UNIVERSITY OF SOUTHAMPTON

Faculty of Environmental and Life Sciences

School of Ocean and Earth Science

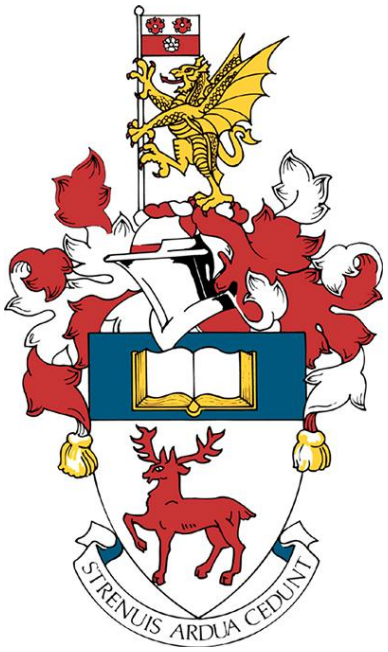

Identification of Seasonal and Interannual Drivers of Primary Production in Two Temperate Estuaries Using High-Frequency Environmental Data

by

Africa Paulina Gómez Castillo

Thesis for the degree of Doctor of Philosophy

March 2022

'The roots of education are bitter, but the fruit is sweet'

~ Aristotle

Identification of Seasonal and Interannual Drivers of Primary Production in Two Temperate Estuaries Using High-Frequency Environmental Data

by

Africa Paulina Gómez Castillo

Supervised by:

Prof. Duncan A. Purdie & Prof. Professor Toby Tyrrell

UNIVERSITY OF SOUTHAMPTON

Faculty of Environmental and Life Sciences
School of Ocean and Earth Science

Abstract

Thesis for the degree of Doctor of Philosophy

Identification of Seasonal and Interannual Drivers of Primary Production in Two Temperate Estuaries Using High-Frequency Environmental Data

by

Africa Paulina Gómez Castillo

Estuaries are one of the most productive coastal regions and, within them, phytoplankton is the most important primary producer. Net community production, the balance between production and consumption, provides an integrated measure of the trophic state, determining if the system is accumulating or depleting organic matter and whether is a net sink or source of O_2 and CO_2. Given that interactions between physical and biological processes within estuaries tends to vary over diurnal and semi-diurnal timescales, this study used high-frequency environmental data to estimate interannual and seasonal drivers of primary production of two contrasting temperate estuaries, the Southampton Water estuary (2014–2020) and Christchurch Harbour estuary (2014–2018). An analysis of the correlation between phytoplankton blooms (from chlorophyll 'a') and environmental conditions, demonstrated correlations between the spring bloom initiation and week-long periods with >800 Wh m^{-2} d^{-1} peaks in surface light availability. Christchurch displayed the typical dynamics described for coastal temperate estuaries, displaying spring and autumn blooms, whereas Southampton presented blooms in spring and summer. Blooms in Southampton developed during neap tides and dissipated on the following spring tide, suggesting reduced estuarine flushing and possible stratification enhancing phytoplankton biomass growth during neap tides. Application of the open water diel oxygen method proved to be a reliable technique to integrate daily estimations of ecosystem production and respiration rates in both estuaries, as long as assumptions are appropriately addressed. Results from this method suggested Southampton Water had become more net heterotrophic (-1.3 to -48.7 mmol O_2 m^{-2} d^{-1}), while Christchurch Harbour seemed had turnes net autotrophic (-11.7 to 19.8 mmol O^2 m^{-2} d^{-1}). An examination of the metabolic balance (GPP:ER) classified both estuaries between oligotrophic and mesotrophic states, with Southampton leaning towards mesotrophic conditions. Estimations of the estuarine carbonate system parameters were performed in Southampton (2019-2020). The estuary was identified to be a source of CO_2 to the atmosphere, agreeing with the net heterotrophic classification from dissolved oxygen derived net community production measurements. Inconsistencies among estimations were attributed to possible seasonal stratification, underestimation of wind speed and estuarine flushing times. Frequency and magnitude of riverine inputs influenced the distribution of carbonate system parameters. Biological processes were identified as a major factor controlling the pH/oxygen saturation dynamics and CO_2 fluxes were observed to follow the pattern of dissolved inorganic carbon concentration. The heterogeneity of coastal zones is of global concern and results from this study will allow a better understanding of local and regional primary production dynamics as well as provide a baseline to assess future anthropogenic impacts and climate change alterations to the aquatic trophic state of the Southampton Water and Christchurch Harbour estuaries.

Table of Contents

List of Tables

List of Figures

Research Thesis: Declaration of Authorship

I, *Africa Paulina Gómez Castillo,* declare that this thesis and the work presented in it are my own and have been generated by me as the result of my own original research.

Identification of seasonal and interannual drivers of primary production in two temperate estuaries using high-frequency environmental data.

I confirm that:

1. This work was done wholly while in candidature for a research degree at this University;
2. Where any part of this thesis has previously been submitted for a degree or any other qualification at this University or any other institution, this has been clearly stated;
3. Where I have consulted the published work of others, this is always clearly attributed;
4. Where I have quoted from the work of others, the source is always given. With the exception of such quotations, this thesis is entirely my own work;
5. I have acknowledged all main sources of help;
6. Where the thesis is based on work done by myself jointly with others, I have made clear exactly what was done by others and what I have contributed myself;
7. At the time of submission, parts of this work have been submitted as:

Gomez-Castillo, A.P., Panton A. & Purdie, D. A. 2022. Temporal variability of phytoplankton biomass and net community production in a macrotidal temperate estuary. Submitted to *Estuarine, Coastal and Shelf Science*.

_____

Date:_____

Symbols and abbreviations

C^*	Calculated oxygen concentration in equilibrium with the atmosphere as a function of temperature and salinity (Feistel, 2008)
C_0	Oxygen concentration at $t = 0$
C_1	Oxygen concentration at the time step (for the present study, 1 hour)
F_{O2}	Gas exchange from diffusive and bubble processes
H_2O	Dihydrogen monoxide; chemical formula for water
I_0	Daily surface irradiance
I_m	Daily mean water column irradiance
K_w	Gas transfer velocity coefficient
$Mn(OH)_3$	Manganese (III) hydroxide
OH^{1-}	Hydroxide ion
P_a	Hourly rates of apparent primary production
P_{atm}	Atmospheric pressure standard value of 101,325 Pa,
P_{slp}	Atmospheric air pressure at sea level
R_n	Hourly rates of apparent night-time respiration
${S_2O_3}^{2-}$	Thiosulfate ion
SE_d	Sum for daily solar energy
Sch_{O_2}	Schmidt number; a dimensionless number defined as the ratio of momentum diffusivity (kinematic viscosity) and mass diffusivity for O_2
T_{Alk}	Total alkalinity
U_i	Standardised wind speed value (9 m s^{-1}) for a smooth boundary regime defined by Wanninkhof (2014)

fCO_2	Fugacity of CO_2
k_{PAR}	Diffuse attenuation coefficient
ρCO_2	Partial pressure of CO_2
ρCO_{2air}	Partial pressure of CO_2 in the atmosphere
ρCO_{2sw}	Partial pressure of CO_2 in seawater
$\frac{\partial C}{\partial t}$	Oxygen concentration change through time
$[O_2]$	Dissolved oxygen concentration
$\Delta\rho CO_2$	Difference between partial pressure of CO_2 in seawater and the atmosphere
$^{14}CO_2$	Radioactive Carbon 14 isotope
A	Autumn
ABPmer	Associated British Ports Marine Environmental Research
ANOVA	Analysis of variance
BOP	Biological oxygen production
Chl ‘a’	Chlorophyll ‘*a*’ concentration
CHR	Christchurch Harbour estuary
CO_2	Carbon dioxide
CO_2^{calc}	A user-friendly seawater carbon calculator for Windows, Max OS X, and iOS(iPhone)
COSYS	Software developed for CO_2 system calculations
DEL	Delaware estuary
DIC	Dissolved inorganic carbon
DO	Dissolved oxygen
ELK	Elkhorn Slough estuary
FCO_2	Air-sea carbon dioxide flux
FO_2	Air-sea oxygen flux
FTU	Formazine Turbidity Unit

h	Mixed layer depth
HAB	Harmful algal blooms
L4	Coastal water representative location from the Western Channel Observatory oceanographic time-series
MIDAS	Met Office Integrated Data Archive System; open access archive of UK weather data
O_2	Oxygen
O_2%	Dissolved oxygen in percentage saturation
OLS	Ordinary least squares
PAR	Photosynthetically active radiation
PC	Principal component
PC1	First principal component
PC2	Second principal component
PCA	Principal component analysis
PDB	Padilla Bay
psu	Practical salinity unit
S-3 EuroHAB	Sentinel-3 satellite products for detecting Eutrophication and Harmful Algal Bloom events in the French-English CHANNEL
Sal	Salinity of the water column
SOT	Southampton Water estuary
Sp	Spring
Su	Summer
Temp	Surface seawater temperature
Tide	Tidal range
TS	Time series
Tur	Turbidity in the water column

VINDTA	Versatile INstrument for the Determination of Total inorganic carbon and titration Alkalinity
W	Winter
WEL	Wells estuary
WKS	Weeks Bay
B	Diffusion through bubbles
BOP	Biological oxygen production
C	Oxygen concentration in the surface mixed layer
E	Entrainment of oxygen through changes in the mixed layer depth
ER	Daily ecosystem respiration
GPP	Daily gross primary production
KJ	Hourly solar energy
Mn	Manganese
NCP	Daily net community production
TCO_2	Sum of dissolved CO_2
U	Wind speed measured at 10m above sea level
t	Transfer velocity correction

Acknowledgments

Firstly, I want to thank CONACyT for the funding for my PhD through the grant 'CONACyT-Gobierno del Estado de Sinaloa' (reference 472065) and to GSNOCS to fund part of my tuition fees.

To my supervisors Duncan and Toby, thank you for your advice. Special gratitude to Duncan; I feel very fortunate to have had you as my leading guide through all this process, I was lucky to catch you before your retirement!

Anouska, many thanks for showing me around the lab and for taking so many samples for me, my PhD wouldn't have happened without your help. To the Callista Crew, thanks for all the trips to the Buoy.

To my PhD friends: Alex Hately, Stacey, Maarten, Alex Trib & Holly, you were my first group of friends here, and I'll always be grateful to have met you guys. Duncan, we would always have Castle Street memories. Elena, Pablo, Lina y Nathan, gracias por ser 'mi comunidad' en NOC. And to everyone in the building who contributed to making this a pleasing experience.

Linda y Patty, agradezco tanto haberlas conocido, no quiero ni imaginarme mis años en Southampton sin ustedes, y me llena de alegría saber que aquí seguirán a mi lado por muchos más. Stephanie, mudarme habría sido imposible sin tu ayuda, gracias por todo. Vecinos (Eric y Monse), que gusto tenerlos cerca y poder compartir pasteles con ustedes.

Elda, yo no estaría acá sin todo el apoyo que me has brindado. Siempre has creído en mí, muchas veces hasta más que yo misma. Gracias infinitas.

A mis hermanas del alma, Erica, Pam y Diana; no importa la distancia, yo las llevo aquí en mi corazón siempre.

A mi mamá, siempre has sido un ejemplo de perseverancia, y de que se pueden alcanzar las metas si te esfuerzas lo suficiente por ellas: éste logro también es tuyo. A mi papá, por los mensajes continuos, siempre preguntando como estoy. A mis hermanos, Erick y Fer, por las risas cada vez que nos juntamos.

Lastly but not least, to Jacob. Nothing of this work would have materialised without your infinite support and love. Thank you for always being my #1 fan, I promise one day I will do the same for you. Meeting you has been the best part of this long journey. I love you.

Chapter 1

Introduction

1.1 Importance of estuarine ecosystems

Coastal zones include lower-river basins (<100 km from shore), estuaries, coastal wetlands, and shelves (Cai, 2011). They represent only 7% of the total ocean surface area (Kanuri *et al*., 2017) however, they play a major role in hydrographic and biogeochemical characteristics of coastal marine ecosystems by acting as natural vectors for land-sea interactions (Ruiz *et al*., 2013). Coastal waters provide habitats to support local biodiversity and sometimes migratory species (Liu *et al*., 2015) and also a variety of ecological services such as water clarity, carbon uptake, erosion control and primary production (Mahoney & Bishop, 2017; Ruiz-Ruiz *et al*., 2017). While different coastal zones share similar characteristics, their response to changes in climate variables fluctuates according to many factors, such as geomorphology and anthropogenic pressures. Among these regions, estuaries can be highlighted due to their unique physical, chemical, and biological characteristics and complex ecological interactions and spatial and temporal variability (Lemley *et al*., 2020; Newton *et al*., 2014).

Estuaries are commonly defined as “semi-enclosed coastal bodies of water that have a free connection with the open sea and within which seawater is measurably diluted with freshwater derived from land drainage” (Borges & Abril, 2011). They can act as fast biogeochemical reactors as a consequence of the continuous input of environment nutrients and organic matter from riverine

sources (Cloern *et al*., 2014). These natural inputs of nutrients from rivers caused by weathering, have been disturbed in the last few decades by human activities, such as agriculture, wastewater treatment and consumption of fossil fuels (Rodríguez-Gallego *et al*., 2017) leading to an alteration of the biogeochemical processes and the biological community structure (Davidson *et al*., 2015; Staehr *et al*., 2017). Human population growth around estuaries can lead to an increase in nutrient and organic inputs (Caffrey et al., 2014; Guenther *et al*., 2015) resulting in major water quality problems, emphasising the importance of determining the current state of representative ranges of estuarine ecosystems.

1.2 Distribution of phytoplankton in coastal waters

Phytoplankton communities are the basis of many marine ecosystems, regulating the energy transfer efficiency through the food web but also the efficiency of the biological carbon pump, and furthermore, are responsible for roughly half of global primary production (Behrenfeld *et al*., 2006; Rose & Caron, 2007). In estuaries, phytoplankton exhibit rapid responses to environmental variations by modifying their temporal and spatial species distribution, usually highly amplified when compared to the open ocean (e.g. Leterme *et al*., 2014). Therefore, phytoplankton is commonly acknowledged as an excellent bioindicator of the impact of natural and man-driven changes in coastal ecosystems (Leterme et al., 2014; López-Abbate et al., 2017).

The most common parameter used to measure phytoplankton biomass variability is the concentration of the chlorophyll '*a*' (Chl '*a*') pigment (Niu *et al*., 2016; Winder & Cloern, 2010). Given the strong relation between chl '*a*' and primary production, there is an implication that the observed variability in one parameter can indirectly describe processes associated with the other. Therefore, the

phytoplankton biomass distribution in an estuary can indicate the dynamics of the seasonal and annual variability of the ecosystem properties such as water quality, community metabolism, and carrying capacity for fish and shellfish (e.g. Cloern & Jassby, 2010).

Phytoplankton blooms are common occurrences in many coastal ecosystems, and estuaries are no exception (e.g. Rose & Caron, 2007). A bloom is a rapid increase in phytoplankton biomass caused by temporary imbalances between the rate of primary production and the rate of loss of photosynthetically fixed carbon due to respiration, grazing, and advection (e.g. Iriarte & Purdie, 1994). To classify an event as a bloom, it is widely accepted that a substantial deviation above background phytoplankton biomass for the individual ecosystems is needed (e.g. Carstensen *et al*., 2015). More than a single event, blooms are usually a series of fluctuations where the biomass and the species composition of the phytoplankton population change rapidly (Cloern, 1996; Godrijan *et al*., 2013), and can affect positively or negatively food web structure and carbon flow (Narasimha *et al*., 2017; Trombetta *et al*., 2019).

1.2.1 Seasonal blooms

Phytoplankton communities and biomass change on many scales simultaneously (e.g. Bucci *et al*., 2012). Estuaries present an extensive range of variability patterns, with some dominated by a seasonal fluctuation, others dominated by annual oscillation and others dominated by the residual component, including exceptional bloom events such as red tides (e.g. Cloern & Jassby, 2010).

In an extensive review of phytoplankton bloom dynamics in coastal ecosystems, Cloern (1996) introduced a classification for seasonal blooms into three types: (i) recurrent seasonal events that usually persist over weeks, (ii) aperiodic events

that often last for days, and (iii) exceptional events that are typically dominated by few species (sometimes noxious or toxic forms) and can persist for months. Seasonal blooms can be observed in spring, summer, autumn, and winter and these events are often dominated by different species each season as the phytoplankton community adapts to changes in resources and the physical environment (e.g. Cloern & Jassby, 2010). In Cloern (1996) review, he suggested that most ecosystems show a narrow range of annual variability and that those with substantially large annual variability can attribute this to disturbance from natural events or human actions.

Undoubtedly, the most often described seasonal pattern is the spring bloom (Carstensen *et al*., 2015; Martellucci *et al*., 2021; Niu *et al*., 2016; Trombetta *et al*., 2019; Zingone *et al*., 2010); an occurrence mainly observed in all aquatic systems in temperate and subpolar regions as a response to seasonal increases in temperature and solar radiation, and the subsequent thermal stratification after winter mixing redistributing nutrients to surface water (e.g. Leterme *et al*., 2014). The spring bloom typically persists for a few weeks to months, with eventually nutrient limitation, cell sinking and grazing causing the bloom to collapse. A secondary biomass peak stimulated by excess nutrients can develop in late summer or autumn (e.g. Winder & Cloern, 2010).

1.2.2 Environmental conditions affecting blooms

The magnitude, timing and duration of phytoplankton blooms across ecosystems varies greatly (Leterme *et al*., 2014). Even though much of phytoplankton variability can be driven by the annual cycles of solar radiation and atmospheric input, in such complex and dynamic systems like estuaries, fluctuation in phytoplankton biomass is generated by additional processes that occur across

their interfaces with land, ocean, atmosphere, and underlying sediments (e.g. Cloern & Jassby, 2010). Consequently, blooms are generated from a combination of different critical factors and interactions between them (Henson *et al*., 2006; Niu *et al*., 2016).

Temperature affects phytoplankton physiology and metabolic process, changing the composition and trophic interactions of plankton communities; for instance, in non-limited nutrient conditions, rises in temperature can increase nutrient uptake (e.g. Trombetta *et al*., 2019). In addition, surface blooms can be promoted by establishing strong thermal stratification in the water column due to the sudden increase of temperature (e.g. Carstensen *et al*., 2015).

However, light availability is usually the critical driver of bloom initiation in coastal environments. Interannual variability within estuaries is modulated by surface irradiance (PAR), oscillation and weather conditions affecting it, such as cloud cover. Moreover, water transparency and surface mixed layer depth affect the amount of light available for phytoplankton (e.g. May *et al*., 2003).

Light availability in turbid estuaries can limit phytoplankton growth, but blooms regularly occur when turbidity decreases. In most shallow estuaries, the main cause of changes in turbidity is vertical mixing driven by tidal currents with variations between ebb and flood phases as well as between neap and spring tides (Bucci *et al*., 2012). Tides can affect sediment resuspension rates and, therefore, turbidity. Additionally, a higher tidal range means a larger intrusion of coastal water than with a low tidal range, which is generally less turbid, and this would tend to counteract the effect of bottom resuspension (e.g. Iriarte & Purdie, 2004). Moreover, the presence of suspended materials from river runoff can also

affect estuarine turbidity depending on its particle load as a result of precipitation rates (e.g. Martellucci *et al*., 2021).

Nutrient input from runoff can supply systems with nutrients, stimulating phytoplankton production and leading to the accumulation of biomass and bloom formation (e.g. Trombetta *et al*., 2019). However, changes in nutrient loads due to human activities have the potential to modify the periodicity and magnitude of phytoplankton blooms or may cause an environment to become eutrophic (e.g. Davidson *et al.*, 2012). Horizontal and vertical water movements largely influence the availability of nutrients, and in shallow estuaries, the intensity and direction of winds can strongly influence the nutrient supply by sediment resuspension (e.g. Silkin *et al*., 2019). Freshwater inflow can favour phytoplankton by promoting vertical salinity stratification retaining phytoplankton in a nutrient-rich and well-illuminated zone. Nevertheless, in small estuarine systems, intense freshwater pulses can flush out the phytoplankton community (Bucci *et al*., 2012; Cloern & Jassby, 2010; Peierls *et al*., 2012).

1.3 Estuarine biogeochemical processes

Biogeochemistry is defined by Bianchi (2012) as the integrative field in which interactions between biological, chemical, and geological processes are studied to determine sources, sinks, and fluxes of elements through different reservoirs within ecosystems. Given that estuaries are complex ecosystems where processes do not work independently from one another (Laane & Middelburg, 2011), in recent years, this holistic approach has been used to improve the understanding of estuaries and the role they play in defining the hydrographic and biogeochemical characteristics of coastal marine ecosystems (e.g. Ruiz *et al*., 2013).

In estuaries, the spatial and temporal scales of biogeochemical cycles can vary considerably within days and even hours (Bianchi, 2012), thus, the importance of estimating atmospheric fluxes of biogases in estuaries and their impact on global budgets cannot be overestimated (e.g. Frankignoulle & Middelburg, 2002).

1.3.1 Dissolved oxygen in the water column

In estuarine environments, the concentration of dissolved oxygen (DO) is a key indicator of water quality due to its direct relation with biological and environmental processes (Yuan *et al*., 2016). In surface waters, DO concentrations are determined by inputs from the atmosphere and aquatic plant photosynthesis, and outputs, which are dominated by respiration and other processes that consume oxygen (Friedrich *et al*., 2014). Furthermore, low DO concentrations can cause adverse responses from aquatic organisms such as slower growth rates, elevated stress levels and in some cases death (e.g. O'Boyle *et al*., 2009). Due to the above, it is not surprising that most of the methods applied to assess eutrophication include water column DO measurements. Even when it has been classified as a secondary symptom of eutrophication (e.g. Bricker *et al*., 2008), dissolved oxygen is a major indicator of how an ecosystem responds following an increased runoff of nutrients.

In coastal ecosystems, and mainly in those affected by eutrophication, the developing plant biomass leads to increased photosynthetic oxygen production. This elevated oxygen concentration is soon reduced by respiratory oxygen consumption of organic matter indicated by a biological demand for oxygen. A large oxygen demand can result in two of the most important oxygen-related conditions of hypoxia and/or anoxia (e.g. Nezlin *et al*., 2009).

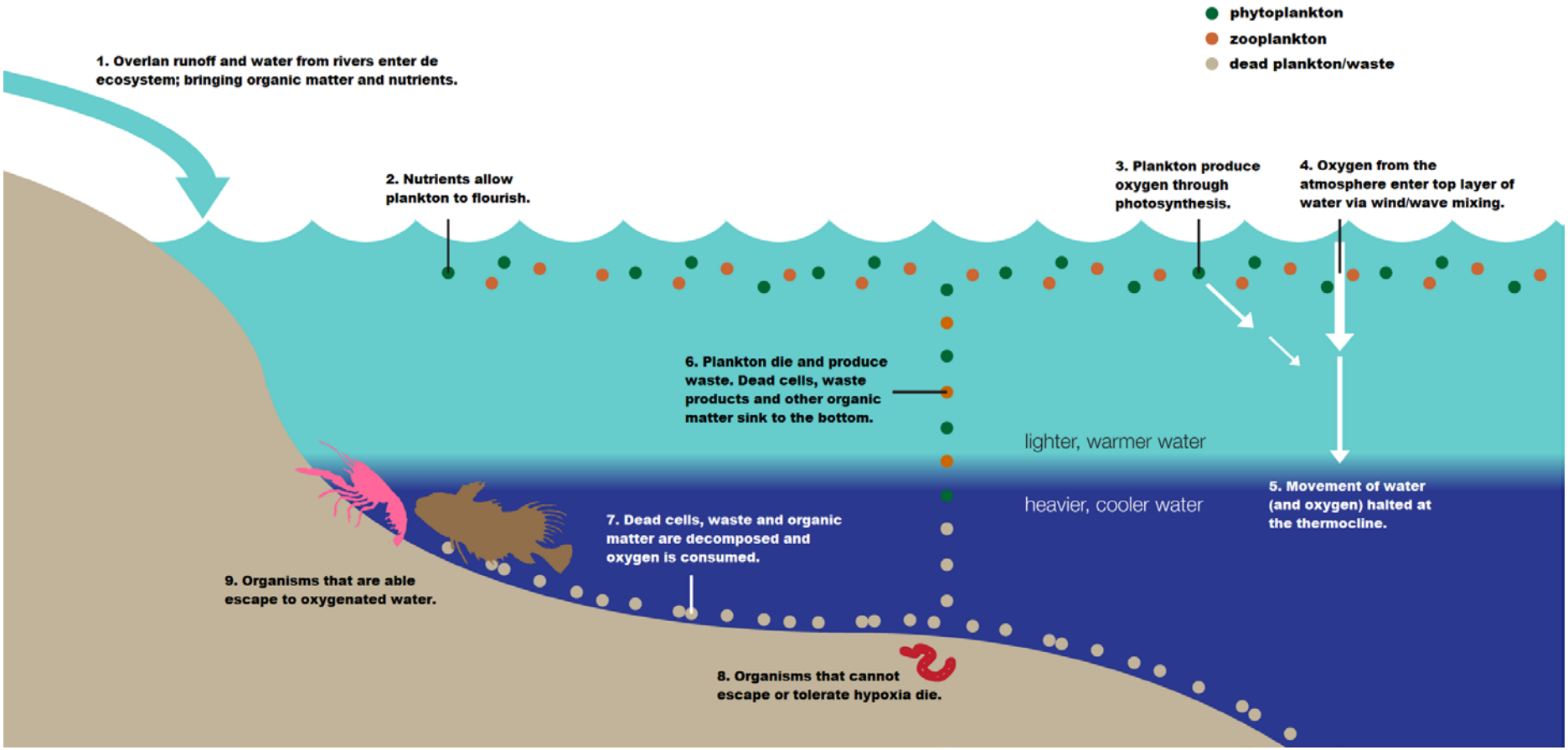

Fig. 1.1 Description of hypoxia process. Infographic from (NOAA. Great Lakes Environmental Research Laboratory, 2017).

Hypoxia is normally defined as when the DO concentration in a water body falls below 2 mg O_2 L^{-1} (~62.5 µmol O_2 L^{-1}) and is influenced by a complex interaction of physical and biochemical processes (Gammal *et al*., 2017; Xia & Jiang, 2015).

Although, it has been pointed out that this value is very low, and a higher one (i.e., 3.5 mg O_2 L^{-1} or 109.4 µmol O_2 L^{-1}) should be used mainly for sites with more sensitive species (Steckbauer *et al*., 2011). Coastal hypoxia is often associated with increases in ecosystem production and respiration, presenting higher net autotrophy in surface layers but higher net heterotrophy in underlying waters (e.g. Kemp & Testa, 2011).

Moreover, anoxia occurs when DO concentration, in the ecosystem, is below 0.2 mg O_2 L^{-1} (~6.3 µmol O_2 L^{-1}); these events are also known as no-oxygen events (O'Boyle *et al*., 2009). Hypoxia and/or anoxia events can reduce the tolerance of organisms to other stressors, disturbing their metabolic activities and eventually causing their death (Cai *et al*., 2017; Steckbauer *et al*., 2011; Xia & Jiang, 2015).

Monitoring oxygen-deficient events in coastal waters is very important, not only due to their impact on marine life but also because of the close relation oxygen has with biogeochemical cycles and nutrient recycling (Ahlgren *et al*., 2017; Zhu *et al*., 2017). Hypoxia can modify the amount of P and N released from the sediments that then becomes available for biota (e.g. Gammal *et al*., 2017), which helps to extend eutrophication conditions.

1.3.2 Net community production

An accurate estimate of the oxygen flux at the air-sea interface can be achieved from the determination of the net primary production of the ocean (e.g. Tilstone *et al*., 2009). Several techniques are used to determine aquatic rates of net primary production, the most common being the method introduced by

Steemann-Nielsen (1952) where radioactive carbon 14 isotope ($^{14}CO_2$) uptake and photosynthetic conversion to reduced particulate organic carbon by a natural community of microplankton, is measured after growth in bottles (Chavez *et al*., 2011; Johnson & Bif, 2021; Oczkowski *et al*., 2016).

Alternatively, changes in DO can be measured in small-volume glass bottle incubations in the dark and light to detect respiration and net production (Langdon & Garcia-Martin, 2021). However, the problems inherent in these short-term, small volume incubation techniques are exacerbated in the highly dynamic heterogeneous coastal zone, where the seasonal oxygen change shows marked variability (Queste *et al*., 2016). Interaction between physical and biological processes within estuaries tends to vary over diurnal, semi-diurnal and sometimes episodic timescales, making acquiring frequent data critical to accurately assess ecosystem health for these periods (e.g. Nidzieko *et al*., 2014).

An alternative and more integrative method to estimate primary production relies on the calculation of the *in situ* oxygen mass-balance from continuous measurements of DO: the open water diel oxygen method, first proposed by Odum (1956) and later modified to apply it to estuarine systems (Caffrey, 2003; Emerson *et al*., 2008). The difference in DO concentration across a specific period of time has been widely used to quantify O_2 flux due to the release of oxygen during photosynthesis and uptake during aerobic respiration, allowing these separate processes to be determined together (Caffrey, 2003, 2004; Herrmann *et al*., 2014). In addition, to DO, it is necessary to monitor other parameters such as light and water clarity, temperature, nutrient and organic matter loading, water residence time and water depth since these are key environmental factors that influence productivity rates (Herrmann *et al*., 2014).

The use of the open water diel oxygen method provides a practical approach to capturing events and ecosystem changes over time, given that DO variability can be recorded continuously and for sustained periods (e.g. Beck *et al*., 2015). This method quantifies the *in situ* diel oscillations in DO concentration to estimate daily integrated gross primary production (GPP), ecosystem respiration (ER) and net community production (NCP) (Demars *et al*., 2015).

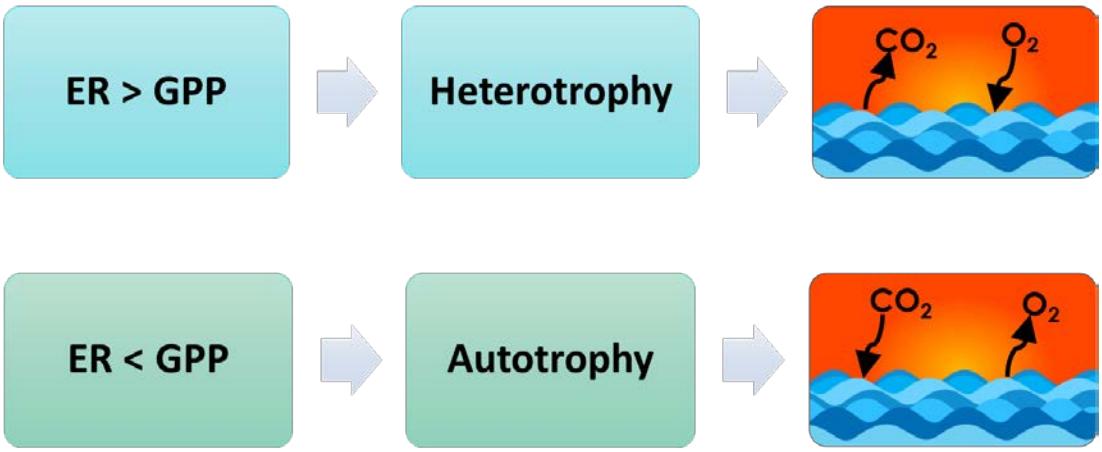

Fig. 1.2 Aquatic ecosystem trophic state through the relationship between ecosystem respiration (RE) and gross primary production (GPP), and its influence in the air-sea exchange of O_2 and CO_2.

NCP, also known as net ecosystem metabolism (e.g. Needoba *et al*., 2012), is a community-level process that integrates all of the processes affecting the balance between production and consumption and can be defined as the overall balance between GPP and ER (Duarte & Regaudie-De-Gioux, 2009; Garcia-Corral *et al*., 2021). It provides an integrated measure of the trophic state of an aquatic ecosystem, determining if the system is accumulating or depleting organic matter and whether there is net uptake or release of O_2 and CO_2 as illustrated in Figure 1.2 (Guenther *et al*., 2017; Haskell *et al*., 2019; Hopkinson & Smith, 2005). A positive NCP (net autotrophic) indicates that autochthonous organic matter

sources dominate in the ecosystem. In contrast, a negative net community production (net heterotrophic) suggests external organic sources dominate (Feng *et al*., 2012; McAndrew *et al*., 2007; Shen *et al*., 2020; Shen *et al*., 2019b).

Although the open ocean has been considered on time scales of months and longer to be a net autotrophic ecosystem that exports organic carbon to depth and produces more oxygen than it consumes (e.g. McAndrew *et al*., 2007), recent reports have revealed a wider prevalence of heterotrophic communities, particularly in the least productive oceanic regions (Aranguren-Gassis *et al*., 2011; Duarte *et al*., 2013b; Williams *et al*., 2012). However, in estuarine regions, a shift from an autotrophic to a heterotrophic state, mainly related to seasonal changes in water temperature and light availability, has been reported (Azevedo *et al*., 2006; Tang *et al*., 2015).

NCP varies between ecosystems, as seen in Table 1.1, which emphasises the importance of determining this parameter in a representative range of marine ecosystems. This will provide the information needed to constrain biogeochemical models used to determine regional and global biogeochemical fluxes (e.g. Beck *et al*., 2015) since NCP represents the net effect of all biological processes contributing to CO_2 and O_2 fluxes in coastal ecosystems (Demars *et al*., 2015; Valenzuela-Siu *et al*., 2007).

1.3.3 Estuarine carbonate system

Estuaries are a major global source of CO_2 to the atmosphere (Bianchi *et al*., 2013), given that they are considered efficient ‘traps’ of a large fraction of terrestrial organic carbon delivered by rivers (e.g. Hu *et al*., 2020). However, coastal environments are usually neglected in global carbon budgets because this region only covers about ~7% of the total ocean system (Kanuri *et al*., 2017).

Despite their small area, according to Chen & Borges (2009), near-shore ecosystems account for ~30% of the CO_2 uptake by the open oceans based on pCO_2 measurements and carbon mass-balance calculations. The coastal ocean is one of the most biogeochemically active regions of the biosphere where production and degradation of organic matter are several times higher than in the open ocean and, in consequence, air-sea CO_2 fluxes are disproportionately more intense than their relative surface area (e.g. Borges *et al*., 2006)

The overall picture of air-sea CO_2 distribution is that temperate open continental shelves are net autotrophic; hence, net exporters of oxygen and potential sinks for atmospheric CO_2 (Borges *et al*., 2004). Whereas the consensus regarding estuaries is that they are considered net heterotrophic, acting as sources of CO_2 to the atmosphere (Bianchi, 2012; Cai, 2011; Frankignoulle *et al*., 1998; Hu *et al*., 2020; Yao *et al*., 2020). This is mainly attributed to the large inputs of terrestrial organic carbon that these ecosystems receive (Guenther *et al*., 2017), resulting in a respiration increase of detrital organic matter, which in turn produces large quantities of dissolved CO_2 that generate very high fluxes to the atmosphere (Frankignoulle & Middelburg, 2002). In general, CO_2 degassing flux is more intensive in lower latitude estuaries than in high latitudes (e.g. Bianchi *et al*., 2013), and more specifically, in European estuaries, the production of large quantities of dissolved CO_2 is related to intense anthropogenic disturbance, reflected in elevated loadings of detrital organic matter which induces high respiration rates (e.g. Frankignoulle *et al*., 1998).

Table 1.1. Annual average rates of net community production determinate by the open water diel oxygen method in different estuaries mmol O_2 m^{-2} d^{-1}.

Site	Year	Ecosystem description	Annual NCP	Reference
Chesapeake Bay, USA	1995-2000	The largest estuary in the US. The Bay estuarine system comprises the Bay proper and more than 50 tributaries	-65.6	(Caffrey, 2004)
Mullica River, USA		Shallow, polyhaline embayment with extensive salt marshes.	-67.6	
Old Woman Creek, USA		Freshwater estuary. The estuary's outlet mouth may be close for extended periods as the result of wave action and the formation of a barrier beach.	-112.5	
Narragansett Bay, USA		Is a phytoplankton-based ecosystem with relatively little salt marsh or macroalgae.	-40.6	
Great Bay, USA		Complex embayment and New Hampshire's largest estuarine system, encompassing tidal portions of five major river systems.	-18.8	
Wells, USA		Back-barrier marsh dominated by strong tidal currents due to the large tidal range in the Gulf of Maine.	28.1	
Weeks Bay, USA	2009-2010	Mid-bay point. Small, shallow sub-estuary of Mobile Bay. Freshwater inputs from two rivers.	-68.8	(Mortazavi *et al*., 2012)
Apachicola Bay, USA	2002-2011	Extensive open water, submerged and emergent wetland vegetation, tidal flats, and unconsolidated bottom.	-50 to -20	(Caffrey *et al*., 2014)
Weeks Bay, USA	2003-2011	Small, shallow sub-estuary of Mobile Bay. Freshwater inputs from two rivers.	-10 to -15	
Grand Bay, USA	2004-2011	Small and relatively pristine estuary with no major river inputs.	-20 to -10	
River Thames plume, UK	2001-2015	Warp Anchorage monitoring station, which is a permanently well-mixed shallow area within the River Thames plume.	-5	(Hull *et al.*, 2016)
Pensacola Bay, USA	2013	Shallow, river-dominated estuary with fringing seagrass beds graduating to deeper unvegetated habitat comprised of sand-silt sediments.	Spring 16.9 Summer 109.5	(Murrell *et al*., 2018)
Ria Formosa, Portugal	2017-2018	Coastal lagoon, depth ~2 m, semi-diurnal tides in a mesotidal regime, well mixed vertically.	-0.1 to -71	(Cravo *et a*l., 2020)

Despite the vast agreement on the role of estuaries as sources of CO_2, the order of magnitude of these contributions are still a matter of debate (Frankignoulle *et al*., 1998). This argument is based on the fact that current global estuarine CO_2 flux estimations are based on a limited dataset that is likely over representing highly heterotrophic estuaries (Shen *et al*., 2020). Furthermore, there is an absence of data resolving the temporal variability of carbon cycling for adequately describing the diversity and spatial heterogeneity in these highly dynamic ecosystems (Borges *et al*., 2008).

Since estuaries act as a convergence zone between the terrestrial environment and the coastal ocean (Kanuri *et al*., 2017), riverine discharge controls the freshwater residence time and the mechanisms of carbon processing (Bianchi *et al*., 2013). When high freshwater discharge occurs, excess CO_2 from riverine flow degases to the atmosphere during estuarine mixing and accounts for most of the CO_2 flux (Borges *et al*., 2006). Conversely, organic matter remineralisation dominates under low freshwater discharge, and dissolved inorganic carbon (DIC) builds up in the estuarine water column resulting in CO_2 emissions (Hu *et al*., 2020). In macrotidal estuaries, most of the mixing between freshwater and seawater occurs within the inner estuary; however, the outer estuary can be a site of intense primary production and can behave as a major sink for atmospheric CO_2 (Frankignoulle *et al*., 1998). Recent work has shown that estuarine plumes can also be net sinks of CO_2, particularly in the outer plume region (e.g. Bianchi, 2012).

The balance between CO_2 absorption and release in estuaries is further regulated by abiotic factors such as wind speed, atmospheric pressure, pH, alkalinity, temperature and salinity, and by biotic factors like primary production and

ecosystem respiration (Guenther *et al*., 2017). Depending on the interaction among these factors, an ecosystem or parts of it, can act as a CO_2 source or sink (Bianchi, 2012). Therefore, to accurately estimate the CO_2 flux and the role of estuaries in the global carbon cycle, spatiotemporal variations and anthropogenic disturbance effects should be considered in budget calculations.

1.4 Optical sensors in coastal observation

Interactions between physical and biological processes in estuaries require making continuous biogeochemical measurements at the tidal, fortnightly, and episodic timescales over which residence time and geochemical rates vary (Nidzieko *et al*., 2014). Moreover, phytoplankton communities and biomass can change on many scales at the same time. Large changes can occur at time scales shorter than a month, and monthly scale changes in Chl '*a*' can arise from processes operating at shorter timescales (Cloern & Jassby, 2010); therefore, Chl '*a*' measured today could easily represent preceding primary productivity (Chavez *et al*., 2011). Biweekly to monthly sampling campaigns are unable to capture such short-term fluctuations, and it has been argued that sampling times very often miss critical or controlling events in estuaries (e.g. Chavez *et al*., 2011).

Recent improvements in sensor and autonomous platform technology are enabling a considerable expansion of the temporal and spatial scope of marine biogeochemical observations (e.g. Nicholson *et al*., 2015). The use of these optical sensors (e.g. optodes) permits the coupling of biogeochemical and physical measurements at sub-hourly intervals for extended durations (e.g. Nidzieko *et al*., 2014). Additionally, long time series constructed with low sampling intervals (minutes) can capture the detail of events that would not be recorded

through conventional on-site discrete sampling, to effectively address episodic events (e.g. Cravo *et al*., 2020).

The literature has widely described examples of the advantages of using optical sensors in coastal observation. One of those is the use of optodes compact enough to be mounted on autonomous underwater vehicles with high enough precision to resolve O_2 diel oscillations smaller than 1 µmol O_2 L^{-1} as reported by Barone et al. (2019). In addition, Rumyantseva *et al*. (2019) described the use of autonomous platforms for studying phytoplankton dynamics due to their ability to obtain frequent depth-resolved profiles of bio-optical and physical properties for inter-seasonal periods of time. Lastly, the estimation of primary production through continuous dissolved oxygen measurements using optodes (Cravo *et al*., 2020; Hull *et al*., 2016) has proven to identify seasonal and even episodic events in estuaries.

In recent years, the use of optical sensors has expanded, and with it global observation networks have developed. Nevertheless, in order to confidently make use of these data, a suite of chemical and biological sensors with adequate characteristics in terms of size, power consumption, precision/accuracy and long-term stability are needed (Bittig *et al*., 2018), and the adequate maintenance and calibration must be performed in order to obtain high-quality and reliable data (Uchida *et al*., 2008).

1.5 Thesis overview

1.5.1 Aims and objectives

The overall aim of this study is to estimate interannual and seasonal changes in the primary production of two contrasting temperate estuaries, the Southampton

Water estuary and Christchurch Harbour estuary, and identify the environmental factors influencing its variability by using continuous high-frequency environmental data. It is hypothesised that *a net heterotrophic state will dominate in the two estuaries, implying a depletion of organic C and a net CO_2 release to the atmosphere, and that a shift to autotrophy will only be episodic and driven by phytoplankton blooms.*

In order to test the hypothesis, the following main objectives were addressed:

- To investigate *temporal phytoplankton bloom dynamics* and the environmental factors driving them in Southampton Water (2014 – 2020) and Christchurch Harbour (2014 – 2018).
- To examine *seasonal and interannual variation in productivity rates* and the interactions between them and environmental variables in Southampton Water (2014 – 2020) and Christchurch Harbour (2014 – 2018).
- To explore the *primary controls and temporal variability of carbonate system parameters* in Southampton Water (2019 – 2020) and their influence on air-sea CO_2 fluxes.

1.5.2 Thesis structure

This thesis is presented in six chapters, which are described below:

Chapter 1: Introduction.

The first chapter provides a general background on the topics addressed within the thesis; including the importance of estuaries in coastal regions, the temporal distribution of phytoplankton in the form of seasonal blooms and environmental conditions triggering them, the estuarine biogeochemical processes that interact with net community production, and the relevance of optical sensors in coastal

observations. The main objectives are described and the thesis structure is explained.

Chapter 2: Methods.

This chapter introduces the study sites and provides background information for Southampton Water and Christchurch Harbour estuaries. The data collection and processing methods are given for continuous sensor monitoring, field sampling and external data acquisition. Equations formulating the open water diel oxygen method are reviewed, as well as calculations included in the CO_2^{calc} software. Statistical analyses used in the following chapters are described.

Chapter 3: Temporal variation of phytoplankton blooms associated with changes in environmental conditions in the Southampton Water and Christchurch Harbour estuaries.

In chapter 3, the seasonal and interannual variability of environmental factors is explored graphically and statistically. Variability in the timing, magnitude and duration of the blooms and environmental drivers is discussed. For Southampton Water, an in-depth analysis of the influence of tides on phytoplankton blooms is also included.

Chapter 4: Variability of net community production, gross primary production, and ecosystem respiration in two contrasting estuaries.

Chapter 4 reviews productivity rates derived from high-frequency measurements of surface water dissolved oxygen concentration (in both estuaries) using the open water diel oxygen method. Environmental factors influencing ecosystem respiration, gross primary production and net community production are analysed. Implications on the aquatic trophic state of both estuaries are

addressed, and the relationship between ecosystem respiration and gross primary production is evaluated.

Chapter 5: Plankton carbon metabolism and air-sea CO_2 fluxes of Southampton Water estuary.

In chapter 5, a characterization of the seasonal and interannual carbonate chemistry parameters, for the Southampton Water estuary in 2019 and 2020, using the CO^{2calc} software is presented. An analysis of the connection between air-sea CO_2 flux and net community production, as well as its implication on the CO_2 release and/or assimilation in the estuary is evaluated.

Chapter 6: Synthesis and conclusions.

The final chapter summarises the research presented in this thesis. It includes the main findings and implications for future work.

The appendix and all references are listed at the end of this work.

At the time of submission of this thesis, data for the Southampton Water estuary in 2019, included in Chapter 4 and Chapter 5, have been submitted as:

Gomez-Castillo, A.P., Panton A. & Purdie, D. A. 2022. Temporal variability of phytoplankton biomass and net community production in a macrotidal temperate estuary. Submitted to *Estuarine, Coastal and Shelf Science*.

Chapter 2

Methods

2.1 Study sites

The present study determined environmental conditions and their relationship with productivity rates in two South Coast UK estuaries: Southampton Water and Christchurch Harbour. Southampton Water was the central area of investigation due to its accessibility to different data sets and sensor calibration availability.

2.1.1 Southampton Water

The Southampton Water estuary is part of the Solent estuarine system, considered the largest on the south coast of the UK (Fig. 2.1). It is an approximately linear body of water about 2 km wide and 10 km long with a central channel continuously dredged to a minimum depth of 12.2 m below the local Chart Datum. Three main rivers discharge into Southampton water: the Rivers Test and Itchen towards the head of the estuary and the river Hamble, nearer to the mouth on the eastern side (Iriarte & Purdie, 2004).

The estuary is characterised by a semi-diurnal tidal regime where each tide consists of a double high water, ~2 h apart, followed by a short ebb tide. The tidal range varies between 1.5 m on neaps and 5.0 m on springs (Crawford *et al*., 1997). It is considered a partially mixed system, with minimal stratification occurring throughout the semi-diurnal tidal cycle with the highest vertical density

gradient occurring at low water and well-mixed conditions at high water (Levasseur *et al*., 2007).

2.1.2 Christchurch Harbour

The Christchurch Harbour estuary is a shallow harbour located on the South coast of England with an approximate area of 2.39 km^2 (Fig. 2.1). It is mainly fed by two rivers, the Hampshire Avon and the Stour, that combine and flow into the western end of the system; a third small river, the Mude, drains into the estuary near the outlet. The system meets the English Channel through a 47-m-wide narrow opening known as the Run (Panton *et al*., 2020).

The estuary presents an average tidal range of 1.2m during spring tides and has a mean water depth of 0.5m outside the main channel. It give flows in the summer months when river flows are minimal and typically well-mixed characteristics (Huggett *et al*., 2021a). Due to its shallow nature, the estuary is a tidally driven system with salinity values mainly depending on tide flow, presenting freshwater conditions at low tides and near fully saline conditions during high tides (Huggett *et al*., 2021b).

2.2 Continuous monitoring

2.2.1 Multiparametric probe: EXO2

<u>Southampton</u>

Water quality data were collected using a YSI EXO2 sonde deployed on a solar-powered EMM700 Data Buoy (Xylem Analytics, UK) located at 50.871° N, -1.373° W, in the Southampton Water estuary (Fig. 2.1). The sonde was placed into an open flow PVC tube fixed to the Data Buoy at a depth of 1.6 m below the sea surface; the average water depth at the site was 10 m. Parameters recorded by

the sonde included dissolved oxygen (DO) concentration (mg L^{-1}) and oxygen saturation (%), temperature (°C), salinity, chlorophyll '*a*' (µg L^{-1}), turbidity (FTU) and pH. The sonde has a central wiper that rotates at regular intervals to remove biofouling from the optical sensors mechanically.

The sonde is connected to a Storm data logger situated within the Data Buoy system that regularly uploads data, via a mobile phone connection, to a dedicated webpage within the Storm Central cloud data collection service (https://stormcentral.waterlog.com/).

Data was recorded at high frequency from May 2014 to December 2020, with a total of 178,677 records (Table 2.1). During the first two months, data were recorded every 10 minutes, and after that, the rest of the measurements were logged every 15 minutes. For this study, hourly averages were calculated for all years.

During the seven year deployment of the data buoy a number of gaps in data collection occurred; major periods of data gaps included (i) During 2014, a 25-days gap from 30/06/14 to 25/07/14 and (ii) in 2015, a gap of 22-days from 19/10/2015 to 09/12/2015. (iii) For 2017, data were recorded from the beginning of the year but only for three months (until 29/03/17), since the probe was recovered, (iv) and not deployed back again until 07/03/18. In 2019 two significant gaps occurred, (v) the first one between 13/02/2019 and 19/03/2019 (34 days) caused by the sonde being recovered while the data buoy mooring chain was replaced and the sonde and PVC tube cleaned of biofouling, and (vi) the second one from 23/11/2019 to 04/12/2019 (11 days) due to some problems backfilling data when the Storm Central server migrated from one IP address to another. Finally, (vii) a 3-day gap from 24/08/20 to 27/08/20 when the sonde was

recovered for cleaning and review sensors. It is worth mentioning that, in 2020, from 15/04/20, temperature and salinity sensors stopped recording, but since the COVID-19 restrictions were in place, it was not until 27/08/20 that sensors could be calibrated and replaced. Temperature and salinity values for this period were estimated based on daily averages from data from 2014 to 2019. The pH sensor was removed at the end of the 2017 and a new sensor was not added until 22/07/2019.

Finally, all data were carefully inspected for unreliable values, and outliers plus negative or occasional inconsistent high magnitude values (typically caused by biofouling) and these removed manually.

Christchurch

Parameters including (DO) concentration (mg L^{-1}) and oxygen saturation (%), temperature (°C), salinity (psu), chlorophyll '*a*' (µg L^{-1}) and turbidity (FTU), were recorded using a YSI EXO2 sonde deployed at the Ferry pontoon located at 50.719° N, -1.744°W, in Christchurch (Fig. 2.1). The probe remained at surface water level at all times since the pier moved along with tides; the average water depth at the site is 1.75 m. The EXO2 was connected to a solar-powered system to provide energy, and to a Storm data logger that uploaded data every 2 hours, via a mobile phone connection, to a dedicated webpage within the Storm Central cloud data collection service; data between the 2-hour periods was logged into the internal storage system and downloaded manually afterwards.

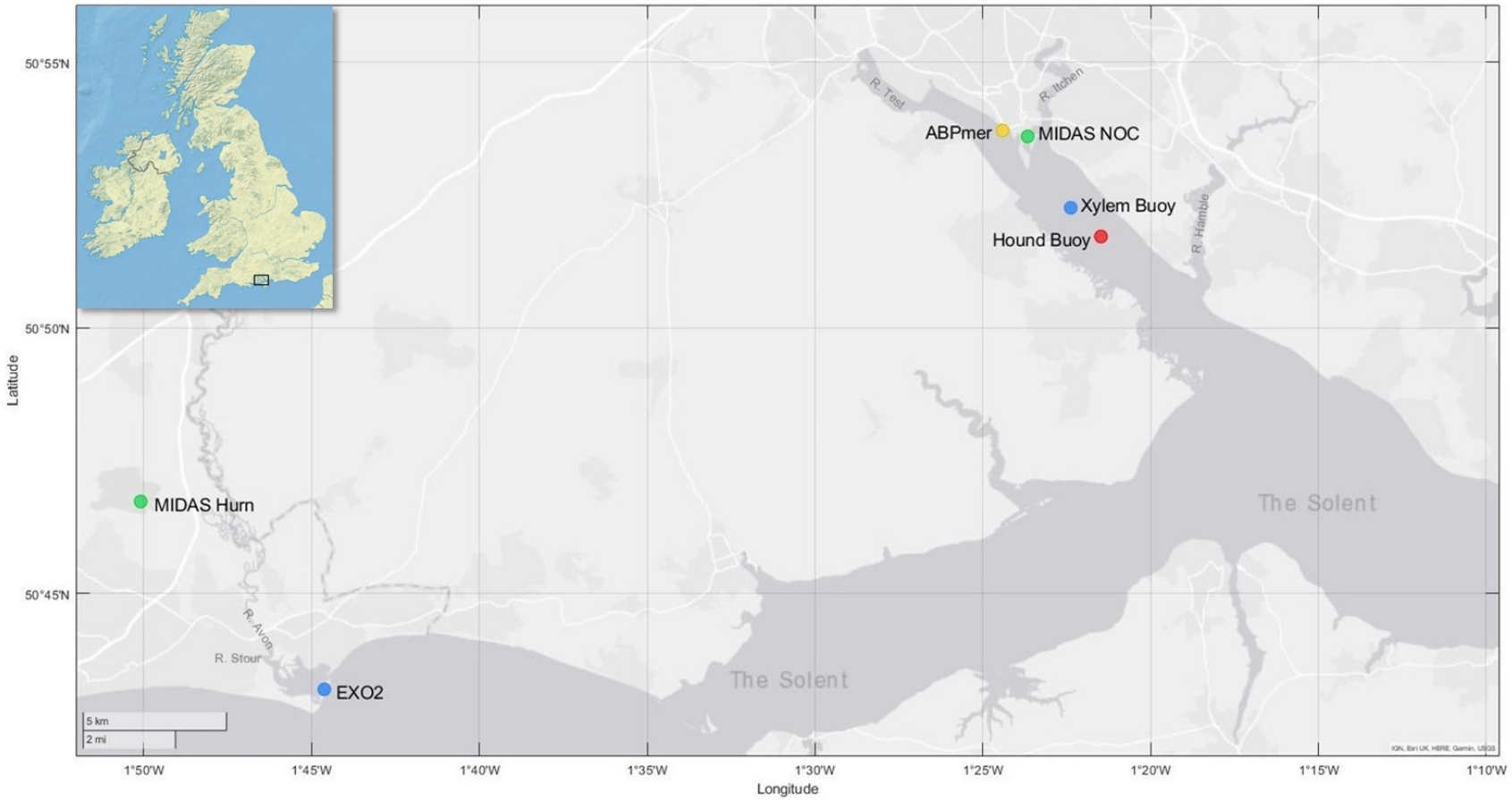

Fig. 2.1 Southampton Water and Christchurch Harbour, and their major tributaries, in the south coast of the UK (inset). Multiparametric probe deployment sites in each estuary are indicated in blue ●, meteorological stations from the Met Office's MIDAS are indicated in green ●, Environment Agency sample site is indicated in red ● and ABP Marine Environmental Research tide gauge location is indicated in yellow ●.

Water quality data was collected at high frequency intervals of 10 minutes from May 2014 to December 2018, for a total of 180,533 records; with the only exception of the period between 30/07/14 and 23/09/2014, when the measurements were taken every 2 hours (Table 2.1). For this study, hourly averages were calculated for all years, when possible.

A few major gaps in data collection were observed; (i) in 2014 a 5-day gap from 25/06/14 to 30/06/14 for all parameters and (ii) a month-gap (06/07/14 – 07/0814) for temperature and DO concentration. (iii) During 2015, from 19/05/15 to 02/09/15 data was not collected. (iv) The 2016 time series lacks 83 days, with data collection started on 18/02/16 and finishes in 26/11/2016. (v) In 2017, there is a 39-day gap between 03/02/17 and 15/03/17, as well as a 10-day late-start and a 7-day early ending. Lastly, (vi) 2018 time series started in 29/03/18 and ended in 13/12/18, missing a total of 105 days.

Table 2.1. Catalog of water quality and meteorological data used to compile time series for Southampton Water estuary and Christchurch Harbour.

	Southampton Water			Christchurch Harbour		
	# records	Date start	Years	# records	Date start	Years
Multiparametric probe	178,677	12/05/14	6.6	180,533	12/05/14	4.6
Met Office MIDAS	59,146	01/01/14	6.8	43,612	01/01/14	5
Environment Agency	74	04/02/14	6.8	--	--	--
ABPmer	3,679,200	01/01/14	7	--	--	--
Probe	--	--	--	8	27/05/14	0.3
Discrete sampling	27[ab]	16/07/18	2.4	16[b]	27/05/14	0.6

[a] Dissolved oxygen water samples.

[b] Chlorophyll '*a*' water samples.

Complete time series data was filtered manually, discarding unreliable values and outliers, plus negative or occasional inconsistent high magnitude values (typically caused by biofouling).

2.2.2 Optode-based oxygen sensor validation: Southampton

Semi-continuous oxygen measurements were determined from the EXO2 sonde deployed optode. Optodes have proven in recent years to be very useful in describing biogeochemical processes as they represent multiple advantages, including no oxygen consumption and long-term stability (Bittig & Körtzinger, 2015). To ensure the optode is recording high-quality dissolved oxygen data, comparison against more precise and accurate DO measurements from discrete water samples is recommended (Uchida *et al.*, 2008) as well as a dependable rectification of DO calculations (Haskell *et al*., 2019). The optode was protected from fouling with a copper mesh pad as suggested by the manufacturer and the following correction steps were made prior to using the oxygen time-series data to calculate NCP rates: (i) Some missing salinity measurements from the time series were estimated since the optode DO sensor installed on the EXO2 sonde measures oxygen saturation and then uses salinity and temperature data to calculate DO concentration. Across the whole time series, the salinity sensor fitted on the sonde showed some periods of mainly negative drifting, and a more reliable sensor could not be installed until late November 2019. Understanding a drift as a variation of the sensor response across a specific time frame and under identical conditions (Ando et al., 2005). Thus, Environment Agency discrete samples of salinity were compared against existing and reliable salinity data from EXO2 sonde though the least squares method and the equation for the best fitted curve was used to substitute missing salinity data (Appendix B). This process

was done for every year included in the time series, except 2018 where salinity values did not show evidence of any drift. (ii) Recalculating DO concentration values from polynomial temperature and salinity dependant equations provided by the sonde manufacturer (Xylem). (iii) Lastly, discrete oxygen measurements from Winkler titrations (June 2018 to November 2020) were used to formulate a standard linear regression model (Fig. 2.2) to correct optode derived DO concentration values.

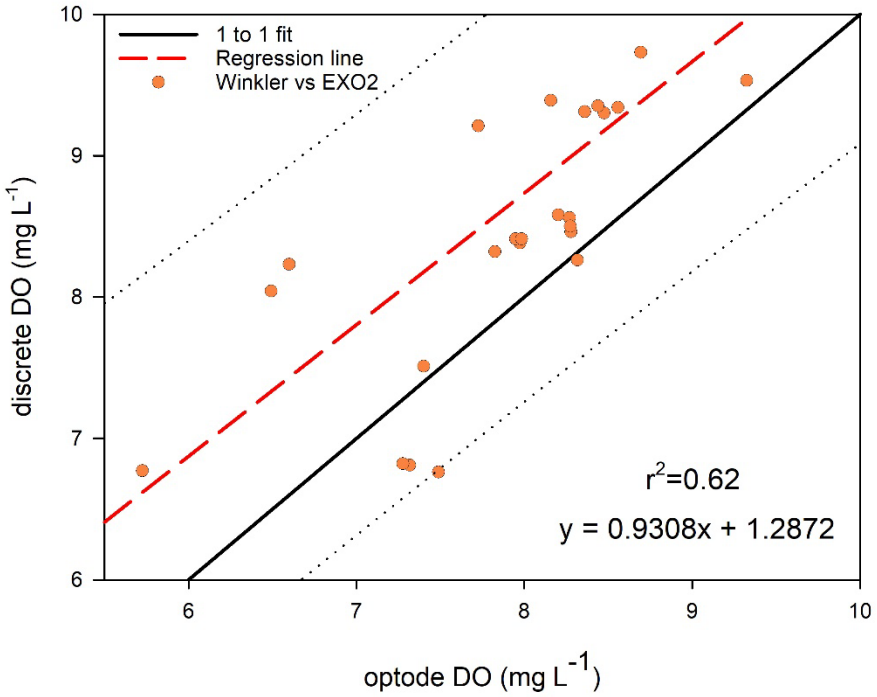

Fig. 2.2 Linear regression – (r^2 0.62) and prediction intervals (…) from the comparison between dissolved oxygen from the Data Buoy system against the Winkler titration analysis ● (2018-2020). 1 to 1 fit line is defined as –.

2.3 Field sampling

2.3.1 Dissolved oxygen by Winkler titration

At the study site, sets of three replicate glass bottles (~60ml), on 27 different dates between June 2018 and November 2020, were filled with water using two methods: (i) from the pump system on RV Callista and (ii) deploying a 5 L Niskin Bottle just below the surface from a RIB close to the data buoy.

A continuous flow was kept in order to fill bottles carefully to minimise agitation and bubble formation. Immediately after, 0.5 ml of manganese chloride solution was added to each glass bottle, followed by 0.5 ml of alkali-iodide solution. Bottles were closed using the bottle stopper, inverted gently around 30 times to ensure chemical mixing and stored underwater to prevent evaporation while awaiting titration and analysis.

The chemical determination of oxygen concentrations in seawater is based on the iodometric titration method first proposed by Winkler (1888) and later modified by Parsons *et al*. (1984). Titrations for this study were performed using a photometric end-point detector as specified in Carrit & Carpenter (1966).

Determination of dissolved oxygen concentration in water is based on a multi-step oxidation described in Hansen (1999):

Manganese chloride is added to a known volume of water, and Manganese (II) is precipitated as hydroxide (Eq. 1),

$$Mn^{2+} + 2OH^{1-} \rightarrow Mn(OH)_2 \quad (1)$$

and oxidized to Manganese (III) hydroxide in a heterogeneous reaction (Eq. 2).

$$2Mn(OH)_2 + \frac{1}{2}O_2 + H_2O \rightarrow 2Mn(OH)_3 \quad (2)$$

Next, the iodide ions added are oxidized to iodine by the Manganese (III) ions, which are reduced to manganese (II) ions, as shown in Eq. 3.

$$2Mn(OH)_3 + 6H^{1+} + 2I^{1-} \rightarrow 2Mn^{2+} + I_2 + 6H_2O \quad (3)$$

In the final step, the iodine is titrated with a thiosulphate solution (Eq. 4).

$$I_3{}^{1-} + 2S_2O_3{}^{2-} \rightarrow 3I^{1-} + S_4O_6{}^{2-} \quad (4)$$

The thiosulphate solution is not stable and, therefore, must be standardised prior to any titration. Before every set of samples was analysed, a standardisation was carried out using the photometric end-point detector and a standard potassium iodate solution to determine the precise concentration of thiosulphate in the titrating solution. An average of six standards was taken to determinate thiosulphate normality as follows:

$$N_1 = \frac{N_2 V_2}{V_1} \quad (5)$$

where N_2 is the iodate normality (0.01 N), V_2 is the iodate volume added (5 ml) and V_1 is the thiosulphate volume added (titre value/50 in ml).

2.3.2 Dissolved inorganic carbon and total alkalinity

Discrete water samples for dissolved inorganic carbon (DIC) and total alkalinity (T_{alk}) were taken using the pumping system connected to the Anderaa SOOguard Ferry Box on the RV Callista or by deploying a 5L Niskin bottle from a RIB. From March to November 2019, samples were taken biweekly (24) and every week from February to November 2020 (30). During 2020 a 3-month gap in sample collection occurred, from mid-March to Mid-June, due to restrictions during the COVID-19 pandemic. In addition, during the 2020 sampling, measurements were performed in the laboratory using a Delta 350 pH meter (Mettler-Toledo, Switzerland) for pH and temperature, and a TetraCon® 325 S (WTW, Germany) four-electrode conductivity cells electrode, for salinity and temperature. Training and analysis of 2020 DIC and T_{Alk} samples were performed by Dr C. Dumousseaud.

250 ml borosilicate glass bottles were filled with water from a continuous flow from a 5 L Niskin Bottle, allowing a head space of 1% for water expansion, and

immediately poisoned with 5 µl of saturated solution of mercuric chloride to stop any biological activity. Samples were stored for later analysis in the Carbon Research Lab using the VINDTA 3C (Marianda, Germany). This equipment combines the proven 'Versatile INstrument for the Determination of Total inorganic carbon and titration Alkalinity' (VINDTA) alkalinity titration concept with a simplified extraction unit for coulometric DIC measurement.

Following Dumousseaud *et al.* (2010), DIC samples were analysed using a coulometric titration and T_{Alk} was determined using a closed-cell titration equipped with a pH half-cell electrode and an Ag/AgCl reference electrode. On the day of analysis, all samples were kept at 25°C with temperature regulation using a water-bath. Certified Reference Materials (from A.G. Dickson, Scripps Institution of Oceanography) were analysed as standards (n≥3) to calibrate the instrument at the beginning and end of each day of analysis. The precision of measurements on these CRMs was within ±3.1 µmol kg^{-1} for DIC and ±1.6 µmol kg^{-1} for T_{Alk}.

2.4 External data acquisition

2.4.1 Met Office's MIDAS database

The MIDAS database is a collection of meteorological observations made available (granting access by request) by the Met Office and includes data from meteorological stations around the UK from around the late 19th Century, and stored in the Met Office's 'MIDAS Open' database (Met Office, 2020).

Southampton Water

The met station at the Southampton Oceanography Centre (50.892° N, -1.394° W) was identified as the closest (2.8km) MIDAS location to the Southampton

Water Data Buoy system (Fig. 2.1). Hourly barometric pressure and wind speed measurements were downloaded and added to the meteorological time series of the Southampton Water site (Table 2.1). Additionally, hourly solar radiation observations were acquired from the National Oceanography Centre weather data archive (https://oesnet.noc.soton.ac.uk/meteorological-station).

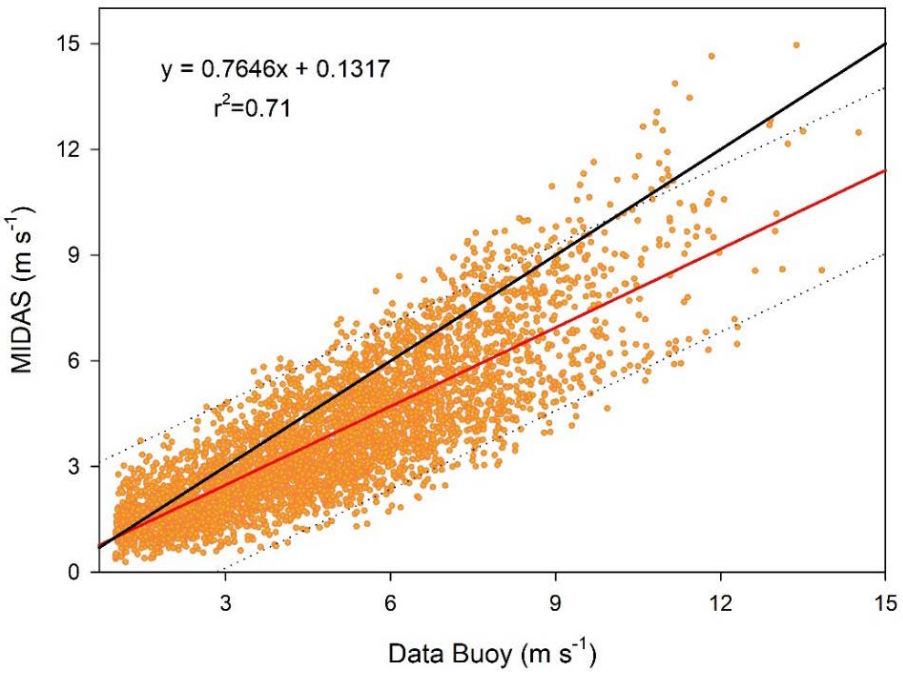

Fig 2.3 Linear regression – (r^2 0.71), prediction intervals (…) and 1 to 1 fit – between hourly wind measurements from met sensor fitted on the Data Buoy system and data from the Southampton Oceanography Centre Met Office MIDAS station ●, from March to September 2018.

The Data Buoy system was fitted with a 200WX WeatherStation® (AIRMAR, France) sensor during the deployment in March 2018, but this stopped recording on 12/09/18 due to damage from a boat collision. Overlapping wind speed data from both the data buoy met sensor and the met sensors on the Oceanography Centre building were compared to determine if the difference in elevation (approximately 26 meters above sea level) of the MIDAS station could present a significant difference. After a liner regression analysis (Fig. 2.3), it was considered that data from the Met Office station could be used to represent conditions at

Southampton Water data buoy site, however, it is apparent a wider spread between data sets at higher wind speeds producing an underestimation of wind values above ~10 m s^{-1}.

Christchurch

The nearest MIDAS station (9.8km) to the Christchurch Harbour pontoon location (Fig. 2.1) is the one identified as Hurn and is situated at the Bournemouth International Airport (50.779° N, -1.835° W). Hourly barometric pressure, wind speed and solar radiation measurements were obtained and added to the meteorological time series of the Christchurch Harbour site (Table 2.1).

2.4.2 Environment Agency Water Quality Archive

The Environment Agency Water Quality Archive (https://environment.data.gov.uk/water-quality/view/download/new) is an open access collection of measurements taken regularly at sampling points around England, which includes coastal and estuarine waters.

A set of water quality measurements was acquired from the Hound navigation buoy sampling site (50.861° N, -1.358° W), selected to compare with the Southampton Water data buoy location measurements due to its close proximity (Fig. 2.1). Environment Agency data (Table 2.1) included ~ monthly surface records of DO (mg L^{-1} and % sat.), temperature (°C), salinity (psu), chlorophyll '*a*' (µg L^{-1}), and turbidity (FTU).

2.4.3 Associated British Ports Marine Environmental Research

The Associated British Ports Marine Environmental Research (ABPMer) provided minute-interval sea surface elevation data measured with a Tidalite tide gauge located at Dock Head, Eastern Docks Southampton (Fig. 2.1). Daily minimum

and maximum values were extracted from the raw time series (Table 2.1), and the difference was plotted to indicate changes in the daily tidal range.

2.4.4 S-3 EuroHAB project

This 4-year EU funded project is working on improving the monitoring and prediction of harmful algal blooms (HABs) using satellite images in the English Channel. As part of the project, the University of Southampton is combining past knowledge from the scientific literature with analysis of multiple datasets collected throughout the Channel to discover the factors that drive bloom development in this region. One of their sample sites is situated next to the Data Buoy System in Southampton Water estuary. Chlorophyll 'a' and nutrients sampling and analysis were performed by Dr A. Panton.

Chlorophyll 'a'

Discrete water samples were taken at ~1m under surface water using either the pumping system connected to the Anderaa SOOguard FerryBox on the RV Callista or using a Niskin bottle deployed from a RIB. Samples to determine phytoplankton biomass (chlorophyll 'a') were taken biweekly during spring-summer from 2018 to 2020, then three replicates of 50 mL were filtered through a Whatman GF/F filter within an hour of collection. Filters were frozen before analysis according to Strickland & Parsons (1972) methodology. Pigmemts were extracted from filters with 90% acetone before their analysis on a precalibrated fluorometer TD-700 (Turner Designs, USA).

Nutrients

Surface water (~1m) was collected biweekly, during spring-summer from 2018 to 2020, into acid-cleaned HDPE bottles then frozen prior to later inorganic nutrient

analysis as described in Panton *et al*. (2020). Samples were collected through the pumping system connected to the Anderaa SOOguard FerryBox on the RV Callista or using a 5 Niskin bottle deployed from a RIB. A QuAAtro segmented flow auto-analyser (Seal Analytical, UK) was used to determinate concentration of silicate SiO_2, phosphate PO_4 and nitrate NO_3.

2.4.5 River inflow data

Average daily river flow data was accessed from gauging stations on the River Avon, located at Knapp Mill, and on the river Test at Broadlands obtained from National River Flow Archive; downloaded from https://nrfa.ceh.ac.uk/data.

2.5 Mean water column irradiance

Hourly solar energy (KJ m^{-2} h^{-1}) data from the Met Office's MIDAS database was computed into daily solar energy values and converted to Wh m^{-2} d^{-1} using the equation shown in Eq. (1).

$$\frac{KJ}{m^2} = \frac{0.27W}{m^2} \quad (1)$$

In order to calculate the proportion of light that can be utilised by plants for photosynthesis reaching the surface, also known as photosynthetic active radiation (PAR), the constant proposed by Peperzak (1993) was used as in Eq. (2).

$$I_0 = 0.45\, SE_d \quad (2)$$

with I_0 as the daily surface irradiance and SE_d as the sum for daily solar energy, both terms in (Wh m^{-2} d^{-1}).

PAR within the water column varies according to changes in surface incident solar irradiance, turbidity, and depth (Cloern *et al*., 2014). Therefore, the mean water column irradiance (I_m) was calculated (Eq. 3) following Riley (1967):

$$I_m = I_0 \frac{(1-e^{-k_{PAR}h})}{k_{PAR}h} \quad (3)$$

where k_{PAR} is the diffuse attenuation coefficient (m^{-1}) and h is the mixed layer depth (10m for Southampton and 1.75m for Christchurch). The diffuse attenuation coefficient was estimated from the slope of a linear regression of turbidity against k_{PAR} data previously generated for Southampton Water estuary by Iriarte & Purdie (2004), with k_{PAR} ranging between 0.2 and 2.0 m^{-1}.

2.6 Open water diel oxygen method

2.6.1 Biological Oxygen Fluxes

The open water diel oxygen method was applied to calculate rates of NCP from oxygen probe data obtained from both estuarine systems. This was achieved by following the quantification of primary production described by Needoba *et al*. (2012) by calculating oxygen mass-balance in the mixed layer. The hourly biological oxygen production (BOP) calculation incorporated equations used by (Hull *et al*., 2016) and (Murrell *et al*., 2018).

An essential assumption of this model is that all measurements come from a well-mixed water column; therefore, the water mass recorded presents the same metabolic history (Caffrey *et al*., 2014). The average water depth at the Southampton Water Data Buoy is 10 m; therefore, vertical profiles of temperature, salinity and dissolved oxygen were made in 2018 and 2019, with a different EXO2 sonde (Fig. 2.4) to show that the water column was well mixed at that position in the estuary. Dates of vertical profiles include months when surface water usually

presents higher temperatures since warming of the upper water layer could induce stratification (Gomoiu *et al*., 2014), and the typical seasons (spring and summer) characterizing bloom dynamics of coastal temperate systems (Martellucci *et al*., 2021).

A second assumption is that other oxygen-consuming processes in the water column, such as nitrification, are insignificant compared to phytoplankton respiration (Hull *et al*., 2016); particularly in high light transparency and low nutrients ecosystems (Murrell *et al*., 2018).

The model calculates the change in oxygen concentration in a certain period of time, given the physical parameters measured (Eq. 4).

$$h\frac{\partial C}{\partial t} = E + FO_2 + BOP \quad (4)$$

Where h is the water depth, $\frac{\partial C}{\partial t}$ is the oxygen concentration change through time, E is the entrainment of oxygen through changes in the mixed layer depth, F_{O2} is the gas exchange from diffusive and bubble processes (Eq. 5), and BOP is the biological oxygen production (Eq. 8).

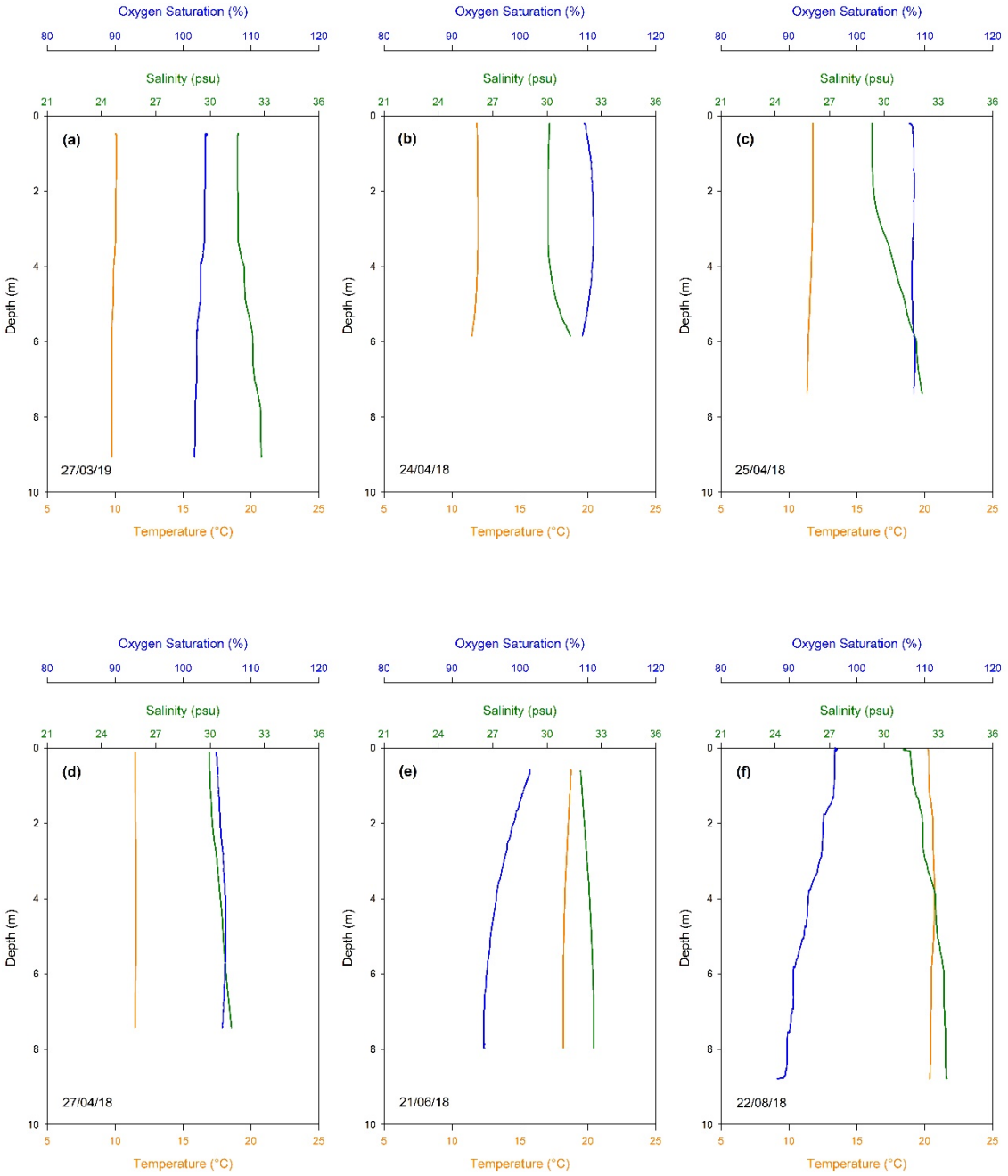

Fig. 2.4 Vertical profiles of oxygen saturation (—), temperature (—) and salinity (—) at the Data Buoy site during spring (a, b, c & d) and summer (e & f).

Given the assumption that the water column in the estuary is fully mixed at the position of the Data Buoy, the term E, which represents changes in mixed-layer depth through time, can be neglected. Similarly, the entrainment term $\frac{\partial h}{\partial t}$ is set to zero in Eq. (5) and (9).

$$F_{O2} = \frac{K_w}{h} C^* (1 + B) \frac{P_{slp}}{P_{atm}} + \frac{1}{h} \frac{\partial h}{\partial t} C \quad (5)$$

The diffusive exchange of gases across the air– sea interface F_{O2} (Eq. 5) was calculated as a function of gas transfer velocity K_w (Eq. 6) and diffusion through bubbles B (Eq. 7). It is worth noting, values for k_w needed to be converted from cm h^{-1} to m s^{-1} before being used in Eq. (5). P_{atm} corresponds to an atmospheric pressure standard value of 101,325 Pa, P_{slp} is the atmospheric air pressure at sea level, C^* is the calculated oxygen concentration in equilibrium with the atmosphere as a function of temperature and salinity (Feistel, 2008) and C is the oxygen concentration in the surface mixed layer.

$$K_w = 0.251 U^2 \left(\frac{Sch_{O_2}}{660}\right)^{-0.5} \quad (6)$$

The coefficient of gas transfer velocity K_w calculated in Eq. (6) is the parameterisation proposed by Wanninkhof (2014), and is a function of salinity and temperature through the relation between the Schmidt number Sch_{O_2} for oxygen and the normalised Schmidt number for CO_2 at 20°C and salinity of 35 (constant value of 660 in Eq. 6). U corresponds to wind speed measured at 10m above sea level but as stated above can be considered the same as at sea level at the position of the Data Buoy.

$$B = 0.01\left(\frac{U}{U_i}\right)^2 \quad (7)$$

Bubbles can induce gas exchange B, therefore its incorporation into the gas transfer calculation (Eq. 5). This was determined using a parametrisation according to measured wind speed U and a standardised wind speed value U_i for a smooth boundary regime (Wanninkhof, 2014).

The biological oxygen production (BOP) is expressed as a mass transfer per surface area and time, in mmol O_2 m^{-2} h^{-1} (Needoba *et al*., 2012). In Eq. (8) C_0 is the oxygen concentration at $t = 0$ and C_1 oxygen concentration at the time step (for the present study, 1 hour), and it is analytically solved by using the air-sea diffusion flux calculation F_{O2} and a transfer velocity correction t, caused by wind-induced turbulence in the water column (Eq. 9).

$$BOP = th\left(\frac{C_1 - C_0}{1 - e^{-rt}} + C_0\right) - F_{O2}h \quad (8)$$

$$t = \frac{k_w}{h} + \frac{1}{h}\frac{\partial h}{\partial t} \quad (9)$$

Then, BOP data were averaged separately during the day and night periods to compute hourly rates of apparent primary production (P_a) and night-time respiration (R_n). Light data collected from the MIDAS Met station was used to integrate complete daily photoperiods and dark periods. Each diel cycle was formed by a light period plus a dark period, starting with the photoperiod.

2.6.2 Ecosystem respiration and productivity

The model assumes respiration rates to be constant during a diel cycle; therefore, respiration was extrapolated to 24 hours to calculate daily ecosystem respiration ER (Eq. 10) for the mixed water column (h).

$$ER = R_n(24)(h) \tag{10}$$

Daily gross primary production GPP was determinate (Eq. 11) as a function of apparent primary production (P_a) and night-time respiration (R_n).

$$GPP = (P_a + R_n)(daylight\ hours)(h) \tag{11}$$

As the final step, daily net community production NCP was calculated (Eq. 12) in mmol O_2 m^{-2} d^{-1} according to Murrell *et al*. (2018).

$$NCP = GPP - ER \tag{12}$$

Positive values of NCP (net autotrophy) indicate organic carbon is being produced over the local respiration demand. On the contrary, negative values (net heterotrophy) suggest the ecosystem requires additional input of organic carbon to be sustained.

2.7 Air-sea CO_2 flux model

2.7.1 CO_2^{calc}

The program COSYS was initially developed by Lewis & Wallace (1998) to perform calculations of parameters involved in the carbon dioxide (CO_2) system in seawater and freshwater, and it was later modified for its use in Microsoft Excel by Pierrot *et al*. (2006). $CO2^{calc}$ is the latest update to the

CO2SYS program application, and it was created by Robbins *et al*. (2010), consisting of a user-friendly application compatible with most operating systems (OS) with an improved graphical user interface for data entry and results (Fig. 2.5). CO_2^{calc} offers several improvements, including the possibility of calculating air-sea CO_2 fluxes for surface waters and the ability to process multiple files in a batch-processing mode.

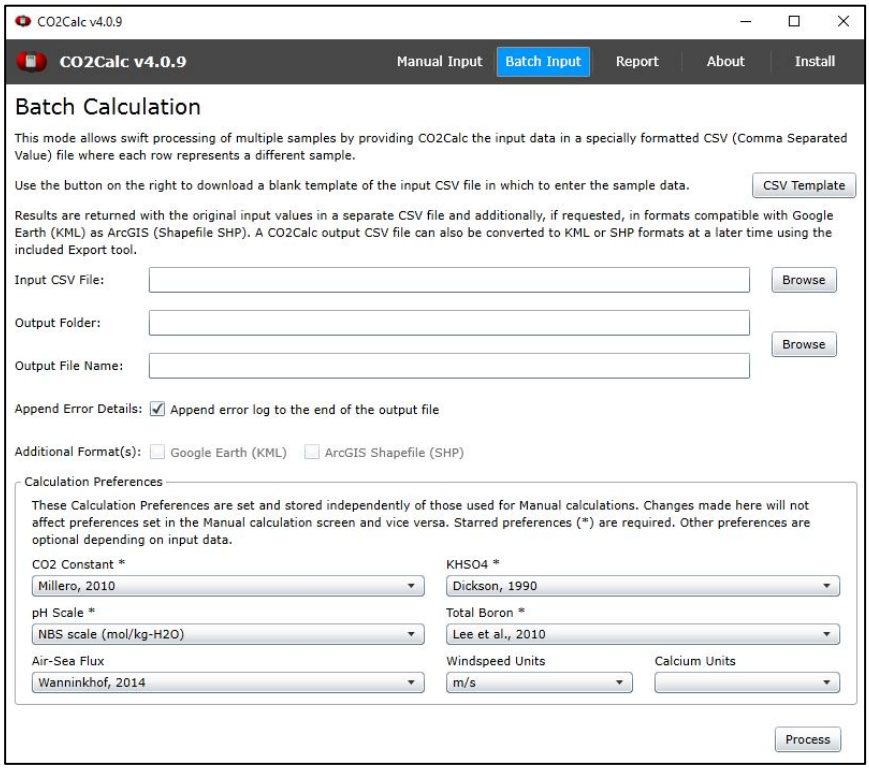

Fig. 2.5 CO_2^{calc} (version 4.0.9) software batch input data interface.

The CO_2 system in seawater is characterized by five measurable parameters: (i) total alkalinity T_{alk}, (ii) total carbon dioxide TCO_2, as the sum of the dissolved CO_2, the carbonate and bicarbonate; (iii) pH, and (iv) partial pressure of carbon dioxide ρCO_2 or (iv) fugacity of carbon dioxide fCO_2. The basis of the model is that by providing it with two of the five measurable CO_2 system parameters, along with temperature, pressure and salinity, CO_2^{calc} then calculates the concentration of the remaining parameters (Robbins *et al*., 2010). In addition,

it also calculates the Revelle factor (homogeneous buffer) and the saturation states (Ω) for aragonite and calcite. It also offers the option to include nutrient data (silicate and phosphate) into the calculations and provides air-sea CO_2 flux, if wind speed and ρCO_2 of air are provided.

In order to calculate CO_2 parameters, a set of constants and preferences need to be selected among different options, as well as scales for certain parameters:

- The solubility of CO_2 in seawater K_0 and the conversion between ρCO_2 and fCO_2 are from Weiss (1974). The program sets them as default.
- Two dissociation constants for carbonic acid (K_1 and K_2) are used in the calculations, the recently added constants for estuarine waters determined by Millero (2010), were selected.
- There are two options for the dissociation constants of potassium sulphate (K_{SO4}), selecting the formulations described by Dickson (1990) for sea water.
- The Lee *et al*. (2010) constant for total Boron was selected since it was developed in accordance to the carbonic acid constants selected (Millero, 2010).
- Among the pH scales, NBS was selected since it is the same as that used by the pH probes collecting data to produce the time series. All constants are converted to the selected pH scale before calculations are made.
- For the calculation of air-sea CO_2 fluxes, the gas transfer velocity coefficient K_w parametrisation proposed by Wanninkhof (2014) was selected in order to correspond to the air-sea O_2 fluxes calculations described in section 2.6.1.

2.7.2 Carbonate system calculations

Total alkalinity extrapolation

In order to estimate CO_2 fluxes for the entire time series available between 2019 and 2020 in Southampton Water, T_{alk} and DIC were analysed as functions of sea surface salinity, since it has been shown that variability of these parameters, expressly T_{alk}, in the surface ocean is controlled mainly by freshwater mass movements (Jeffrey *et al*., 2018; Lee *et al*., 2006). Once these associations were analysed (Fig. 2.6), it was decided to only use T_{alk} equation relating it to salinity since it presented a better fit than DIC and, as mentioned previously, it has been more frequently described in literature. The result of the equation the linear regression between salinity and T_{alk} was then used to extrapolate T_{alk} data from salinity data along the1-hour step time series from July 2019 to December 2020.

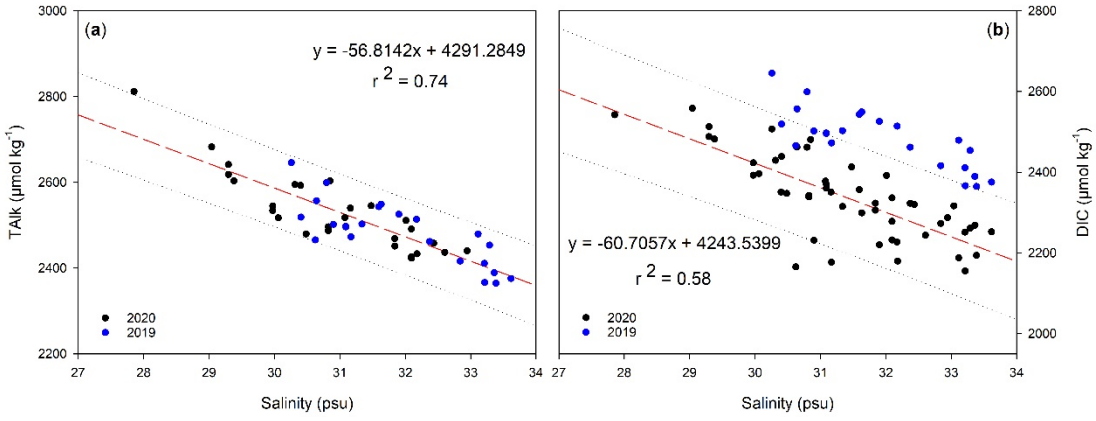

Fig. 2.6 Linear regressions – and prediction intervals (…) for salinity from Data Buoy and (a) total alkalinity (r^2 0.74) and (b) dissolved inorganic carbon (r^2 0.58). Data for 2019 is shown in blue circles ● and for 2020 in black circles ●.

pH data calibration

Three independent pH data sets were created: (i) pH records from the EXO2 probe (Data Buoy) deployed in the estuary, (ii) pH measurements made with

a calibrated Delta 350 pH meter (Mettler-Toledo, Switzerland) in the laboratory for every DIC and T_{alk} sample, and (iii) pH data generated with CO_2^{calc} application, from DIC and T_{alk} data.

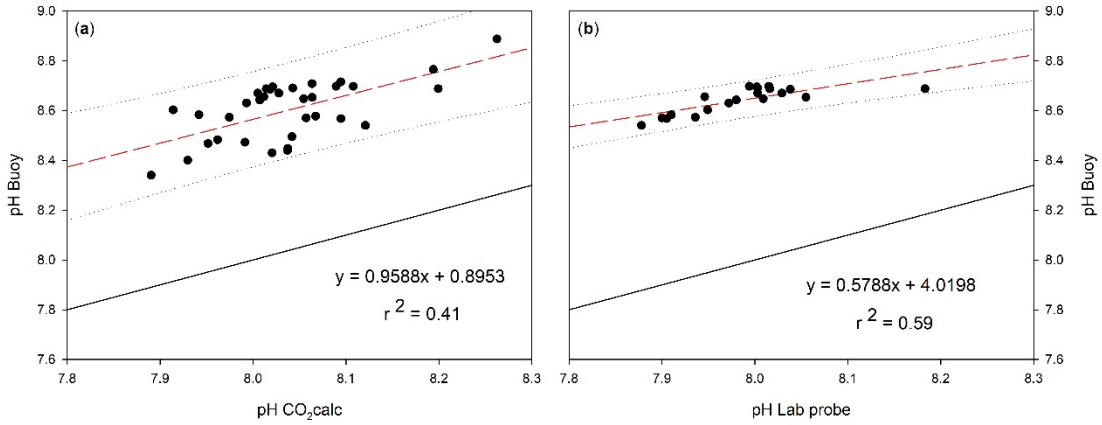

Fig. 2.7 Linear regressions –, prediction intervals (…) and 1 to 1 fit – for pH from Data Buoy against (a) pH derived from DIC and Talk using the CO_2^{calc} application (r^2 0.41) and (b) pH measured in laboratory (r^2 0.59). Individual data is shown in black circles ●.

pH from the Data buoy was recorded from July 2019 to December 2020, however, since measurements for 2020 showed a positive offset, a calibration was established. pH data calculated with the CO_2^{calc} software was taken as the most accurate, therefore, pH from the Data Buoy was standardised using equation $y = 0.9588x + 0.8953$ (Fig. 2.7a).

pH data from the CO_2^{calc} software and pH standardised data were analysed using a one-way ANOVA in which assumptions of normality and homogeneity of variances were met, and a *p* value of <0.05 was considered significant. Data sets presented no significant (p=0.116) difference between each other (Fig. 2.8); therefore, pH standardised data were selected to be used in carbonate system parameters.

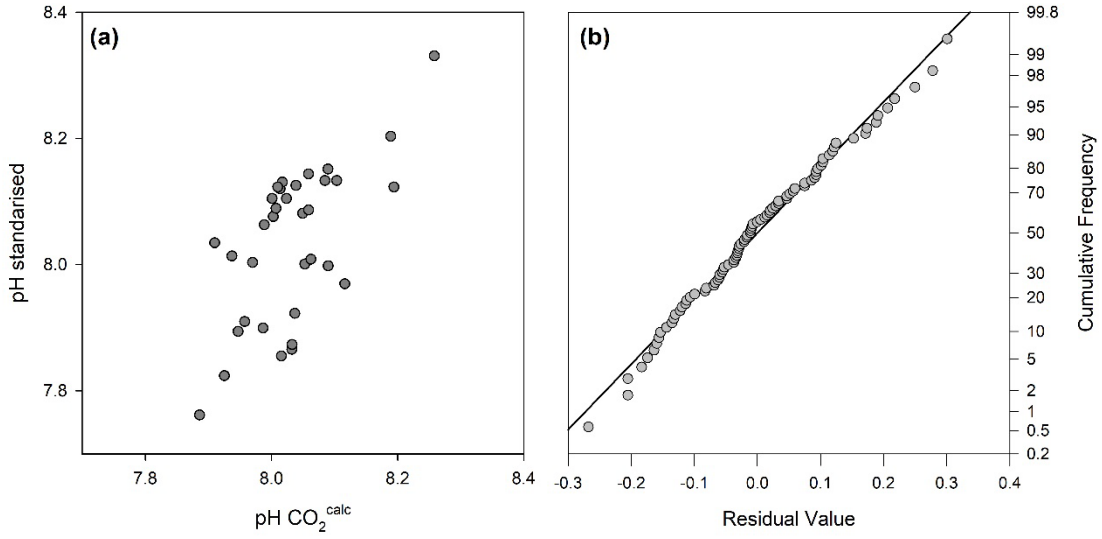

Fig. 2.8 Scatter plot (a) and normal probability plot (b) of pH from CO_2^{calc} application and pH from the Data Buoy standardised with equation $y = 0.9588x + 0.8953$.

CO_2 fluxes

Once T_{alk} and pH data sets were compiled, they were introduced into the CO_2^{calc} application to formulate seawater CO_2 partial pressure ρCO_{2sw} for the 2019 - 2020 hourly time series.

Subsequently, hourly air CO_2 partial pressure ρCO_{2air} data was downloaded from the NOAA archive (Dlugokencky *et al.*, 2021), collected by the Ryan Institute's Mace Head Atmospheric Research Station (Galway, Ireland) as part of the Earth System Research Laboratories (ESRL) Global Monitoring Laboratory. This parameter, in addition to ρCO_{2sw} and wind speed, were introduced to the CO_2^{calc} programme. Air-sea CO_2 fluxes F_{CO2} in mmol C m^{-2} d^{-1} were calculated following Eq. 13:

$$F_{CO2} = K_w \, K_0 \, \Delta\rho CO_2 \tag{13}$$

where $\Delta\rho CO_2$ (Eq. 14) is estimated as the difference between CO_2 partial pressure in seawater ρCO_{2sw} and the atmosphere ρCO_{2air}

$$\Delta\rho CO_2 = (\rho CO_{2sw} - \rho CO_{2air}) \quad (14)$$

Positive $\Delta\rho CO_2$ values indicate a net CO_2 flux from the sea to the atmosphere, in other words, the aquatic system is a source of CO_2. Conversely, $\Delta\rho CO_2$negative values indicate CO_2 flowing from the atmosphere to the sea, meaning the aquatic system behaves as a sink of CO_2.

2.8 Statistical analysis

All statistical analysis was performed using the statistical package in SigmaPlot version 13.0. The data matrix was organized with dates as rows and environmental conditions and productivity rates as columns. Chlorophyll '*a*' (Chl '*a*') blooms were considered when hourly average concentration values exhibited values >5 µg L^{-1} for Southampton Water and above >10 µg L^{-1} for Christchurch Harbour. The difference between thresholds is attributable to Christchurch Harbour receiving a higher input of nutrients (Panton *et al*., 2020), and being a semi-enclosed system presents reduced flushing abilities compared to Southampton, a system with open boundaries to the sea (Huggett *et al*., 2021a). This enhanced the process of eutrophication and, sometimes, increases the maximal concentrations of phytoplankton biomass an ecosystem can sustained (Adams *et al*., 2020; Turner *et al*., 2015).

Seasons were defined by astronomical dates for the Northern hemisphere: spring begins on the spring equinox, summer begins on the summer solstice, autumn begins on the fall equinox, and winter begins on the winter solstice.

2.8.1 Spearman's correlation

Time-series data were tested for normality using the Shapiro-Wilk Test. None of the environmental data nor productivity rates were normally distributed, despite different transforms being applied. The association between variables was investigated by the correlation analysis, a valuable tool, highly used in coastal marine assessments (Kitsiou & Karydis, 2011).

Therefore, the non-parametric Spearman's Rank-Order Correlation Coefficient ($p<0.05$) was used to (i) understand the relationship between chl 'a' blooms and various measured environmental parameters in the Southampton Water and Christchurch Harbour estuaries (Chapter 3); (ii) to identify predictors of calculated productivity rates and measured environmental variables throughout the study period in both estuaries (Chapter 4); and (iii) assess the relationship between carbonate system parameters, environmental conditions and primary production (Chapter 5).

2.8.2 Principal components analysis

The principal component analysis (PCA) allows reducing the dimensionality of large datasets without losing its variability by transforming original variables into a new and smaller set of uncorrelated variables (principal components PCs). The first PC accounts for as much variation as possible, and each subsequent component explains progressively less (Jollife & Cadima, 2016).

In the graphic representation of a PCA, the arrows represent the variables. When arrows are far from the centre and close to each other, they are positively correlated, meanwhile when they are symmetrically opposed, they are negatively correlated (Trombetta *et al*., 2019).

In Chapter 3, PCA was used to assess the influence of environmental conditions on the appearance of each major bloom event in both estuaries for each year of study. For Chapter 4, the analysis was used to evaluate the relationship between the seasonal distribution of productivity rates and environmental conditions and the relative contributions of GPP and ER to NCP. Finally, in Chapter 5, the PCA method was used to explain the seasonal variation of carbonate chemistry parameters, productivity rates and environmental factors affecting the response of FO_2 and FCO_2.

2.8.3 Ordinary least squares

Ordinary least squares (OLS) regression is a statistical method of analysis that estimates the relationship between one or more independent variables and a dependent variable; the method estimates the relationship by minimizing the sum of the squares in the difference between the observed and predicted values of the dependent variable configured as a straight line (Pohlmann & Leitner, 2003). In Chapter 4, OLS was used to examine the relationship between ER and GPP, allowing the estimation of the threshold values of GPP necessary to achieve metabolic balance (GPP:CR=1) in Southampton Water and Christchurch Harbour.

2.8.4 Analysis of Variance

In chapter 5, data were divided into seasons for 2019 and 2020. Subsequently, a two-factor analysis of variance (two-way ANOVA) was conducted to examine the response of the estuarine carbonate system to seasons and the difference between years studied. A significant ANOVA model with significant interaction between the factors (seasons and year) indicates that the change in the

dependent variable (the tested carbonate system parameter) in response to one factor depends on the level of the other factor (Kitsiou & Karydis, 2011). When differences were detected, the Holm–Šídák method was applied. This is an all-pairwise multiple comparison procedure that helps isolate the groups differing.

2.8.5 Regression analysis

In correlation analysis there is no distinction between dependent and independent variables but both are influenced by the same factor (Kitsiou & Karydis, 2011), therefore, a simple regression analysis was applied to describe pH and oxygen saturation dynamics influence by metabolic rates. In addition, a multiple regression was carried out to study the dependence of pH on two independent variables: oxygen saturation and salinity.

Chapter 3

Temporal variation of phytoplankton blooms associated with changes in environmental conditions in the Southampton Water and Christchurch Harbour estuaries

Abstract

Estuarine blooms are typically identified by measuring changes in phytoplankton biomass. In addition, seasonal and interannual patterns can be described by paring this data with hydrological and meteorological parameters.

The present chapter includes an analysis of the correlation between phytoplankton blooms and environmental conditions using high-frequency water quality data collected in the Southampton Water (2014 – 2020) and Christchurch Harbour estuaries (2014 – 2018). It was possible to associate the initiation of the spring bloom in both systems with abrupt rises in the water column light availability and temperature. Furthermore, the Christchurch Harbour estuary was characterised by spring and autumn blooms, while Southampton Water presented a pattern with blooms mainly in spring and summer. In addition, an analysis of the neap-spring tidal cycle in the Southampton Water estuary identified a correlation between initiation of blooms and the lower mixing conditions during neap tides.

3.1 Introduction

Phytoplankton in estuaries

Coastal systems are highly variable ecosystems where chemical, physical and biological processes interact at different spatial and temporal scales (Bucci et al., 2012; Martellucci et al., 2021). Within this area, estuaries act as connection vectors for land–sea interactions, mostly transferring substances and energy through riverine discharges into the marine environment (Ruiz et al., 2013).

Phytoplankton is the most important primary producer of coastal areas, acting as a key driver of biogeochemical cycles and playing a central role in determining water quality (Paerl & Justic, 2013). The concentration of chlorophyll 'a' (Chl '*a*'), a proxy of phytoplankton biomass, can provide a rapid assessment of the disturbance of nutrient enrichment (e.g. van der Struijk & Kroeze, 2010) affecting the first trophic levels and consequently the whole ecosystem (Bucci et al., 2012).

A phytoplankton bloom is defined as the fast growth and accumulation of phytoplankton, and are mainly controlled by light energy availability and nutrient supply (Shi et al., 2016). However, coastal phytoplankton communities typically show strong seasonal and spatial distributions (Paerl & Justic, 2013), since they are strongly related to the physical forcing (e.g., wind, rain, rivers, waves, and tides) that drives coastal current and runoff dynamics (Bucci *et al*., 2012; Lauria *et al*., 1999); making an understanding of estuarine phytoplankton dynamics extremely difficult to obtain (Martellucci et al., 2021).

This chapter aims to investigate the variability in the timing, magnitude and duration of the blooms and environmental conditions driving them in Southampton Water and Christchurch Harbour.

3.2 Southampton Water time series of environmental factors

The time series data collected from the Xylem sonde mounted under the data buoy based in the Southampton Water estuary includes 15-minute measurements from 2014 to 2020, except for 2017. In 2017, measurements were only available from the Data Buoy system for the first 3 months of the year; therefore, this data was not included in the results presented here. In addition, Environment Agency data from their ~ monthly surface sampling was included in plots to compare the magnitude and pattern of parameters.

Although analysis was done on a daily basis, for the present work in the Southampton Water estuary, a chlorophyll '*a*' (Chl '*a*') bloom was considered when hourly average concentration values exhibited values >5 µg L^{-1}. Despite previous work in the region (Arantza Iriarte & Purdie, 2004) stating 10 µg L^{-1} as the threshold for major phytoplankton blooms in the estuary, the findings of the current research demonstrated that 5 µg L^{-1} better reflected the production activity, since smaller blooms were being missed if a higher threshold value was set.

3.2.1 Year 2014

Measurements for 2014 from the Data Buoy system started in May and extended to December, with a noticeable gap for most of July.

The temperature presented a marked seasonal change (Fig. 3.1a), with values ranging from 8.7°C in December to 22.7°C in July. Surface salinity did not show much variation in the mid estuary (30.8 ± 1.0 psu), with a minimum of 28.0 psu and a maximum of 33.2 psu (Fig. 3.1b).

Oxygen concentration was higher during June, presenting the yearly maximum of 335.5 µmol O_2 L^{-1}, and showing the lowest values in the successive month (July), with the yearly minimum of 214.1 µmol O_2 L^{-1} (Fig. 3.1c). June also presented the highest daily oxygen variability in concentration and saturation, particularly towards the end of the month. The yearly average (102.2 ± 5.9 %) for oxygen in percentage showed a near overall balance in saturation. Oversaturation, conditions prevailed mostly from June to September, with a maximum value of 140.9% at the end of June, and the minimum of 92.5% in May, although, under saturation values were commonly observed from October to December (Fig. 3.1d).

Chl '*a*' concentration varied between 0.2 (December) and 18.2 µg L^{-1} (June) throughout the year (Fig. 3.1e), with intermittent increases from June to September, when five distinctive blooms were observed: (i) the first bloom lasting 5 days starting the 2nd week of June with an average of 4.4 µg L^{-1}, and in the same month, (ii) the peak with the highest average (9.3 µg L^{-1}) was observed for 10 days and probably lasted for a few more days but unfortunately the sonde stopped recording in the subsequent weeks. (iii) The longest bloom event (18 days) was detected in the last days of July and beginning of August, just as sonde recordings re-started, with an average of 6.5 µg L^{-1}. (iv) A small bloom can be seen in the early days of September, with an average of 3.4 µg L^{-1} during 3 days, and lastly into the 3rd week of September, (v) a 6-days long bloom with a mean value of 3.6 µg L^{-1}.

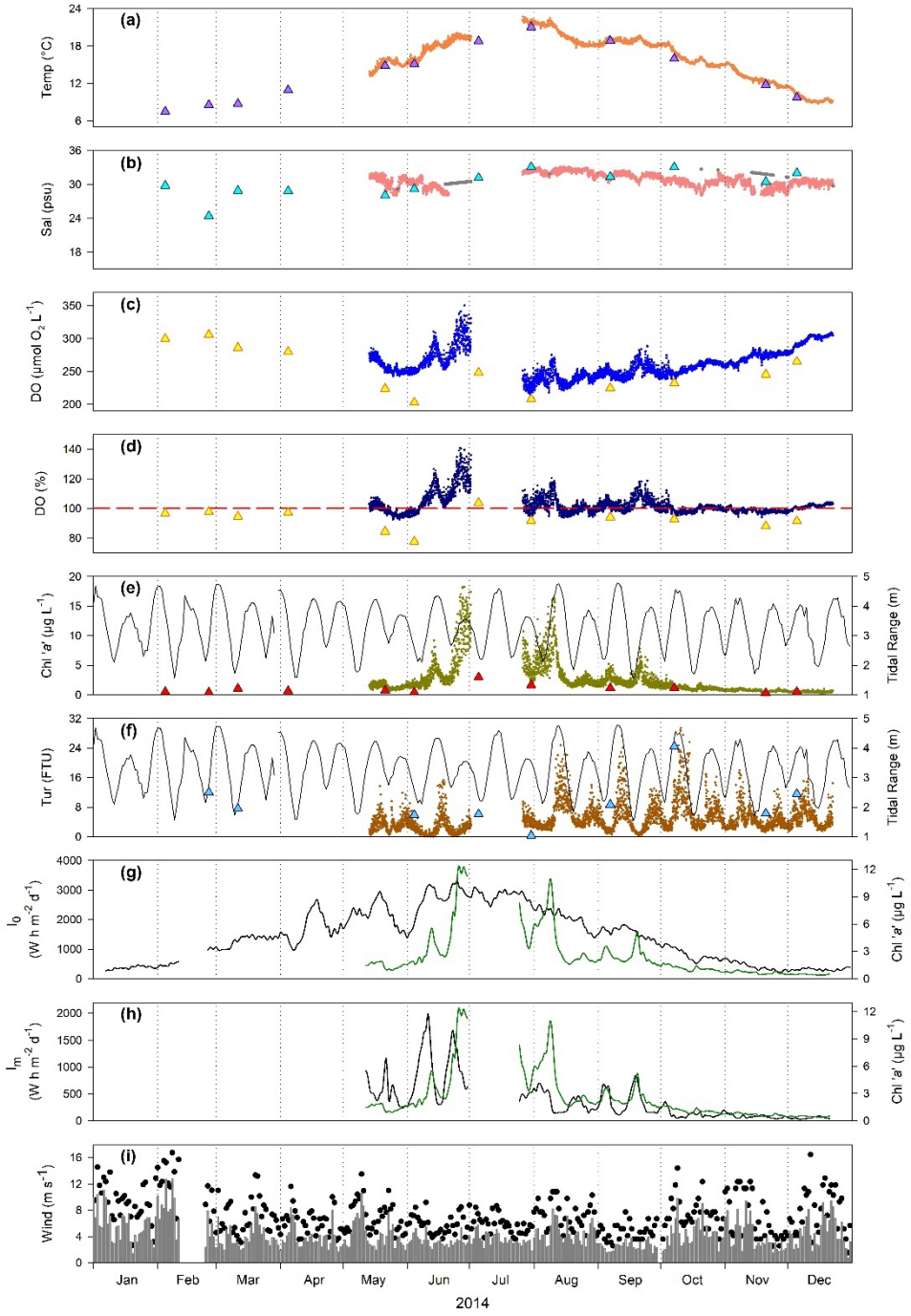

Fig 3.1 Time series of environmental conditions at the Data Buoy in Southampton Water in 2014. (a) Temperature, (b) salinity, (c) DO in concentration and (d) DO in percentage saturation, (e) chlorophyll '*a*' and (f) turbidity are presented as hourly values with dots ● of different colours. In (b), salinity values generated by a model are shown as grey dots ●. In (d), the red dashed line – – represents 100% of saturation. In (e) and (f), the daily tidal range is indicated as a black line —. Environmental agency sampling points are shown as triangles ▲ in different colours in (a) to (f). 7-day running mean of (g) surface irradiance I_0 and (h) mean water column irradiance I_m are presented as black lines —, with daily mean chlorophyll '*a*' concentration included as a green line —. (i) Wind speed is represented as daily mean in vertical bars ▮ and maximum daily values in black circles ●.

Turbidity presented higher monthly variability from August to October, showing a maximum value of 29.4 FTU in October while the year minimum was 0.1 FTU and was observed in June (Fig. 3.1f). A clear correspondence between peaks of turbidity and greater tidal range values was detected.

Surface PAR (I_0) varied on a seasonal pattern, with higher values towards the summer, reaching a maximum of 3312.9 Wh m^{-2} d^{-1} in June (Fig. 3.1g). Daily values started to noticeable increase in April and then decreased from September onwards.

Mean water column irradiance (I_m) presented its highest values from May to September, then rapidly started to decrease towards the end of the year. Two major peaks with values above 1500 Wh m^{-2} d^{-1} were observed during June and one above 1000 Wh m^{-2} d^{-1} in May (Fig. 3.1h). The maximum daily value for 2014 was observed during the 1st peak in June, reaching 1992.9 Wh m^{-2} d^{-1}.

The winter months (December, January and February) showed the highest daily wind speeds, with several daily averages above 10 m s^{-1}. However, a few peaks in wind speed almost reaching this value occurred in May, October and November (Fig. 3.1i). June, July, and September showed the lowest monthly average wind speeds below 3.6 m s^{-1}.

3.2.2 Year 2015

In 2015 there was a significant gap in data collection from the data buoy lasting from mid-October to early December and a smaller gap at the end of March.

The yearly range in water temperature varied from 5.0°C to 20.4°C showing a distinctive seasonal pattern with lowest values in February (Fig. 3.2a), and then

rising again in the middle of that month, towards the summer, with the highest monthly average in July (19.3°C).

Salinity average value for the year was 32.1 ± 1.1 psu, again displaying minimal seasonal variation with a minimum value of 27.9 psu in December and a maximum of 33.5 psu in August (Fig. 3.2b). Daily values from mid-June to October were estimated from Environment Agency data.

Dissolved oxygen did not show large peaks in concentration, with the exception of one detected in April when the maximum yearly value (357.4 µmol O_2 L^{-1}) was recorded (Fig. 3.2c). From June to August, daily variation was higher than during the rest of the year, with the minimum value of 209.3 µmol O_2 L^{-1} detected in August. A similar increased daily variation for the same period (June to August) was observed for oxygen saturation (Fig. 3.2d). Oversaturated conditions mostly prevailed from April to August, with the highest value of 131.2% during a peak in April. Outside this period, constant undersaturation values were observed, reaching a minimum in September (85.7%).

In 2015, no major peaks in chl '*a*' concentration were detected; however, five small blooms were identified between the period from April to September (Fig. 3.2e). During the rest of the year, daily chl '*a*' averages remained below 1.3 µg L^{-1}. (i) The first and most noticeable bloom occurred in April, with a 3.9 µg L^{-1} average during the 3 days it lasted. (ii) The longest bloom (6 days) was observed between the last days of June and first days of July, but due to it being more spread out, its average concentration was only 3.0 µg L^{-1}. In August, in the space of two weeks, two blooms were identified, (iii) the first one lasting only 2 days and presenting a concentration of 3.2 µg L^{-1}, and (iv) the second bloom observed for 3 days, which reached 4.0 µg L^{-1} making it the highest concentration of the year.

Lastly, (v) in the middle of September, a 2-day bloom could be observed with a mean value of 3.1 µg L^{-1}.

Turbidity showed greater daily values at the beginning of the year, reaching a maximum value of 22.9 FTU in March, just before the sonde stopped recording but with a similar pattern observed during April (Fig. 3.2f). From June to August, daily mean values remained mostly below 10 FTU and a minimum of 0.1 FTU was detected in July. Throughout the year again a clear pattern of turbidity values correlating with tidal range was observable, with higher turbidity during spring tides.

A big spike in I_0 was seen in the first days of April, where, in approximately a week, values increased from ~1400 to ~2500 Wh m^{-2} d^{-1}, to then drop again to ~1800 Wh m^{-2} d^{-1} after 20 days of sustained high I_0 values (Fig. 3.2g). Following this, a more gradual increase in values was observed reaching 3097.5 Wh m^{-2} d^{-1} in July. From mid-October onwards, daily values remained below 1000 Wh m^{-2} d^{-1} with a minimum of 162.9 Wh m^{-2} d^{-1} detected in December.

A high monthly variability could be observed for I_m from April to October, (correlating with neap tides and reduced turbidity values) with the highest values recorded in June (1727.7 Wh m^{-2} d^{-1}) and noticeable starting to decrease from the end of September. For the rest of the year, daily values remained below 500 Wh m^{-2} d^{-1} (Fig. 3.2h).

During January, November and December periods of high winds occurred, with recurrent daily maximums above 10 m s^{-1} and averages around 6.2 m s^{-1} (Fig. 3.2i). In contrast, from April, wind speeds started to decline until October where only two days were observed to exceed 10 m s^{-1} gusts and daily averages remained below 7 m s^{-1}.

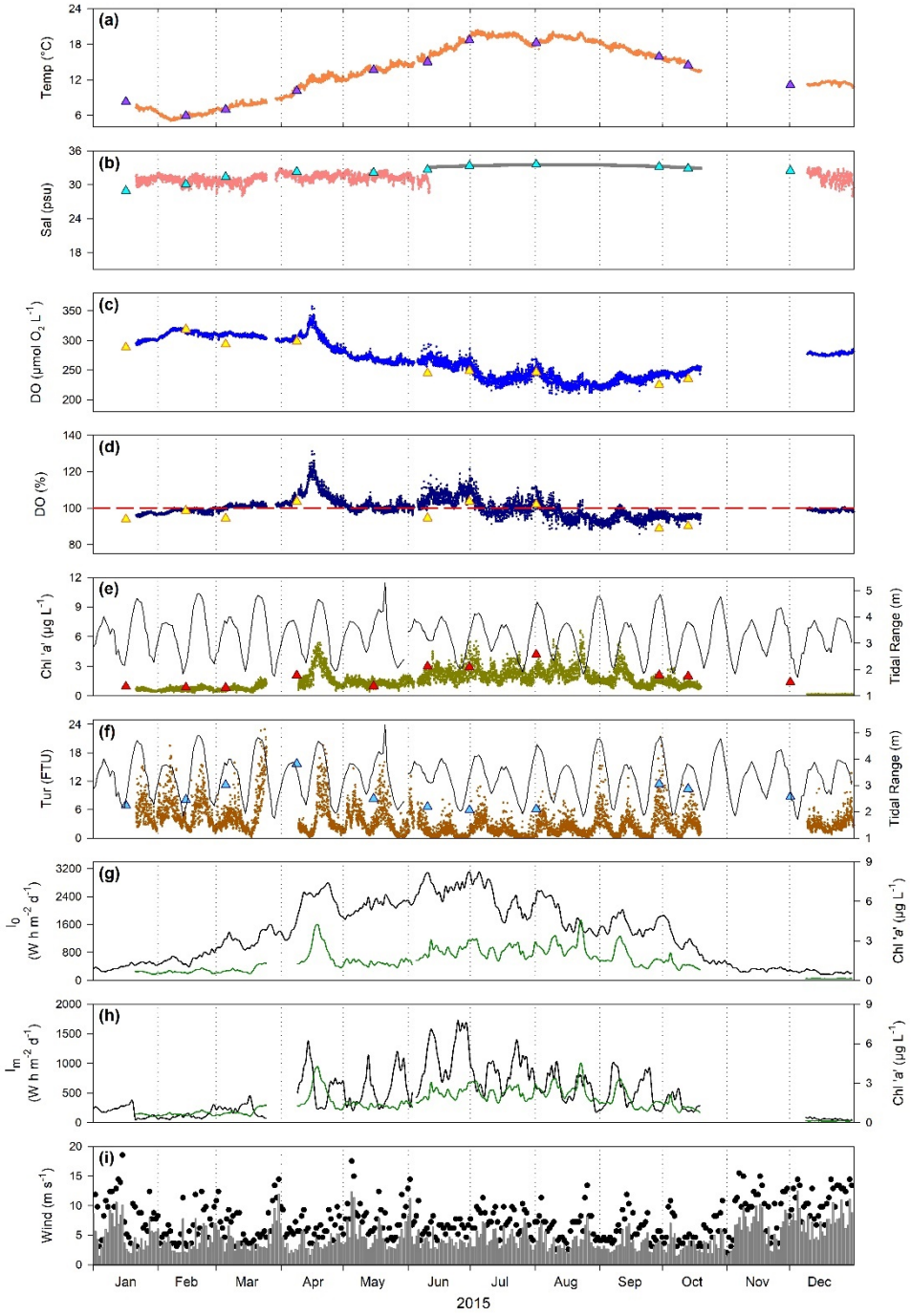

Fig 3.2 Time series of environmental conditions at the Data Buoy in Southampton Water in 2015. (a) Temperature, (b) salinity, (c) DO in concentration and (d) DO in percentage saturation, (e) chlorophyll '*a*' and (f) turbidity are presented as hourly values with dots ● of different colours. In (b), salinity values generated by a model are shown as grey dots ●. In (d), the red dashed line – – represents 100% of saturation. In (e) and (f), the daily tidal range is indicated as a black line —. Environmental agency sampling points are shown as triangles ▲ in different colours in (a) to (f). 7-day running mean of (g) surface irradiance I_0 and (h) mean water column irradiance I_m are presented as black lines —, with daily mean chlorophyll '*a*' concentration included as a green line —. (i) Wind speed is represented as daily mean in vertical bars ▮ and maximum daily values in black circles ●.

3.2.3 Year 2016

In 2016, there were no major gaps in measurements across all parameters apart from salinity (the probe became unreliable from May for the rest of the year). However in May, chl '*a*' displayed a 9-day disruption after filtering the data due to erratic values being detected.

Water temperature varied from 6.8°C in March to 21.5°C in August (Fig. 3.3a) with values initially decreasing throughout the first three months of the year then started to rise at the end of March until they stabilised around 19.5°C for the summer period (July to September). Temperature then slowly decreased until reaching values of 9°C in December.

Salinity from the Data Buoy system is displayed until May; after that, values are estimated from a model using Environment Agency data (Fig. 3.3b). The range of values was from 28 to 32.8 psu, without any clear seasonal variation.

During the month of May, oxygen concentration showed higher values than the rest of the year, with the maximum of 413.3 µmol O_2 L^{-1} in the first week of the month during a peak that lasted 8 days (Fig. 3.3c). May and June presented elevated daily variability, with the yearly minimum of 160 µmol O_2 L^{-1} in the middle of June. The rest of the year showed relatively constant daily values, particularly during the first four months. The period from July to September, displayed only minimal daily variations in concentration. Regarding oxygen percentage, the period from May to August displayed clear oversaturation conditions for prolonged periods (~1 month); however, between June and July 30 days of undersaturation values were also recorded (Fig. 3.3d). During other months, oxygen remained slightly undersaturated and the yearly values ranged from 64.8% in June to 147.6% in May.

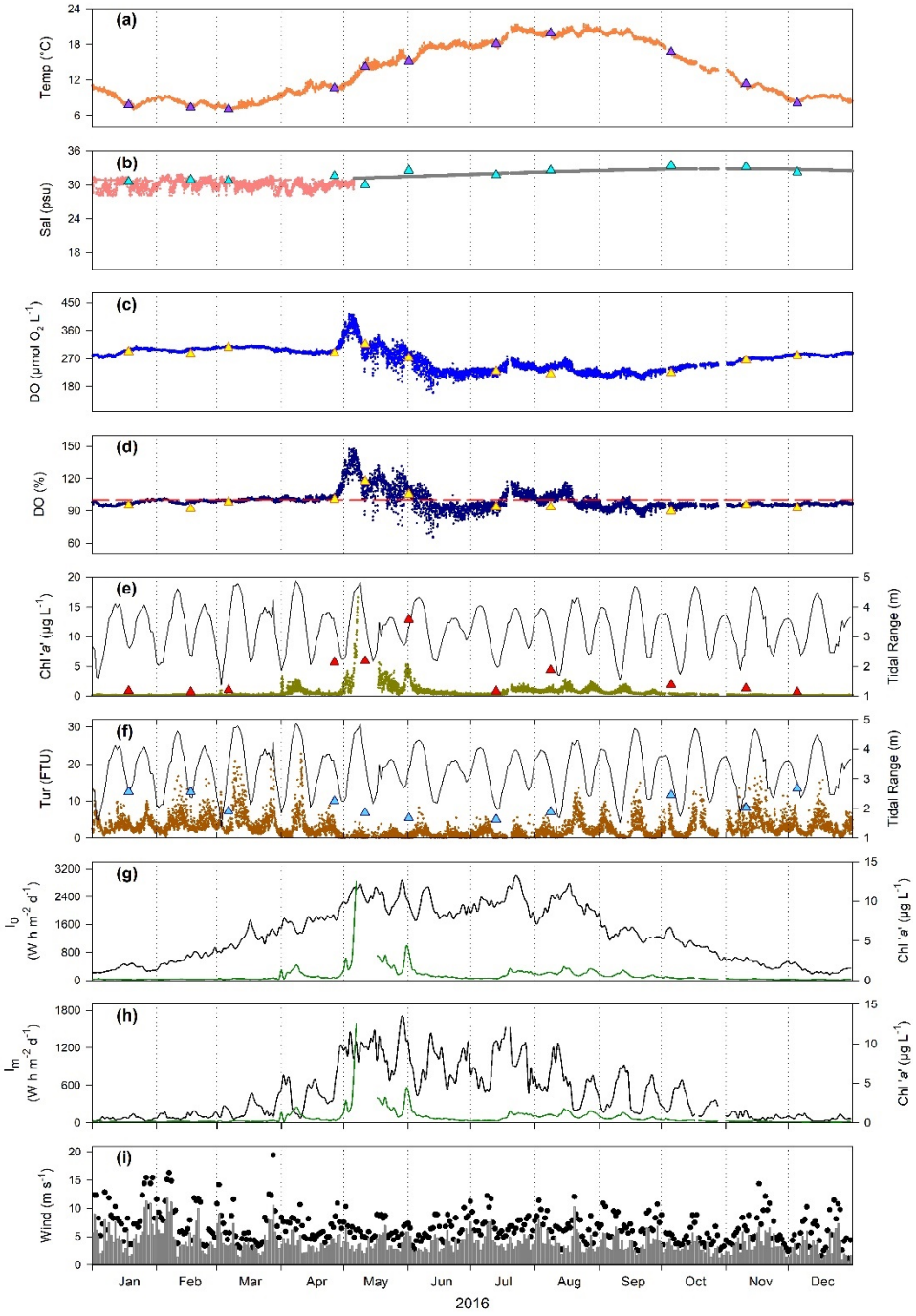

Fig 3.3 Time series of environmental conditions at the Data Buoy in Southampton Water in 2016. (a) Temperature, (b) salinity, (c) DO in concentration and (d) DO in percentage saturation, (e) chlorophyll '*a*' and (f) turbidity are presented as hourly values with dots ● of different colours. In (b), salinity values generated by a model are shown as grey dots ●. In (d), the red dashed line – – represents 100% of saturation. In (e) and (f), the daily tidal range is indicated as a black line —. Environmental agency sampling points are shown as triangles ▲ in different colours in (a) to (f). 7-day running mean of (g) surface irradiance I_0 and (h) mean water column irradiance I_m are presented as black lines —, with daily mean chlorophyll '*a*' concentration included as a green line —. (i) Wind speed is represented as daily mean in vertical bars ▮ and maximum daily values in black circles ●.

Chl '*a*' showed a very distinct peak at the beginning of May, where the yearly maximum value of 16.6 µg L^{-1} was detected (Fig. 3.3e). This spike in chl 'a' included an average value of 9.9 µg L^{-1} for 2 days but data was then interrupted and when recording restarted, concentrations above 5 µg L^{-1} were still detected for another 3 days which suggested it was part of a prolonged peak. A small chlorophyll peak was then identified at the end of May with an average value of 4.1 µg L^{-1}. From July to September, some variability in chl 'a' concentration was detected but with all values below 5 µg L^{-1}.

February and March presented the highest monthly average turbidity values, although, the maximum hourly value (22.7 FTU) was observed in April (Fig. 3.3f). An extended period of low turbidity was detected from mid-April to mid-August, where values did not exceed 9 FTU. From then onwards, turbidity increased again but values were not as high as in the beginning of the year. A perceptible correspondence pattern could be observed between turbidity and tidal range.

A seasonal variability was observed for I_0, with lower values in winter months increasing towards the summer, until reaching a maximum of 2993 Wh m^{-2} d^{-1} in July (Fig. 3.3g). The period between May and August presented values above 1950 Wh m^{-2} d^{-1} that were not observed during the rest of the year.

I_m remained below 500 Wh m^{-2} d^{-1} until the end of March, when several peaks occurred during the same period observed in November and December (Fig. 3.3h). In April, a large spike in I_m was observed where in 4 days with values increasing from ~400 to ~1240 Wh m^{-2} d^{-1}. Immediately after, for 24 consecutive days, daily values remained above 950 Wh m^{-2} d^{-1}. Regular peaks surpassing this value were identified from the end of April to mid-August. The yearly maximum I_m value (1707.3 Wh m^{-2} d^{-1}) occurred during a peak at the end of May.

Daily wind speed oscillated between 0.7 and 11.9 m s^{-1} throughout the year (Fig. 3.3i). January to March was the period with highest monthly averages (~5 m s^{-1}) and variability, after that, daily averages remained under 10 m s^{-1}, with the exception of one day in August, and monthly average values were less than 4.3 m s^{-1}.

3.2.4 Year 2018

The Xylem data buoy commenced recordings in early March 2018. An extensive sensor clean-up was performed in the first few days of September and the result of some biofouling on the optical sensors can be noticed in parameters such as chl '*a*' and turbidity.

Temperature values varied between 4.7°C in March and 23.7°C in July (Fig. 3.4a), following a seasonal distribution with monthly high averages of ~20°C during summer months (June to September).

Salinity presented an annual average of 30.6 ± 0.9 psu, with a minimum of 28 psu and a maximum of 33.4 psu (Fig. 3.4b). Two important sensor positive drifts were noticed, one at the end of October increasing subsequent values by ~1 psu for around two weeks, and another in November where data dropped almost 4 psu in two days. This last event was reflected in the oxygen concentration data since salinity and temperature values are used to calculate O_2 concentration from O_2 saturation.

Oxygen concentration showed consistently higher values between March and May, with a maximum of 337.8 µmol O_2 L^{-1} in April (Fig. 3.4c). Following this period, concentration remained below 290 µmol O_2 L^{-1} until mid-December. The lowest concentration (152.3 µmol O_2 L^{-1}) was detected in July. For both oxygen

parameters, concentration and saturation, daily variability was maximal from the end of May to mid-August then much reduced from September onwards. Saturation percentage exhibited a minimum value in July (67%) and a maximum in May (127.1%). From May to August, saturation values fluctuated between undersaturated and oversaturated conditions then from September, for the rest of the year oxygen remained undersaturated (Fig. 3.4d).

Ten chl '*a*' peaks with values reaching at least 5 µg L^{-1} occurred between March and October 2018 , with evidence of major production activity in July (Fig. 3.4e); outside this period, the average concentration was 0.2 µg L^{-1}. (i) The first bloom of the year appeared at the end of March, lasting 9 days and presenting a mean value of 5.6 µg L^{-1}; (ii) two weeks later, a bloom with an average 3.7 µg L^{-1} was sustained for 5 days, (iii) In May, an 11-day event was detected (4.1 µg L^{-1}) and (iv) three weeks later, in the middle of June, a bloom averaging 4.7 µg L^{-1} was observed for 4 days. (v) during the first days of July, the most extended bloom of the year was sustained for 19 days and presented an average of 4.1 µg L^{-1}; (vi) in the same month, just a week later, an 8-day bloom with a maximum value of 13.7 µg L^{-1} and an average of 4.9 µg L^{-1} appeared. (vii) four days later a peak lasting a week averaged 4.2 µg L^{-1} (viii) The smallest bloom (3.5 µg L^{-1}) was identified at the end of August, lasting 2 days. (ix) The hourly year maximum (17.8 µg L^{-1}) was observed during the bloom at the beginning of September, the data for this event is for 6 days and ceased when the sensor cleaning occurred, and it is believed that this was caused by sensor biofouling. (x) Finally, in October a less clear bloom was noticed where within a week, 3 different days showed hourly values exceeding 5 µg L^{-1}, however, daily values stayed below 2.3 µg L^{-1}.

From March to mid-May, turbidity maxima with hourly values greater than 12 FTU were commonly observed (Fig. 3.4f). In May and early June an unusual 25-day period where turbidity values remained below 5 FTU was detected. For the rest of the year, only on two occasions did the daily mean values exceed 10 FTU; the biofouling event starting at the end of August and finishing when sensors were cleaned, and two days in the middle of December.

Periods from January to mid-April and October to December, showed daily sums of I_0 below 1400 Wh m^{-2} d^{-1} (Fig. 3.4g). The highest values of the year were noticed from May to August, where data remained constantly above 1900 Wh m^{-2} d^{-1}, and the year daily maximum of 3739 Wh m^{-2} d^{-1} was observed in early July.

The largest variability in computed I_m values was observed between the end of May and the beginning of September (Fig. 3.4h), daily vales stayed consistently under 600 Wh m^{-2} d^{-1}. In May, a significant peak in I_m occurred when, within a week, data values increased from ~212 Wh m^{-2} d^{-1} to the year maximum of 1509.8 Wh m^{-2} d^{-1}. Although this peak reduced after 7 days, a second peak then occurred with values higher than 700 Wh m^{-2} d^{-1} for a total of 23 days between May and June.

Daily wind velocity values rarely surpassed 10 m s^{-1}; although irregular wind gusts during the year occasionally exceeded this value (Fig. 3.4i). A period of average low wind (<7 m s^{-1}) was observed between May and July, and greater monthly variation was during January and December.

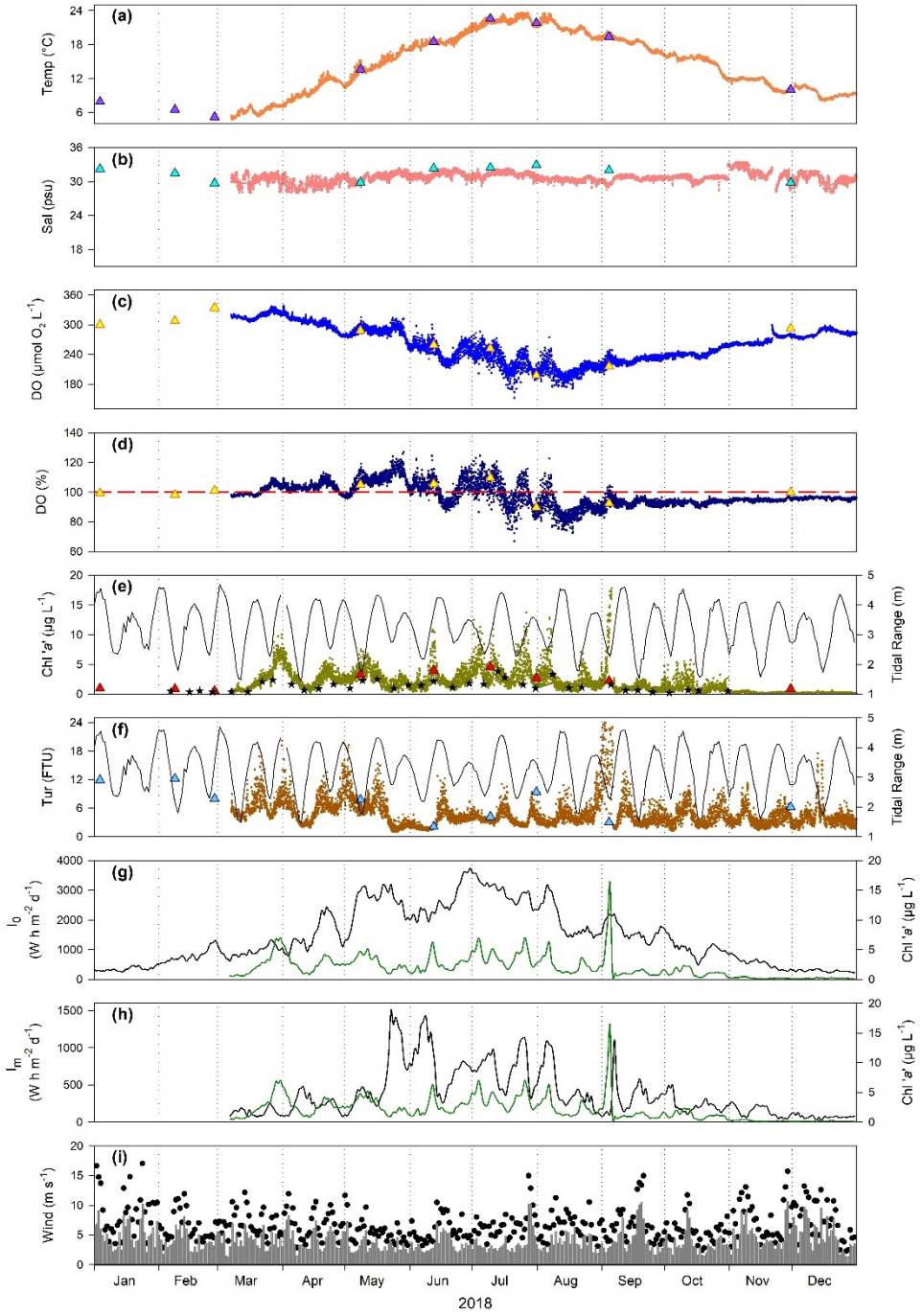

Fig 3.4 Time series of environmental conditions at the Data Buoy in Southampton Water in 2018. (a) Temperature, (b) salinity, (c) DO in concentration and (d) DO in percentage saturation, (e) chlorophyll '*a*' and (f) turbidity are presented as hourly values with dots ● of different colours. In (d), the red dashed line – – represents 100% of saturation. In (e) ★ represent discrete chlorophyll samples taken independently. In (e) and (f), the daily tidal range is indicated as a black line —. Environmental agency sampling points are shown as triangles ▲ in different colours in (a) to (f). 7-day running mean of (g) surface irradiance I_0 and (h) mean water column irradiance I_m are presented as black lines —, with daily mean chlorophyll '*a*' concentration included as a green line —**.** (i) Wind speed is represented as daily mean in vertical bars ▮ and maximum daily values in black circles ●.

3.2.5 Year 2019

Measurements from all sensors were available for most of the 2019, but with two noticeable short gaps. The first one of ~30 days between February and March occurred when the probe was removed from the buoy for maintenance, and the second gap of about 10 days was in late November.

The temperature reflected a seasonal warming, with monthly average values of ~7°C during January and February (Fig. 3.5a), then steadily increasing until reaching an average of 20.3°C for July and August and later decreasing to a value of 8.7°C in December 2019.

Salinity showed low variation across the whole year, with an average of 31.8 ± 1.2 psu (Fig. 3.5b). Failure of the conductivity sensor during two periods required salinity values to be estimated from the salinity model derived from Environmental Agency samples: almost all dates in May and from early July to November.

Oxygen concentration presented a year minimum of 165 µmol O_2 L^{-1} during July and a maximum of 450.4 µmol O_2 L^{-1} in June (Fig. 3.5c). Elevate daily values were detected between April-July; however, periods before April and after July showed more constant values. The oxygen concentration during the first 3 months remained at ~300 µmol O_2 L^{-1} while from August to December, a gradual monthly average increase occurred, taking averages from 225.2 to 287.3 µmol O_2 L^{-1}. An average value of oxygen saturation over the whole year of 100.8% indicated an overall balance in the oxygen saturation (Fig. 3.5d). However, oxygen percentage presented mainly oversaturated conditions between April and July and, in the same way as oxygen concentration, consistently showed the greatest daily variations, with the lowest value in July (71.1%), while the highest in June (183.5%). During the rest of the year, saturation conditions remained

mainly undersaturated. Both oxygen parameters displayed peaks during the high productivity period, comprising days of continuous values above 115% saturation and 300 µmol O_2 L^{-1} concentration.

Chl '*a*' showed a clear period of increased concentration from late April to late August (Fig. 3.5e). Outside of this period, average chl '*a*' concentration remained below 1.5 µg L^{-1}. During this augmented production activity period, four phytoplankton bloom events of different duration and magnitude were observed: (i) in late April, a peak was observed for 14 days with an overall average of 4.2 µg L^{-1} and, (ii) at the end of May, a bloom was sustained for 15 days with an average of 8.7 µg L^{-1} and reached a maximum hourly value of 27.1 µg L^{-1}. (iii) The most prolonged bloom was observed for about 48 days during June-July, presenting the year maximum value of 28.3 µg L^{-1} and an average of 7.5 µg L^{-1} and finally, (iv) a short bloom event was observed at the end of August for 5 days with a mean concentration of 5 µg L^{-1}. The major bloom events in late April, early June and late August developed following a spring tide and peaked during the next neap tide. The more prolonged bloom in July started on a neap tide in late June but was then sustained over two further spring/neap periods until late July.

Turbidity measurements ranged between 1.2 and 16.6 FTU, with a marked period from May to July of low turbidity when daily averages remained below 6 FTU (Fig. 3.5f). Higher daily variation was observed from September to December, but this could have been caused by some biofouling of the turbidity sensor while chl '*a*' for this period remained unaffected. Highest turbidity values corresponded to maximum tidal ranges, especially during spring tides.

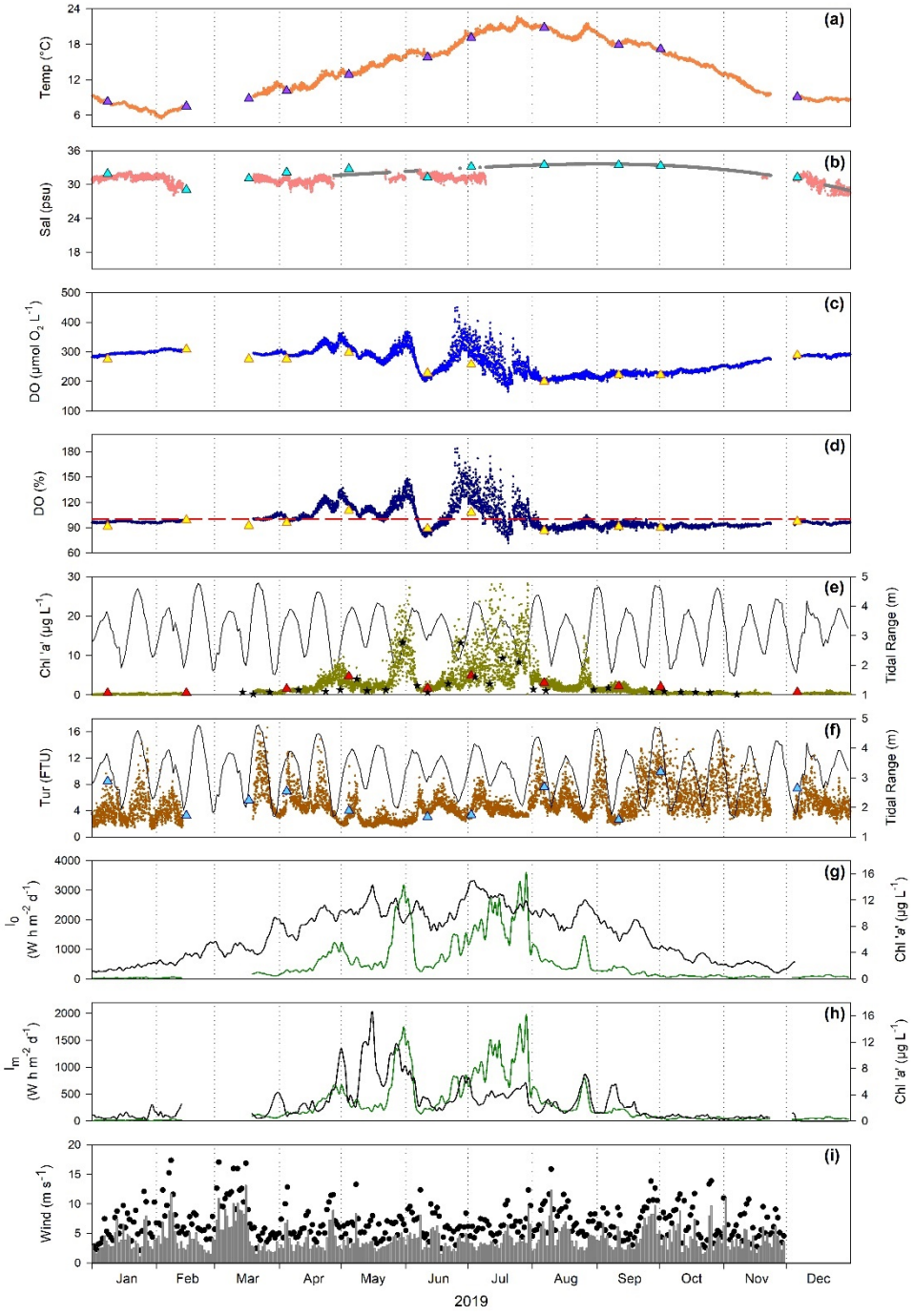

Fig 3.5 Time series of environmental conditions at the Data Buoy in Southampton Water in 2019. (a) Temperature, (b) salinity, (c) DO in concentration and (d) DO in percentage saturation, (e) chlorophyll '*a*' and (f) turbidity are presented as hourly values with dots ● of different colours. In (b), salinity values generated by a model are shown as grey dots ●. In (d), the red dashed line – – represents 100% of saturation. In (e) ★ represent discrete chlorophyll samples taken independently. In (e) and (f), the daily tidal range is indicated as a black line —. Environmental agency sampling points are shown as triangles ▲ in different colours in (a) to (f). 7-day running mean of (g) surface irradiance I_0 and (h) mean water column irradiance I_m are presented as black lines —, with daily mean chlorophyll '*a*' concentration included as a green line —. (i) Wind speed is represented as daily mean in vertical bars ▮ and maximum daily values in black circles ●.

For I_0, values ranged between 165.9 and 3313.6 Wh m^{-2} d^{-1} in January and July, respectively (Fig. 3.5g). A sudden increase in values was observed at the end of March, reaching slightly above 2000 Wh m^{-2} d^{-1} but then decreasing to ~1300 Wh m^{-2} d^{-1} for two weeks, before increasing again and remaining mainly above 2000 Wh m^{-2} d^{-1} for the period between April and August.

I_m showed a large variation throughout the year, with a monthly range from 55.9 Wh m^{-2} d^{-1} in November to 1004.6 Wh m^{-2} d^{-1} in May (Fig. 3.5h). Sustained values above the annual average of 321.4 Wh m^{-2} d^{-1} were observed from April to late September, after which a drop in values remained for the rest of the year.

An exceptionally high I_m period occurred in late April and throughout the whole of May, with three different events, lasting from 3 to 9 days, of sustained values above 1000 Wh m^{-2} d^{-1}.

The first 15 days of March, showed high wind in comparison to the rest of the year, with sustained daily values above 6 m s^{-1} and gusts reaching up to ~16.8 m s^{-1}. Directly after those two weeks, a period lasting until the end of July of lower wind intensity (>5 m s^{-1}) was identified (Fig. 3.5i).

3.2.6 Year 2020

In mid-April, temperature and conductivity sensors stopped logging data, and due to COVID-19 social distancing restrictions, it was not possible to reach the Data Buoy system until the end of August when the sensor was replaced. In order to fill the ~4.5 month data gap, a daily average of all data buoy values for water temperature and salinity from 2014 to 2019 for the same annual period were used. Without these estimated data values, it would have not been possible to calculate oxygen concentration for the productive period of the year. It should

also be noted that there was no Environment Agency sampling between early March and early October 2020 due to Covid restrictions.

The water temperature during the first 3 months of the year was ~8.5°C then started to steadily increase from April, until reaching an estimated yearly maximum of 21.6°C in July (Fig. 3.6a). From then on, temperature declined with the monthly average of 9.2°C measured in December. It is possible to notice, at the end of November, a negative drift with values decreasing suddenly ~1.0°C.

The salinity yearly average was 30.9 ± 1.1 psu. Although greater daily variation in the monthly averages can be observed from October to December, this was less than 1.0 psu. An additional month of salinity data values was added from the salinity model derived from Environment Agency data, from mid-March to mid-April, since values recorded were drifting downward about ~10 psu (Fig. 3.6b).

A very pronounced oxygen concentration peak could be observed in the middle of April, where values above 400 µmol O_2 L^{-1} were sustained for a week and the yearly maximum of 542.4 µmol O_2 L^{-1} was identified (Fig. 3.6c). The May to August period showed greater daily variability and several other peaks, however, none exceeded 370 µmol O_2 L^{-1}. The lowest concentration of the year was displayed during this period, 102.8 µmol O_2 L^{-1} in July. Oxygen in percentage presented a very similar distribution pattern to oxygen concentration, with a major peak in values in April (Fig. 3.6d), when the highest saturation of the year (190.7%) was detected. Oversaturation conditions could be mainly observed from April to August, although during July the lowest measurements of the year (~50%) were detected. Outside this period, undersaturation prevailed with monthly averages ranging from 91.0 to 98.8%.

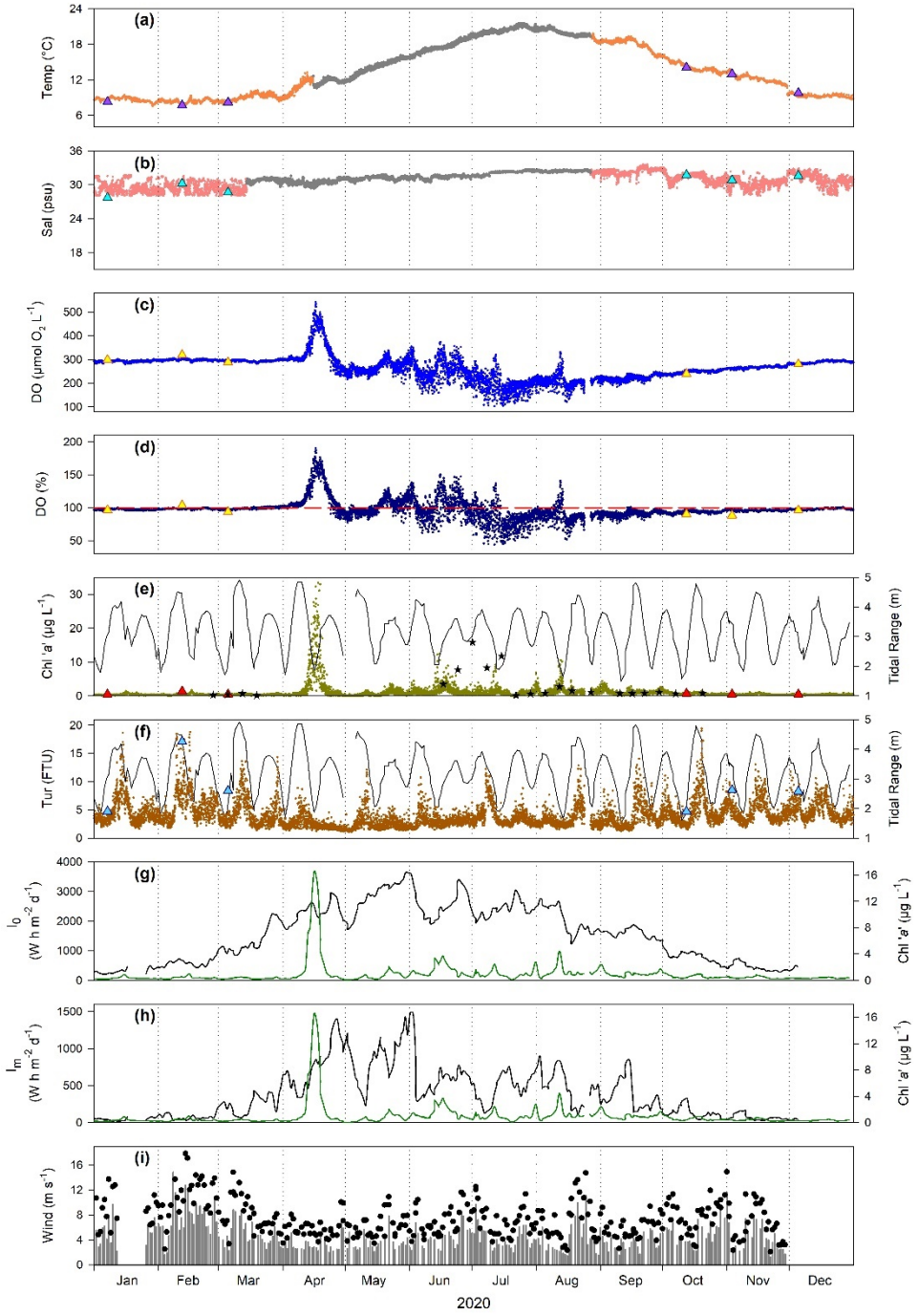

Fig 3.6 Time series of environmental conditions at the Data Buoy in Southampton Water in 2020. (a) Temperature, (b) salinity, (c) DO in concentration and (d) DO in percentage saturation, (e) chlorophyll '*a*' and (f) turbidity are presented as hourly values with dots ● of different colours. In (a) and (b), temperature and salinity values generated by a model are shown as grey dots ●. In (d), the red dashed line – – represents 100% of saturation. In (e) ★ represent discrete chlorophyll samples taken independently. In (e) and (f), the daily tidal range is indicated as a black line —. Environmental agency sampling points are shown as triangles ▲ in different colours in (a) to (f). 7-day running mean of (g) surface irradiance I_0 and (h) mean water column irradiance I_m are presented as black lines —, with daily mean chlorophyll '*a*' concentration included as a green line —. (i) Wind speed is represented as daily mean in vertical bars ▮ and maximum daily values in black circles ●.

A significant peak of chl '*a*' was identified in April, presenting the highest concentration of the year (33.4 µg L^{-1}) and this event averaged 8.2 µg L^{-1} during the 11 days it lasted (Fig. 3.6e). In addition, four minor blooms were identified from June to August: (i) In mid-June a 11 days bloom could be observed, averaging 2.5 µg L^{-1}. (ii) Almost three weeks later, for 2 days, higher values were described, reaching 12.4 µg L^{-1} and a mean of 2.1 µg L^{-1}. (iii) In early August, a small bloom appeared, exceeding the 5 µg L^{-1} threshold value for 1 day and averaging 2.7 µg L^{-1}, and a week later (iv) a 3-day event averaged 3.4 µg L^{-1}. Outside the April-August period, monthly mean values remained below 1 µg L^{-1}.

The first three months of the year presented, in general, the most elevated values for turbidity during the year, with peaks ranging from 13.4 to 18.6 FTU. Nevertheless, the year maximum was recorded in a peak (19.4 FTU) during October (Fig. 3.6f). April presented the lowest monthly average (2.5 FTU), and from that month until June, peaks were observed every 30 days instead of every 15 days, like during the rest of the year.

Values for I_0 started increasing steadily from ~283 Wh m^{-2} d^{-1} in January, but at the end of March a spike of ~1000 Wh m^{-2} d^{-1} took daily sums from 1240 to 2250 Wh m^{-2} d^{-1} in about 9 days (Fig. 3.6g). After this, several peaks in I_0 were observed with a major one at the end of May reaching 3639.4 Wh m^{-2} d^{-1}. In a period of 8 days in mid-August, values dropped more than 1300 Wh m^{-2} d^{-1} keeping daily sums for the rest of the year below 1800 Wh m^{-2} d^{-1}.

Distribution of I_m for this year was very irregular, with the highest values concentrated in 42 days between April and June, this being the only time when daily sums exceeded 900 Wh m^{-2} d^{-1} during the year (Fig. 3.6h). However, within this period of major activity, a pronounced decrease occurred in May with values

as low as 250 Wh m^{-2} d^{-1}. In addition, in early June, values exhibited a sudden drop, from ~1480 to 290 Wh m^{-2} d^{-1} in less than a week, and then remained under 900 Wh m^{-2} d^{-1} until mid-September. After that, values remained below 350 Wh m^{-2} d^{-1}.

February presented the highest monthly average wind speeds, with 7.6 m s^{-1} on average and gusts above 12 m s^{-1}, especially in the last two weeks of the month (Fig. 3.6i); August and October presented gusts surpassing 12 m s^{-1}, but recorded less often. From mid-March to the end of June, low wind conditions were observed, with daily means staying, commonly, under 5.8 m s^{-1}.

3.3 Christchurch Harbour time series of environmental factors

The data collected from the deployment of an EXO2 multi parameter sonde from the Ferry Pontoon in Christchurch Harbour is available from 2014 to 2018.

For this study site, a chlorophyll '*a*' (Chl '*a*') major bloom was considered whenever an hourly average value exceeded 10 µg L^{-1}. Since the main analysis has been based on daily mean values, any day where Chl '*a*' concentration exceeded the threshold value of 10 µg L^{-1} was included as a 'bloom' event. The Environment Agency did not routinely sample in the Christchurch Harbour estuary between 2014 and 2018 however some spot sampling was done throughout the estuary including at the Ferry pontoon by the Christchurch Harbour Macronutrients research team in 2014 (Panton *et al*., 2020).

3.3.1 Year 2014

For 2014, measurements recorded with the EXO2 probe in the estuary commenced in May. A 5-day gap in data at the end of June affected all water quality parameters and a second 5-day gap in mid-July disturbed both oxygen

variables. From 30th July to 23th September 2014, data was collected every 2 hours instead of the 10 minutes displayed for the rest of the Christchurch Harbour time series.

Water temperature values were not available due to sensor malfunction for almost two months from July to September. In order to fill the gap, independent measurements made about every two weeks with a similar probe were used to produce a temperature model and predicted values were introduced into the time series (Fig. 3.7a). These estimated temperature values were used to calculate oxygen concentration (from percentage saturation) for the same period. During the year, water temperature ranged between 4.2°C in December and 20.9°C in August.

For the first month of measurements, between May and June, estimated salinity only varied between 26.2 and 31.5 psu although this reflected high tide values (Fig. 3.7b). However, during the rest of the year salinity often showed widely fluctuating values between 0.3 to 31.3 psu within one day due to the daily tidal fluctuations. This high variation resulted in a yearly average of 22.8 ± 7.7 psu at the Christchurch Harbour site.

Oxygen concentration showed high daily and monthly variability during July and August, and during these months the minimum (Aug) and maximum (Jul) values were detected (189.9 and 636.4 µmol O_2 L^{-1} respectively). July's monthly average of 380.2 µmol O_2 L^{-1}, was considerably higher than for other months, displaying the maximum of 299 µmol O_2 L^{-1}; October presented the lowest monthly average of 247.9 µmol O_2 L^{-1} (Fig. 3.7c). Both oxygen concentration and saturation exhibited a sudden drop in values during the first week of August, and after that,

concentration did not exceeded 355 µmol O_2 L^{-1} and saturation remained below 150%.

Oxygen saturation ranged from 70% in August to 242% in July. Oversaturated conditions prevailed in June and July and were common in August and September. Undersaturated conditions dominated during other months.

Chl '*a*' registered a minimum of 0.1 µg L^{-1} in December and a maximum of 22.1 µg L^{-1} in September, however, July monthly average was the highest of the year, with 4.9 µg L^{-1}. At the end of June, a small peak in Chl 'a' could be observed, with only 1 day exceeding the threshold of 10 µg L^{-1}. In addition, four major blooms were detected between July and September as observed in Figure 3.7e. (i) Lasting more than three weeks (24 days), the longest bloom of the year was observed in July with an average of 5.1 µg L^{-1} and maximum hourly values up to 19 µg L^{-1}. Approximately a week later, (ii) the second bloom was maintained for 6 days averaging 5.8 µg L^{-1}. (iii) In early September, the bloom presented the maximum average of 6.4 µg L^{-1}, lasted 9 days; and a week later (iv) a 3-day bloom with an average of 5.3 µg L^{-1} was detected.

From May to September, hourly values of turbidity remained below 20 FTU, with the exception of a few days in August (Fig. 3.7f). During this period, monthly average values did not exceed 7.5 FTU. However, from October to December, the monthly values increased from 11.2 to 18.3 FTU, and a maximum of 77.2 FTU was observed in November.

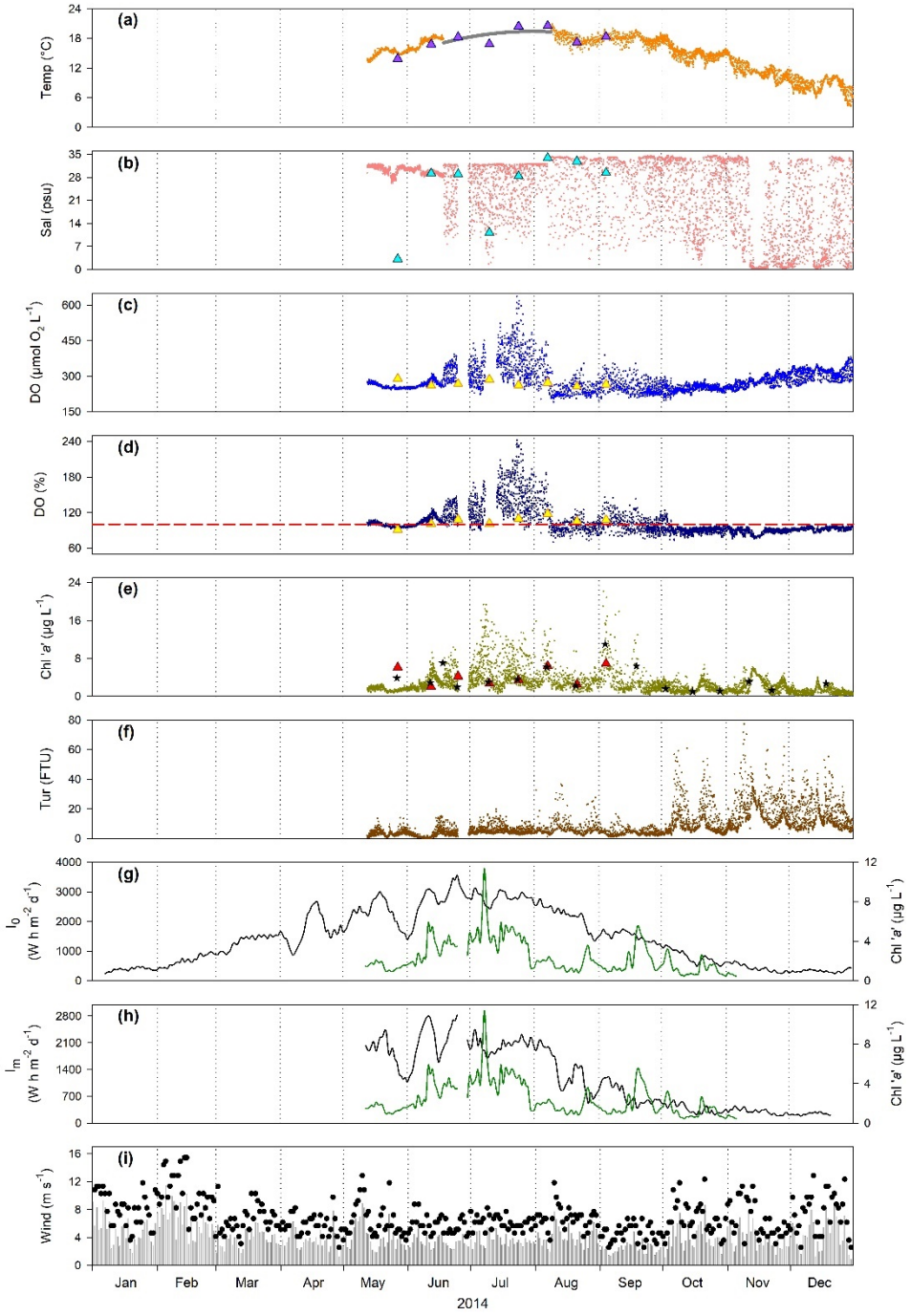

Fig 3.7 Time series of environmental conditions at the Data Buoy in Christchurch Harbour Ferry Pontoon in 2014. (a) Temperature, (b) salinity, (c) DO in concentration and (d) DO in percentage saturation, (e) chlorophyll '*a*' and (f) turbidity are presented as hourly values with dots ● of different colours. In (a), temperature values generated by a model are shown as grey dots ●. In (d), the red dashed line – – represents 100% of saturation. Measurements taken with an independent probe are shown as triangles ▲ in different colours in (a) to (e). In (e) ★ represent discrete samples taken independently. 7-day running mean of (g) surface irradiance I_0 and (h) mean water column irradiance I_m are presented as black lines —, with daily mean chlorophyll '*a*' concentration included as a green line —. (i) Wind speed is represented as daily mean in vertical bars ▮ and maximum daily values in black circles ●.

I_0 steadily increased during the first three months of the year, until in early April a peak of more than 1500 Wh m^{-2} d^{-1} stirred values from ~900 to ~2600 Wh m^{-2} d^{-1} in less than two weeks (Fig. 3.7g). From then until the end of August, daily sums above 1750 Wh m^{-2} d^{-1} were commonly observed; unlike the rest of the year when values did not reach this threshold. A maximum of 3556.9 Wh m^{-2} d^{-1} was detected in June.

Since I_m is partly derived from turbidity, the time series for this parameter started in May, with values around 2000 Wh m^{-2} d^{-1}. At the beginning of June, a big peak was observed, moving daily sums from ~1100 to ~2800 Wh m^{-2} d^{-1}. A second peak appeared in late June, including the year maximum of 2824.9 Wh m^{-2} d^{-1} just as estimated values ceased due to a gap in turbidity data (Fig. 3.7h). Values above 1550 Wh m^{-2} d^{-1} were only identified between May and mid-August.

January, February and December exhibited higher daily wind speeds, which was reflected in their monthly averages ~ 6 m s^{-1}. From these three months, February presented the maximum gusts of wind, generally above 13 m s^{-1}. Moreover, in May, a peak of high wind speed (>11 m s^{-1}) was identified for over a week (Fig. 3.7i). On the contrary, June and July maintained daily values consistently below 6 m s^{-1} with maximum values never exceeding 9 m s^{-1}. Moreover, September presented the lowest monthly value of 2.5 m s^{-1}.

3.3.2 Year 2015

In 2015, from mid-May to the end of August (105 days), data from the EXO2 sonde were not recorded due to a data logger malfunction. Additionally, data in December was only collected during the first week of the month. However, this year was included in the results since phytoplankton activity in the form of chl ‘a’ blooms were detected in months either side of this data gap.

Temperature varied between 3.6 and 18.5°C, in February and September respectively (Fig. 3.8a). Since data from the summer months were not available, it can only be assumed that temperature did not go above 20°C because of missing data during the generally warmest period of the year.

Regarding salinity, a minimum of 0.2 psu and a maximum of 37.4 psu was observed during the year (Fig. 3.8b). During the first 3 months of the year salinity values were often below 2 psu due to high freshwater river inputs to the estuary then for a period of about 3 weeks, data remained above 7 psu. Once measurements resumed in September, salinity appeared to displayed a negative drift of ~1 psu for about a month, since before this period values did not exceed 35 psu.

Both oxygen parameters, concentration and percentage, showed a major peak in values in April, when the year maximums (481.4 µmol O_2 L^{-1} and 160.8%) were detected. Oxygen concentration exhibited, on average, highest values in the first months of the year, with monthly means of ~319 µmol O_2 L^{-1} compared with ~284 µmol O_2 L^{-1} from September onwards (Fig. 3.8c). In a similar way, data recorded between January and March showed, mostly, undersaturated conditions, while the rest of the year had larger daily variation, reflecting rapid within day changes between over saturated and undersaturation in shortly periods (Fig. 3.8d).

Chl '*a*' concentration increased in April and Oct but remained below 5 µg L^{-1} in other monitored months. For 2015, seven major blooms were identified and are displayed in Figure 3.8e. (i) The first one started in late March and lasted 7 days, averaging 4.9 µg L^{-1}. (ii) During mid-April, the longest event (24 days) was evident, presenting an 8.3 µg L^{-1} average and the year maximum of 48.2 µg L^{-1}. Two days later, (iii) a smaller bloom (6.1 µg L^{-1}) could be observed for about 3

days. Almost a week after measurements restarted in September, (iv) an event where for 12 days several hourly values exceed 10 µg L^{-1} was identified. (v) The bloom presenting the highest average of the year of 12.6 µg L^{-1}, was observed between September and October for over 12 days, and almost immediately a (vi) smaller peak (5.8 µg L^{-1}) appeared for 4 days. This last bloom could have been due to the remnants of the larger one, but it is included as it was separated by two days of lower concentrations. (vii) At the end of October, the last bloom of the year was observed for 15 days and averaging 9.2 µg L^{-1}.

Turbidity in October and November presented highest monthly values (>20 FTU) compared to the rest of the year and the maximum value for the year (91.6 FTU) was detected in November (Fig. 3.8f). However, during the first three months of the year some high values were also detected with values as high as 66 FTU.

Higher daily sums for I_0 were observed between April and September (Fig. 3.8g), with values from 1228 to 2484 Wh m^{-2} d^{-1}. Until July, values stayed close to 2000 Wh m^{-2} d^{-1}, and for the next 3 months daily peaks occurred from ~1350 to ~2900 Wh m^{-2} d^{-1}.

Similarly, to I_0, a sudden increase to ~1000 Wh m^{-2} d^{-1} in early April, was detected for I_m. With the year maximum of 2350.2 Wh m^{-2} d^{-1} appearing in the following week (Fig. 3.8h). From April to mid-September, I_m values exceeded 1370 Wh m^{-2} d^{-1}, but it is worth noting that a 3-month gap within this period is shown.

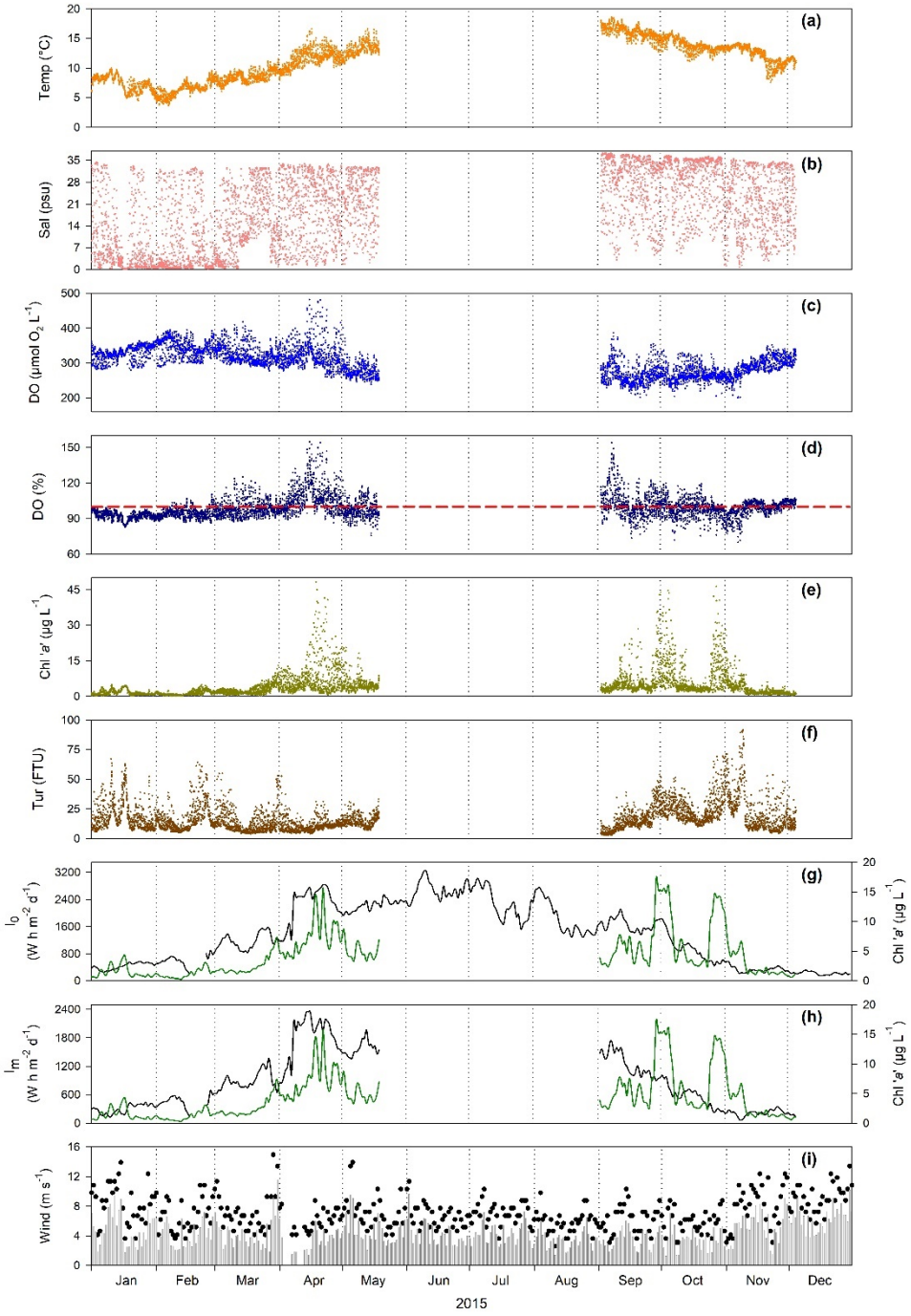

Fig 3.8 Time series of environmental conditions at the Data Buoy in Christchurch Harbour Ferry Pontoon in 2015. (a) Temperature, (b) salinity, (c) DO in concentration and (d) DO in percentage saturation, (e) chlorophyll '*a*' and (f) turbidity are presented as hourly values with dots ● of different colours. In (d), the red dashed line – – represents 100% of saturation. 7-day running mean of (g) surface irradiance I_0 and (h) mean water column irradiance I_m are presented as black lines —, with daily mean chlorophyll '*a*' concentration included as a green line —. (i) Wind speed is represented as daily mean in vertical bars ▮ and maximum daily values in black circles ●.

Windier conditions were seen in November and December, when most maximum daily gusts recorded were above 9 m s^{-1} and monthly average ~5.8 m s^{-1}. Nevertheless, daily values above 10 m s^{-1} with gusts >13 m s^{-1} occurred at the end of March (Fig. 3.8i). On the contrary, an extended period of lower measured wind speeds were detected from June to October, presenting monthly values ~3.8 m s^{-1} and gusts below 10.5 m s^{-1}.

3.3.3 Year 2016

Measurements for 2016 started in mid-February and finished at the end of November, with no gaps during the period in-between.

Temperature varied seasonally, presenting higher monthly averages (~18.8°C) in the summer months with a year maximum of 23.7°C in July (Fig. 3.9a). In addition, February showed the coldest temperature of the year 5.3°C and the lowest monthly value (7.8 °C).

From February to May, salinity showed a larger variation than for the rest of the year, with peaks approximately every two weeks, as seen in Figure 3.9b. It is also noticeable that from June to September, hourly values rarely dropped below 5 psu and, at the end of November, a similar decrease in salinity as detected in the first few months, was observed.

Oxygen concentration exhibited higher values (~354 µmol O_2 L^{-1}) from February to May, but then in June started showing slightly lower values (~283 µmol O_2 L^{-1}) for the rest of the year (Fig. 3.9c). Several oxygen peaks could be observed from May to August, but especially during May when the highest value of 485.3 µmol O_2 L^{-1} was recorded. In terms of oxygen saturation, the year presented an overall average oversaturation (107.1 ± 9.0%), with most of the undersaturated

conditions detected from May to September, but never lasting for extended periods (Fig. 3.9d).

Chl '*a*' concentrations in 2016, presented four different bloom events, with a particularly extended one between May and June, as can be clearly seen in Figure 3.9e. (i) The first bloom was detected at the end of April for about 5 days and reached a mean value of 4.6 µg L^{-1}. A week later, (ii) a substantial bloom was recorded for a total of 45 days, averaging 14 µg L^{-1} for the total event and reaching a maximum value of 130 µg L^{-1}. Following this, a period of about two months remained with relatively low productivity, until August when two separate days showed hourly values exceeding 10 µg L^{-1} and presenting daily values of (iii) 3.5 µg L^{-1} and (iv) 5.3 µg L^{-1}.

A clear period of low turbidity, with values never surpassing 30 FTU was detected for about 4 months (Apr-Aug), in the middle of the year (Fig. 3.9f). Outside of this period, turbidity presented regular peaks over 50 FTU, and even a major increase in November reaching 84.1 FTU.

From February, I_0 showed a gradual increase in daily values (Fig. 3.9g). The period between April and August displayed several changes in the light intensity, but values permanently remained above 1600 Wh m^{-2} d^{-1}. In May and July, peaks increased to 2926.9 and 2946.1 Wh m^{-2} d^{-1}, respectively. A decrease in values later in the year was observed from mid-September when in 4 days values declined from 1603.2 to 742.5 Wh m^{-2} d^{-1}.

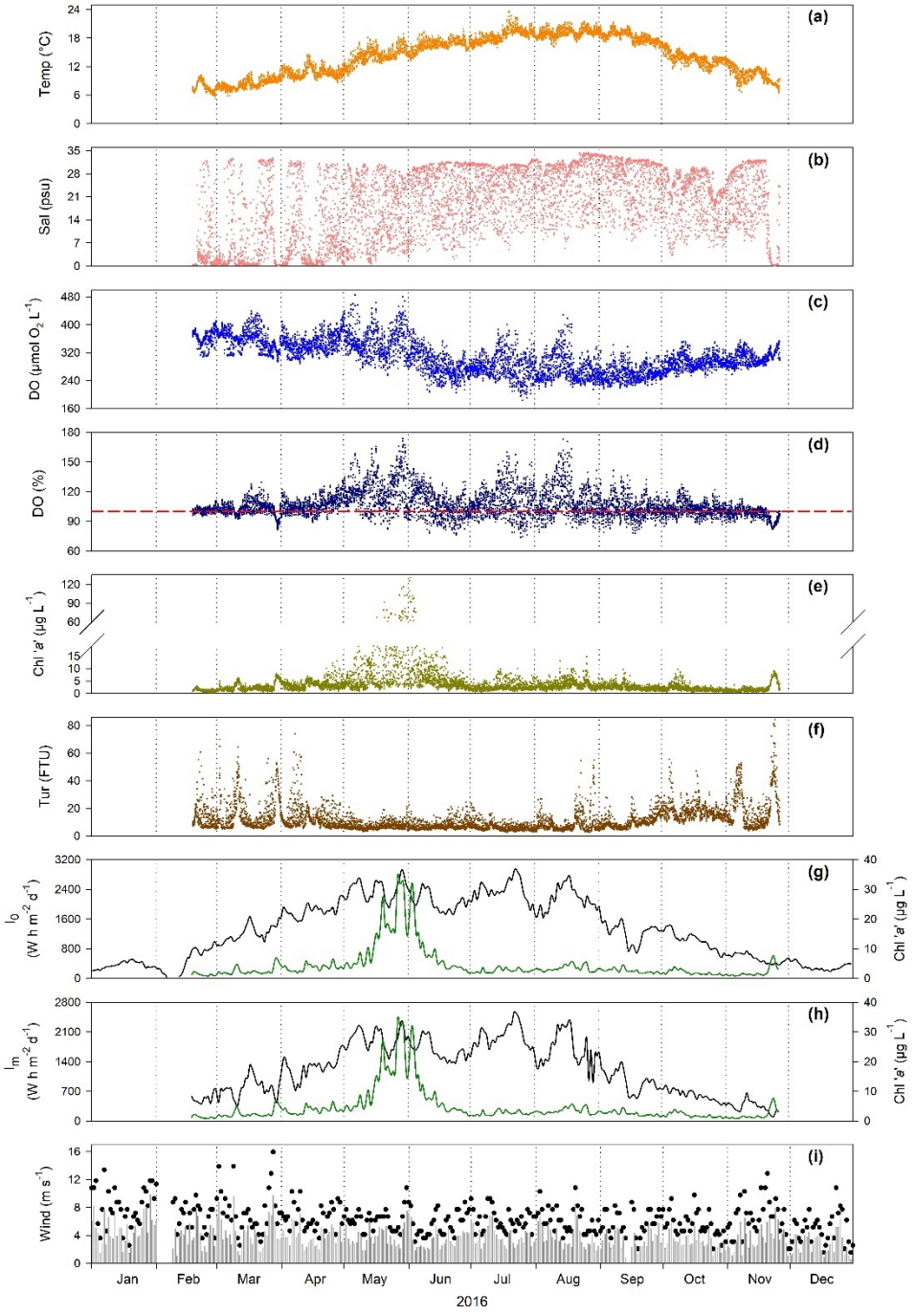

Fig 3.9 Time series of environmental conditions at the Data Buoy in Christchurch Harbour Ferry Pontoon in 2016. (a) Temperature, (b) salinity, (c) DO in concentration and (d) DO in percentage saturation, (e) chlorophyll '*a*' and (f) turbidity are presented as hourly values with dots ● of different colours. In (d), the red dashed line – – represents 100% of saturation. 7-day running mean of (g) surface irradiance I_0 and (h) mean water column irradiance I_m are presented as black lines —, with daily mean chlorophyll '*a*' concentration included as a green line —. (i) Wind speed is represented as daily mean in vertical bars ▮ and maximum daily values in black circles ●.

I_m calculations varied greatly across the year as seen in Figure 3.9h, showing several spikes in values, with the maximum in July (2555.6 Wh m^{-2} d^{-1}). Although peaks identified during May were only around 2250 Wh m^{-2} d^{-1}, this month presented a very similar average to July, ~2000 Wh m^{-2} d^{-1}.

During the first three months of the year, higher wind speeds were detected (Fig. 3.9i), with monthly averages of ~4.5 m s^{-1}, and reaching gusts of up to 16 m s^{-1}. For the rest of the year, monthly averages never exceeded 3.9 m s^{-1} and daily values remained often below 7 m s^{-1}.

3.3.4 Year 2017

In 2017, there is missing water quality data for the first and the last week of the year, as well as a 40-day gap between February and March.

Water temperature at the beginning of the year was ~6°C then started to progressively increase from the end of January, until reaching a maximum of 24.8°C in June, to then decrease to temperatures near 7°C in December (Fig. 3.10a).

A considerable variability was observed in salinity, with values ranging from 0.3 to 34.8 psu (Fig. 3.10b). Early in the year large daily fluctuations in salinity are evident due to higher river flows in the estuary and later from May salinity did not decrease below about 10-15psu during reduced river flow rates and effect of tidal water inputs to the estuary.

Large daily variability was detected from June to August in terms of oxygen concentration (Fig. 3.10c). The yearly minimum (171.2 µmol O_2 L^{-1}) and maximum (462.7 µmol O_2 L^{-1}) values were identified within this period, in July and June respectively. Monthly averages showed September as the lowest (272.1

µmol O_2 L^{-1}) and January as the month presenting the highest oxygen concentration (357.6 µmol O_2 L^{-1}). Regarding oxygen saturation, overall the year was oversaturated with a mean of 107.7 ± 9.7%. Values below 100% saturation were mainly detected from May onwards, and were less evident in the last few months of the year, as seen in Figure 3.10d.

This year displayed a relatively low Chl '*a*' concentration (Fig. 3.10e), with an average of 2.8 ± 1.3 µg L^{-1}. Three different events reached the conditions specified to be classified as major blooms at the Ferry Pontoon in the estuary. (i) In early-June, over two days the hourly values reached the threshold of 10 µg L^{-1} and the bloom presented a mean of 3.1 µg L^{-1}. Later in the summer, (ii) at the beginning of August, a bloom was detected lasting 7 days and reaching a maximum of 11.2 µg L^{-1}, however, the yearly maximum of 11.6 µg L^{-1} was observed during (iii) the 3-day bloom in October. A few days after the last bloom, a downward drift in data of about 1.1 µg L^{-1} was identified.

Peaks in turbidity exceeding 50 FTU were regularly detected during the year, particularly in January and December when maximum values were close to 80 FTU (Fig. 3.10f). Nevertheless, long periods (>2 months) when turbidity remained below 20 FTU were evident in April-May and June-August.

I_0 showed greater variation and several peaks, during the period between April and August (Fig. 3.10g). Additionally, daily values remained above 1700 Wh m^{-2} d^{-1}. The maximum of 3509.1 Wh m^{-2} d^{-1} was detected during the peak in the middle of June, the same month that presented the highest monthly average of 2607.6 Wh m^{-2} d^{-1}.

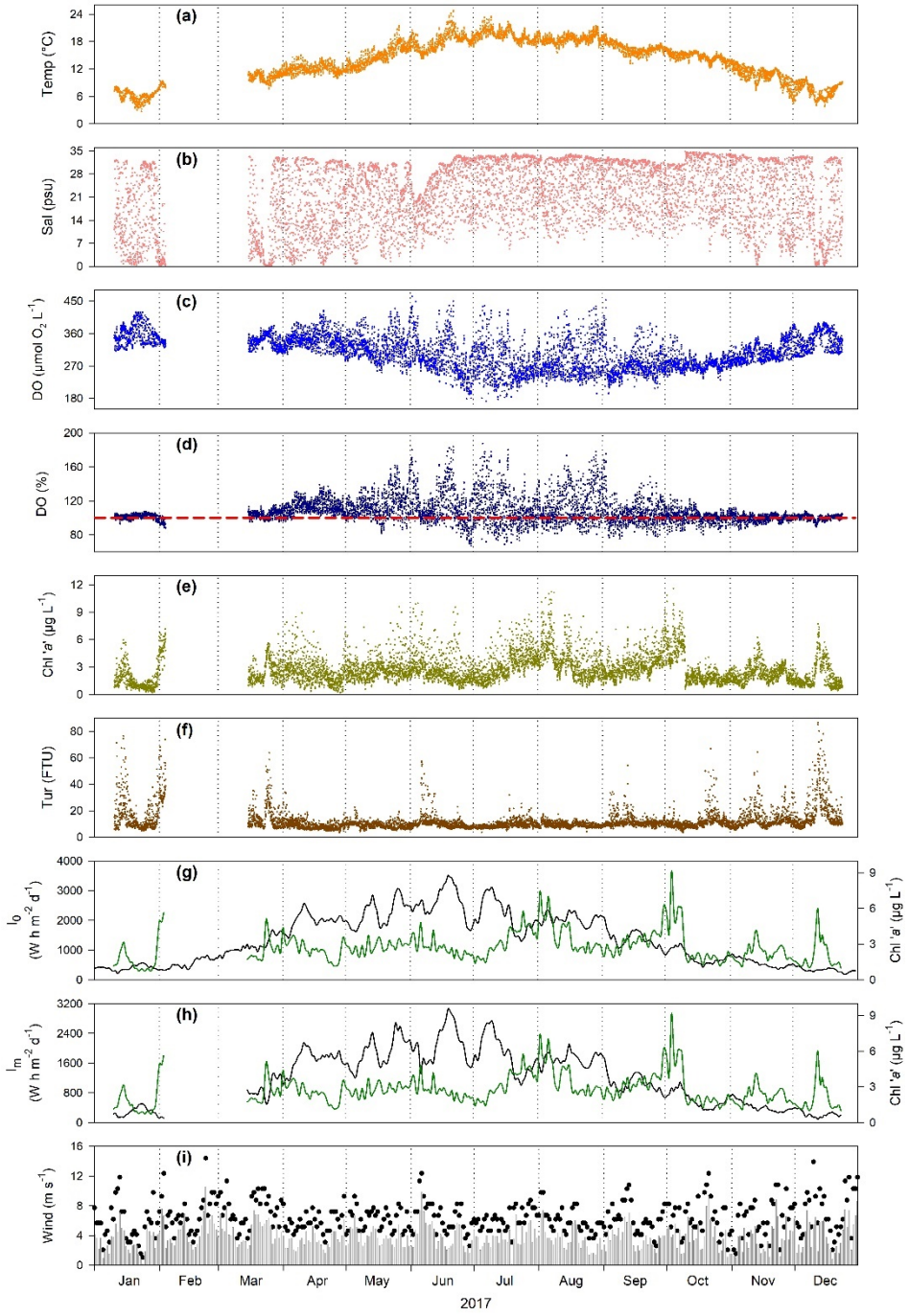

Fig 3.10 Time series of environmental conditions at the Data Buoy in Christchurch Harbour Ferry Pontoon in 2017. (a) Temperature, (b) salinity, (c) DO in concentration and (d) DO in percentage saturation, (e) chlorophyll '*a*' and (f) turbidity are presented as hourly values with dots ● of different colours. In (d), the red dashed line – – represents 100% of saturation. 7-day running mean of (g) surface irradiance I_0 and (h) mean water column irradiance I_m are presented as black lines —, with daily mean chlorophyll '*a*' concentration included as a green line —. (i) Wind speed is represented as daily mean in vertical bars ▮ and maximum daily values in black circles ●.

In a very similar pattern to I_0, calculations of I_m varied significantly from April to August (Fig. 3.10h). For this parameter, daily values surpassed 1300 Wh m^{-2} d^{-1} almost the whole time within this period, an exception could be observed in late July, and a peak during June presented the highest value of the year (3055.8 Wh m^{-2} d^{-1}).

Daily average wind speeds rarely exceeded 8 m s^{-1} during the year, as it can be seen in Figure 3.10i. Monthly averages remained below 5 m s^{-1} for the whole year, with the lowest in April (3.3 m s^{-1}) and the highest in March (4.7 m s^{-1}). Periods of about two weeks, presenting higher gusts were measured in March and December.

3.3.5 Year 2018

Water quality data was not available in 2018 until the last days of March, and at the end of the year the probe stopped logging data two weeks before the end of December.

Water temperature increased gradually from around 7 °C in March until reaching a maximum of 24.3 °C in July, and then progressively decreased to values of ~6.5°C at the end of the year (Fig. 3.11a). However, in the last weeks of April an unusual drop in temperature to near 8°C for a couple of days, to then rapidly increase back to ~16.5°C.

Salinity is a widely variable parameter at this study site, ranging from 0.1 to 34 psu in this particular year, as shown Figure 3.11b. However, two periods where data stayed consistently below 1 psu for days were observed. The first one lasting 14 days in early-April and the second period for almost all of July (28 days); these are believed to be caused by a sensor failure. In addition, during the last three

months of the year, values for salinity clearly drifted down steadily, again probably due to sensor malfunction.

Oxygen concentration ranged from 176.6 µmol O_2 L^{-1} in September to a value of 506.8 µmol O_2 L^{-1} in July. Nevertheless, the first three months average above 340 µmol O_2 L^{-1} which made this the period with the highest concentration of oxygen of the year (Fig. 3.11c). The period between June and August presented the highest daily variability in oxygen saturation (Fig. 3.11d), with the yearly limit values observed within this period: 64.2% in July and 187.1% in June. The year presented a general oversaturated average (108.8 ± 10.6%) with all monthly averages above 100% saturation. Regular peaks in oxygen concentration and saturation were identified from May to September.

From 11th August, Chl '*a*' data had to be fitted since a drift of about ~1.0 µg L^{-1} every 2 weeks was detected; values revised by applying a linear model are highlighted in Figure 3.11e. A total of seven peaks of Chl '*a*' were distinguished across the year, (i) with the first and longest from May to June (28 days), presenting the year maximum of 38.1 µg L^{-1} and bloom average of 8 µg L^{-1}. (ii) Very soon after, a peak lasting 6 days that could have still been part of the bigger bloom was observed (3.9 µg L^{-1}). (iii) In July a 3-day bloom occurred and averaged 4.3 µg L^{-1}. After almost 2 months of no major productivity, (iv) in mid-September a significant peak sustained for 21 days got a 6.8 µg L^{-1} mean value. (v) In early November, a spike in Chl '*a*' data was noticed for about 3 days, although values above 10 µg L^{-1} mainly appeared during one day. This particular peak, behaves more like a drift in the sensor data than a bloom since values dropped from one hour to the next by almost 7.7 µg L^{-1}. Two close peaks showed in the last weeks of measurements; (vi) one for 7 days and averaging 9.2 µg L^{-1}

and less than a week after (vii), a 5-day peak with a mean value of 8.5 µg L^{-1}. The last three peaks mentioned, appeared in a time of the year when blooms in this estuary are not that common and were not reflected in the oxygen saturation time series.

Several peaks of turbidity were observed in 2018, especially in the period from November onwards (Fig 3.11f). The maximum value of the year (57.1 FTU) was detected within this time, however, a spike in August reached 49.9 FTU and one in April, 49.1 FTU. Turbidity presented a period of almost two months (June and July) of values remaining below 18 FTU.

Daily values of I_0 remained under 1500 Wh m^{-2} d^{-1} until an increase that took them to ~2440 Wh m^{-2} d^{-1}, in less than two weeks, in late-April (Figure 3.11g). From then, until August, the maximum monthly averages (>1950 Wh m^{-2} d^{-1}) were observed and the highest daily value of 3774.2 Wh m^{-2} d^{-1} was identified as part of the peak in late-June. Values after October mainly stayed below 1000 Wh m^{-2} d^{-1}.

I_m calculations presented daily values above 1550 Wh m^{-2} d^{-1} for the period between May and early August, with the highest point of 3116.4 Wh m^{-2} d^{-1} in June and being July the month with the highest average (2357.5 Wh m^{-2} d^{-1}), just as observed in Figure 3.11h. It is noticeable that during August; a similar range of values seen across the first three months was detected from 2726 to 429 Wh m^{-2} d^{-1} in about 20 days.

The windiest month was January followed by December (Fig. 3.11i), both presenting regular gusts above 11 m s^{-1}. From May to August, daily averages remained below 7.5 m s^{-1} and only two separate days surpassed 9 m s^{-1} gusts.

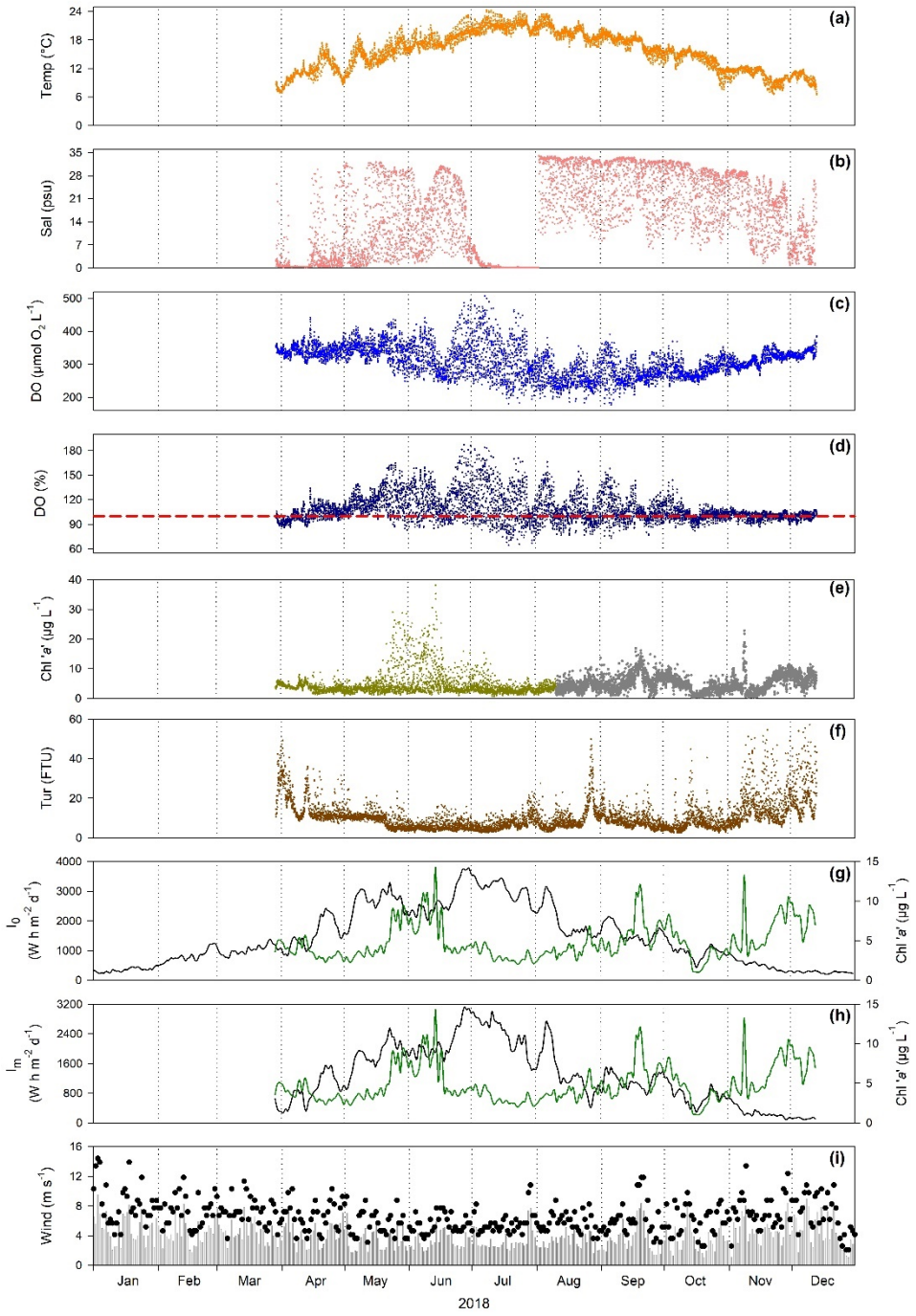

Fig 3.11 Time series of environmental conditions at the Data Buoy in Christchurch Harbour Ferry Pontoon in 2018. (a) Temperature, (b) salinity, (c) DO in concentration and (d) DO in percentage saturation, (e) chlorophyll '*a*' and (f) turbidity are presented as hourly values with dots ● of different colours. In (d), the red dashed line – – represents 100% of saturation. In (e), chlorophyll 'a' values generated by a model are shown as grey dots ●. 7-day running mean of (g) surface irradiance I_0 and (h) mean water column irradiance I_m are presented as black lines —, with daily mean chlorophyll '*a*' concentration included as a green line —. (i) Wind speed is represented as daily mean in vertical bars ▮ and maximum daily values in black circles ●.

3.4 Seasonal and interannual trends and comparison between estuaries

3.4.1 Phytoplankton correlation with abiotic parameters

The most frequently used parameter to measure or estimate changes in phytoplankton biomass in marine and freshwater environments is the concentration of chl '*a*' (Cloern, 1996), and with the addition of hydrological and meteorological parameters, spatial and temporal patterns can be inferred. However, the relationship between chlorophyll and abiotic parameters is not fixed but site-specific (Niu *et al*., 2016); it is often shown that it is not just one physical factor controlling the initiation of blooms but instead interactions between processes (Henson *et al*., 2006), hence the importance of monitoring as many systems as possible and including a vast range of environmental parameters. Spearman's rank coefficients were used to understand the relationship between chl '*a*' concentration and various measured environmental parameters in both the Southampton Water (SOT) and Christchurch Harbour (CHR) estuaries (Table 3.1).

Analysing the complete time series for the two systems, I_0 is revealed as the parameter that correlates strongly with chl '*a*' in SOT for the complete time series (ρ=0.71) but less strongly in CHR (ρ=0.39). Considering individual years, all but 2020 (ρ=0.46) in SOT showed strong positive correlations to I_0 (ρ>0.55), and similarly in CHR from 2014 to 2016 (ρ>0.55), whereas in 2017 (ρ=0.31), a weaker correlation was observed. A very similar relationship among sites for the complete time series could be observed for I_m, with SOT presenting a strong correlation (ρ=0.54) while CHR a weaker one (ρ=0.35). In SOT, 2014-2016 and 2019

showed strong correlations (ρ>0.55), 2018 a moderate (ρ=0.49) and 2020 a weaker relationship (ρ=0.32). Meanwhile, for CHR, only 2016 showed a strong correlation with I_m (ρ=0.62), while 2014 and 2015 a moderate (ρ=0.53 and ρ=50) and 2017 a weak relationship (ρ=0.26). Noticeably, 2018 in CHR presented an irregular negative correlation with both I_0 and I_m (ρ=-0.30 and ρ=-0.24) which certainly affected the degree of correlation for this site's complete time series analysis. Light availability has previously been described as a critical driver of bloom initiation for SOT (Iriarte & Purdie, 1994) and correlations point at CHR presenting the same behaviour.

Besides the parameters related to light availability, temperature showed, at both sites, a significant correlation for the whole time series and at each individual year. A strong correlation (ρ>0.55) between temperature and chlorophyll concentration was present for the whole times series at SOT and most individual years apart from 2018. At the CHR site, a less strong relationship was evident for the whole time series (*p*=0.31) and with moderate relationships (0.40<ρ<0.54) for 2016 and 2017. For 2018 at CHR, a negative correlation (ρ=-0.25) between temperature and Chl '*a*' suggested that the chlorophyll data may have been less accurate towards the end of the year. It is known that temperature affects phytoplankton physiology and metabolic processes (Trombetta *et al*., 2019), and in a previous study at a coastal site in the Western English Channel, it was identified that phytoplankton biomass growth was potentially governed by temperature control on enzymatic processes associated with carbon fixation (Barnes *et al*., 2015).

Table 3.1. Spearman's correlation coefficients relating chlorophyll concentration with environmental conditions.

Location	Period	I_0	I_m	Tidal range	Wind speed	Temp	Sal	O_2%	Turb	River flow
Southampton Water	Whole TS	**0.71**	**0.54**	ns	**-0.09**	**0.61**	**0.19**	**0.39**	ns	**-0.32**
n=	2014	**0.86**	**0.78**	ns	**-0.16**	**0.92**	**0.44**	**0.56**	**-0.17**	**-0.42**
	2015	**0.81**	**0.71**	ns	**-0.12**	**0.79**	**0.70**	**0.25**	**-0.27**	**-0.65**
	2016	**0.85**	**0.76**	ns	ns	**0.73**	ns	**0.31**	**-0.40**	**-0.19**
	2018	**0.76**	**0.49**	ns	**-0.14**	**0.43**	ns	**0.43**	**0.29**	**0.18**
	2019	**0.89**	**0.77**	ns	ns	**0.76**	**0.25**	**0.44**	**-0.20**	**-0.65**
	2020	**0.46**	**0.32**	**0.18**	ns	**0.62**	**0.49**	**-0.11**	ns	**-0.56**
Christchurch Harbour	Whole TS	**0.39**	**0.35**	---	ns	**0.31**	ns	**0.35**	**-0.09**	**-0.12**
n=	2014	**0.61**	**0.53**	---	ns	**0.58**	ns	**0.57**	**-0.26**	**-0.35**
	2015	**0.62**	**0.50**	---	ns	**0.66**	**0.45**	**0.31**	**0.27**	**-0.56**
	2016	**0.65**	**0.62**	---	ns	**0.28**	ns	**0.50**	**-0.39**	**0.18**
	2017	**0.31**	**0.26**	---	**0.12**	**0.38**	ns	ns	ns	ns
	2018	**-0.30**	**-0.24**	---	**0.18**	**-0.25**	**0.24**	ns	ns	ns

Values in bold $p < 0.05$. Values underlined represent absolute coefficient with strong correlation, $\rho > 0.55$.
ns = no significant relationship

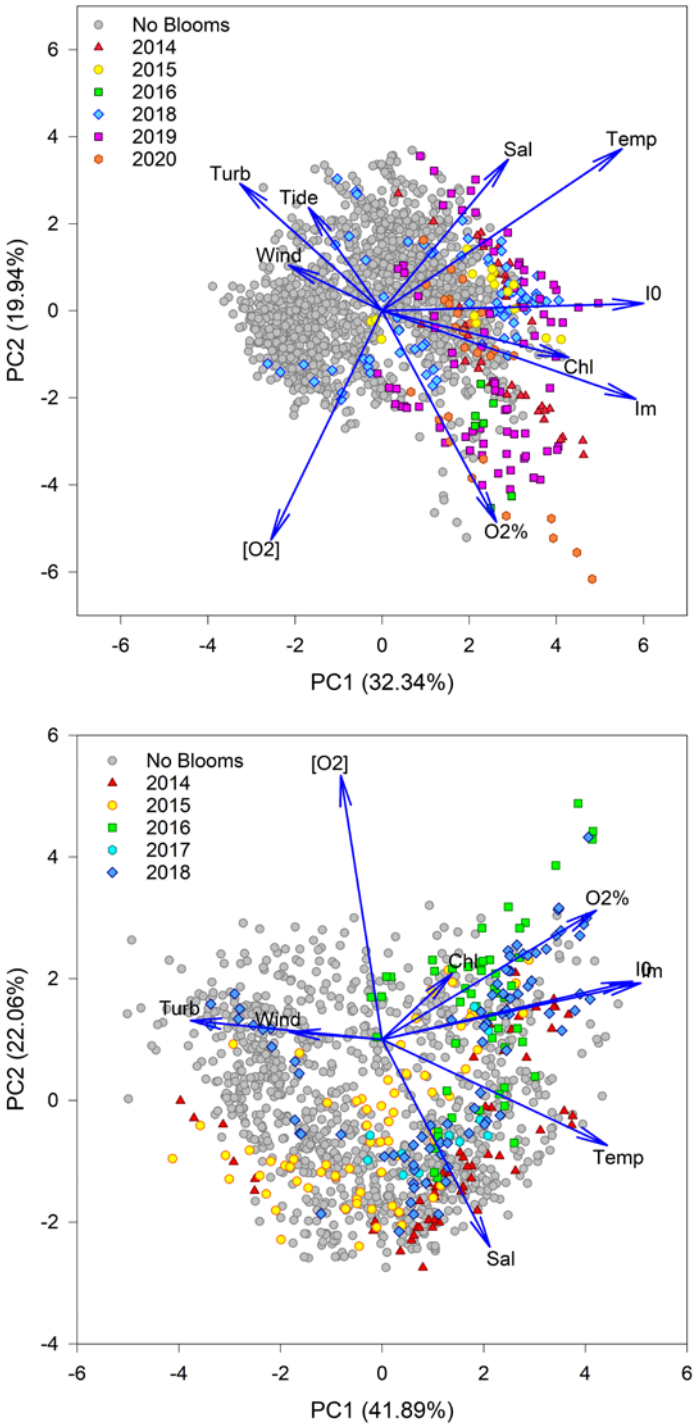

Fig 3.12 Principal Component Analysis (PCA) of environmental conditions for (a) Southampton Water and (b) Christchurch Harbour Ferry Pontoon. Bloom events and years have been used as factors to illustrate the clusters: No blooms in all years (grey circles ●), 2014 blooms (red triangles ▲), 2015 blooms (yellow circles ●), 2016 blooms (green squares ■), 2017 blooms (light blue hexagons ⬢), 2018 blooms (blue diamonds ◆), 2019 blooms (pink squares ■) and 2020 blooms (orange hexagons ⬢). Arrows → represent the variable and the direction of an arrow indicates its relation with the Principal Component (PC) and other variables. Temp=temperature, Sal=salinity, Chl=chlorophyll '*a*', I0=surface water irradiance, Im=mean water column irradiance, O2%=DO in percentage saturation, [O2]=DO concentration, Wind=wind speed, Turb=turbidity and Tide=tidal range.

Regarding oxygen parameters, oxygen saturation presented moderate positive correlations with chlorophyll at both sites for the complete data set (SOT ρ=0.39 and CHR ρ=0.35). For 2014, a stronger (ρ>0.55) correlation was evident in both systems. A moderate relation (0.40<ρ<0.54) was exhibited in SOT in 2018 and 2019 and CHR in 2016. Weaker correlations (ρ<0.39) were observed in SOT and CHR in 2015 and 2016 only in SOT. Dissolved oxygen concentration in coastal regions is controlled by physical processes such as atmospheric exchange and ocean circulation as well as water temperature (Cravo *et al*., 2020). However, its close relationship to phytoplankton biomass is due to its direct release and consumption during photosynthesis and respiration respectively (Yuan *et al*., 2016).

Chl '*a*' showed no direct relationship with turbidity for the complete time series for both sites; however, individual years at both sites presented some significant correlations; e.g. in SOT negative correlations (ρ<-0.40) in 2015, 2016 and 2019 and a positive correlation (ρ=0.29) in 2018, while CHR presented negative correlations (ρ<-0.39) in 2014 and 2016 and positive correlation for 2015 (ρ=0.27). Turbidity relates to decreasing phytoplankton biomass since it reduces light availability, but variations in turbidity can be driven by interactions between physical and biological processes such as wind and tides (e.g. May *et al*., 2003).

Daily rates of riverine inflow measurements from the River Test were used in the analysis for SOT and from the River Avon for CHR. This parameter showed an overall moderate negative correlation to Chl '*a*' in SOT (ρ=-0.32) and a very weak correlation in CHR (ρ=-0.12). However, considering individual years, data for CHR in 2015 presented a strong negative correlation (ρ=-0.56), and in 2014 a moderate one (ρ=-0.35). In the case of SOT, 2015, 2019 and 2020 showed strong

negative correlations (ρ<-0.55) and 2014 a moderate relation (ρ=-0.42). Freshwater inflow can favour phytoplankton growth; nevertheless, in small estuarine systems, intense pulses of freshwater can flush out the phytoplankton community (Cloern & Jassby, 2010; Peierls *et al*., 2012).

Influence of environmental conditions on major bloom events, at both estuaries, for each year of study is shown in Figure 3.12. SOT being a deeper ecosystem showed a closer relationship with I_m and with Chl 'a', and an inverse connection to turbidity, wind speed and tides, with O_2 being more related (inversely) to temperature and salinity. The shallower estuary (CHR), related strongly to Chl 'a' and to O_2, and slightly to I_0 and I_m, and inversely to turbidity and wind with O_2 related inversely to salinity as well. In terms of blooms, SOT has stronger relationship to I_m and O_2 than CHR, which presents more spread in data and weaker influence of Chl 'a' in bloom event separation. The classification of blooms through the PCA analysis did not reflect any major influence of tidal range, turbidity, or wind speed; however, it was observed for both estuaries, that late-year blooms in 2018 correlated with such parameters.

3.4.2 Timing of blooms

Temporal patterns of bloom distribution can be inferred from the PCA results (Fig. 3.12). The majority of days classified as within bloom events are explained by parameters affected by seasonality (i.e. temperature, I_0 and I_m), indicating the presence of warmer waters and extended hours of light availability, as well as greater irradiance levels within the water column, favouring the appearance of phytoplankton blooms in both estuaries.

The period when blooms were observed in CHR was longer than in SOT, with an average duration of 153 (~5 months) and 121 (~4 months) days, respectively.

CHR estuary shows (Fig. 3.13b) the typical dynamics of the coastal temperate systems (e.g. Martellucci *et al*., 2021), which are characterised by spring and autumn blooms and significant interannual variability; while SOT follows a different pattern of bloom occurrence, particularly during spring and summer (Fig. 3.13a). Both estuaries showed blooms typically persisting for days or even weeks during spring before dissipating, followed by additional biomass peaks in late summer or autumn that may be stimulated by an excess in nutrients (Winder & Cloern, 2010).

Riverine inflow (and possibly nutrients) increased in both estuaries during the winter months through elevated riverine inflow (e.g. Nedwell *et al*., 2002). Nevertheless, phytoplankton biomass remains low mainly due to limiting surface light availability (Fig. 3.14 & 3.15). Spring blooms marked the beginning of the productivity period each year at both locations, except for 2014 at both sites, where data was not available from the autonomous monitoring until May. Certainly, the most described seasonal pattern in coastal regions is the spring bloom (e.g. Martellucci *et al*., 2021; Niu *et al*., 2016; Trombetta *et al*., 2019; Zingone *et al*., 2010), and it is particularly pronounced in northern latitudes (e.g. Henson *et al*., 2006). Previous work identified the existence of spring blooms in the Southampton Water estuary (Iriarte & Purdie, 2004; Kifle & Purdie, 1993; Wright *et al*., 1997) and an extended study on phytoplankton blooms in estuarine coastal waters around the world (Carstensen *et al*., 2015) found that the spring bloom was the most common seasonal bloom across all regions, occurring in April-May in European coastal regions at similar latitudes to the ones studied in the present research.

A previous 5-year monitoring (1999–2003) of phytoplankton dynamics in SOT characterised the system with distinctive spring and summer blooms (Holley *et al*., 2007) and the main spring bloom occurring around May, similarly to that observed in this research (Fig. 3.13a). In comparison, a study of the temporal variation of chlorophyll '*a*' in a coastal region in the Western English Channel (Smyth *et al*., 2010) showed that the area presents distinct spring and autumn phytoplankton blooms, just as seen for CHR in the present study (Fig. 3.13b). This extended studied site is highly influenced by the Tamar estuary and presents very well mixed waters during the autumn and winter months and a more stratified water column in spring-summer. A similar temperature-driven stratification process, but in much lesser magnitude, could be occurring in SOT since temperature seems to play a major role in bloom initiation. However, in CHR, given that years when autumn blooms were highly marked (2015 & 2018) correlated with salinity, a possible stratification due to horizontal and vertical density gradients generated by difference in salinity could be reducing turbulence and enhancing resuspension (Zehrer *et al*., 2015).

Blooms are generated from a combination of different critical factors, and most of the time, through interaction between them (e.g. Niu *et al*., 2016). The initiation of the spring bloom in all years evaluated in SOT occurred when I_0 values were above 1314 Wh m^{-2} d^{-1} in combination with light penetration in the water column (I_m values) above 188 Wh m^{-2} d^{-1} as observed in Figure 3.14. A similar value of I_0 (1245 Wh m^{-2} d^{-1}) was identified for CHR spring bloom initiation, but as it can be appreciated in Figure 3.15, for this system I_m data was consistently above 640 Wh m^{-2} d^{-1} mostly due to the shallower water column. I_0 values are an indication of patterns in bloom development shaped by the annual cycle of solar radiation

(e.g. Rumyantseva *et al*., 2019), differing from I_m which is affected by other shorter timescale processes, like tidal currents. I_0 values found at the initiation of blooms in SOT and CHR are above the range (500 – 800 Wh m^{-2} d^{-1}) found by Martellucci *et al*. (2021) for an ecosystem on the Italian coast with very marked spring and autumn blooms, but below previous values reported for the Southampton Water estuary by Iriarte & Purdie (2004) where blooms occurred consistently with I_0 > 2000 Wh m^{-2} d^{-1}. Regarding I_m, the critical theoretical value, according to Riley (1967), for a sustained increase in phytoplankton biomass, in temperate coastal and estuarine waters is 193 Wh m^{-2} d^{-1}; with results from the current study suggesting a similar value of I_m for SOT. However, for the CHR a much larger value of I_m above Riley's value, was evident which could relate to the shallower conditions in CHR since PAR within the water column varies according to changes in depth (e.g. Cloern *et al*., 2014). Previous research done in the Southampton Water estuary by Iriarte & Purdie (2004) reported that Chl '*a*' levels above 10 µg L^{-1} occurred when I_m averaged for the previous 7 days exceeded 380 Wh m^{-2} d^{-1}.

When considering turbidity measurements at the onset of blooms, <8.4 FTU for SOT and <31.7 FTU for CHR, it is no surprise that a lower I_m value was registered for SOT. Furthermore, CHR is a more turbid estuary presenting an average during blooms of 11.2 ± 9.0 FTU, while SOT mean value was 4.1 ± 2.7 FTU. Nevertheless, phytoplankton growth in CHR does not seem to be light-limited since blooms initiate at a similar time of the year as in SOT; this is likely to be due to its shallower water column depth that allows enough light energy required for photosynthesis (e.g. Cloern, 1996), despite the elevated turbidity present.

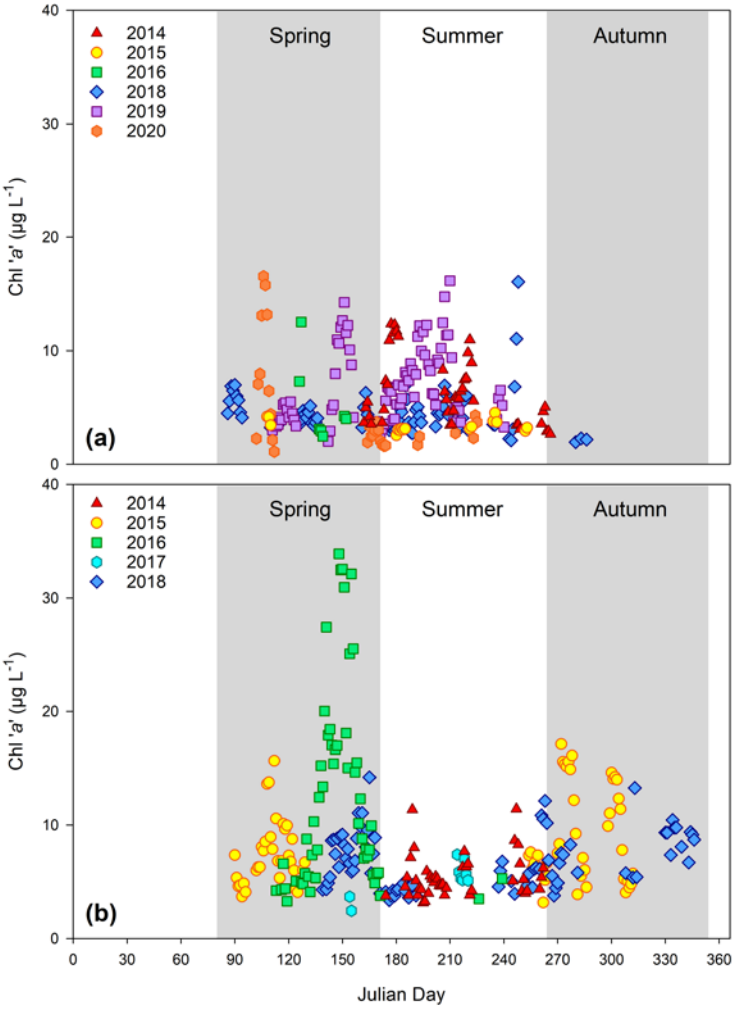

Fig 3.13 Chlorophyll '*a*' daily concentration during bloom events from 2014 to 2020 in (a) Southampton Water estuary and (b) Christchurch Harbour Ferry Pontoon. The Spring and Autumn bloom periods have been background shaded in light grey, while the Sumer bloom period has a white background.

The temperature was also identified as a primary driver of the spring blooms, with SOT events commonly appearing when water reached values >11.8°C and an average of 12.2 ± 0.3°C, excluding 2014 when measurements started later in the year (May), hence, by the time the first bloom was recorded temperature had reached 17.7°C. For CHR, the temperature at the beginning of the spring bloom ranged from 9.8°C in 2015 to 17.2°C in 2017, showing no clear set value to initiate events. This wider range of water temperature can perhaps indicate that blooms in this estuary are initiated by an increase in water temperature rather than a

threshold temperature value, similar to that described by Trombetta *et al*. (2019) for a Mediterranean shallow coastal lagoon with a similar yearly temperature range to the CHR site.

3.4.3 The magnitude of blooms and interannual variability

Interannual variability of environmental conditions can affect, positively or negatively, the magnitude of blooms within a system (e.g. Leterme *et al*., 2014). Therefore, it is clear the importance of studying extended time series that allows the comparison among years and permits the possibility of predictions.

SOT presented an average of daily Chl '*a*' during bloom events and across the time series of 5.6 ± 3.2 µg L^{-1}, while CHR showed a mean value of 8.2 ± 5.3 µg L^{-1}, approximately 1.5 times higher than the one calculated for SOT. Analysing the range of data, a similar pattern was observed, where CHR (9.5 – 130 µg L^{-1}) presents, in general, higher biomass concentrations than SOT (4.9 – 33.4 µg L^{-1}). With blooms detected in CHR occasionally reaching values above 30 µg L^{-1} (17.2% of bloom observations), while in SOT only during the maximum peak of 2020, was this threshold exceeded (1.2% of bloom observations) as shown in Figures 3.15 and 3.14, respectively.

Holley *et al*. (2007) review of the magnitude of phytoplankton blooms at a Southampton Water mid-estuary location showed that maximum annual Chl '*a*' values range from 17.2 to 38.2 µg L^{-1} during their 5-year study (1999–2003). A similar variation was observed in this study in SOT of 6.6 – 33.4 µg L^{-1}, especially if considering that besides 2015, the other years maxima were above 16 µg L^{-1}. However, Holley *et al*. (2007) states these major peaks occurred around day 140 of the year, a pattern not observed in SOT but seen in CHR (Fig. 3.13b).

A lower Chl '*a*' concentration was used to describe a phytoplankton bloom in the Southampton Water estuary, during the ~100-day monitoring done by Wright *et al*. (1997), where values of 3.6 µg L^{-1} represented an increase from the general range detected of 0.5 – 1.0 µg L^{-1}. This value is closer to the 5.0 µg L^{-1} threshold used to delimit blooms in the current work than the 10.0 µg L^{-1} previously used for the same location by Holley *et al*. (2007) and Iriarte & Purdie (1994). In the same study by Wright *et al*. (1997), the bloom was identified in summer, the same season where SOT higher Chl '*a*' peaks were observed for most years studied (Fig. 3.13a).

Previous measurements of Chl '*a*' made at the L4 site in the Western Channel as representative of coastal waters (~12 km offshore), defined a blooming pattern dominated by autumn blooms from 4.0 µg L^{-1} (Kitidis *et al*., 2012) to 12.0 µg L^{-1} (Smyth *et al*., 2010). Autumn blooms were present almost exclusively in CHR, especially in 2015 and 2018, which could infer that the CHR system presents a similar seasonality pattern to the Tamar estuary, although CHR is a much smaller and shallower estuary than Tamar. Given the general lower biomass observed in coastal waters, the overall lower concentrations of Chl '*a*' in SOT could indicate more oceanic waters entering the system compared to CHR.

The magnitude of coastal phytoplankton blooms is highly variable across the world, ranging from coastal ecosystems with typically low concentrations of Chl '*a*' such as the Mediterranean Thau Lagoon presenting mean values ~ 2 µg L^{-1} during spring blooms and concentrations between 2.8 and 3.6 µg L^{-1} while experiencing winter blooms (Trombetta *et al*., 2019); to systems with marked seasonal changes like the Mediterranean Lagoon and the Bay of Bizerte (Salhi *et al*., 2018), displaying maximum mean values during a summer bloom of 15.8

and 8.5 µg L^{-1}. It is also possible to find highly eutrophicated and stratified systems like the Sundays Estuary in South Africa, where exceptional maximum Chl '*a*' values during autumn blooms above 100 µg L^{-1} have been reported (Lemley *et al*., 2018).

The highest concentration of biomass during a single bloom period in SOT was observed in 2019 during summer when the longest event recorded (48 days) coincided with the highest values of I_0 of the year (3313 Wh m^{-2} d^{-1}) and a reduced moderate turbidity period (<8.8 FTU). However, the maximum chlorophyll peak of the time series was observed in the spring of 2020 during a period of low turbidity (<3.6 FTU), and low wind (<4.7 m s^{-1}) was detected at the time of the year when I_0 started to increase, resulting in a rapid rise of I_m values (Figure 3.14). Unfortunately, there is no additional data to corroborate this chlorophyll peak since there was no regular chlorophyll sampling from March to June 2020 in SOT due to COVID restrictions and similarly, there is no EA data available, as their sampling had also been stopped. In contrast, the lowest chlorophyll values during a bloom in SOT were detected in 2015, although there were no apparent major differences from other years, except a strong correlation between Chl '*a*' and salinity. This could indicate the effect of riverine inflow on the system, given that 2015 was one of the two years presenting the highest correlation with freshwater input (Table 3.1). Even though it is known that a high freshwater runoff in estuarine systems can cause reduced phytoplankton biomass by preventing the accumulation of cells in the mixed layer (Levasseur *et al*., 1984; Peierls *et al*., 2012), this does not seem to be the case for SOT given that although 2015 presented a low river inflow, the lowest annual flow recorded

was in 2019 when the total biomass was much higher than the other years analysed (Fig. 3.14e).

The maximum chlorophyll biomass and peak in CHR was observed in 2016, a year that showed the highest correlation to low turbidity and elevated I_m, which was represented by the biggest peak appearing during an extended low turbidity period (<9.6 FTU) and when the first values above 2000 Wh m^{-2} d^{-1} of I_m appeared in the year. Conversely, the smallest peak and the lower biomass observed in CHR was during the following year, 2017, when daily turbidity varied more (8.3 – 12.9 FTU) and was reflected in pronounced peaks of I_m (Figure 3.15). 2018 was an unusual year in CHR, presenting the latest autumn blooms observed in Figure 3.13b. Although autumn blooms were identified previously in the estuary in 2015, the correction performed to Chl 'a' 2018 data may be the cause for such high concentrations later in the year, and the reason for such unusual negative correlations between Chl '*a*' and both light parameters and temperature (see the previous section). Regarding riverine inflow, as in SOT, the high flow was not a clear driver of higher phytoplankton biomass in CHR; where the highest riverine annual flow, by almost double in magnitude, was observed in 2014, but the blooms during that year were not particularly higher or more numerous (Fig. 3.15e).

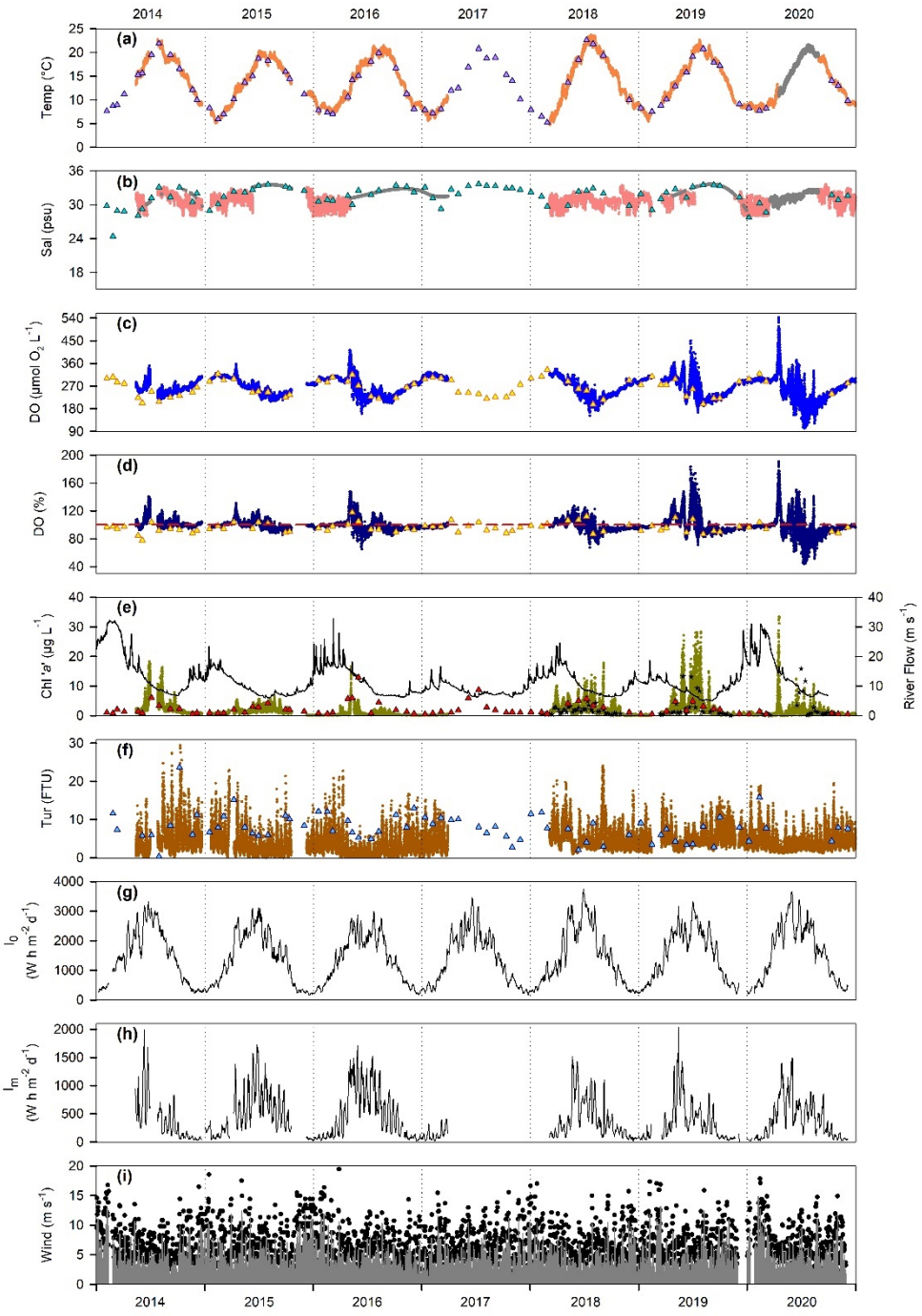

Fig 3.14 Time series of environmental conditions at the Data Buoy in Southampton Water from 2014 to 2020. (a) Temperature, (b) salinity, (c) DO in concentration and (d) DO in percentage saturation, (e) chlorophyll '*a*' and (f) turbidity are presented as hourly values with dots ● of different colours. In (a) and (b), temperature and salinity values generated by a model are shown as grey dots ●. In (d), the red dashed line – – represents 100% of saturation. In (e) ★ represent discrete chlorophyll samples taken independently and the daily river flow is indicated as a black line —. Environmental agency sampling points are shown as triangles ▲ in different colours in (a) to (f). 7-day running mean of (g) surface irradiance I_0 and (h) mean water column irradiance I_m are presented as black lines —. (i) Wind speed is represented as daily mean in vertical bars ▮ and maximum daily values in black circles ●.

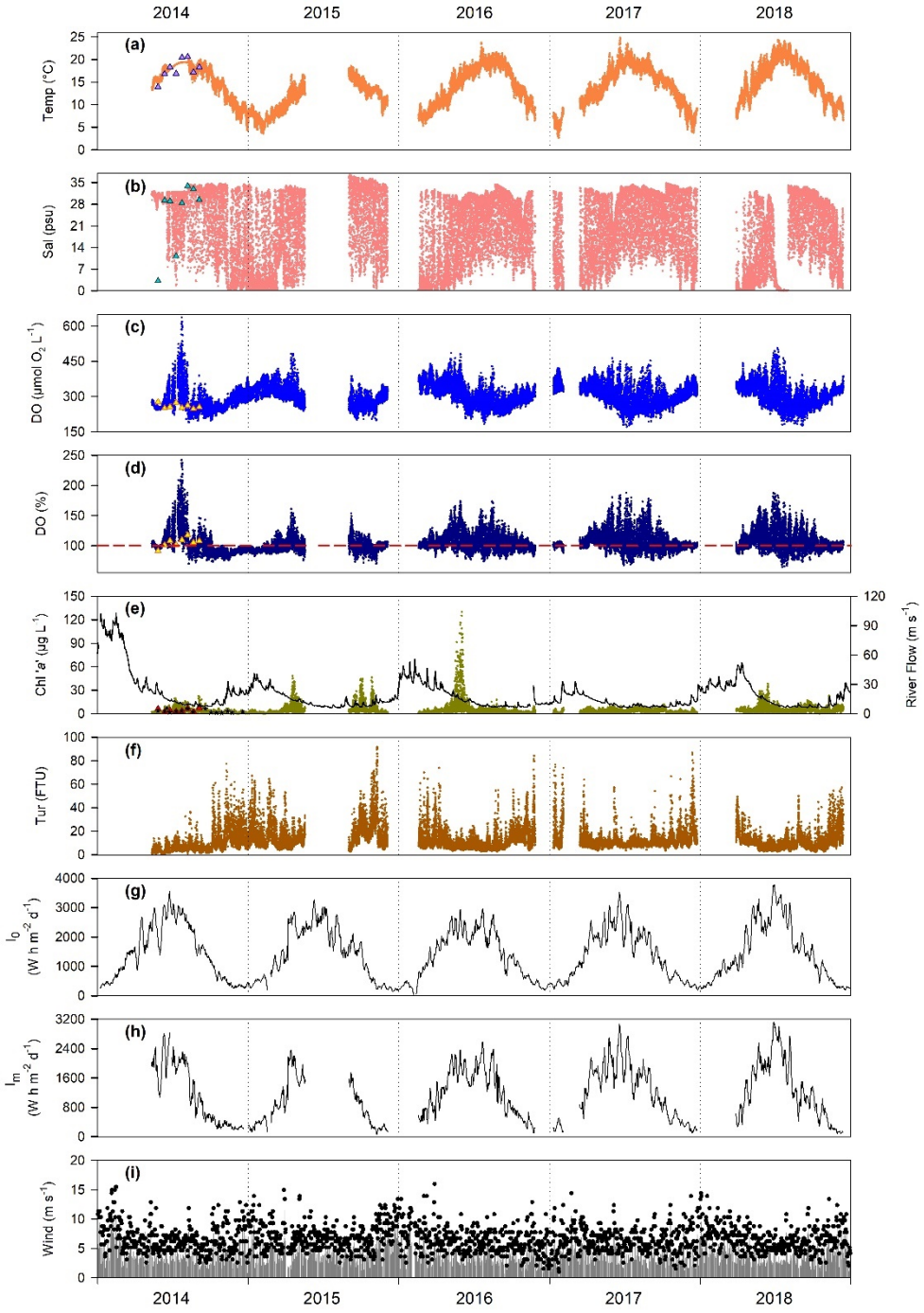

Fig 3.15 Time series of environmental conditions at the Data Buoy in Christchurch Harbour Ferry Pontoon from 2014 to 2018. . (a) Temperature, (b) salinity, (c) DO in concentration and (d) DO in percentage saturation, (e) chlorophyll '*a*' and (f) turbidity are presented as hourly values with dots ● of different colours. In (a) and (b), temperature and salinity values generated by a model are shown as grey dots ●. In (d), the red dashed line – – represents 100% of saturation. In (e) ★ represent discrete chlorophyll samples taken independently and the daily river flow is indicated as a black line —. Measurements taken with an independent probe are shown as triangles ▲ in different colours in (a) to (e). 7-day running mean of (g) surface irradiance I_0 and (h) mean water column irradiance I_m are presented as black lines —. (i) Wind speed is represented as daily mean in vertical bars ▮ and maximum daily values in black circles ●.

Both estuaries showed the highest blooms coinciding with prolonged periods of low turbidity. High turbidity can limit phytoplankton growth by reducing light availability in the water column. In shallow estuaries, the leading cause of changes in turbidity is the tidal variation (e.g. Bucci *et al*., 2012), as can be observed in SOT where frequent water level data was available.

3.4.4 Tidal analysis for Southampton Water

Water level data analysed for the Southampton Water estuary showed a positive correlation (ρ=0.52) between tidal range and turbidity, indicating that turbidity in the system generally increases with the presence of spring tides. In shallow estuaries, the principal cause for changes in turbidity is the vertical mixing driven by tidal currents (e.g. Bucci *et al*., 2012).

Despite the absence of a statistical relationship between Chl '*a*' concentration peaks, more specifically blooms, and tidal range in SOT (Table 3.1), individual blooms were observed to develop mainly during neap tides to then dissipate with the arrival of the following spring tide; this relation was well represented in 2020, the only year of the time series where tidal range and Chl '*a*' showed a small but significant correlation (ρ=0.18); during this year, all five identified blooms occurred during weak neap tides (Fig. 3.6). Bucci *et al*. (2012) described a similar situation, where reported phytoplankton summer blooms in the São Vicente estuary (Brazil) usually occurred towards the end of neap tides, but no significant correlation to found. This lack of correlation to the tidal range, in addition to the strong correlations between phytoplankton peaks and I_m and temperature (as discussed in previous sections), indicate that blooms in SOT are not only regulated by turbulent mixing due to tides but a

combination of factors affecting the solar radiation attenuation throughout the water column (e.g. Cloern *et al*., 2014).

According to a previous study on the phytoplankton dynamics in Southampton Water (Wright *et al*., 1997), the tidal range observed during spring tides in this study (~ 5m) is high enough to decrease water column stability, inhibit growth, and, perhaps, decrease retention time meaning a proportion of phytoplankton can be flushed from the estuary. In most shallow estuaries where the neap-spring cycle is present, like in SOT, fortnightly patterns of reduced mixing during neap tides can be observed and it is during these periods that phytoplankton net biomass growth is enhanced (e.g. Carstensen *et al*., 2015). Such pattern has been extensively reported by Cloern (1996) in his widespread review of phytoplankton bloom dynamics in the San Francisco Bay, a system with a similar depth to SOT (~10m) and a 2m tidal range.

3.5 Conclusions

The collection of high-frequency water quality data combined with meteorological information allowed an accurate and thoroughly comparison of the relationship between physical environmental conditions with the occurrence of phytoplankton blooms in two different temperate estuaries.

Phytoplankton distribution exhibited seasonal variability in both estuaries, with bloom initiation being primarily related to periods of ~7 days when a sudden increase in surface light availability (>800 Wh m^{-2} d^{-1}) was observed. Temperatures above 11.8°C correlated with the appearance of blooms in Southampton Water, while rising water temperature (<10°C) overlapping with

values of solar radiation above 1245 Wh m^{-2} d^{-1}, seemed to initiate blooms at the Christchurch Harbour estuary.

Despite being different in size, shape, average depth, tidal regime, and discharge, both estuaries showed similarities regarding the timing of the spring bloom, developing between April and May. However, whereas Christchurch displayed the typical dynamics described for coastal temperate estuaries, presenting mainly spring and autumn blooms, Southampton presented a pattern with blooms in spring and summer.

Higher concentration of phytoplankton biomass during blooms was associated with values of water column irradiance <188 Wh m^{-2} d^{-1} for SOT and <640 Wh m^{-2} d^{-1} for CHR), corresponding with lower turbidity (<8.4 FTU for SOT and <31.7 FTU for CHR,) and daily wind speed average below 4.7 m s^{-1}.

An additional analysis of the tidal cycle in the Southampton Water estuary identified that blooms typically developed during neap tides and dissipated during the following spring tide. This suggests that the tidal cycle creates stronger mixing conditions during spring tides leading to increased turbidity and creating lower mixing and possible stratification during neap tides that enhance phytoplankton biomass growth.

Chapter 4

Variability of net community production, gross primary production, and ecosystem respiration in two contrasting estuaries

Abstract

Measurements of primary production provide essential information about the trophic status of aquatic ecosystems. In this chapter, the open water diel oxygen method was applied to high-frequency water quality data collected from the Southampton Water (2014 – 2020) and Christchurch Harbour estuaries (2014 – 2018) to estimate ecosystem respiration (ER), gross primary production (GPP), and net community production (NCP). Trends in the overall trophic state of the two estuaries were identified, with Southampton becoming more net heterotrophic over the 7-year time series (from -1.3 to -48.7 mmol O_2 m^{-2} d^{-1}), while Christchurch Harbour showed an increasing net autotrophic state -11.7 to 19.8 mmol O_2 m^{-2} d^{-1}). A pattern was observed, where autotrophic conditions prevailed during summer and spring due to the dominant factors driving metabolic rates being related to seasonal changes in light availability, temperature, and riverine flow. Threshold values for the Southampton estuary and Christchurch Harbour of temperature (10.5 & 10.3 °C), surface water irradiance (1520 & 1240 Wh m^{-2} d^{-1}) and mean water column irradiance (415 & 950 Wh m^{-2} d^{-1}) were related to the appearance of extreme autotrophic and heterotrophic conditions.

The relationship between ecosystem respiration and gross primary production allowed classification of both estuaries between oligotrophic and mesotrophic states, with Southampton particularly leaning to mesotrophic conditions. Variance in Chl '*a*' concentration during phytoplankton blooms was explained by NCP rates in more than 75% for both estuaries. Regarding the methodology assumptions, an overestimation of ER was related to higher air-water transfer rates calculated through the model, due to high wind speeds.

4.1 Introduction

Almost half of global primary production occurs in the oceans (Cloern & Jassby, 2008). Furthermore, estuaries are one of the most productive marine ecosystems (Golubkov *et al*., 2017), especially those receiving an important runoff of nutrients from the basin (Butron *et al*., 2009; Hopkinson & Smith, 2005).

Phytoplankton account for most of ecosystem primary production in the majority of coastal ecosystems (Paerl & Justic, 2013), with phytoplankton primary production playing a central role in the ecological and biogeochemical dynamics of estuaries (Cloern *et al*., 2014). In coastal ecosystems spatio-temporal variability of primary production and phytoplankton biomass are the result of the interaction of a number of factors such as irradiance (May *et al*., 2003), temperature (Trombetta *et al*., 2019), nutrients (Davidson *et al*., 2012) and horizontal and vertical water movements (Silkin *et al*., 2019).

Net community production, also known as net ecosystem metabolism (eg. Shen *et al*., 2015), is a community-level process that integrates all of the processes affecting the balance between production and consumption (Duarte & Regaudie-De-Gioux, 2009; Garcia-Corral *et al*., 2021). It can be defined as the difference between gross primary production (GPP) and ecosystem respiration (R) (Lee *et*

al., 2022). When NCP>0, the ecosystem is net autotrophic, suggesting that the internal production of organic matter dominates. In contrast, if NCP<0, this indicates the system is net heterotrophic and depends on external sources of organic matter (Agusti *et al*., 2018; Herrmann *et al*., 2020; Loken *et al*., 2021). Estuaries are complex, open systems with the potential to be either autotrophic or heterotrophic systems (Hopkinson & Smith, 2005).

In systems with relatively homogeneous water masses, clear signals of diel changes in water-column O_2 and CO_2 concentration are often detectable and associated with net community production (Testa *et al*., 2012). Thus, NCP can be accurately estimated from the calculation of the oxygen flux at the air-sea interface (e.g. Tilstone *et al*., 2009) employing the open water diel oxygen method, first proposed by Odum (1956) and later modified to apply it to estuarine systems (Caffrey, 2003, 2004; Emerson *et al*., 2008).

Interaction between physical and biological processes within estuaries tends to vary over diurnal, semi-diurnal and sometimes episodic timescales (Cloern et al., 2016, Nidzieko *et al*., 2014) making the open water diel oxygen method an advantageous resource to measure the integrated metabolic activity of the entire ecosystem over a short time period since O_2 sensors can be deployed for weeks or more, allowing long-term measurements (Testa *et al*., 2012).

In this chapter, productivity rates (GPP, ER and NCP) were derived from high-frequency measurements of surface water dissolved oxygen concentration, for Southampton Water and Christchurch Harbour, using the open water diel oxygen method. The influence of environmental factors on productivity rates and their implications on the aquatic trophic state were evaluated.

4.2 Southampton Water time series analysis of ecosystem respiration, gross primary production, and trophic state: net community production.

Productivity rate calculations are derived from the dissolved oxygen, temperature, salinity, and wind speed time series data presented in Chapter 3 section 1. Data from 2017 was not included in the following individual-year results since only measurements for the first 3 months of the year were available.

Daily rates of net community production (NCP) can be either positive when gross primary production (GPP) exceeds ecosystem respiration (ER) indicating a net autotrophic state of the estuarine water column or negative reflecting a heterotrophic state of the system (Shen *et al*., 2019b).

4.2.1 Year 2014

For 2014, calculated ER rates presented a high variability throughout the year, ranging from 0.1 mmol O_2 m^{-2} d^{-1} in September to 221.4 mmol O_2 m^{-2} d^{-1} in May, as seen in figure 4.1a. A dynamic period was detected in May-June when the average estimate was 40.4 mmol O_2 m^{-2} d^{-1}, against 9.5 mmol O_2 m^{-2} d^{-1} for the rest of the year. Excluding this active period of ER, October and November presented maximum values of ~ 64.0 mmol O_2 m^{-2} d^{-1}, followed by 48.1 mmol O_2 m^{-2} d^{-1} in mid-August. September was the month with the lowest average value of ER (3.0 mmol O_2 m^{-2} d^{-1}), while the mean value in May of 60.0 mmol O_2 m^{-2} d^{-1} was the monthly highest of the year.

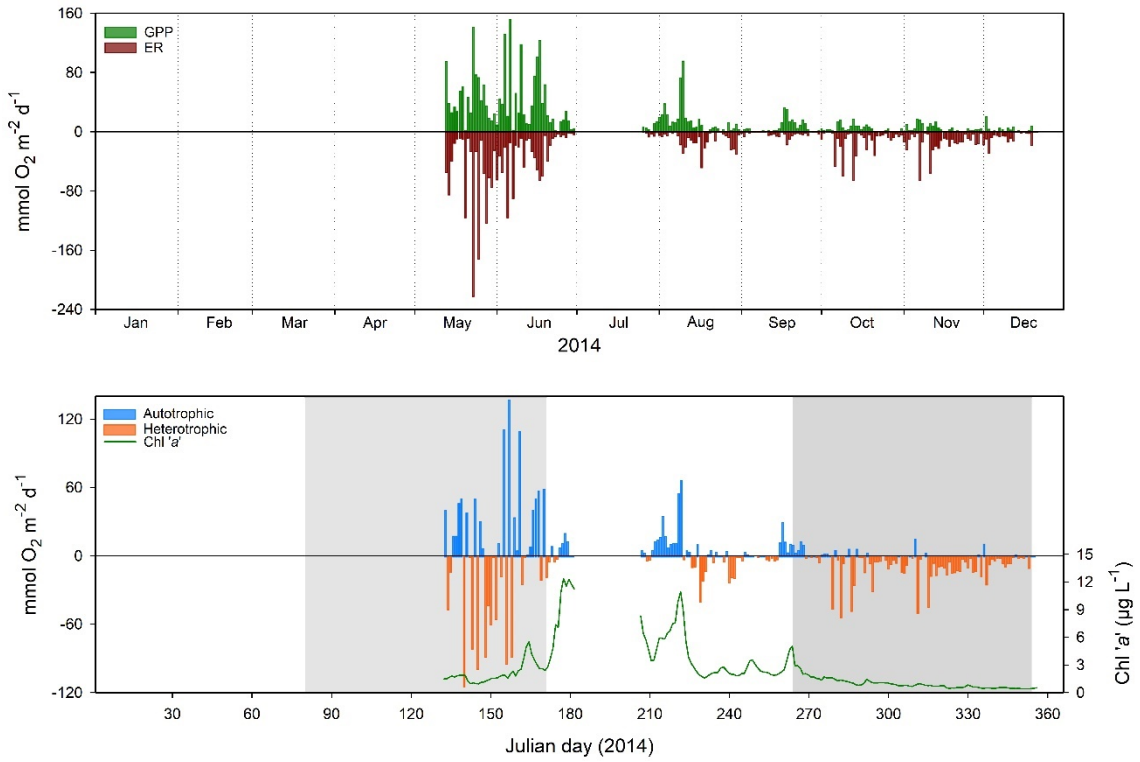

Fig 4.1 Time series for 2014 of (a) calculated daily respiration ER (red bars ▮) and gross primary production GPP (green bars ▮) and (b) calculated net community production in Southampton Water. In (a) ecosystem respiration data are displayed as negative values for convenience of graphing. In (b) negative values indicate net heterotrophic state (orange bars ▮), and positive values indicate net autotrophic state (blue bars ▮). Daily chlorophyll '*a*' is shown as a green line —.

GPP also exhibited noticeably higher calculations during May-June than for the rest of the year, with a mean value of 43.0 mmol O_2 m^{-2} d^{-1} during that period, and the year maximum of 151.5 mmol O_2 m^{-2} d^{-1} in June (Fig. 4.1a). From August to December, an average of 7 mmol O_2 m^{-2} d^{-1} was estimated, and a maximum daily value was observed in August (95.7 mmol O_2 m^{-2} d^{-1}). May presented the highest monthly mean of 47.3 mmol O_2 m^{-2} d^{-1}, followed closely by June with 40.2 mmol O_2 m^{-2} d^{-1}. GPP was low in December (3.0 mmol O_2 m^{-2} d^{-1}), and monthly values remained consistently below 6.5 mmol O_2 m^{-2} d^{-1} from September.

Annual NCP daily average was -1.3 mmol O_2 m^{-2} d^{-1}, indicating a slightly heterotrophic state. During this year there was a noticeable increase in NCP during spring, with the highest autotrophic (137.4 mmol O_2 m^{-2} d^{-1}) and

heterotrophic (-113.6 mmol O_2 m^{-2} d^{-1}) conditions of the year occurring within this season, only 16 days apart (Fig. 4.1b). During spring NCP oscillated between the two trophic states, but with autotrophic conditions dominating in late spring (+1.8 mmol O_2 m^{-2} d^{-1}); indicating a greater balanced between GPP and ER than during summer, which was more autotrophic (4.0 mmol O_2 m^{-2} d^{-1}) and autumn, that showed a general heterotrophic state (-6.6 mmol O_2 m^{-2} d^{-1}). During the summer, positive NCP values matched up with Chl '*a*' concentration peaks, particularly during the middle of summer when from day 211 to 222 NCP averaged +22.4 mmol O_2 m^{-2} d^{-1}, and then later from summer to autumn when NCP was +11.2 mmol O_2 m^{-2} d^{-1}.

4.2.2 Year 2015

ER in 2015 presented an average of 20.0 mmol O_2 m^{-2} d^{-1}, with occasional isolated high daily values from May to October (Fig. 4.2a), when the yearly maximum of 167.5 mmol O_2 m^{-2} d^{-1} was observed in August, followed closely by a peak in May of 160.3 mmol O_2 m^{-2} d^{-1}. However, it is important to highlight that only 4.9% of ER observations in 2015 exceeded 70 mmol O_2 m^{-2} d^{-1}, almost half of them identified in December. March was the month with the lower average ER estimate, of 9.0 mmol O_2 m^{-2} d^{-1}, while December showed a substantial increase in overall daily values, which was reflected in an average value of 55.6 mmol O_2 m^{-2} d^{-1}.

A yearly estimate of 12.0 mmol O_2 m^{-2} d^{-1} was obtained for GPP in 2015. Values remained consistently below 73 mmol O_2 m^{-2} d^{-1} throughout the year, except for one day in early-May that presented a value of 149.5 mmol O_2 m^{-2} d^{-1}, as reflected in figure 4.2a. Months showing an overall high GPP estimate were April (21.5

mmol O_2 m^{-2} d^{-1}) and June (22.4 mmol O_2 m^{-2} d^{-1}), meanwhile, the lowest monthly mean value of 5.1 mmol O2 m^{-2} d^{-1} was in March.

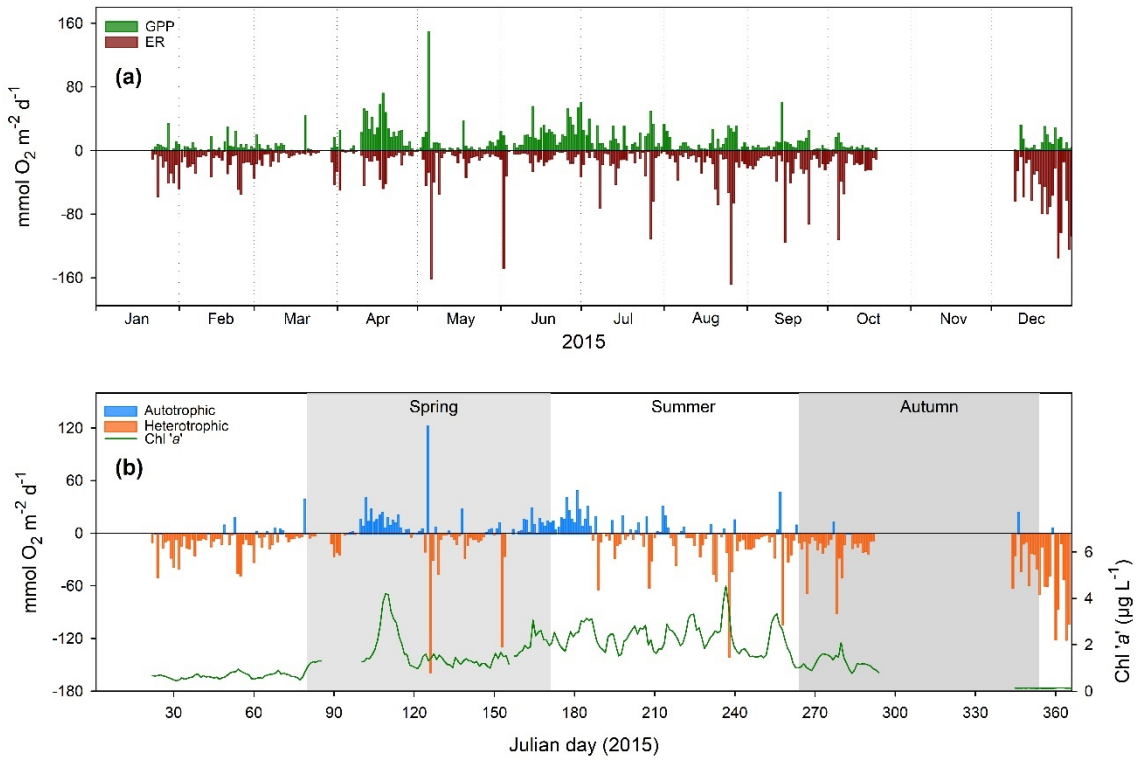

Fig 4.2 Time series for 2015 of (a) calculated daily respiration ER (red bars ▮) and gross primary production GPP (green bars ▮) and (b) calculated net community production in Southampton Water. In (a) ecosystem respiration data are displayed as negative values for convenience of graphing. In (b) negative values indicate net heterotrophic state (orange bars ▮), and positive values indicate net autotrophic state (blue bars ▮). Daily chlorophyll '*a*' is shown as a green line —.

Negative NCP rates dominated for much of the year with an annual average value of -8.2 mmol O_2 m^{-2} d^{-1}. Five daily values of high negative rates of NCP indicating heterotrophic conditions (<-90 mmol O_2 m^{-2} d^{-1}) were observed mainly in spring and summer, in addition to three days at the end of the year (Figure 4.2b). Additional negative NCP values were observed throughout the year without a clear pattern. One outstanding autotrophic daily value of +123.1 mmol O_2 m^{-2} d^{-1} was identified in the middle of spring just before the highest heterotrophic value was estimated (-157.3 mmol O_2 m^{-2} d^{-1}); unlike heterotrophic peaks, in the case of positive NCP of this magnitude, it was an isolated event. A prolonged period

of autotrophic conditions was observed for almost 25 days in the first half of the spring season, averaging 8.8 mmol O_2 m^{-2} d^{-1}. In addition, a second extended period of positive NCP daily values was calculated during the transition between spring and summer for ~30 days, averaging 15.3 mmol O_2 m^{-2} d^{-1}.

4.2.3 Year 2016

During 2016, ER showed a yearly average rate of 26.9 mmol O_2 m^{-2} d^{-1}, and a range of values from 0.1 mmol O_2 m^{-2} d^{-1} in April to a maximum of 244.9 mmol O_2 m^{-2} d^{-1} in May (Figure 4.3a). A period of low rates of ER was observed in March and April, when daily values remained below 52 mmol O_2 m^{-2} d^{-1}, with only one exceptional peak in March of 110.7 mmol O_2 m^{-2} d^{-1}. January presented the highest average rate of ER (45.4 mmol O_2 m^{-2} d^{-1}), followed closely by May (41.2 mmol O_2 m^{-2} d^{-1}) after which monthly values decreased until reaching 18.7 mmol O_2 m^{-2} d^{-1} in December.

GPP rates in 2016 displayed a distinct period of increased values in May (97.9 mmol O_2 m^{-2} d^{-1}), with three daily values above 200.0 mmol O_2 m^{-2} d^{-1}, and in addition a maximum of 334 mmol O_2 m^{-2} d^{-1}, as seen in Figure 4.3a. In contrast, in March, most of April, and from October to December average values below 7 mmol O_2 m^{-2} d^{-1} were estimated.

In 2016, over the whole year, the heterotrophic state dominated with an NCP average of -7.9 mmol O_2 m^{-2} d^{-1}. NCP values representing heterotrophic conditions and exceeding -100 mmol O_2 m^{-2} d^{-1}, were mainly observed during winter and some short periods in summer months (Fig. 4.3b). The main period of autotrophic conditions was identified during spring, when for 40 continuous days the NCP averaged 49.5 mmol O_2 m^{-2} d^{-1} and the maximum of 179.2 mmol O_2 m^{-}

^{2} d^{-1} was observed. The beginning of this extended period of positive NCP values coincided with increased Chl '*a*' concentration.

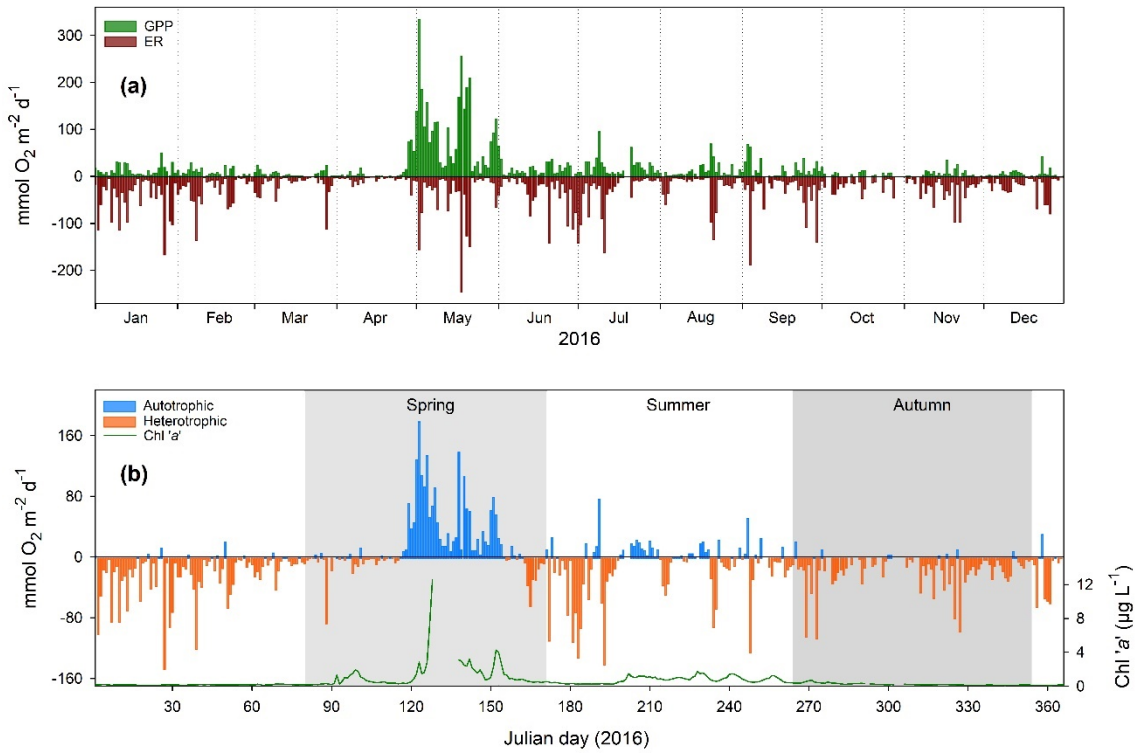

Fig 4.3 Time series for 2016 of (a) calculated daily respiration ER (red bars ▮) and gross primary production GPP (green bars ▮) and (b) calculated net community production in Southampton Water. In (a) ecosystem respiration data are displayed as negative values for convenience of graphing. In (b) negative values indicate net heterotrophic state (orange bars ▮), and positive values indicate net autotrophic state (blue bars ▮). Daily chlorophyll '*a*' is shown as a green line —.

4.2.4 Year 2018

During the first half of the 2018 (Figure 4.4a), ER estimated values remained below 90 mmol O_2 m^{-2} d^{-1}, with April having the lowest monthly average value of the year (8.1 mmol O_2 m^{-2} d^{-1}). At the end of July, peaks in ER started to occur, reaching the yearly daily maximum of 264.1 mmol O_2 m^{-2} d^{-1} in August; however, the highest average monthly ER value was in December (53.2 mmol O_2 m^{-2} d^{-1}). The annual average ER was 30.6 mmol O_2 m^{-2} d^{-1}, with two marked periods of increased rates from March to July with values below 19 mmol O_2 m^{-2} d^{-1}, and the second from August to December when values exceeded 45 mmol O_2 m^{-2} d^{-1}.

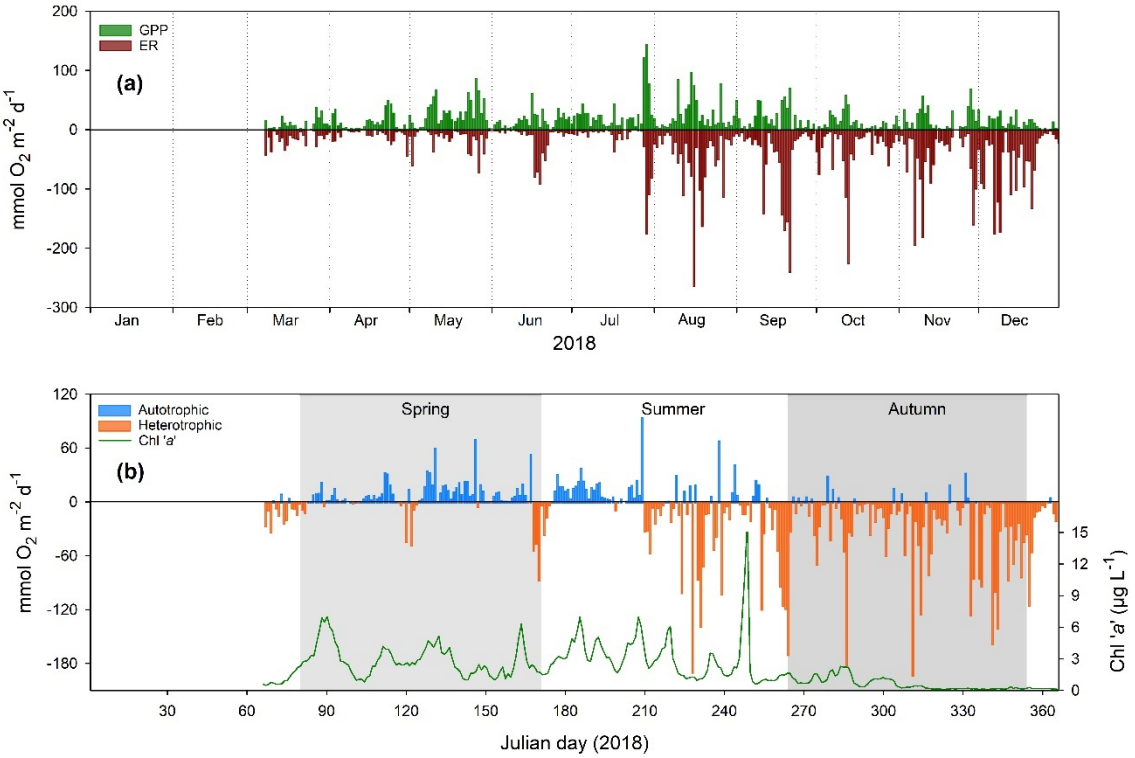

Fig 4.4 Time series for 2018 of (a) calculated daily respiration ER (red bars ▮) and gross primary production GPP (green bars ▮) and (b) calculated net community production in Southampton Water. In (a) ecosystem respiration data are displayed as negative values for convenience of graphing. In (b) negative values indicate net heterotrophic state (orange bars ▮), and positive values indicate net autotrophic state (blue bars ▮). Daily chlorophyll '*a*' is shown as a green line —.

GPP in 2018 presented highly variable daily estimated rates, with peaks of different magnitudes throughout the year, as can be seen in Figure 4.4. A yearly average of 18.4 mmol O_2 m^{-2} d^{-1} was estimated, with a range from 0.1 mmol O_2 m^{-2} d^{-1}, detected in June, to 143.7 mmol O_2 m^{-2} d^{-1}, in July. Only ~2% of daily observations were greater than 80 mmol O_2 m^{-2} d^{-1} and these were registered in July and August, however, the highest monthly value of 29.0 mmol O_2 m^{-2} d^{-1} was estimated for May, followed closely by the 28.4 mmol O_2 m^{-2} d^{-1} calculated for July.

An NCP average of -12.3 mmol O_2 m^{-2} d^{-1} was observed in 2018, indicative of an overall annual heterotrophic state. The highest negative NCP values (>90 mmol O_2 m^{-2} d^{-1}) were detected in the second half of summer and throughout autumn,

as shown in figure 4.4b. It was during these two seasons when ~75% of all negative NCP observations were calculated and reached a maximum of -192.8 mmol O_2 m^{-2} d^{-1}. Both summer and autumn presented overall heterotrophic states with -12.2 and -30.5 mmol O_2 m^{-2} d^{-1} respectively. Positive NCP values mainly occurred during spring and early summer when ~85% of autotrophic daily conditions were detected. Three extended periods (between 34 and 43 days) of almost uninterrupted positive NCP values were identified, averaging 7.0 and 14.5 mmol O_2 m^{-2} d^{-1} in spring, and 15.4 mmol O_2 m^{-2} d^{-1} in early-summer.

4.2.5 Year 2019

Estimated daily values of ER for 2019 are presented in Figure 4.5a. Calculations for this year ranged from 0.1 (June) to 437.5 (August) mmol O_2 m^{-2} d^{-1} with a yearly average of 37.6 mmol O_2 m^{-2} d^{-1}. ER rates did not show a particularly well defined seasonality with occasional periods of ~7 days of peaks in activity throughout the year, mainly from June to November. From August to October, monthly values were above 50 mmol O_2 m^{-2} d^{-1}. Conversely, March presented a particularly low monthly value of 2.9 mmol O_2 m^{-2} d^{-1} (although only 12 days of estimates were available), with the next closest monthly average being for January of 21.8 mmol O_2 m^{-2} d^{-1}.

GPP in 2019 presented an annual daily average of 36.8 mmol O_2 m^{-2} d^{-1} and varied from 0.1 to 411.2 mmol O_2 m^{-2} d^{-1} with both values occurring in the second half of June, only 11 days apart as seen, in Figure 4.5a. A period of increased productivity was noted from late April to mid-August, with the average productivity rate for this time being 58.6 mmol O_2 m^{-2} d^{-1}, compared to only 11.1 mmol O_2 m^{-2} d^{-1} for the rest of the year. In addition, daily values outside this period were

below 100.0 mmol O_2 m^{-2} d^{-1}, while ~20% of daily observations from April to May were above this rate.

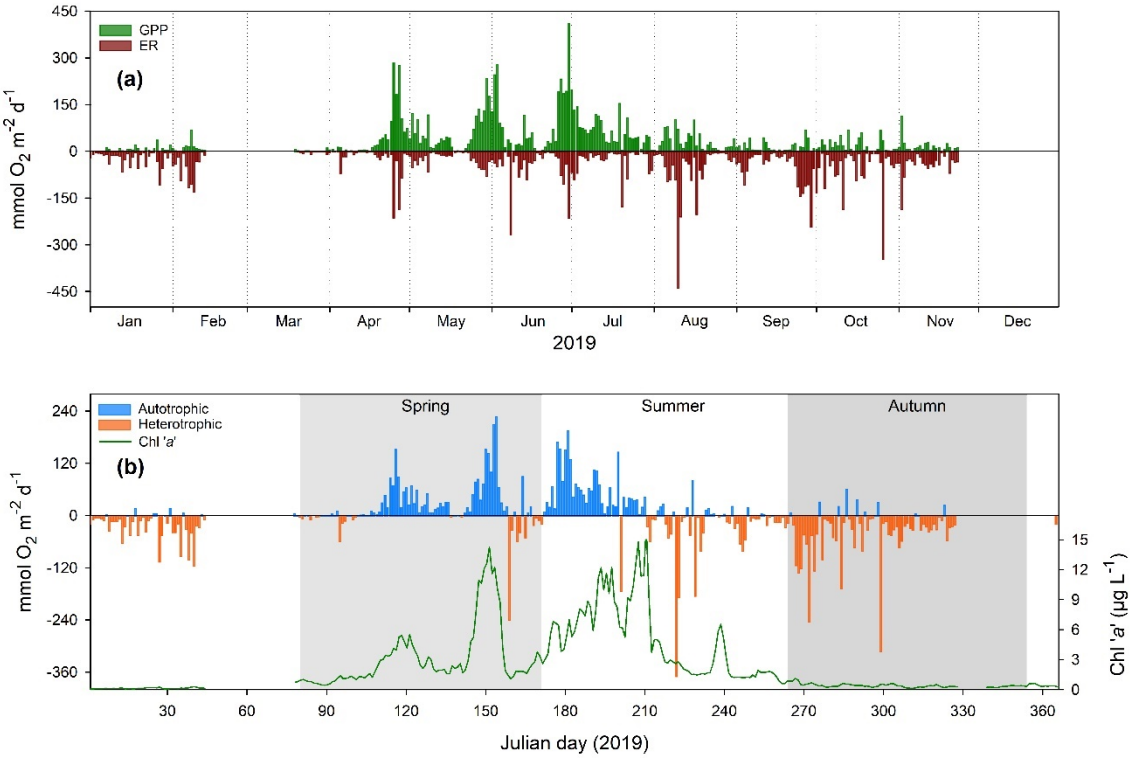

Fig 4.5 Time series for 2019 of (a) calculated daily respiration ER (red bars ▮) and gross primary production GPP (green bars ▮) and (b) calculated net community production in Southampton Water. In (a) ecosystem respiration data are displayed as negative values for convenience of graphing. In (b) negative values indicate net heterotrophic state (orange bars ▮), and positive values indicate net autotrophic state (blue bars ▮). Daily chlorophyll '*a*' is shown as a green line —.

NCP calculated values for 2019 showed a year with a good balance between GPP and ER rates reflected in an annual average of -0.8 mmol O_2 m^{-2} d^{-1}. Positive NCP estimations exhibited a seasonal pattern with a highly productive period during spring and early summer (Fig. 4.5b), reflecting net autotrophic conditions with averages of 22.7 and 10.7 mmol O_2 m^{-2} d^{-1} for each season. The maximum autotrophic daily value (+229.6 mmol O_2 m^{-2} d^{-1}) matched with the maximum Chl '*a*' peak registered in spring, almost at the end of a 57-day period of continuous autotrophic conditions, that averaged +44.1 mmol O_2 m^{-2} d^{-1}. This peak was followed closely by a second observed at the beginning of summer (+197.1 mmol

O_2 m^{-2} d^{-1}), when another extended autotrophic period lasted for 29 days, averaging +72.2 mmol O_2 m^{-2} d^{-1}. Heterotrophic conditions were nearly absent during spring, presenting less than ~15% of total observations in this season. However, in summer some high negative rates of NCP were estimated (e.g. -366.8 mmol O_2 m^{-2} d^{-1}) and in autumn (e.g. 309.8 mmol O_2 m^{-2} d^{-1}). The winter and autumn periods showed a heterotrophic state averaging -21.3 and -37.5 mmol O_2 m^{-2} d^{-1}, respectively.

4.2.6 Year 2020

In 2020, ER estimated daily rates were the highest values of the whole time series, with an annual average of 90.4 mmol O_2 m^{-2} d^{-1}. A notable period between the end of June and the end of August presented the largest peaks (>425 mmol O_2 m^{-2} d^{-1}) and an average of 202.0 mmol O_2 m^{-2} d^{-1}, in contrast to the 64.6 mmol O_2 m^{-2} d^{-1} for the rest of the year (Fig. 4.6a). During July, the highest daily rates of ER were estimated, yielding the maximum monthly value of 224.5 mmol O_2 m^{-2} d^{-1}. However, the maximum daily maximum (664.7 mmol O_2 m^{-2} d^{-1}) was observed in August. In March a low average, of 37.9 mmol O_2 m^{-2} d^{-1} was estimated with most daily values below 100 mmol O_2 m^{-2} d^{-1}.

GPP in 2020 showed a similar pattern to ER, with peaks occurring in a range of months, as shown in Figure 4.6a. The maximum values above 120 mmol O_2 m^{-2} d^{-1} were described from mid-April to August and this almost 5-month period averaged 72.3 mmol O_2 m^{-2} d^{-1}, while the rest of the year showed an average of 18.1 mmol O_2 m^{-2} d^{-1}. The maximum daily value was observed in April (395.4 mmol O_2 m^{-2} d^{-1}), followed closely by a 389.6 mmol O_2 m^{-2} d^{-1} peak in May; even so, the month with highest average GPP overall was July (95.7 mmol O_2 m^{-2} d^{-1}).

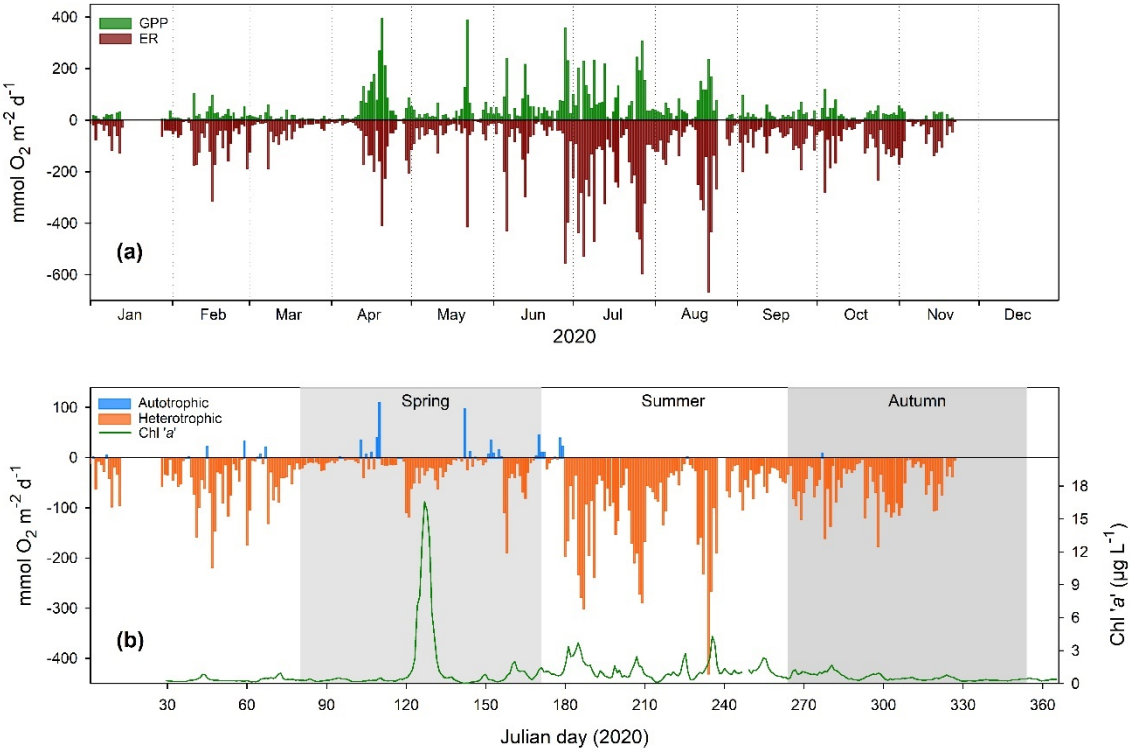

Fig 4.6 Time series for 2020 of (a) calculated daily respiration ER (red bars ▮) and gross primary production GPP (green bars ▮) and (b) calculated net community production in Southampton Water. In (a) ecosystem respiration data are displayed as negative values for convenience of graphing. In (b) negative values indicate net heterotrophic state (orange bars ▮), and positive values indicate net autotrophic state (blue bars ▮). Daily chlorophyll '*a*' is shown as a green line —.

A particularly strong heterotrophic state was calculated for 2020, as clearly seen in figure 4.6b, with an annual daily average of -48.7 mmol O2 m-2 d-1. For this year, all four seasons were classified as heterotrophic, with NCP rates ranging from -13.6 mmol O2 m-2 d-1 during spring, to -84.99 mmol O2 m-2 d-1 in summer. High heterotrophic daily values (>220 mmol O2 m-2 d-1) were observed throughout summer, season where the year maximum of NCP of -428.3 mmol O2 m-2 d-1 was observed. Positive NCP values only represented 12% of total daily observations in 2020, with almost two thirds of these during spring. The maximum positive daily NCP rate of 111.7 mmol O_2 m^{-2} d^{-1} occurred at the same time as the maximum peak in Chl '*a*'. It is important to note that NCP calculations for this year, used temperature and salinity values estimated from daily averages from time series from 2014 to 2019 due to problems with sensor failures and it

being impossible to access the Data Buoy system due to national COVID-19 restrictions, as explained in Chapter 2, section 2.2.1.

4.3 Christchurch Harbour time series analysis of ecosystem respiration, gross primary production, and trophic state: net community production.

Productivity rate calculations within Christchurch Harbour are derived from the dissolved oxygen, temperature, salinity, and wind speed time series data presented in Chapter 3 section 2.

Daily rates of net community production (NCP) can be either positive when gross primary production (GPP) exceeds ecosystem respiration (ER) indicating a net autotrophic state of the estuarine water column or negative reflecting a heterotrophic state of the system (e.g. Shen *et al*., 2019b).

4.3.1 Year 2014

In 2014, ER rates averaged 28.5 mmol O_2 m^{-2} d^{-1} and showed a minimum daily value of 0.1 mmol O_2 m^{-2} d^{-1} in September, while the maximum (228.7 mmol O_2 m^{-2} d^{-1}) was observed in the month of November. ER presented two periods of consistent daily values below 50.0 mmol O_2 m^{-2} d^{-1}, the first from May to mid-July, and the second during the whole of September (Fig 4.7a). However, during July and August, higher ER calculations were described with monthly averages ~30.0 mmol O_2 m^{-2} d^{-1}, but daily values never exceeded 110.0 mmol O_2 m^{-2} d^{-1}, compared to the period from October to December when monthly means were above 39.0 mmol O_2 m^{-2} d^{-1}.

An annual value of 29.0 mmol O_2 m^{-2} d^{-1} was estimated for GPP in 2014. At the start of calculations, in May, daily values were ~5.8 mmol O_2 m^{-2} d^{-1}; then, in

early-June GPP started to gradually increase, despite the two gaps in data in June and July (Fig. 4.7a). By the middle of July, a 19-day period of high daily rates of GPP was observed, reaching the yearly maximum of 239.0 mmol O_2 m^{-2} d^{-1} and averaging 155.9 mmol O_2 m^{-2} d^{-1}. Immediately after this increased productivity period, GPP dropped to ~45.0 mmol O_2 m^{-2} d^{-1} and remained low until showing a few peaks in October and November, but these were less than 75.0 mmol O_2 m^{-2} d^{-1}.

Overall, for the months when data was available in 2014, a slightly autotrophic state was determined, with an annual NCP of 0.6 mmol O_2 m^{-2} d^{-1}. Positive NCP rates (Fig. 4.7b) mostly occurred in summer months and averaged 35.9 mmol O_2 m^{-2} d^{-1} for the period with the highest positive daily NCP rate of the year of 182.9 mmol O_2 m^{-2} d^{-1}. During summer, a period of particularly high rates of positive NCP was evident (~49 days) and during this, more than 35% of the observations were above 60 mmol O_2 m^{-2} d^{-1} with an average of 90.1 mmol O_2 m^{-2} d^{-1} calculated. From mid-summer to the end of the year, positive NCP values remained below 35.0 mmol O_2 m^{-2} d^{-1}. Although the two main Chl '*a*' peaks identified in the year corresponded to autotrophic conditions, only the first was observed during increased NCP values (<100.0 mmol O_2 m^{-2} d^{-1}). Contrary, heterotrophic conditions mainly occurred during autumn. NCP during this season averaged -27.8 mmol O_2 m^{-2} d^{-1} and peaks of more than -85.0 mmol O_2 m^{-2} d^{-1} were commonly observed, including the maximum registered of -161.4 mmol O_2 m^{-2} d^{-1}. Greater values of phytoplankton biomass did not seem to shift conditions to autotrophic during autumn, as compared to the summer.

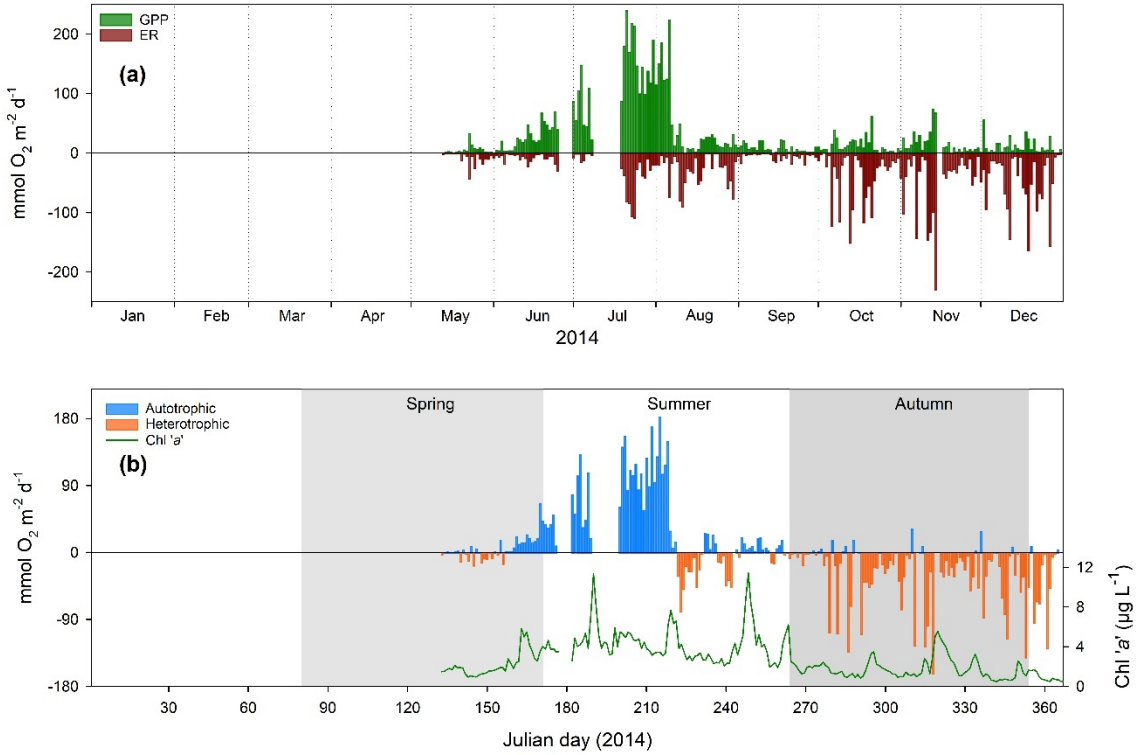

Fig 4.7 Time series for 2014 of (a) calculated daily respiration ER (red bars ▮) and gross primary production GPP (green bars ▮) and (b) calculated net community production in Christchurch Harbour Ferry Pontoon. In (a) ecosystem respiration data are displayed as negative values for convenience of graphing. In (b) negative values indicate net heterotrophic state (orange bars ▮), and positive values indicate net autotrophic state (blue bars ▮). Daily chlorophyll '*a*' is shown as a green line —.

4.3.2 Year 2015

In 2015 there was a major gap in available data between May and September. ER showed a different distribution between the two periods of available data; between January and May and September and December, as seen in figure 4.8a. Although the annual average of ER was 27.0 mmol O_2 m^{-2} d^{-1}, the period from January to May presented a mean value of 35.4 mmol O_2 m^{-2} d^{-1} with the daily maximum of 248.4 mmol O_2 m^{-2} d^{-1} in January, followed by a peak at the end of March of 235.1 mmol O_2 m^{-2} d^{-1}. Noticeably, during this period of increased ER, estimations in April were observed mainly below 15.0 mmol O_2 m^{-2} d^{-1}. For the second part of the year (September to December), ER showed an average of

11.8 mmol O_2 m^{-2} d^{-1} and two peaks of ~65.0 mmol O_2 m^{-2} d^{-1} in October and November.

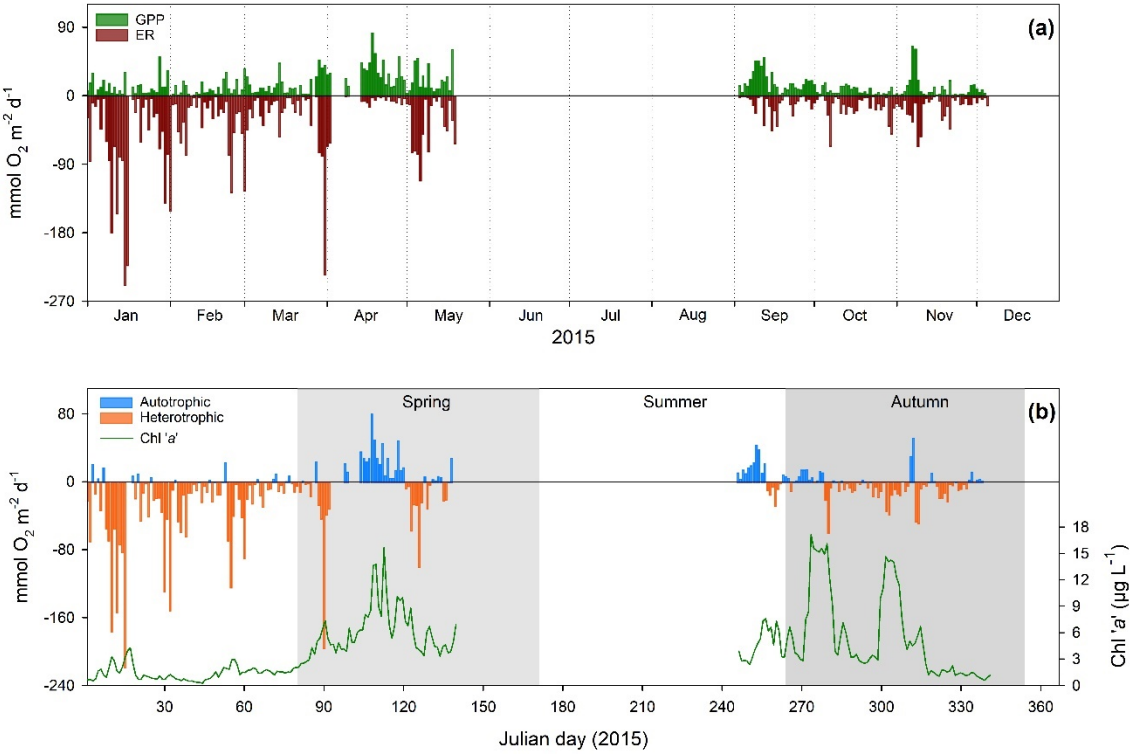

Fig 4.8 Time series for 2015 of (a) calculated daily respiration ER (red bars ▮) and gross primary production GPP (green bars ▮) and (b) calculated net community production in Christchurch Harbour Ferry Pontoon. In (a) ecosystem respiration data are displayed as negative values for convenience of graphing. In (b) negative values indicate net heterotrophic state (orange bars ▮), and positive values indicate net autotrophic state (blue bars ▮). Daily chlorophyll '*a*' is shown as a green line —.

In 2015, values of GPP ranged from 0.2 mmol O_2 m^{-2} d^{-1} in February to 82.5 mmol O_2 m^{-2} d^{-1} in April; however, only 3.7% of observations exceeded 50.0 mmol O_2 m^{-2} d^{-1} and half of these were identified in April and November (Fig 4.8a). The period from January to May averaged 17.6 mmol O_2 m^{-2} d^{-1} and included the month with the highest value, April with 32.1 mmol O_2 m^{-2} d^{-1}. In comparison the period from September to December included the lowest monthly value of 6.8 mmol O_2 m^{-2} d^{-1} (October) and averaged 10.5 mmol O_2 m^{-2} d^{-1}.

An overall heterotrophic state was calculated for 2015 (-11.7 mmol O_2 m^{-2} d^{-1}). However, it is important to note the large gap in available data between day 139

and 245 (Fig. 4.8b), with the annual estimations affected by missing spring and summer data. NCP rates remained mostly negative during the first 100 days of the year, exhibiting values greater than -80.0 mmol O_2 m^{-2} d^{-1} approximately every 20 days. During this period NCP averaged -29.5 mmol O_2 m^{-2} d^{-1} and a maximum of -217.8 mmol O_2 m^{-2} d^{-1} was observed. Daily heterotrophic estimations during summer and autumn stayed below -60 mmol O_2 m^{-2} d^{-1}. During spring, autotrophic conditions prevailed uninterrupted for 23 days, corresponding with higher concentrations of Chl '*a*'. A mean of 27.2 mmol O_2 m^{-2} d^{-1} was calculated for this period, and the highest NCP value observed was 80.5 mmol O_2 m^{-2} d^{-1}. At the end of summer, a similar pattern was identified, with a 11-day lapse averaged 19.7 mmol O_2 m^{-2} d^{-1} but only reached 44.2 mmol O_2 m^{-2} d^{-1}. Although Chl '*a*' showed increased values in autumn, the autotrophic conditions were not as high as during the spring. Two great peaks (>12 µg L^{-1}) of Chl '*a*' were observed in autumn, but only during the first peak, the trophic state shifted from heterotrophic to autotrophic.

4.3.3 Year 2016

In 2016, ER daily values during the year remained below 90 mmol O_2 m^{-2} d^{-1}, apart from only two days at the end of November (Fig. 4.9a) when peaks reached 183.36 and 158.13 mmol O_2 m^{-2} d^{-1}. The year average was 11.1 mmol O_2 m^{-2} d^{-1}, but months of May and November presented mean values of 21.7 and 24.7 mmol O_2 m^{-2} d^{-1}, respectively. Throughout the year, ER calculations showed a bimonthly pattern where values start increasing until reaching a peak to then reduce in magnitude abruptly, particularly noticeable up to August. From September to mid-November, an extended period of low daily ER rates was observed, with values below 25 mmol O_2 m^{-2} d^{-1}.

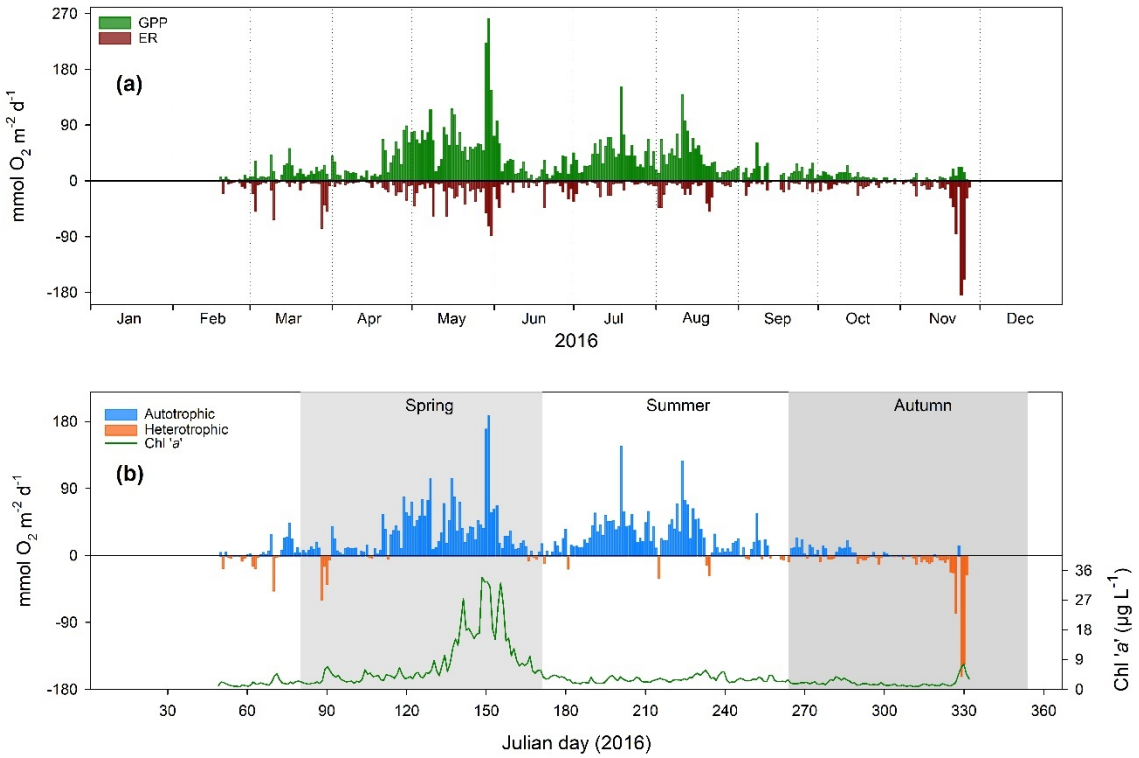

Fig 4.9 Time series for 2016 of (a) calculated daily respiration ER (red bars ▮) and gross primary production GPP (green bars ▮) and (b) calculated net community production in Christchurch Harbour Ferry Pontoon. In (a) ecosystem respiration data are displayed as negative values for convenience of graphing. In (b) negative values indicate net heterotrophic state (orange bars ▮), and positive values indicate net autotrophic state (blue bars ▮). Daily chlorophyll '*a*' is shown as a green line —.

GPP in 2016 presented a mean annual value of 28.4 mmol O_2 m^{-2} d^{-1}, however, most of the productivity was concentrated between April and August (Fig. 4.9a). Estimations of GPP rates averaged ~12.0 mmol O_2 m^{-2} d^{-1} in February and March then increased in mid-April lasting for about 45 days and averaging 71.8 mmol O_2 m^{-2} d^{-1} with the year maximum of 261.5 mmol O_2 m^{-2} d^{-1} in late May. Two other periods when GPP calculations increased and peaked beyond 130.0 mmol O_2 m^{-2} d^{-1} were present in July and August, both lasting ~18 days and averaging 53.2 and 61.5 mmol O_2 m^{-2} d^{-1}, respectively. For the remaining months, daily GPP remained below 40.0 mmol O_2 m^{-2} d^{-1}, except for one day in September.

2016 displayed a general net autotrophic state and an NCP average of 17.3 mmol O_2 m^{-2} d^{-1}. Around 75% of NCP estimations corresponding to autotrophic

conditions were identified during spring and summer (Fig. 4.9b). The spring season averaged 29.1 mmol O_2 m^{-2} d^{-1} of NCP and presented a daily maximum of 189.3 mmol O_2 m^{-2} d^{-1}, while summer showed a mean value of 26.4 mmol O_2 m^{-2} d^{-1} and a daily observation of 148.3 mmol O_2 m^{-2} d^{-1} as the maximum. Phytoplankton biomass displayed high concentrations at the end of the spring season (>20 µg L^{-1}), overlapping with the most autotrophic conditions overserved through the year. Autotrophic conditions during winter did not exceed 45.0 mmol O_2 m^{-2} d^{-1} and autumn displayed even lower values, with calculations remaining below 25.0 mmol O_2 m^{-2} d^{-1}. Negative NCP values accounted for less than the 25% of the yearly calculations and were mainly identified during autumn, the only season to show an overall heterotrophic state (-4.6 mmol O_2 m^{-2} d^{-1}) in 2016. The last few estimates in autumn were characterised by high negative NCP values (>30.0 mmol O_2 m^{-2} d^{-1}), however, this weeklong heterotrophic period was only disturbed for one day when NCP displayed 14.1 mmol O_2 m^{-2} d^{-1}, corresponding to a minor rise in Chl '*a*' concentration.

4.3.4 Year 2017

ER displayed an annual average of 11.7 mmol O_2 m^{-2} d^{-1} in 2017, with the maximum daily value (99.9 mmol O_2 m^{-2} d^{-1}) identified at the beginning of February (Fig. 4.10a) when 3 continuous days exceeded 85.1 mmol O_2 m^{-2} d^{-1}. Throughout the rest of the year the next maximum peak was observed in June (89.4 mmol O_2 m^{-2} d^{-1}). It is notable that less than 3% of ER daily rate calculations for 2017 surpassed 50 mmol O_2 m^{-2} d^{-1}. June displayed the greatest monthly average ER rate of 15.5 mmol O_2 m^{-2} d^{-1}, followed closely by September with 14.1 mmol O_2 m^{-2} d^{-1}.

The average annual GPP rate in 2017 was 29.5 mmol O_2 m^{-2} d^{-1}, but distribution across the year was not even, as observed in figure 4.10a. Between April and August most estimations were >60 mmol O_2 m^{-2} d^{-1} and the year maximum of 220.7 mmol O_2 m^{-2} d^{-1} was detected in May, with an average of 50.5 mmol O_2 m^{-2} d-1, for said period. In March, September and October a rapid decline in values was evident averaging 14.3 mmol O_2 m^{-2} d^{-1}. Lastly, months at the beginning and end of the year (January, November and December), presented the lowest GPP values of 3.6 mmol O_2 m^{-2} d^{-1}.

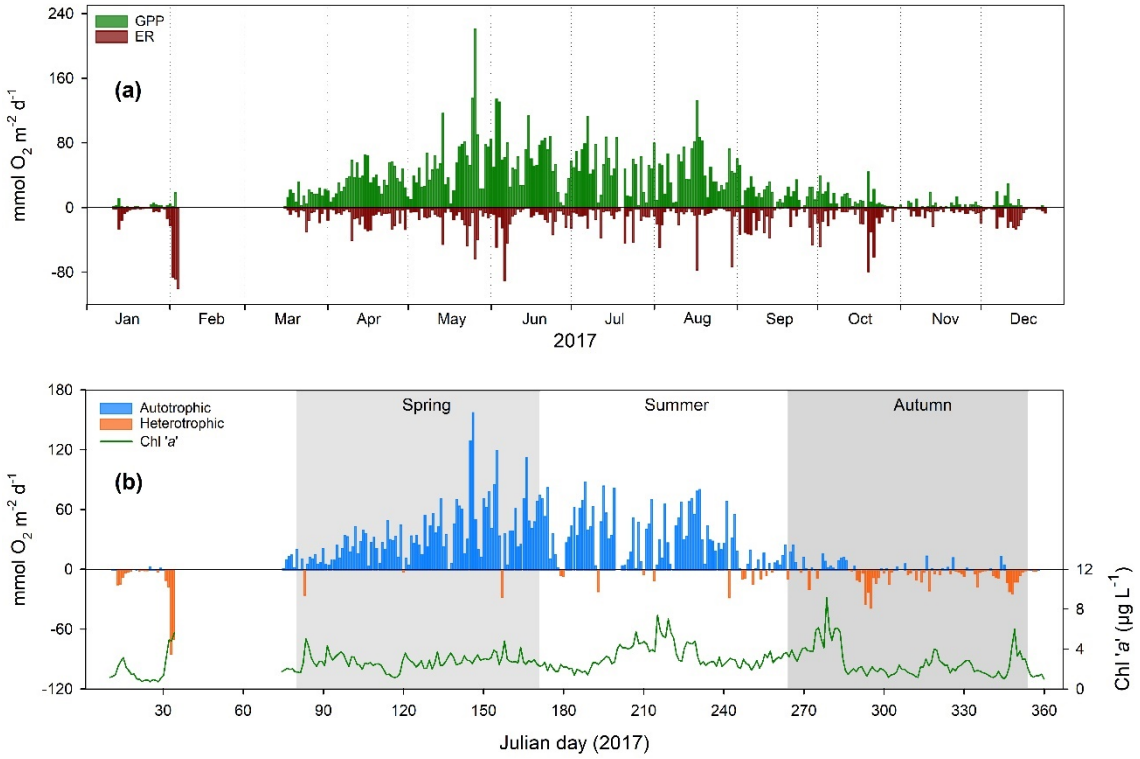

Fig 4.10 Time series for 2017 of (a) calculated daily respiration ER (red bars ▮) and gross primary production GPP (green bars ▮) and (b) calculated net community production in Christchurch Harbour Ferry Pontoon. In (a) ecosystem respiration data are displayed as negative values for convenience of graphing. In (b) negative values indicate net heterotrophic state (orange bars ▮), and positive values indicate net autotrophic state (blue bars ▮). Daily chlorophyll '*a*' is shown as a green line —.

An overall net autotrophic state was calculated for 2017, showing an average NCP of 18.1 mmol O_2 m^{-2} d^{-1}. During this year, more than 73% of the total NCP estimations corresponded to autotrophic conditions and were present during

spring and summer seasons, as clearly seen in figure 4.10b. Spring displayed the highest daily NCP value of the year (158.1 mmol O_2 m^{-2} d^{-1}) and an average of 34.8 mmol O_2 m^{-2} d^{-1}, although the summer season also exhibited an autotrophic state, it was not as marked as the one for spring since the maximum value observed was 88.5 mmol O_2 m^{-2} d^{-1} and presented a mean of 29.6 mmol O_2 m^{-2} d^{-1}. Autumn and winter showed weak daily autotrophic conditions, given that values remained constantly below 25.0 mmol O_2 m^{-2} d^{-1}. It was during these two seasons that heterotrophic conditions prevailed, with winter averaging -5.1 mmol O_2 m^{-2} d^{-1} and autumn -1.9 mmol O_2 m^{-2} d^{-1}. However, peaks in negative NCP were greater at the begging of the year, reaching -83.7 mmol O_2 m^{-2} d^{-1}.

4.3.5 Year 2018

For 2018, ER annual daily average rate was 12.0 mmol O_2 m^{-2} d^{-1}. Across the year, daily values mostly remained less than 40.0 mmol O_2 m^{-2} d^{-1}, with only 6.2% of calculations exceeding this threshold, half of them in April and May, even though the highest value of ER in the year (86.5 mmol O_2 m^{-2} d^{-1}) was observed in July (Fig. 4.11a). Despite April and May displaying peaks of ER, their monthly averages (15.9 and 17.5 mmol O_2 m^{-2} d^{-1}) were not as high as the one calculated for December, 22.7 mmol O_2 m^{-2} d^{-1}. June to July was the longest uninterrupted period showing values below 30 mmol O_2 m^{-2} d^{-1}.

The GPP observed in 2018 was mainly concentrated between May and July (Fig 4.11a), months when two major periods of increased GPP were identified. Lasting almost the entire month of May (22 days), a productivity lapse averaging 71.2 mmol O_2 m^{-2} d^{-1} and reaching values above 140 mmol O_2 m^{-2} d^{-1}, on two occasions, was detected. A similar period appeared three weeks later, when for 27 days (between June and July), enhanced GPP daily values reached a

maximum of 169.8 mmol O_2 m^{-2} d^{-1} and displayed an average of 80.6 mmol O_2 m^{-2} d^{-1}. April, August and September seemed to act as transition periods given that increasing values were observed towards the major production months; monthly averages of them ranged from 21.8 to 28.8 mmol O_2 m^{-2} d^{-1}. From October to December GPP did not exceed 25 mmol O_2 m^{-2} d^{-1} and this three-month period showed an average value of 6.5 mmol O_2 m^{-2} d^{-1}.

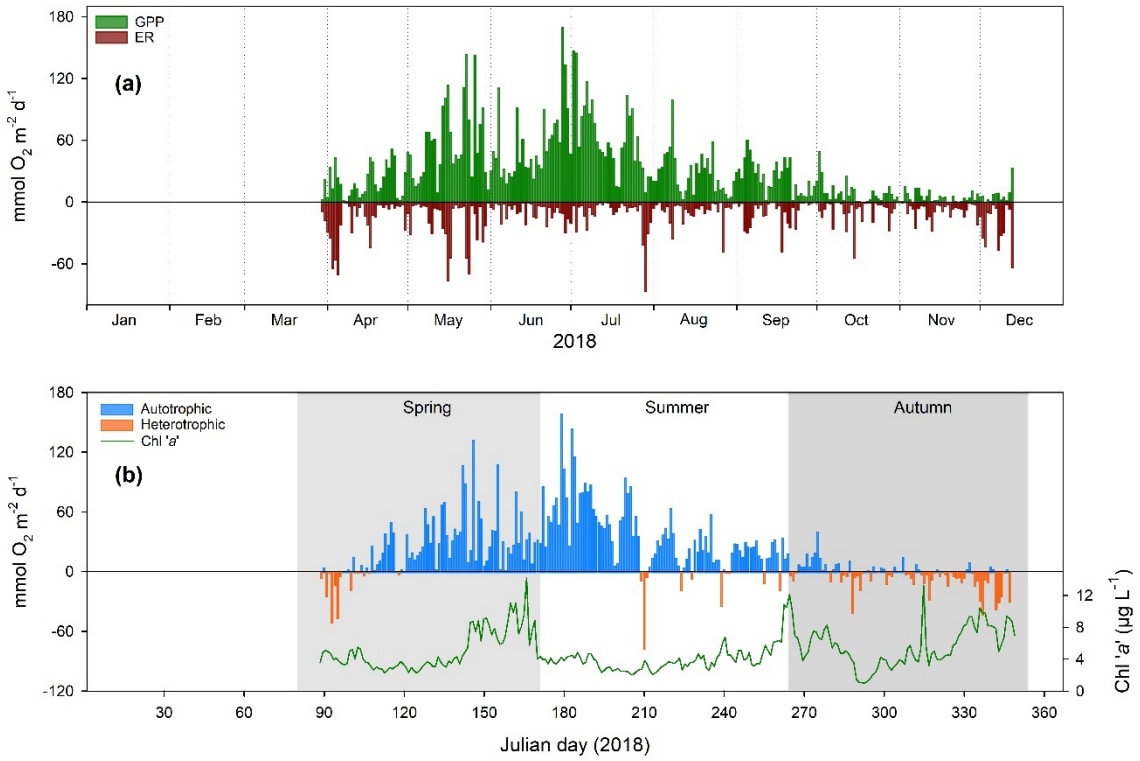

Fig 4.11 Time series for 2018 of (a) calculated daily respiration ER (red bars ▮) and gross primary production GPP (green bars ▮) and (b) calculated net community production in Christchurch Harbour Ferry Pontoon. In (a) ecosystem respiration data are displayed as negative values for convenience of graphing. In (b) negative values indicate net heterotrophic state (orange bars ▮), and positive values indicate net autotrophic state (blue bars ▮). Daily chlorophyll '*a*' is shown as a green line —.

In 2018, an autotrophic state dominated the year, represented with an average NCP value of 19.8 mmol O_2 m^{-2} d^{-1}. Nearly 80% of total positive NCP daily values were visible between spring and summer, as shown in figure 4.11b. Both seasons reflected autotrophic states, with 24.3 and 36.1 mmol O_2 m^{-2} d^{-1} averages, respectively, and a maximum of 132.5 mmol O_2 m^{-2} d^{-1} during spring and the

years highest daily NCP value (159.3 mmol O_2 m^{-2} d^{-1}) in summer. However, the period of the year when values of NCP above 70.0 mmol O_2 m^{-2} d^{-1} occurred, was between day 142 and 209, taking place during the transition period between spring and summer seasons. This period averaged 52.9 mmol O_2 m^{-2} d^{-1} and did not present any change to heterotrophic conditions. In addition, for the first 30 days it corresponded to the highest and prolonged increase in phytoplankton biomass observed in the year. Heterotrophic conditions were mainly identified in autumn, that averaged -2.5 mmol O_2 m^{-2} d^{-1} but only presented values below -45.0 mmol O_2 m^{-2} d^{-1}. Unlike spring, that surpassed -50 mmol O_2 m^{-2} d^{-1} on two occasions and summer that showed a particular highly negative NCP value of -77.0 mmol O_2 m^{-2} d^{-1} right after the long-positive NCP period mentioned previously. At the end of summer and during autumn, increasing values of Chl '*a*' seemed to help shift heterotrophic to autotrophic conditions.

4.4 Drivers of productivity rates

4.4.1 Environmental factors regulating productivity rates

There are many physical, chemical, and biological processes that regulate the balance between production and consumption of organic matter in estuarine ecosystems (Kemp & Testa, 2011). To assess the influence of different environmental factors on productivity rates, Spearman's correlation coefficient was calculated (Table 4.1) for the Southampton Water estuary (SOT) and Christchurch Harbour Ferry Pontoon (CHR).

Analysing the whole time series for SOT and CHR, both, NCP and GPP correlated with parameters denoting light availability, I_0 and I_m, especially in CHR (ρ>0.66). This is no surprise given that light availability is considered the

critical driver for photosynthesis, hence, photosynthetic rates generally follow daily and seasonal variations in solar intensity (e.g. Kemp & Testa, 2011). However, ER showed very weak negative correlations with light parameters ($\rho<-0.16$) agreeing with the open water diel oxygen method assumption that respiration rates are constant during day and night (e.g. Caffrey *et al*., 2014).

Temperature in CHR showed a strong correlation with NCP ($\rho=0.50$) and a more moderate correlation with GPP ($\rho=0.47$), while SOT only presented a weak relationship between GPP and temperature ($\rho=0.29$). In temperate estuaries, GPP generally shows a strong correlation with temperature by following closely seasonal variations, while NCP can strongly be affected by seasonal and interannual fluctuations that are sometimes difficult to detect (Kemp & Testa, 2011).

Chl '*a*' has become the most widely used indicator of phytoplankton biomass even though its relation to phytoplankton carbon changes significantly with light intensity, nutrient availability, and species composition (e.g. Hopkinson & Smith, 2005). When analysing chlorophyll concentration in relation to productivity rates in the estuarine systems studied here, positive correlations were observed for both estuaries, SOT ($\rho>0.30$) and CHR ($\rho>0.27$), with NCP and GPP; meaning that higher phytoplankton biomass was related to autotrophic conditions, particularly between NCP and Chl '*a*' in SOT ($\rho=0.45$).

Wind speed strongly correlates with ER in SOT ($\rho=0.54$) and CHR ($\rho=0.51$), and moderately correlates with GPP ($\rho>0.23$). The negative correlations observed between NCP and wind speed, are a clear indication of the influence of winds in ER driving the trophic state into net heterotrophic. It has been reported that

increased wind periods could drive sediment resuspension events and induce apparent negative NCP (Hull *et al*., 2016; Staehr *et al*., 2012).

Oxygen saturation (O_2%) negatively correlated with ER in SOT (ρ=-0.41) and CHR (ρ=-0.30), while positively related to NCP in both estuaries (ρ>0.58) and only to GPP in CHR (ρ=0.62). This relationship between O_2% and conditions more representative of net autotrophy, point towards the estuarine systems releasing DO to the atmosphere (e.g. Haskell *et al*., 2019); a trend more clearly observed in CHR than in SOT. Although DO variations in the water column of coastal systems depend mainly on the balance between respiration and photosynthesis (e.g. Alonso-Pérez *et al*., 2015), it has been reported that atmospheric exchange of DO could represent about 10% of the estimation of DO production and consumption, thought to be by biological processes (e.g. Cravo *et al*., 2020).

In CHR, NCP and GPP declined (ρ=-0.49 and ρ=-0.30) as water clarity decayed, while ER appeared to increase with turbidity (ρ=0.28). This correlation was only apparent in CHR since being a much shallower system turbidity effects are greater. It is known that water clarity is a critical factor influencing light availability for photosynthesis (e.g. May *et al*., 2003) , moreover, in many shallow estuaries there is a strong correlation between turbidity and suspended sediment concentrations.

River inflow rates, similar to turbidity, was significantly correlated with NCP (ρ=-0.22) and ER (ρ=0.23) in CHR, implicating that freshwater inflow, in this estuary, seemed to not only determine light availability in the water column but also enhanced respiration due to possible organic inputs (Azevedo *et al*., 2006).

Table 4.1. Spearman's correlation matrix relating environmental conditions and productivity rates in Southampton Water and Christchurch Harbour Ferry Pontoon.

Location	Productivity rates	I_0	I_m	Tidal Range	Wind Speed	Temp	Sal	O_2%	Chl '*a*'	Turb	River flow
Southampton Water n=1668	NCP	**0.39**	**0.37**	0.00	**-0.27**	**0.12**	0.00	**0.58**	**0.45**	**-0.16**	0.00
	GPP	**0.39**	**0.25**	0.01	**0.35**	**0.29**	**0.09**	**0.08**	**0.30**	0.00	**-0.09**
	ER	**-0.10**	**-0.16**	0.00	**0.54**	**0.04**	**0.04**	**-0.41**	**-0.18**	**0.13**	-0.03
Christchurch Pontoon n=1241	NCP	**0.70**	**0.73**	---	**-0.17**	**0.50**	**0.08**	**0.81**	**0.27**	**-0.49**	**-0.22**
	GPP	**0.67**	**0.66**	---	**0.23**	**0.47**	-0.04	**0.62**	**0.33**	**-0.30**	**-0.07**
	ER	**-0.11**	**-0.16**	**---**	**0.51**	**-0.13**	**-0.20**	**-0.30**	0.03	**0.28**	**0.23**

Values in bold $p < 0.05$. Values underlined represent absolute coefficient with strong correlation, $\rho > 0.50$.

4.4.2 Site-specific variables regulating season effects on NCP, GPP and ER

Seasonal patterns in primary production variability can be identified with multivariate techniques such as principal component analysis (PCA) (Cloern, 1996). By considering daily rates throughout the complete time series, for both estuaries, PCA analysis was performed to assess the relationship between the seasonal distribution of productivity rates and environmental conditions as well as the relative contributions of GPP and ER to NCP. Figure 4.12 shows a representation of the first two principal components (PCs), accounting for ~46% of the total variance in SOT and ~59% in CHR. Day rates have been labelled based on season and trophic state.

For SOT, PC1 explained 26.5% of the total variability in the dataset and PC2 explained 19.5%. The main factors contributing to PC1 positive eigenvalues (R^2>0.40) were I_0, temperature and I_m, and to a lesser extent (R^2>0.20) Chl '*a*', salinity and NCP. PC1 negative values (R^2>-0.22) were attributed to riverine inflow and turbidity. The factor loading scores in biplots (Fig. 4.12a) show a seasonal difference among daily rates following the gradient of PC1, with positive values attributed to spring and summer and negative to autumn and winter. This could denote an association with physical parameters dependent on seasonality, favouring the appearance of higher phytoplankton biomass and primary production due to warmer waters and extended hours of light availability. A similar analysis in the Western English Channel (Barnes *et al*., 2015) revealed an identical clustering of seasons and related it to stratification and primary production governed by temperature control on enzymatic processes and phytoplankton succession. Variables describing positive values for PC2 were ER

and temperature (R^2>0.30), followed by salinity and wind speed (R^2>0.20). NCP, O_2 %, dissolved oxygen concentration ([O_2]), and river inflow contributed to negative eigenvalues (R^2>-0.30) of PC2. Heterotrophic conditions were mainly associated with positive values of PC2, while negative loadings related to an autotrophic state (Fig. 4.12a). This indicates that ER correlates to irregular events, like high wind periods, and drives NCP into a net heterotrophic state, while increases in O_2 saturation and concentration reflect a closer relation to autotrophic conditions and, seemingly, to riverine inflow. This correlation between ER and high wind speeds was demonstrated in the Spearman's correlation coefficient (Table 4.1). Moreover, it has been demonstrated that in large estuaries, such as Chesapeake Bay (Winder & Cloern, 2010), high river flow can deliver nutrients and freshwater to establish salinity stratification and enhance phytoplankton blooms.

PCA analysis for CHR revealed that PC1 explained 38.6% of the total variance, while PC2 explained 20.2%. Factors contributing positively to PC1 (R^2>0.30) were I_m, I_0, NCP, O_2%, temperature and GPP (Fig. 4.12b). In comparison, river flow and turbidity correlated with negative eigenvalues of PC1 (R^2>-0.20). In the same way as the pattern observed for SOT, CHR component loadings of PC1 associated positive eigenvalues to daily rates in spring and summer and negative values to observations in autumn and winter. In addition, heterotrophic conditions seemed to only correlate with negative values.

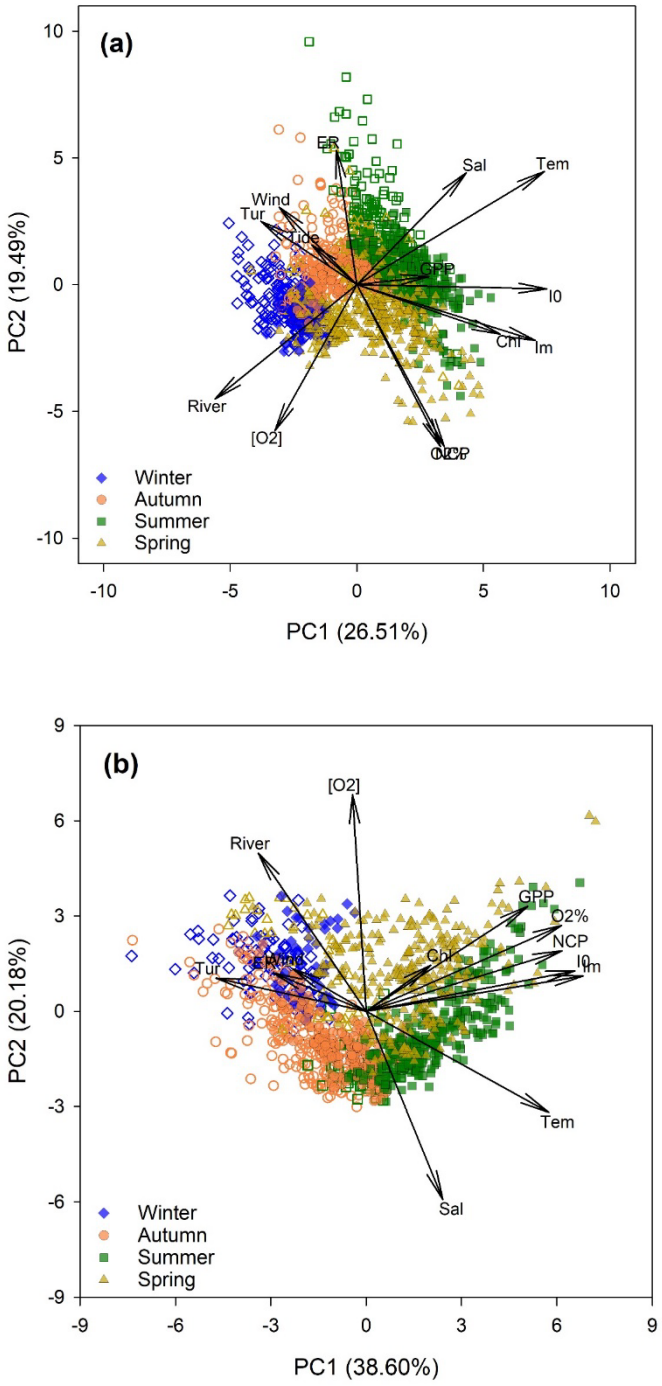

Fig. 4.12 Principal Component Analysis (PCA) for (a) Southampton Water and (b) Christchurch Harbour Ferry Pontoon. Seasons have been used as factors to illustrate the clusters: winter (blue diamonds ♦), autumn (orange circles ●), summer (green squares ■) and spring (yellow triangles ▲). Filled symbols designate autotrophic conditions while open symbols indicate heterotrophic conditions. Arrows → represent the variable and the direction of an arrow indicates its relation with the Principal Component (PC) and other variables. Tem=temperature, Sal=salinity, Chl=chlorophyll '*a*', I0=surface water irradiance, Im=mean water column irradiance, O2%=DO in percentage saturation, [O2]=DO concentration, Wind=wind speed, Tur=turbidity, Tide=tidal range, River=river inflow, GPP=gross primary production, ER=ecosystem respiration and NCP=net community production.

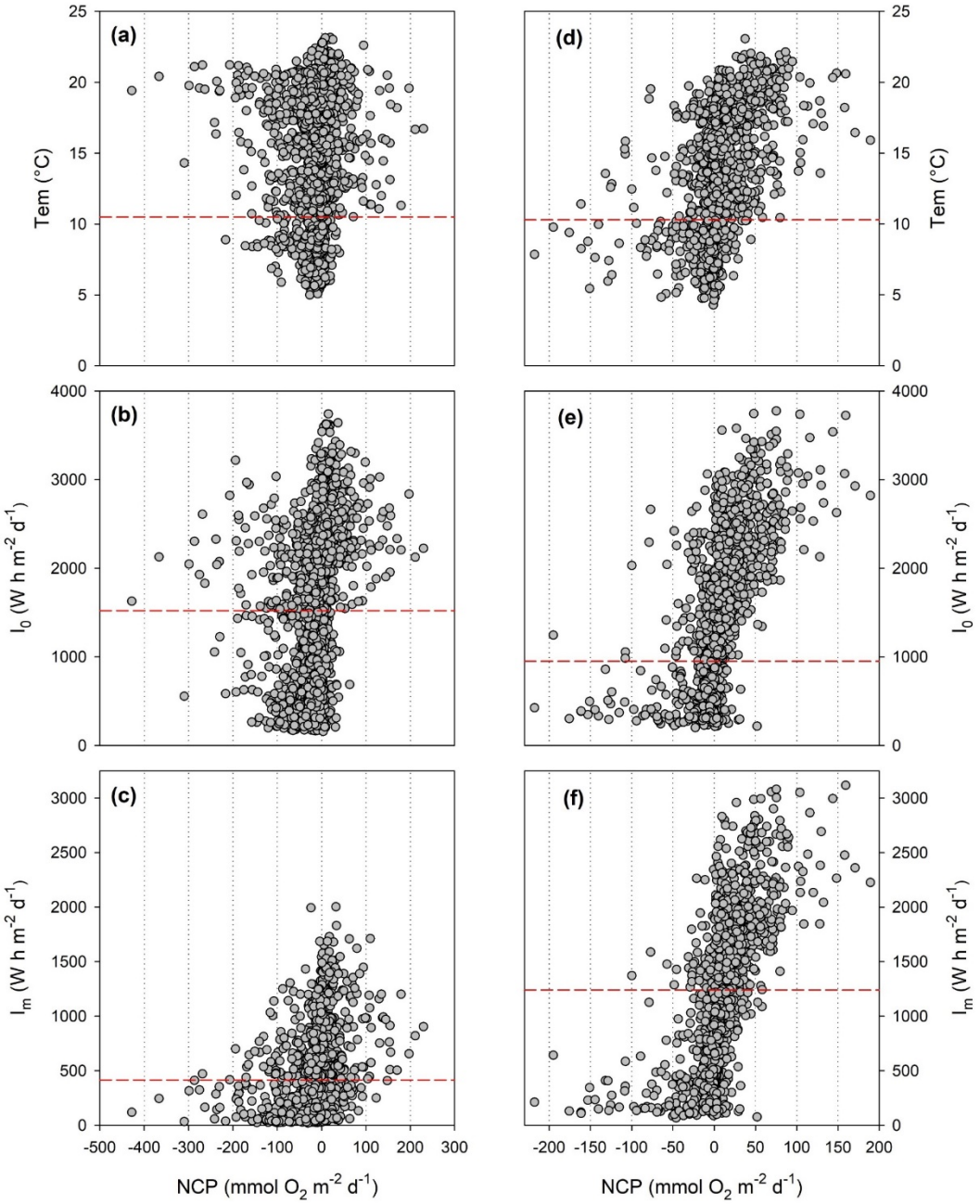

Fig. 4.13 Net Community Production (NCP) compared with temperature (a, d), daily surface irradiance I_0 (b, e) and water column irradiance I_m (c, f), in Southampton Water (a, b, c) and Christchurch Harbour Ferry Pontoon (d, e, f). Red dashed lines – – indicate threshold values.

PCAs results in this study display a strong seasonal classification, however, previous research on the factors controlling primary production in the Duoro estuary, Portugal (Azevedo *et al*., 2006), described a distinct arrangement of winter and summer samples in opposite extremes of PCs but a spring and fall spreading across the middle of the factor loading biplot. PC1 for CHR indicates that light availability and temperature increase relate to higher GPP, and in turn the great influence of GPP on NCP in this estuary. This suggests that seasonal fluctuations in phytoplankton biomass positively correlate with annual cycles of temperature and solar radiation, a characteristic pattern usually observed in coastal ecosystems (e.g. Leterme *et al*., 2014). Positive values of PC2 were mainly described (R^2>0.40) by [O_2] and riverine inflow, followed by GPP and O_2% (R^2>0.22). Conversely, salinity (R^2=-0.49) and temperature (R^2=-0.26) contributed to negative eigenvalues (Fig. 4.12b). The seasonal distribution of primary production in CHR appears to be a response to seasonal fluctuations in the riverine inflow into the estuary and its influence on primary production, as previously described by (Cloern, 1996) for San Francisco Bay, USA. However, the relationship between phytoplankton primary production and river discharge is complex and ecosystem specific (Cloern *et al*., 2014). This intricate relation was highlighted in the comparison of two neighbouring, shallow, microtidal estuaries in North Carolina, USA (Peierls *et al*., 2012), where negative and positive responses between estuarine phytoplankton biomass and river discharge were found in both estuaries, similarly to results from the PCA in CHR.

The main factors limiting water column primary production in shallow coastal systems located in temperate latitudes are light availability (e.g. Brito &

Newton, 2013) and temperature (e.g. Trombetta *et al*., 2019), which are highly seasonal parameters. A comparison between productivity rates against temperature and light availability (Fig. 4.13) showed that, for SOT, a surface water temperature threshold of 10.5 °C, I_0 values above 1520 Wh m^{-2} d^{-1} and I_m greater than 415 Wh m^{-2} d^{-1}, corresponded to the maximum NCP calculated rates, meaning positive values above 100 mmol O_2 m^{-2} d^{-1} and negative NCP beyond -200 mmol O_2 m^{-2} d^{-1}. In CHR, this same comparison revealed that NCP exceeding positive and negative values above 50 mmol O_2 m^{-2} d^{-1}, were consistent with the appearance of water temperatures above 10.3 °C, values above 1240 Wh m^{-2} d^{-1} for I_0 and I_m higher than 950 Wh m^{-2} d^{-1}, as seen in Fig. 4.13.

In both studied estuaries, it was difficult to separate the effects of light and temperature on primary production. The same covariance between these two parameters was identified in the 3-year study of phytoplankton biomass variability of two shallow (<5m), microtidal estuaries in North Carolina (USA) (Peierls *et al*., 2012). Identifying these borderline values of temperature is an important precedent since both community production and respiration will increase in a possible scenario of sea temperature rise (López-Urrutia *et al*., 2011). While solar radiation is an important factor enhancing photosynthesis, in coastal waters the light available for primary production depends on water column light attenuation (e.g. Caffrey *et al*., 2014). This was particularly recognised for CHR since it required a higher value of I_m than SOT but a lower I_0, an indication of its shallower water column being affected by turbidity increases due to suspended sediment associated to river flow (e.g. Hall *et al*., 2015). Reduction in estuarine primary production has been linked to the

increase in water turbidity promoted by dredging and differential sediment transport (Bucci *et al*., 2012).

4.4.3 Relation between ecosystem respiration and gross primary production: implications on aquatic trophic state

The concept of 'trophic' or 'metabolic' state of an aquatic system is based on the metabolic theory of ecology (López-Urrutia *et al*., 2011), and it is defined as the ratio between GPP and ER, with a system being net autotrophic if it produces more organic matter than it consumes it (GPP:ER > 1), and net heterotrophic if organic matter consumption exceeds production (GPP:ER < 1) (Caffrey, 2003; McKinnon *et al*., 2017).

Examination of the relationship between GPP and ER using Ordinary Least Squares (OLS) allows the estimation of the threshold values of GPP necessary to achieve metabolic balance (GPP:ER = 1) (Duarte & Regaudie-De-Gioux, 2009). The metabolic balance in SOT and CHR is described in Figure 4.14 where the solid line is the 1:1 relationship, the dashed line is the regression of the log-transformed ER and GPP data, and where the lines intercept indicates the threshold for metabolic balance (GPP:ER) for each system.

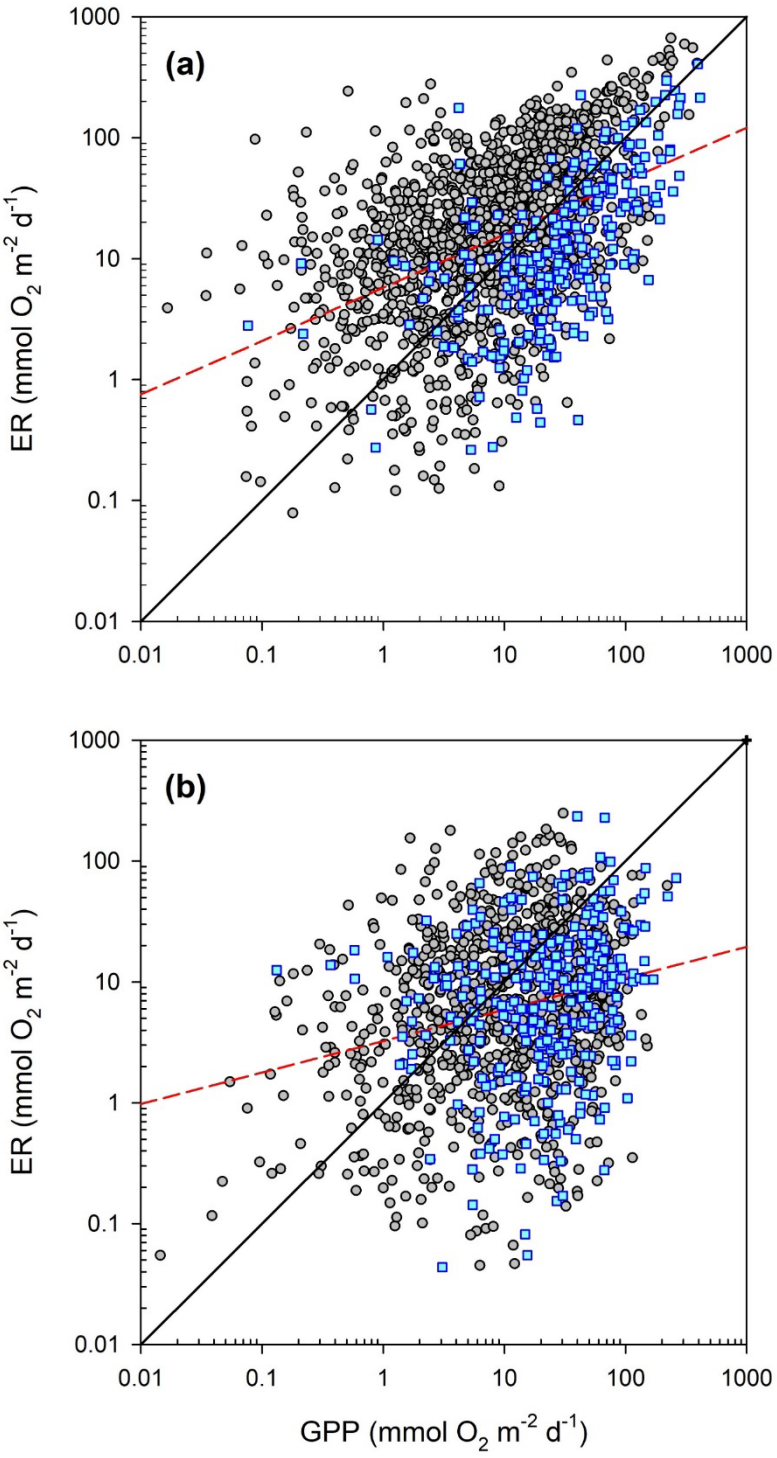

Fig. 4.14 Relationship between daily ecosystem respiration (ER) and daily gross primary production (GPP) for (a) Southampton Water estuary and (b) Christchurch Harbour Ferry Pontoon. Both rates are expressed in mmol O_2 m^{-2} d^{-1}. Grey circles ● show data for days classified as No Blooms and blue squares ■ show data for days classified as Blooms (see Chapter 3). The red dashed line --- represents the ordinary least-squares regression of the log-transformed data: (a) $ER = 5.74x^{0.44}$, $r^2 = 0.22$, $n = 1720$, and (b) $ER = 5.74x^{0.44}$, $r^2 = 0.06$, $n = 1249$. The black continuous line — represents 1:1.

For SOT, a GPP threshold of 22.4 mmol O_2 m^{-2} d^{-1} was calculated (Fig. 4.14a) while for CHR, a value of 4.9 mmol O_2 m^{-2} d^{-1} was estimated (Fig. 4.14b). This results implicate that the production needed to drive SOT towards net autotrophic metabolism is higher than in CHR (Kemp & Testa, 2011). There is a considerable variation in the GPP threshold among marine ecosystems, with the open ocean considerably lower than coastal water as described by Duarte & Agustí (1998) in their cross-comparative survey of metabolism in coastal and adjacent waters. In this work, a GPP threshold of 12.96 mmol O_2 m^{-2} d^{-1} was about a factor of 10 or higher in these environments compared to open-ocean waters. A comparable value was reported as the primary production required to drive estuaries into a net autotrophic state (12.8 mmol O_2 m^{-2} d^{-1}) by Duarte & Prairie (2005). Both of these limits are lower than the one reported for SOT but higher than what was calculated for CHR. Moreover, in a study of the coastal waters adjacent to Northern Australia (McKinnon *et al*., 2017) the mean threshold of GPP was 45 mmol O_2 m^{-2} d^{-1}. Much elevated values than the ones calculated in the present study have been reported for the whole European coast (Duarte & Regaudie-De-Gioux, 2009), with 212.5 mmol O_2 m^{-2} d^{-1} originated from experiments and 288.0 mmol O_2 m^{-2} d^{-1} derived from a cross-comparative synthesis of different studies. An even more significantly higher threshold was reported by Hopkinson & Smith (2005) for whole-system metabolism of estuaries (500 mmol O_2 m^{-2} d^{-1}). The discrepancy between some of the highest thresholds reported for estuarine and coastal systems, and values found for CHR and SOT, can be related to the amount and importance of allochthonous organic matter inputs received by the estuaries (e.g. Serret *et al*., 2002). For SOT and CHR, riverine inflow seems to not be as strongly correlated with productivity rates as some of the estuarine systems included in the studies mentioned above (Table 4.1).

An additional tool to describe the balance between the flow of organic matter required to maintain community metabolic balance and that available for growth or export away from the ecosystem (NCP) is the GPP/ER ratio (Caffrey, 2003). The daily GPP/ER ratio for SOT was 0.63 while the value for CHR was 1.52, indicating a state of heterotrophy for SOT and net autotrophy for CHR. A GPP/ER ratio of 1.91 was described for Matilda Bay (Australia), a temperate estuary located in Western Australia (Agusti *et al*., 2018). This ratio classifies the estuary as autotrophic, and like in CHR, the system is influenced by riverine input but also experiences significant inflow of oceanic waters. The GPP/ER ratio varies greatly among ecosystems; examples of this fluctuation can be observed in the analysis presented by Duarte & Agustí (1998) for global coastal waters (0.03 – 34.3), as well as the range described for coastal and shelf waters adjacent to Northern Australia (McKinnon *et al*., 2017) where the ratio ranged from 0.84 to 5.21. Differences in GPP/ER ratios can be attributed to light and nutrient availability and changes in phytoplankton community structure and cell size (e.g. McKinnon *et al*., 2017).

In both systems, it was observed a prevalence of ER>GPP at lower rates, and similarly, a tendency for GPP>ER at higher metabolic rates. This same pattern has been recognised before for coastal waters, by Duarte & Prairie (2005) in their study of metabolism in different aquatic systems, implying that ER takes longer than GPP to decline, within less productive ecosystems. This observation that less productive aquatic ecosystems tend to be more heterotrophic at lower productivity rates, implies that these systems rely on allochthonous inputs of organic matter (Azevedo *et al*., 2006; Duarte & Agustí, 1998) and that metabolic balance of plankton communities in coastal areas is mainly regulated by factors

controlling autotrophic processes, such as nutrient inputs and temperature (e.g. Agusti *et al*., 2018).

Changes along the GPP:ER diagonal represent variations in ecosystem vitality, thus, systems can be classified by their metabolic state ranging from oligotrophic at low rates to eutrophic at high rates, with mesotrophic conditions being intermediate (Kemp & Testa, 2011). Using this approach both estuaries seemed to be situated between oligotrophic and mesotrophic states, with SOT particularly leaning to mesotrophic conditions.

In order to apply the more traditional trophic classification based on the yearly organic Carbon supply of an ecosystem (Nixon, 1995), NCP calculated in O_2 needed to be converted to organic carbon equivalents. This can be accomplished by using a productivity PQ and a respiratory quotients RQ; whereas the PQ corresponds to the ratio of gross photosynthetic O_2 production GPP to DIC fixation, and the RQ reflects the ratio among O_2 consumed during respiration ER and DIC (Jeffrey et al., 2018; Taddei, Cuet, Frouin, Esbelin, & Clavier, 2008). Often is assumed constant values for PQ and RQ, commonly ranging from 0.6 to 1.5 (Robinson, 2019). For the present study, the PQ and RQ were assumed equal to 1 following the proposal for the European coastal zone proposed by Gazeau *et al*., (2004). Using the coastal marine eutrophication classification proposed by Nixon (1995), both estuaries were classified as mesotrophic (100-300 g C m^{-2} y^{-1}), with CHR positioned slightly higher (~131 g C m^{-2} y^{-1}) than SOT (~128 g C m^{-2} y^{-1}) on the scale.

The simplest model used to estimate primary production describes it as a linear function of phytoplankton biomass, and is generally measured through values of the concentration of Chl '*a*' (e.g. Cloern *et al*., 2014). In Figure 4.14, daily rates

classified as within Blooms in Chapter 3 were highlighted to assess the viability of Chl '*a*' as a predictor or primary production and trophic state, in the two estuaries studied. The analysis was carried out under the premise that rates classified as blooms would be below the metabolic balance line (GPP:ER = 1). SOT presented 78.8% of total NCP observations explained by phytoplankton biomass (Fig. 4.14a). In SOT, almost two thirds (64.3%) of the daily rates classified as Blooms and identified as heterotrophic, were estimated for 2020. Another implication of the NCP model not responding well to calculations based on estimated salinity and temperature values assumed due to the 4.5-month gap after temperature and conductivity sensors stopped logging data and were not accessible because of COVID-19 social distancing restrictions. In CHR, 75.1% of Bloom daily rates were related to positive values of NCP (Fig. 4.14b). Nearly half of these estimations (47.8%) were documented in 2015, a year where data for most of spring and summer is missing. Seasons that, according to the whole time series, are the most productive in the estuary.

Phytoplankton biomass in estuarine ecosystems is highly variable and can fluctuate up to 500-fold across these systems, as demonstrated in the compilation by Cloern & Jassby (2008) of Chl 'a' measurements from more than 100 coastal ecosystems representing the global diversity of marine habitats. Moreover, coastal chlorophyll integrated primary production can differ by a factor of 3 to 4 against direct measurements of production (e.g. Chavez *et al*., 2011) since interannual variability in biomass corresponds to even larger variability in primary production (e.g. May *et al*., 2003). Nevertheless, results of NCP rates explained by daily variation of phytoplankton biomass in SOT and CHR are better than the prediction of variance in Chl '*a*' from a pH/O_2 model in Narragansett Bay

(Oczkowski *et al*., 2016) where only 27–60% could be explained. A closer explanation of the daily variability of phytoplankton productivity from fluctuations of Chl '*a*' is the 64% reported for the Saanich Inlet (Grundle *et al*., 2009) a British Columbia fjord (Canada). Lastly, the highest variability of annual phytoplankton primary production explained by oscillation of the annual mean of Chl '*a'* found in the literature review was 81%, as reported by (Keller *et al*., 2001) for the Boston Harbor-Massachusetts Bay (USA).

4.4.4 Seasonal and interannual fluctuations of productivity rates

The PCA analysis presented in Figure 4.12, permitted a separation of productivity rates by season. For SOT the metabolic balance among seasons, showed a net autotrophic state only during spring (6.4 mmol O_2 m^{-2} d^{-1}) with a few sporadic daily rates during summer also presenting positive NCP values (Fig. 4.15b). This reduced the average NCP for summer months to a less heterotrophic state (-16.9 mmol O_2 m^{-2} d^{-1}) than that observed for autumn and winter (~ -25.0 mmol O_2 m^{-2} d^{-1}). Spring and summer GPP rates (~33.5 mmol O_2 m^{-2} d^{-1}) were almost three orders of magnitude higher than the rates for winter and autumn (~11.2 mmol O_2 m^{-2} d^{-1}). However, spring showed a slightly lower rate of ER than the other seasons which, in addition to the elevated GPP rates, derived in net autotrophic conditions for spring. The trophic balance for CHR (Fig. 4.16b) described summer and spring as net autotrophic (30.8 and 22.6 mmol O_2 m^{-2} d^{-1}, respectively), and autumn as heterotrophic (-8.6 mmol O_2 m^{-2} d^{-1}). Although winter was also classified as heterotrophic, it is important to notice that NCP calculations for this season were not available for 2014 and 2018, and more than half of observations were found in 2015. Winter and spring were separated from autumn and summer at CHR by the influence of riverine inflow which is higher during these seasons

(see Fig. 3.15e, section 3.3). River runoff was also correlated to [O_2] which the open water diel oxygen method indicates is mainly driven by GPP.

In both estuaries, the dominant factors driving metabolic rates appeared to be related to seasonal changes in light availability and temperature, with the addition of freshwater flow affecting CHR rates. This produced a shift from heterotrophic to autotrophic state associated with the season (Azevedo *et al*., 2006; Tang *et al*., 2015). The same seasonal dominance over the trophic state by light and temperature, was previously documented by Murrell *et al*. (2018) for a shallow, river-dominated estuary in Pensacola Bay (USA).

Strong temperature effects on respiration rates have been reported in estuarine systems (Caffrey, 2003; McKinnon *et al*., 2017), however, this was not the case for the present study. Additionally, ecosystems in regions such as the north-eastern Gulf of Mexico (Caffrey *et al*., 2014) and Matilda Bay (Australia) (Agusti *et al*., 2018) have not found clear seasonal trends in either GPP or ER throughout the year.

The extensive compilation of productivity rates in estuaries across the U.S. made by Caffrey (2004) found that all ecosystems located in the mid-Atlantic region exhibited summer production and respiration rates around 1.5–2 times higher than in other seasons, similar in magnitude to GPP rates observed in SOT and CHR, but not ER since rates were more evenly spread throughout the year.

Weaker heterotrophic conditions during spring and summer were observed in the Ria Formosa Lagoon (Portugal), when the study area was considered slightly autotrophic for very short periods (Cravo *et al*., 2020). In addition, a mainly heterotrophic state was reported for winter in the shallow bank site at the mouth

of the River Thames (Hull *et al*., 2016). These studies aligned with similar findings for SOT and CHR.

ER magnitude seems to be increasing across the SOT time series by around 22% each year, with the exception of 2020 that increased by three orders of magnitude against the previous years (Fig 4.15a). A similar trend was observed for GPP but not to the same degree as ER, thus, annual net heterotrophic conditions have been steadily increasing and were only brought to almost metabolic balance in 2019 (Fig 4.15b). In comparison in CHR, the rate of GPP has seen an increase throughout the time series, particularly from 2016 when GPP doubled in comparison to the previous year, and after that, annual averages remained above 28 mmol O_2 m^{-2} d^{-1}. From 2015 to 2016, ER decreased by ~50% and remained at similar values (11.6 mmol O_2 m^{-2} d^{-1}) until the end of the time series (Fig. 4.16a). Therefore, a net autotrophic state has prevailed in the estuary since 2015 (Fig. 4.16b). According to Cai (2011), research has strongly suggested that the coastal ocean, and particularly estuarine ecosystems, are significant sources of CO_2 to the atmosphere, therefore, a net heterotrophic state generally prevails. Moreover, it has been reported that increased nutrient inputs to this region could shift ecosystems towards net heterotrophy (e.g. Mortazavi *et al*., 2012).

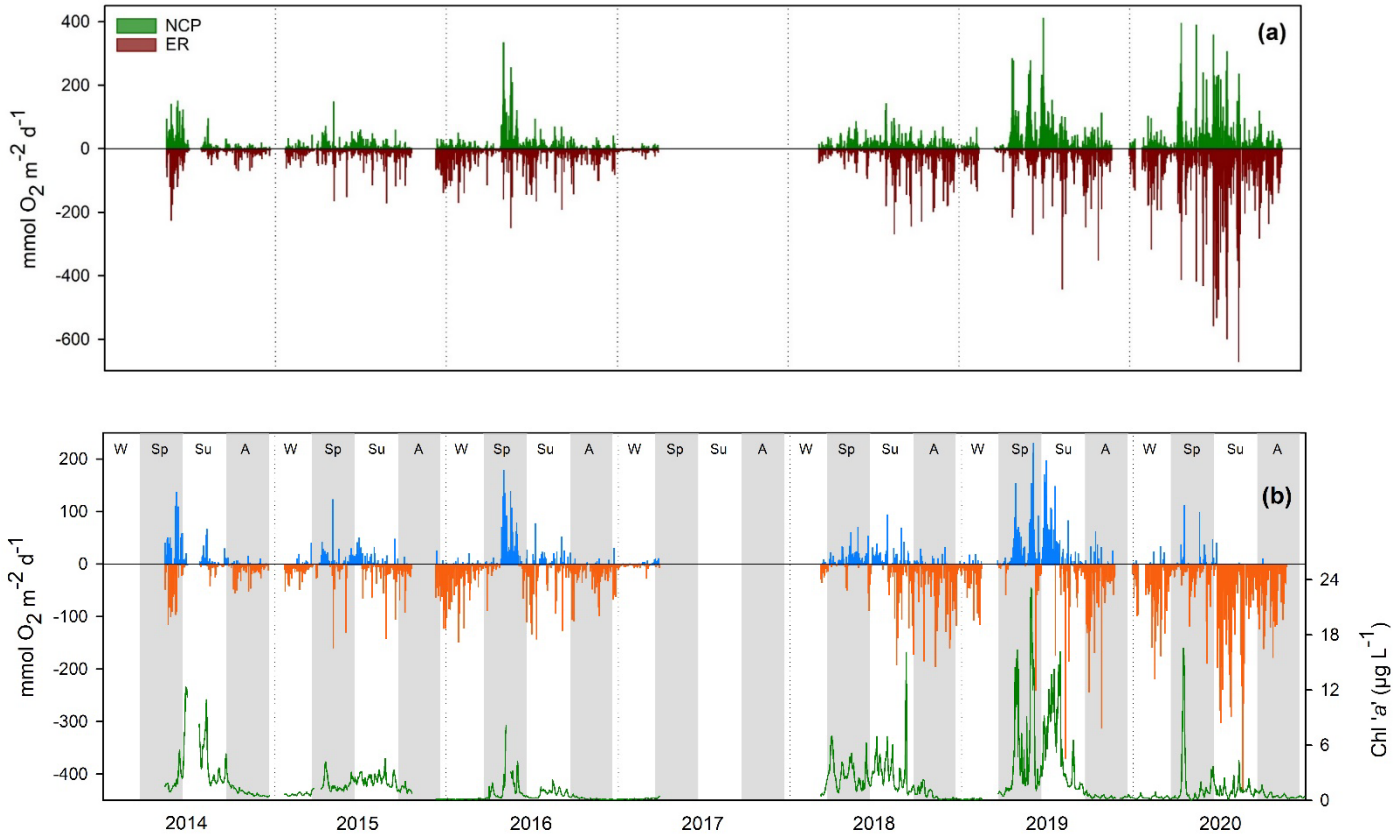

Fig 4.15 Time series from 2014 to 2020 of (a) calculated daily respiration ER (red bars ▮) and gross primary production GPP (green bars ▮) and (b) calculated net community production in Southampton Water. In (a) ecosystem respiration data are displayed as negative values for convenience of graphing. In (b) negative values indicate net heterotrophic state (orange bars ▮), and positive values indicate net autotrophic state (blue bars ▮). Daily chlorophyll '*a*' is shown as a green line —. Seasons are represented with white and grey bars; W=winter, Sp=spring, Su=summer and A=autumn.

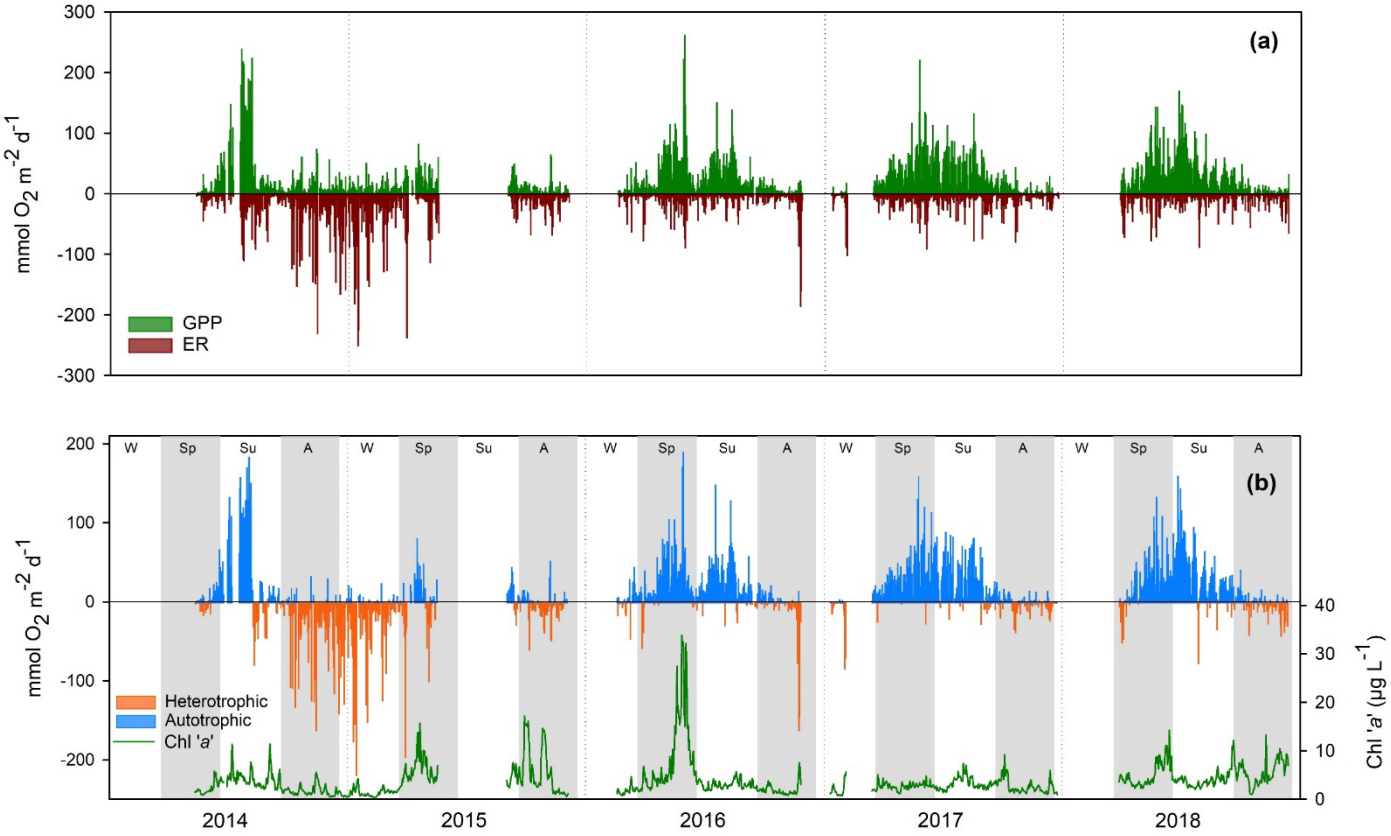

Fig 4.16 Time series from 2014 to 2018 of (a) calculated daily respiration ER (red bars) and gross primary production GPP (green bars) and (b) calculated net community production in Christchurch Harbour Ferry Pontoon. In (a) ecosystem respiration data are displayed as negative values for convenience of graphing. In (b) negative values indicate net heterotrophic state (orange bars), and positive values indicate net autotrophic state (blue bars). Daily chlorophyll '*a*' is shown as a green line —. Seasons are represented with white and grey bars; W=winter, Sp=spring, Su=summer and A=autumn.

Average ER in SOT (38.6 mmol O_2 m^{-2} d^{-1}) was more than two orders of magnitude higher than the mean ER for CHR (16.5 mmol O_2 m^{-2} d^{-1}). In addition, ER across the time series ranged between 0.1 and 664.7 mmol O_2 m^{-2} d^{-1} in SOT, and from 0.1 to 284.4 mmol O_2 m^{-2} d^{-1} in CHR, with values for both estuaries in agreement with the variation reported by Robinson & Williams (2005) for community respiration in coastal areas (0.9 – 670 mmol O_2 m^{-2} d^{-1}). Furthermore, on their review of open–water portion of estuaries, Hopkinson & Smith (2005) reported ER based on O_2 incubations (Feb–Sep 1972) for Southampton Water to be an average of 93 mmol O_2 m^{-2} d^{-1} and have ranged from 0.1 to 246 mmol O_2 m^{-2} d^{-1}. Their higher ER average, compared to the result of this study, is perhaps a result of incubations excluding less productive months (Oct–Jan), while a smaller range is an indication of the interannual variability.

Even though GPP average was very similar for SOT and CHR (24.5 and 25.0 mmol O_2 m^{-2} d^{-1} respectively), the maximum observed in SOT of 411.2 mmol O_2 m^{-2} d^{-1} was almost double the peak observed in CHR (284. 4 mmol O_2 m^{-2} d^{-1}). A similar maximum GPP (256 mmol O_2 m^{-2} d^{-1}) to that in CHR was reported among systems in the northeast coast of the U.S. (Caffrey, 2004), while only systems in southern California matched the peak registered in SOT.

Annual NCP estimations for SOT (-48.7 to -0.9 mmol O_2 m^{-2} d^{-1}) are comparable with ranges reported for other estuaries presenting mainly heterotrophic conditions (-71.0 to -0.1 mmol O_2 m^{-2} d^{-1}) (Caffrey, 2004; Cravo *et al*., 2020; Hull *et al*., 2016; Mortazavi *et al*., 2012; Murrell *et al*., 2018). In contrast, CHR showed a tendency to become more autotrophic and its annual NCP calculations (-11.7 to 19.8 mmol O_2 m^{-2} d^{-1}) were comparable to the ones described for a eutrophic ecosystem in Western Australia (-9.3 to 76.99 mmol O_2 m^{-2} d^{-1}) (McKinnon *et al*.,

2017). However, CHR is a considerable smaller, shallower estuary and does not present sustained periods of high chl '*a*' concentration or any other signs of eutrophication in the outer estuary region (Huggett *et al*., 2021a).

Most research describing primary production, in terms of GPP and ER, has been done in the northern hemisphere between 30°N and 50°N. However, these measurements have been collected largely in the open ocean and coastal areas (<20m) and mainly during the temperate and austral spring (e.g. Robinson & Williams, 2005). This information highlights the necessity of estimations of NCP including paired ER and GPP measurements to be made in estuaries, given that these systems are highly dynamic, presenting fluctuations in primary production over short temporal scales (days to hours) (e.g. Guenther *et al*., 2017) and present an opportunity to evaluate the health of these areas in order to prevent adverse effects such as eutrophication (e.g. Liu *et al*., 2015).

4.4.5 Open water diel oxygen method implications

The open water diel oxygen method coupled with high- frequency water quality monitoring is a powerful tool to help understand the influence of physical and biological processes on DO changes through time, particularly since the principal biological process influencing the ocean's declining DO concentration is phytoplankton respiration (Robinson, 2019). The increasing availability of improved and affordable instrumentation has made it possible to create high-frequency time-series from which more reliable estimations of net community production can be derived and evaluate different scales of spatial and temporal variability within ecosystems (Aristegi *et al*., 2009; Staehr *et al*., 2012).

As with any other method, assumptions must be made in order to apply the approach to different ecosystems and data availability. Since it frames the

possibility of applying the open water diel oxygen method to a particular ecosystem, one of the main assumptions is that the water column monitored must be reasonably homogenous and well mixed (e.g. Caffrey *et al*., 2014). Therefore, vertical profiles of temperature, salinity and dissolved oxygen were made in SOT in 2018 and 2019, with a different EXO2 sonde (see Chapter 2, section 2.6), this analysis presented temperature differences between the surface and bottom waters ranged from 0.1°C in late April to 2.0°C in July. DO saturation through the water column presented higher variability in August (9%) and did not correspond with the profile presenting the greater temperature variation or the highest temperature (July). Both DO saturation and temperature showed less variability through the water column than data in Murrell et al. (2018) study (26% and ~4°C) where the open water diel oxygen method was applied in a shallow, river-dominated estuary located in the northeaster Gulf of Mexico.

Among other complications previously encountered using this methodology, is the necessity to separate air-sea O_2 exchange (Staehr et al., 2012; J M Testa & Kemp, 2011). Direct measurements of air-water exchange can present great difficulty, and some past works have opted for assumed constant values for similar systems (e.g. Caffrey, 2004). Since air-water exchange can vary with fluctuations in surface turbulence, water viscosity and the solubility of O_2 (e.g. Holtgrieve *et al*., 2010); to minimised error propagation, in the present study it was calculated for every time-step (1 hour) as a function of diffusion through bubbles and gas transfer velocity, which in turn included the Schmidt number encapsulating influences of water temperature and salinity. Contribution from partially dissolved bubbles and overestimation in the air-water transfer has been reported previously (Haskell *et al*., 2019; Liang *et al*., 2013), without explicit

consideration of bubble-mediated supersaturation, NCP can be significantly overestimated (e.g. Nicholson *et al*., 2015).

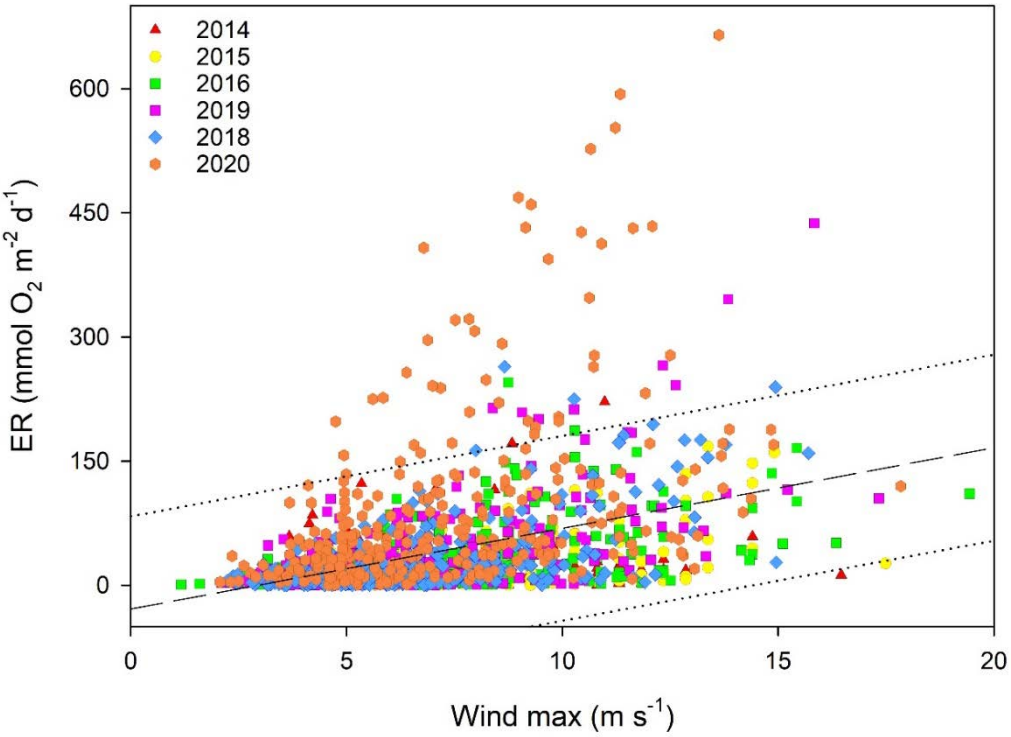

Fig 4.17 Comparison of maximum daily wind speed and daily ecosystem respiration (ER). Symbols and colours differentiate years: 2014 (red triangles ▲), 2015 (yellow circles ●), 2016 (green squares ■), 2017 (light blue hexagons ⬢), 2018 (blue diamonds ◆), 2019 (pink squares ■) and 2020 (orange hexagons ⬢). Linear regression is represented with a dash black line (– –) and prediction intervals with a dotted line (…).

However, both estuaries showed a strong correlation between values of calculated ER and wind speed (Table 4.1). In Fig. 4.17 it is noticeable that isolated elevate ER calculations correspond to wind gusts above ~9 m s^{-1}, thus, inducing negative NCP and perhaps overestimating heterotrophic conditions. Although it is known that in shallow ecosystems high wind gusts can induce rates of sediment resuspension, affecting the magnitude and balance between GPP and ER (Hull *et al*., 2016; Staehr *et al*., 2012; Testa & Kemp, 2011), in the current study seems to be an overprediction of the biological oxygen production (BOP) calculation due to the poor performance of the wind speed curve fitting at higher winds (see Chapter 2, Fig. 2.3). Moreover, 2020 calculations for SOT, seemed to

have worsen the BOP overestimation (Fig. 4.17) through DO approximations from yearly averages of temperature and salinity (see Chapter 2, section 2.2.1).

A final generalisation is that ER rates are assumed constant through the diel cycle since CO_2 fixation through chemoautotrophic processes is usually smaller than that fixed by photosynthesis. However, in systems where nitrification is an important process, overlooking it could result in overestimating ER and underestimating NCP (Hull *et al*., 2016; Murrell *et al*., 2018). Nitrification could represent up to 20% of total organic matter production around the maximum turbidity zone (e.g Gazeau *et al*., 2005c) and it can be increase by organic matter inputs from water runoff (Hopkinson & Smith, 2005). Given the characteristics of high light transparency and low nutrients in the estuaries studied, particularly SOT, nitrification and photooxidation were assumed to be insignificant compared to estimates of 'night respiration' (Demars *et al*., 2015; Kemp & Testa, 2011).

There are several methods to estimate aquatic primary production, but few provide the opportunity to calculate direct continuous productivity rates for long periods at a low cost and fieldwork intensity, and at the same time, make available easy validation using independent estimations, like the open water diel oxygen method (e.g. Briggs *et al*., 2018). Climate change and variability in environmental conditions will have an effect on both ER and GPP and, consequently, on NCP (Staehr *et al*., 2012), therefore, it is vital to increase understanding of how these factors influence productivity rates across a broader range of coastal regions, and in a scale that allows prevention and mitigation management in future years.

4.5 Conclusions

The present study identified trends suggesting between 2014 and 2020 the Southampton Water estuary had become more net heterotrophic (from -1.3 to -

48.7 mmol O_2 m^{-2} d^{-1}), while between 2014 and 2018 Christchurch Harbour seemed to be turning more net autotrophic (-11.7 to 19.8 mmol O_2 m^{-2} d^{-1}).

In both estuaries, the dominant factors driving metabolic rates were related to seasonal changes in light availability and temperature, with the addition of riverine inflow affecting Christchurch Harbour. This produced a shift from heterotrophic to autotrophic state mainly in spring and summer.

An analysis between productivity, temperature and light availability showed that, for Southampton, a surface water temperature threshold of 10.5 °C, surface water irradiance above 1520 Wh m^{-2} d^{-1} and mean water column irradiance greater than 415 Wh m^{-2} d^{-1}, corresponded maximum NCP calculated rates, meaning positive values above 100 mmol O_2 m^{-2} d^{-1} and negative NCP beyond -200 mmol O_2 m^{-2} d^{-1}. Furthermore, the same analysis revealed that in Christchurch, NCP exceeding positive and negative values beyond 50 mmol O_2 m^{-2} d^{-1}, were consistent with the appearance of water temperatures above 10.3 °C, values above 1240 Wh m^{-2} d^{-1} for surface water irradiance and mean water column irradiance higher than 950 Wh m^{-2} d^{-1}. This analysis concluded that Christchurch Harbour being a shallower and more turbid water column is more affected by disturbances in the mean water column irradiance.

The examination of the relation between ecosystem respiration and gross primary production permitted values for metabolic balance (GPP:ER) for each system to be estimated (22.4 mmol O_2 m^{-2} d^{-1} for Southampton and 4.9 mmol O_2 m^{-2} d^{-1} for Christchurch). This results implicate that production needed to shift the Southampton from net heterotrophy to net autotrophy is four orders of magnitude higher than what is needed in Christchurch. This approach also allowed classification of both estuaries between oligotrophic and mesotrophic states, with

Southampton particularly leaning towards mesotrophic conditions. A tendency of ecosystem respiration exceeding gross primary production at lower rates along the metabolic balance (GPP:ER) analysis was observed, implying that metabolic balance in these systems relies to some extent on allochthonous inputs of organic matter.

A comparison between days classified as within bloom events, using chlorophyll ‘a’ concentration, and net autotrophic daily rates, highlighted the viability of chlorophyll ‘a’ as a predictor or primary production and trophic state since more than 75% observations overlapped.

The open water diel oxygen method proved to be a reliable technique to integrated daily estimations of ecosystem production and respiration rates in both estuaries. Ecosystem respiration showed no clear dependence on water temperature, in agreement with the assumption that respiration rates are constant during day and night. However, the methodology has the disadvantage of requiring a very precise air-sea correction that can be easily disturbed by over or underestimation of wind speed, which in turns results in uncertainty in the O_2 air-sea calculation. In the present study, in order to minimised error propagation, the diffusive exchange of O_2 across the air– sea interface was calculated for every time-step (1 hour) as a function of diffusion through bubbles and gas transfer velocity, instead of using a constant.

Chapter 5

Plankton carbon metabolism and air-sea CO_2 fluxes at Southampton Water estuary

Abstract

Coastal zones account for about 20% of total ocean CO_2 flux, nevertheless, a comprehensive description and analysis of the spatial and temporal variability of CO_2 fluxes and their relation to environmental factors in estuaries is scarce. In this chapter, an estimation of carbonate system parameters (CO_2 flux, partial pressure of CO_2, dissolved inorganic carbon, total alkalinity and pH) was carried out at hourly intervals for a position in the Southampton Water estuary in 2019 and 2020 using the software CO_2^{calc}, described in Chapter 2, using inputs of discrete sampling of dissolved inorganic carbon and total alkalinity and the continuous monitoring of pH. The estuary exhibited an annual average of 6.56 ± 10.43 mmol C m^{-2} d^{-1}, acting as a source of CO_2 to the atmosphere and agreeing with the overall net heterotrophic classification performed in Chapter 4. Discrepancies among estimations were attributed to possible seasonal stratification, wind speed affecting the calculation of O_2 fluxes and estuarine flushing times. Frequency and magnitude of riverine inputs influenced the distribution of carbonate system parameters, presenting supersaturated CO_2 conditions in summer when there was reduced daily river discharge and undersaturated CO_2 corresponding to high riverine inflow during winter. Biological processes were identified as a major factor controlling the pH/oxygen saturation

dynamics and CO_2 fluxes were observed to follow the pattern of DIC, indicating its association with metabolic rates.

5.1 Introduction

Estuaries are one of the most biogeochemically active systems of the coastal zone due to intense inputs of nutrients and carbon from land through rivers and from the open ocean at continental margins (Borges *et al*., 2006). Yet, despite the importance of dissolved gases in many of the biogeochemical cycles of estuaries and coastal waters, only during the last two decades have large-scale collaborative efforts addressed the importance of air-sea exchange in estuaries (Bianchi, 2012).

The consensus regarding estuaries, is that they are considered net heterotrophic, acting as sources of CO_2 to the atmosphere (Bianchi, 2012; Cai, 2011; Frankignoulle et al., 1998; Hu et al., 2020; Yao et al., 2020), particularly in the outer plume region (Bianchi, 2012). This is mainly attributed to the large inputs of terrestrial organic carbon that these ecosystems receive (Guenther *et al*., 2017), resulting in increased respiration of detrital organic matter, which in turn produces large quantities of dissolved CO_2 that generate very high fluxes to the atmosphere.

One of the main drivers of estuarine CO_2 emissions to the atmosphere is the rate of primary production (the photosynthetic production of carbon and oxygen) (Frankignoulle & Middelburg, 2002), since it acts as a fundamental component of the global carbon cycle and initiating the biogeochemical cycling of major nutrients (Henderikx *et al*., 2020).

It has been reported that air-sea CO_2 fluxes and net community production (NCP) in estuaries show a consistent pattern of being a source of CO_2 coupled to net heterotrophy (Borges *et al*., 2006; Gazeau *et al*., 2005c; Gupta *et al*., 2008; Raymond *et al*., 2000), yet the link between the exchange of CO_2 with the atmosphere and the metabolic status is not direct since the variability of air-sea CO_2 fluxes is also a function of the physical settings of estuaries, in particular with respect to the occurrence of vertical stratification, and residence time of the water mass (Borges & Abril, 2011). To better understand how CO_2 and O_2 are transferred across the air–sea boundary, the environmental parameters driving their dynamics in estuarine waters need to be examined (Shen *et al*., 2019a).

The aim of this chapter is to provide a depiction of the seasonal and interannual carbonate chemistry parameters for the Southampton Water estuary and explore drivers of the carbonate system parameters and its connection to net community production.

5.2 Seasonal oscillation of the carbonate system in Southampton Water

Parameters for the carbonate system in the Southampton Water estuary were calculated using the program CO_2^{calc} (see Chapter 2, section 2.7.1). Time series of hourly calculations are presented for 2019 and 2020 for Southampton Water.

5.2.1 Estuarine carbonate chemistry

pH

A strong seasonality was observed for pH across the 2-year time series (Fig. 5.1a), with both years showing the same general pattern. This parameter presented the highest seasonal average during Winter (8.17 ± 0.01), to then start

decreasing values throughout spring (8.10 ± 0.03). Observations reached the lowest seasonal mean of 8.02 ± 0.01 in summer (Table 5.1). At the end of this season, values started increasing continuously, a trend that prevailed all through autumn (8.09 ± 0.03). Although 2019 showed the maximum (8.21) and the minimum (7.98) of the time series, the yearly averages were identical, with 2019 presenting 8.09 ± 0.04 and 2020 showing 8.09 ± 0.07 as a mean value. Annual minimum pH was detected for both years in July, while maximums were detected in February.

pH variability was significantly higher during spring and autumn than in winter and summer, indicating that spring and autumn were acting more as transitional seasons (p<0.001, Table 5.2), whereas winter and summer appeared to be more stable. However, winter in 2020 was considerably less variable than in 2019, when a high peak pH value was observed (Fig. 5.1a).

Dissolved inorganic carbon and total alkalinity

Dissolved inorganic carbon (DIC) and total alkalinity (T_{alk}) presented an analogous fluctuation between the seasons and years, as can be seen in figure 5.1b & c. For both parameters, winter was the season showing the highest average values, with 2413 ± 68 µmol kg^{-1} for DIC and 2578 ± 63 µmol kg^{-1} for T_{alk}. During spring, values started to steadily decrease, particularly in 2020, reaching season averages of 2365 ± 32 µmol kg^{-1} for DIC, and 2533 ± 29 µmol kg^{-1} for T_{alk}. This trend extended throughout the summer season when the lowest mean values were observed for DIC and T_{alk} (2295 ± 30 and 2467 ± 28 µmol kg^{-1}, respectively). At the end of summer, DIC and T_{alk} values started rising again. However, hourly maximums did not reach those registered for winter in either of the studied years (Table 5.1). Seasonal averages in autumn were 2360 ± 70 µmol

kg^{-1} for DIC, and 2529 ± 66 µmol kg^{-1} for T_{alk}. For 2019 and 2020, maximum values occurred in February, whereas minimums during September were identified for both parameters.

Although spring and autumn presented very similar seasonal averages, the variation among data was higher in autumn, particularly in 2020, where spring showed a smaller fluctuation than in 2019 (Fig. 5.1b & c). Furthermore, winter in 2019 exhibited a marked peak in values in the middle of the season that was not observed in 2020, when values oscillated greatly but between a very specific range, 2329 – 2544 for DIC and 2497 – 2701 for T_{alk}. This made a significant difference between winter within the two years studied (p<0.001, Table 5.2), and favoured a larger influence in the seasonal average by the 2020 data.

Partial pressure of CO_2 in the aquatic system

The estuarine partial pressure of CO_2 (ρCO_2) showed a large seasonal variation (Fig. 5.1d), with a similar annual pattern for 2019 and 2020. Starting with low values throughout winter, reflected in the lowest seasonal average of 450.5 ± 28.6 µatm, ρCO_2 started increasing continuously during spring and presented a mean value of 544.8 ± 52.5 µatm. Summer displayed the highest records of ρCO_2 with a 672.4 ± 27.5 µatm average for the season (Table 5.1). At the end of summer, values started to show a decline that continued throughout autumn (557.1 ± 37.3 µatm). Maximum values were identified during July, whilst minimums were observed in February for the two years included.

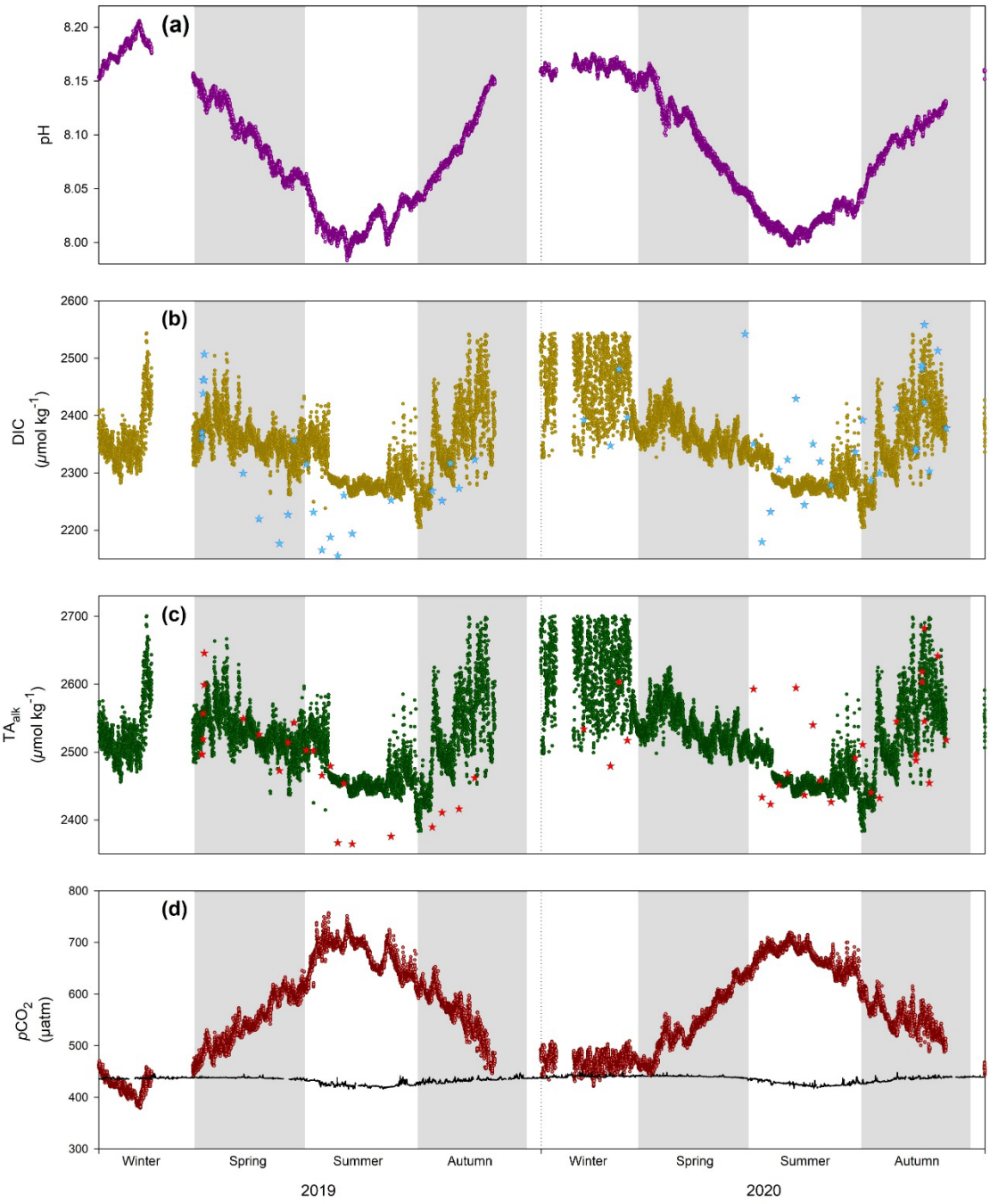

Fig 5.1 Seasonal variations of carbonate system parameters: (a) pH, (b) dissolved inorganic carbon [DIC], (c) total alkalinity [T_{alk}] and (d) partial pressure of CO_2 [pCO_2], calculated with the CO_2^{calc} software for Southampton Water from 2019 to 2020. In (d) the black line represents the atmospheric pCO_2, data from the Ryan Institute's Mace Head Atmospheric Research Station (Galway, Ireland). In (b) and (c) ★ indicate discrete samples.

Table 5.1. Annual and seasonal average, standard errors and range of hourly hydrologic (O_2%), carbonate system parameters (pH, DIC, $T_{alk}, \rho CO_{2\ air}, \rho CO_{2\ sw}$), O_2 (FO_2) and CO_2 (FCO_2) fluxes in Southampton Water from 2019 to 2020.

Parameter	Annual n=730	Winter n=181	Spring n=183	Summer n=184	Autumn n=182
pH	8.09 ± 0.06 (7.98 – 8.21)	8.17 ± 0.01 (8.14 – 8.21)	8.10 ± 0.03 (8.04 – 8.17)	8.02 ± 0.01 (7.98 – 8.06)	8.09 ± 0.03 (8.04 – 8.15)
DIC (µmol kg^{-1})	2351 ± 65 (2205 – 2544)	2413 ± 68 (2282 – 2544)	2365 ± 32 (2262 – 2508)	2295 ± 30 (2216 – 2421)	2360 ± 70 (2205 – 2541)
T_{alk} (µmol kg^{-1})	2520 ± 61 (2383 – 2700)	2578 ± 63 (2456 – 2700)	2533 ± 29 (2437 – 2667)	2467 ± 28 (2394 – 2585)	2529 ± 66 (2383 – 2698)
$\rho CO_{2\ air}$ (µatm)	433.6 ± 6.8 (415.8 – 449.6)	439.0 ± 2.5 (434.5 – 449.6)	438.7 ± 2.1 (431.9 – 447.7)	425.4 ± 4.6 (415.8 – 441.6)	433.3 ± 4.0 (423.2 – 447.8)
$\rho CO_{2\ sw}$ (µatm)	568.4 ± 86.6 (378.7 – 756.8)	450.5 ± 28.6 (378.8 – 509.0)	544.8 ± 52.5 (442.2 – 653.4)	672.4 ± 27.4 (589.9 – 756.8)	557.1 ± 37.3 (445.9 – 652.6)
FCO_2 (mmol m^{-2} d^{-1})	-6.6 ± 10.4 (-133.3 – 20.5)	-1.7 ± 4.1 (-38.9 – 20.5)	-3.7 ± 5.2 (-48.0 – 0.1)	-11.5 ± 14.2 (-133.3 – -0.1)	7.7 ± 10.2 (-105.1 – 0.1)
FO_2 (mmol m^{-2} d^{-1})	13.3 ± 18.5 (0.1 – 247.2)	23.9 ± 28.5 (0.1 – 247.2)	8.9 ± 10.5 (0.1 – 94.5)	10.2 ± 14.4 (0.1 – 116.1)	14.9 ± 17.5 (0.1 – 219.0)
O_2 %	98.9 ± 13.5 (43.9 – 190.7)	97.2 ± 1.4 (91.9 – 101.1)	107.1 ± 15.9 (61.5 – 190.7)	96.1 ± 17.8 (43.9 – 183.5)	93.4 ± 2.2 (81.0 – 9.7)

There was greater variance during spring and autumn than in winter and summer (p<0.001, Table 5.2). Even though both years showed a similar range in values through spring (~200 µatm), autumn in 2019 varied ~200 µatm while in 2020, only ~140 µatm. Moreover, 2019 presented a wider annual range than 2020, with ~378 µatm and ~300 µatm, respectively.

5.2.2 Temporal variability of O_2 and CO_2 air-sea fluxes

O_2 flux

Annual mean air-sea O_2 flux (FO_2) was 13.3 ± 18.5 mmol O_2 m^{-2} d^{-1} (Table 5.1). The range of values during 2019 were from 0.1 to 219.0 mmol O_2 m^{-2} d^{-1} and an average of 11.4 ± 15.2 mmol O_2 m^{-2} d^{-1} was calculated. The following year, maximum value increased to 247.2 mmol O_2 m^{-2} d^{-1} and the mean value 1.3 orders of magnitude larger (15.2 ± 20.9 mmol O_2 m^{-2} d^{-1}). The overall seasonal tendency was for high values during winter (>50 mmol O_2 m^{-2} d^{-1}), then decreasing and remaining mainly below ~25 mmol O_2 m^{-2} d^{-1} during spring and summer, to then increase again (~30 mmol O_2 m^{-2} d^{-1}) at the end of year (autumn), although not as much as in winter.

A significant difference among the distribution of O_2 flux between 2019 and 2020 was identified (p<0.001, Table 5.2). This was mainly driven by the variance between the winter seasons in 2019 (14.2 ± 20.0 mmol O_2 m^{-2} d^{-1}) and 2020 (30.5 ± 31.4 mmol O_2 m^{-2} d^{-1}), given that the average season value in 2020 was doubled that for 2019. Additionally, data in winter for 2020 was distributed in several peaks against just one perceivable peak identified in 2019 (Fig. 5.2a). A minor source of variance was identified within 2020 (p<0.001, Table 5.2) since spring and summer showed lower average values and lesser variation than winter and autumn.

CO_2 flux

Air-sea CO_2 flux (FCO_2) presented and annual average of -6.6 ± 10.4 mmol C m^{-2} d^{-1}. Averages among years investigated were very similar, with -6.6 ± 11.2 mmol C m^{-2} d^{-1} for 2019 and -6.5 ± 9.7 mmol C m^{-2} d^{-1} for 2020 (Table 5.1). However, the range of values decreased from one year to another, from -133.3 to 20.5 mmol C m^{-2} d^{-1} to -100.7 to 5.6 mmol C m^{-2} d^{-1}. Positive values, indicating net flux from the atmosphere to the aquatic system, were observed only during winter of both years, and winter 2019 was the only season that averaged above zero, presenting 0.7 ± 2.1 mmol C m^{-2} d^{-1} (Fig. 5.2b). Summer was visibly the season with the lowest values, showing an average of -11.5 ± 14.2 mmol C m^{-2} d^{-1}. It was followed by autumn, which did not present an average as decreased as summer (-7.7 ± 10.2 mmol C m^{-2} d^{-1}), although maximum values were close, and well above the other seasons. Winter and spring averages remained above -4 mmol C m^{-2} d^{-1} in both years.

There was a significant difference between seasons but not between the years studied (p<0.001, Table 5.2). This variance among seasons was mainly attributed to the lower values observed in winter of 2019, when for a period of 18 days, negative CO_2 fluxes were recorded. An additional source of variance was credited to the fluctuation of winter and spring averages within years, given that in 2019 the difference between seasons was 4.8 mmol C m^{-2} d^{-1}, while in 2020, the fluctuation reduced to 0.1 mmol C m^{-2} d^{-1}.

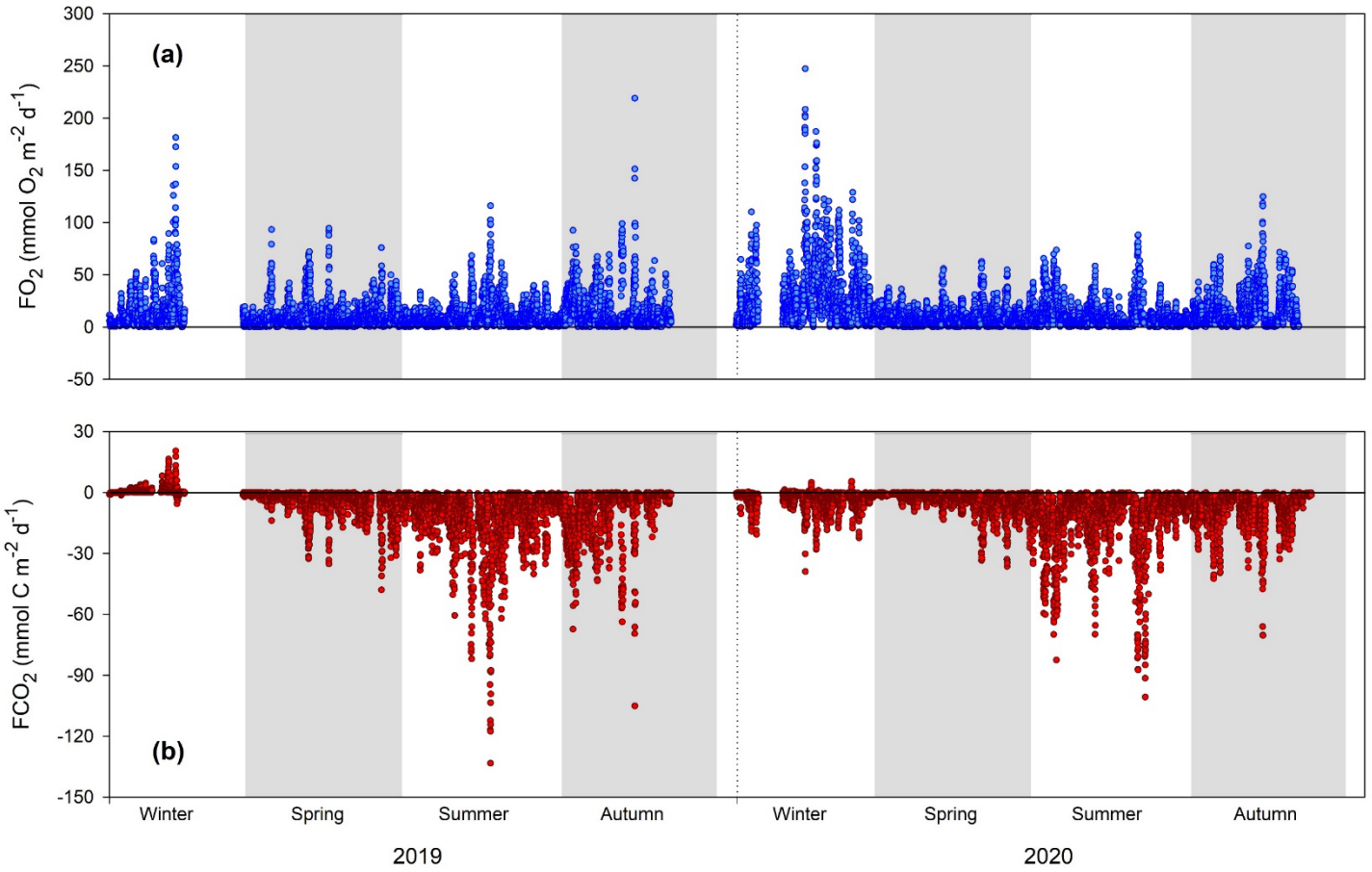

Fig 5.2 Seasonal variation of air-sea (a) O_2 (mmol m^{-2} d^{-1}) and (b) CO_2 (mmol m^{-2} d^{-1}) fluxes in Southampton Water from 2019 to 2020. In (a) and (b) positive values indicate net flux from the atmosphere to the aquatic system. O_2 fluxes were calculated with the open water diel method. CO^2 fluxes were calculated with the CO_2^{calc} software.

Table 5.2. Two-way ANOVA of daily carbonate system parameters, testing for season (winter, spring, summer and autumn) and year (2019 and 2020) effects, and their interactions.

Parameter	Factor	dF	SS	MS	F	P
pH	Seasons	3	1.6	0.5	945.0	<0.001
	Year	1	0.0	0.0	1.5	0.226
	Seasons*Year	3	0.0	0.0	4.8	0.002
DIC	Seasons	3	980755.0	326918.3	216.9	<0.001
	Year	1	85119.2	85119.2	56.5	<0.001
	Seasons*Year	3	165541.8	55180.6	36.6	<0.001
T_{alk}	Seasons	3	859044.3	286348.1	216.9	<0.001
	Year	1	74555.8	74555.8	56.5	<0.001
	Seasons*Year	3	144997.9	48332.6	36.6	<0.001
$\rho CO_{2\,sw}$	Seasons	3	3743544.2	1247848.1	901.1	<0.001
	Year	1	10298.6	10298.6	7.4	0.007
	Seasons*Year	3	54519.2	18173.1	13.1	<0.001
FCO_2	Seasons	3	8526.1	2842.0	48.5	<0.001
	Year	1	44.8	44.8	0.8	0.382
	Seasons*Year	3	526.7	175.6	3.0	0.03
FO_2	Season	3	14594.4	4864.8	28.6	<0.001
	Year	1	2545.1	2545.1	15.0	<0.001
	Seasons*Year	3	5729.7	1909.9	11.2	<0.001

Holm-Šídák post hoc test $p<0.05$. dF=degrees of freedom, SS=sum of squares, MS=mean squares, F=factorial test, and P= *p*-values for treatments (season and year).

5.3 Analysis of variation in air-sea exchange from biogeochemical processes

5.3.1 Main factors impacting air-sea O_2 and CO_2 fluxes

Estuaries are a major boundary in the land-ocean interaction zone where the gathering of different biogeochemical processes results in high air-sea O_2 and CO_2 fluxes, making them more dynamic and complex than the open ocean (Cai, 2011; Duarte *et al*., 2013a). To assess the relationship between environmental factors and carbonate chemistry parameters with FO_2 and FCO_2, the Spearman's correlation coefficient was calculated (Table 5.3) for the Southampton Water estuary, for 2019 and 2020 individually, and the complete time series.

FO_2 showed a strong correlation ($\rho>0.97$) with wind speed throughout the time series. This is expected since wind is a key parameter in calculating the biological oxygen production used to compute net community production (NCP). Although it has been stated before that, in shallow ecosystems, high wind gusts can affect the magnitude and balance between gross primary production (GPP) and ecosystem respiration (ER) due to wind-induced mixing (Hull *et al*., 2016; Kemp & Testa, 2011; Staehr *et al*., 2017), in this research, it was established that NCP calculations were most likely overestimating heterotrophic conditions, and the correlation between ER and wind, although present, was over amplified (see Chapter 4, section 4.4.5).

A clear influence of the relations calculated for FO_2 in 2020 on those estimated for the complete time series is observed (Table 5.3), since patterns for both years are more similar to those in 2020. Apart from wind and ER, FO_2 in 2019 only presented a moderate correlation ($\rho=0.44$) with GPP. Conversely, for 2020, a

moderate positive correlation was found with ER (ρ=0.48) and river inflow (ρ=0.42), while negative modest correlations were identified with I_m (ρ=-0.51) and NCP (ρ=-0.47). Weaker direct correlations (0.30<ρ<0.37) were observed between FO_2 and T_{alk}, DIC, pH and GPP, whilst negative with $\rho CO_{2\ sw}$ (ρ=-0.27), I_0 (ρ=-0.39) and temperature (ρ=-0.33). FO_2 is linked to primary production due to the release of oxygen during photosynthesis and uptake during aerobic respiration (Caffrey, 2003, 2004; Herrmann *et al*., 2020).

FCO_2 was strongly negatively correlated to most of the carbonate system parameters (Table 5.3); T_{alk} (ρ=-0.69), DIC (ρ=-0.69) and pH (ρ=-0.99), indicating that CO_2 release to the atmosphere was closely related to increases in those parameters. The correlation of ρ=1.0 between FCO_2 and ρCO_{2sw} was anticipated since FCO_2 is estimated from the difference between CO_2 partial pressure in seawater ρCO_{2sw} and the atmosphere ρCO_{2air} (see Chapter 2, section 2.7.2). The close connection among the carbonate system parameters is an expected outcome due to their participation in different states of the C buffering process in aquatic systems (Duarte *et al*., 2013a, b; Millero, 2010). However, data for 2020 showed a slightly higher relationship between FCO_2, DIC and T_{alk} than in 2019.

Regarding parameters related to primary production, FCO_2 presented a strong correlation with Chl '*a*' in 2019 (ρ=0.73) and 2020 (ρ=0.60). In a similar pattern, GPP had a stronger relation in 2019 (ρ=0.44) than in 2020 (ρ=0.38), but not as elevated as Chl 'a' (Table 5.3). NCP was positively correlated in 2020 (ρ=0.27) and negatively in 2020 with FCO_2 (ρ=-0.30), possibly driven by ER which only presented a substantial correlation with FCO_2 this year (ρ=0.37). It has been

reported that NCP in estuaries shows a consistent pattern of a CO_2 emission to the atmosphere coupled to net heterotrophy (e.g. Borges & Abril, 2011).

Abiotic factors mainly affected by the annual cycle of solar radiation (I_0 ρ>0.55 and temperature ρ>0.98) showed strong correlations with FCO_2 (Table 5.3); in addition, I_m a parameter also affected by light availability (I_0), presented a moderate relationship (ρ=0.47). Furthermore, oxygen concentration [O_2] negatively correlated in both years (ρ>-0.54), while oxygen saturation (O_2%) only in 2019 (ρ=-0.57). The correlation between FCO_2 and seasonal drivers of phytoplankton bloom development (I_0, I_m and temperature) (Rumyantseva *et al*., 2019) and [O_2], mainly occurs since CO_2 is involved in various aspects of carbon transport and metabolism in photosynthesis (e.g. Raven *et al*., 2020). Lastly, river flow presented a strong correlation with FCO_2 in 2019 (ρ=-0.93) and 2020 (ρ=-0.90), which is credited to riverine input to the estuary being generally rich in organic carbon (e.g. Salisbury *et al*., 2008a).

A PCA analysis was conducted to further investigate the seasonal variation of carbonate chemistry parameters, productivity rates and environmental factors affecting the response of FO_2 and FCO_2. Spatial and temporal variability in carbonate chemistry parameters in estuaries has been identified before using PCA (Shen *et al*., 2020; Uthicke *et al*., 2014). ρCO_{2sw} was omitted from this analysis as it is directly correlated with FCO_2. For the present work, daily observations were classified within ‘seasons’ (autumn, spring, summer and winter) and were noticeably grouped together in the PCA, as seen in figure 5.3. The first two principal components (PCs) accounted for ~64% of the total variance in data. PC1 explained 44.4% of the total variability while PC2 accounted for 19.3%.

The main factors contributing to PC1 positive eigenvalues (R^2>0.36) were temperature and FCO_2, and in a reduced magnitude (R^2>0.14) Chl '*a*', I_0 and I_m. PC1 negative values (R^2>-0.31) were attributed to river flow, DIC, T_{alk} and pH. Component loadings of PC1 showed a seasonal pattern associating positive eigenvalues to daily observations during summer, while negative values were attributed to winter days. PC1 variability is correlated to river discharge, given that maximum FCO_2 (83.1 mmol C m^{-2} d^{-1}) and temperature (22.0 °C) both occurred in summer of 2019, when there was lower daily discharge (<5 m s^{-1}), and the highest DIC, T_{alk} (2660 and 2501 µmol kg^{-1}, respectively) and pH (8.2) values corresponded to high riverine inflow (> 30 m s^{-1}) during winter. Spring and autumn data were situated right at the transition zone of PC1, given that river discharge average for these seasons (11 m s^{-1}) was among values for summer (6.7 m s^{-1}) and winter (18.3 m s^{-1}). Salisbury (2008b) stated that most river plumes are acidic relative to the adjacent ocean, and therefore, capable of significantly depressing calcium carbonate saturation and increasing concentrations of CO_2 in the aquatic system within marine coastal zones (e.g. Cai *et al*., 2008).

Positive values of PC2 were mainly described by NCP (R^2=0.44), followed by I_m and [O_2] (R^2>0.17). Conversely, wind speed (R^2=-0.48), ER (R^2=-0.46) and FO_2 (R^2=-0.45) contributed to negative eigenvalues (Fig. 5.3). Seasonal separation was not as clear for PC2, even though positive values were mainly attributed to spring, the other seasons were situated in the centre of the component axis. The main drivers of high rates of ER were associated with negative values of PC2, while positive loadings related to indicators of increased phytoplankton biomass like light availability, [O_2] and chlorophyll 'a' (Cloern *et al*., 2014). The correlation between ER and high wind speeds, and their influence on FO_2 was also

recognised by the Spearman's correlation coefficient and it can be observed at the negative end of the PC2 (Fig. 5.3). Carbonate chemistry parameters were not relevant in the description of variability by PC2, however, this does not mean that NCP is not related to the carbonate system, but as Gazeau *et al*. (2005b) detailed, besides NCP the carbonate system can be regulated by different biogeochemical processes such as organic matter production/mineralisation and calcium carbonate ($CaCO_3$) precipitation/dissolution.

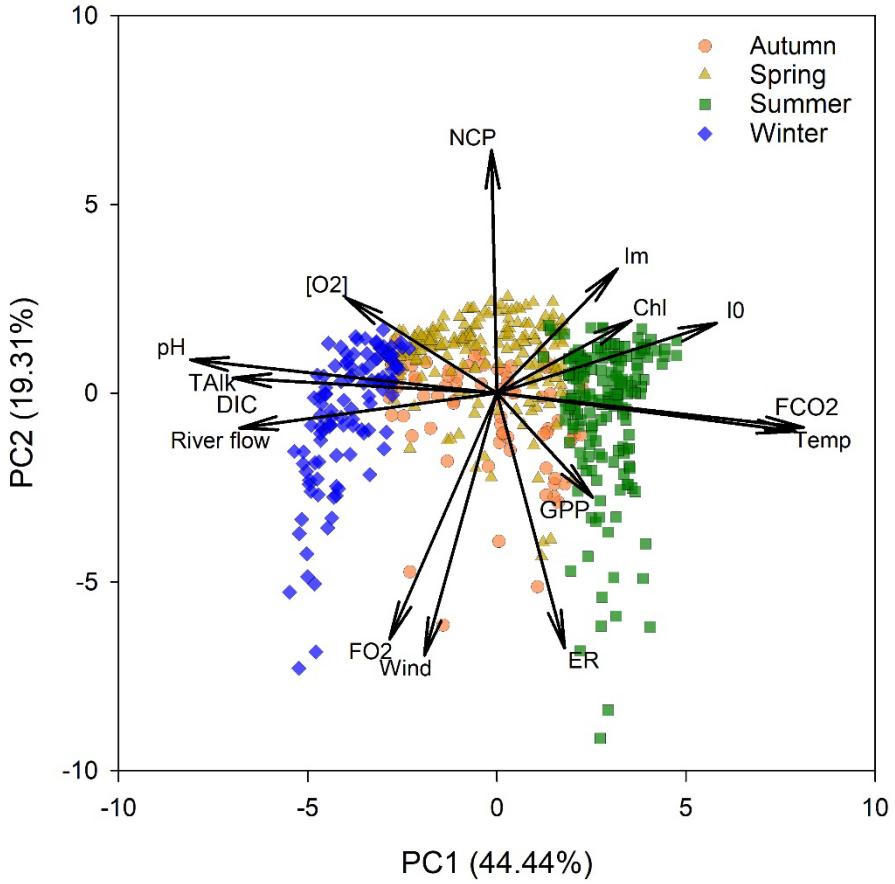

Fig. 5.3 Principal Component Analysis (PCA) for Southampton Water estuary (2019-2020). Seasons have been used as factors to illustrate the clusters: winter (blue diamonds ♦), autumn (orange circles ●), summer (green squares ■) and spring (yellow triangles ▲). Arrows → represent the variable and the direction of an arrow indicates its relation with the Principal Component (PC) and other variables. TAlk=total alkalinity, DIC=dissolved inorganic carbon, pH=pH, FCO2=air-sea CO_2 flux, FO2=air-sea O_2 flux, I0= surface water irradiance, Im= mean water column irradiance, Wind=wind speed, Temp=temperature, [O2]= DO concentration, Chl= chlorophyll '*a*', River=river inflow, NCP=net community production, GPP=gross primary production, ER=ecosystem respiration.

Table 5.3. Spearman's correlation matrix relating O_2 and CO_2 fluxes with carbonate system parameters, abiotic environmental factors and primary production rates in the Southampton Water estuary.

Air-sea fluxes	Year	Carbonate system				Abiotic environmental factors							Primary production			
		T_{Alk}	DIC	pH	$\rho CO_{2\ sea}$	I_0	I_m	Wind speed	Temp	O_2%	[O_2]	River flow	Chl '*a*'	NCP	GPP	ER
FO_2	Total	**0.16**	**0.16**	**0.17**	**-0.14**	**-0.25**	**-0.33**	**0.98**	**-0.17**	-0.06	0.03	**0.20**	**-0.13**	**-0.36**	**0.37**	**0.56**
	2019	**-0.12**	**-0.12**	0.00	-0.01	-0.11	**-0.16**	**0.98**	0.00	**-0.17**	-0.10	-0.02	-0.07	**-0.16**	**0.44**	**0.62**
	2020	**0.37**	**0.37**	**0.32**	**-0.27**	**-0.39**	**-0.51**	**0.97**	**-0.33**	0.08	**0.12**	**0.42**	**-0.15**	**-0.47**	**0.30**	**0.48**
FCO_2	Total	**-0.69**	**-0.69**	**-0.99**	**1.00**	**0.63**	**0.47**	0.03	**0.99**	**-0.32**	**-0.55**	**-0.84**	**0.65**	0.00	**0.41**	**0.22**
	2019	**-0.59**	**-0.59**	**-0.99**	**1.00**	**0.70**	**0.49**	0.11	**0.99**	-0.07	**-0.54**	**-0.93**	**0.73**	**0.27**	**0.44**	**0.14**
	2020	**-0.78**	**-0.78**	**-0.98**	**1.00**	**0.55**	**0.45**	**-0.16**	**0.98**	**-0.57**	**-0.60**	**-0.90**	**0.60**	**-0.30**	**0.38**	**0.37**

Values in bold $p < 0.05$. Values underlined represent absolute coefficient with strong correlation, $\rho > 0.55$.

5.3.2 Relationship between air-sea CO_2 fluxes and net community production

The trophic state of estuaries can be determined by calculating NCP in the water column. NCP integrates all of the processes affecting the balance between production (GPP) and consumption (ER) of organic matter (Duarte & Agustí, 1998; Garcia-Corral *et al*., 2021). If the estimation of NCP is positive, the ecosystem is considered net autotrophic and exports or stores the excess organic carbon and is a potential sink for atmospheric CO_2. Conversely, a net heterotrophic ecosystem is characterised by a negative NCP, requires stored or imported organic matter to maintain its metabolic state and acts as a net CO_2 source (Duarte & Agustí, 1998; Gazeau *et al*., 2004; Nidzieko *et al*., 2014; Raymond *et al*., 2000).

However, the presumed link between FCO_2 and the metabolic status of an aquatic ecosystem is not as direct as expected in coastal environments (e.g. Borges *et al*., 2006) as it can be masked by thermodynamic and hydrodynamic effects on gas exchange and the anthropogenic perturbation of the CO_2 budget (Duarte & Prairie, 2005). Although NCP is the main regulator of air-sea FCO_2 (e.g. Borges & Frankignoulle, 2003), processes such as the exchange of water masses with adjacent ecosystems, decoupling of organic carbon production and the fluctuation of flushing times can alter FCO_2 (Ávila-López *et al*., 2017; Borges & Abril, 2011; Borges *et al*., 2006).

A comparison of monthly FCO_2 and NCP estimates in Southampton Water was carried out for 2019 and 2020, coupling months within seasons (Fig. 5.4). The FCO_2 calculated was supported by NCP measurements for all of 2020 and

2019 for the complete autumn season and two months of summer (August and September). This indicated that the estuary was net heterotrophic and a source of CO_2 for most of the studied period, in agreement with the assumption that most estuaries are net heterotrophic ecosystems where respiration rates exceed gross rates of photosynthesis as stated by Cai (2011) and Raven *et al*. (2020)

Contrary to the conceptual relationship between FCO_2 and the trophic status, values for spring and July (summer) in 2019 indicated that the ecosystem was a source of CO_2 while also classified as autotrophic by the NCP model (Fig. 5.4). This could be a result of the water column being stratified and FCO_2 driven partially by the mixed layer metabolic processes, as was described by (Borges *et al*., 2006) in their evaluation of metabolic process rates and FCO_2, where the Bay of Palma showed positive NCP and an association to be a source of CO_2 due to the seasonally thermally stratification. In addition, NCP is highly influenced by wind speed, hence, notable departures from the relationship with FCO_2 during the season with highest average wind speeds (winter) was expected (e.g. Salisbury *et al*., 2009).

A different unbalance among estimations was observed in winter 2019, when February and January were sinks of CO_2 but showed negative NCP (heterotrophy); nevertheless, March remained close to the equilibrium with both methods (Fig. 5.4). This same discrepancy was reported by Guenther *et al*. (2017) in their comparison of FCO_2 and plankton metabolism in a hypereutrophic estuary (Recife Harbor, Brazil), showing that an excess of CO_2 was entering the ecosystem but was not being entirely incorporated by the primary producers and consequently was being exported to the atmosphere.

Additionally, a numerical disagreement between the magnitude of the metabolic rates was identified with estimations through the NCP model being up to ~6.6 orders of magnitude higher than calculated from FCO_2, especially during summer (Fig. 5.4). This magnitude of discrepancy was also found in the Randers Fjord (Denmark) and in the Scheldt estuary where FCO_2 was 6 to 7 times higher than in the mixed layer NCP (Borges *et al*., 2006; Gazeau *et al*., 2005a).

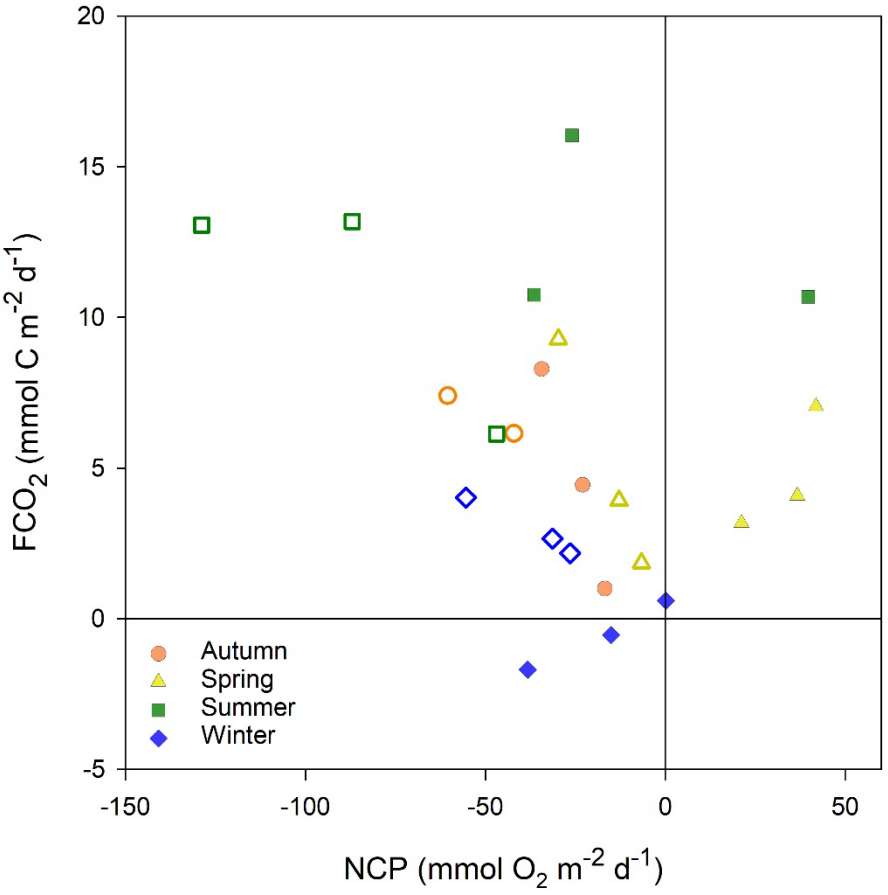

Fig. 5.4 Monthly comparison between air–sea CO2 fluxes (FCO2) and net community production (NCP). Seasons have been used as factors to illustrate the clusters: winter (blue diamonds ♦), autumn (orange circles ●), summer (green squares ■) and spring (yellow triangles ▲). Filled symbols correspond to 2019 while open symbols to 2020.

The water residence time can play a major role in uncoupling FCO_2 and NCP estimations in estuaries (Borges & Abril, 2011; Cai, 2011). In the current research, months with riverine inflow below 10 m s^{-1} showed the highest

monthly DIC averages (> 2415 µmol kg^{-1}), contrary to the findings of Gazeau *et al*. (2005a), indicating that long residence times can lead to a built-up of DIC in the water column and, therefore, higher emissions of CO_2. This is most likely because the system studied by Gazeau *et al*. (2005a) showed residence times between 60 and 90 days, while Southampton Water estuary flushing times range between 5 and 11 days (Shi, 2000), not giving enough time for DIC to accumulate. However, FCO_2 values >10 mmol C m^{-2} d^{-1} corresponded to summer, a season described previously with the most extended residence times in the estuary (e.g. Shi, 2000), while averages below 5 mmol C m^{-2} d^{-1} mostly matched to lower river inflow rates. It has been identified before that short residence times, of a few of days, can flush the water mass quickly enough that biological activity has little or no effect on FCO_2 (e.g. Gazeau *et al*., 2005b).

5.3.3 Metabolically driven pH and oxygen fluctuations

Whereas factors such as temperature, salinity and T_{Alk} influence the pH of coastal waters, rates of production and respiration, and the associated uptake and release of DIC (Laurent *et al*., 2012), induce most of the daily and seasonal changes of pH in estuarine ecosystems (e.g. Nixon et al., 2015). These metabolic effects, tend to be higher in coastal systems than in the open ocean due to hydrological processes dictating the mixing between the two water masses and watershed inputs (e.g. Duarte *et al*., 2013b).

Since coastal pH fluctuations are primarily caused by variable metabolic rates, they are necessarily accompanied by changes in dissolved oxygen concentration (e.g. Baumann *et al*., 2015). Moreover, fluctuation in the pH/dissolved oxygen dynamics can provide an indication of the balance

between autotrophy and heterotrophy (Caffrey, 2004; Cloern, 1996; O'Boyle *et al*., 2013). The strong correlation between pH and dissolved oxygen has been used to broadly characterise the trophic status (Howland et al., 2000; Laurent *et al*., 2012; O'Boyle *et al*., 2009) and trends in acidification (Cai, 2011; Shen *et al*., 2019a; Wallace *et al*., 2014) of estuarine water bodies.

Continuous high-frequency pH and oxygen data can be a powerful tool in determining the trophic status of estuarine ecosystems since it captures the diel oscillation (e.g. O'Boyle *et al*., 2013); hence, it allows identification of the cumulative effects of respiration over photosynthesis during the night, that decrease [O_2] and pH (e.g. Raven *et al*., 2020). Furthermore, using O_2% saturation as an alternative to [O_2] standardises the effects of temperature and salinity variations (e.g. Baumann & Smith, 2018). Supersaturated conditions can reflect the role of biological processes in the water column, just as O'Boyle *et al*. (2009) indicated in their evaluation of estuarine and coastal waters in Ireland, where values >130% correlated to high phytoplankton photosynthesis rates.

Besides O_2%, salinity has been reported to be a significant parameter in explaining a substantial variation of pH in the water column and throughout diel cycles in coastal ecosystems (e.g. Baumann *et al*., 2015). Water masses of low salinity generally have lower alkalinity values and, thus, decreased CO_2 buffering capacity (e.g. Salisbury *et al*., 2009). However the rivers feeding into Southampton water are derived from chalk streams and have higher alkalinity values than the adjacent sea water. T_{Alk} values above 2580 µmol kg^{-1} in this work were related to river inflow over 18 m s^{-1}, therefore, to evaluate the

influence of freshwater on pH variability in the estuary, an analysis was carried out including salinity as a predictor of pH along with O_2%.

In order to assess if trends in pH, O_2% and salinity coupling remain valid across similar ecosystems, an examination of the sensitivity of pH variation through multiple regression analysis was undertaken. In figure 5.5 the regression using O_2% as a predictor of pH is plotted since the analysis using only O_2% (R^2=0.50) performed, to some extent, better than the combination of O_2% and salinity (R^2=0.48). In addition, the relationship between these two parameters from five different estuaries that form part of the US National Estuarine Research Reserve System (NERRS) was included in the comparison. They were selected for being temperate ecosystems that, in the extensive analysis carried out by Baumann & Smith (2018), better relate pH to O_2% than also adding salinity, like with Southampton Water (SOT).

A similar trend in the association of pH and O_2% was observed with the Wellls (WEL), Elkhom (ELK) and Delaware (DEL) estuaries (Fig. 5.5); systems with a tidal range between 1 and 2.8 m and average depth ~3.5 m (Baumann *et al*., 2015). WEL and DEL presented a comparable pH average (7.9 and 8.0, respectively) to the one identified for SOT (8.1) but were undersaturated for longer periods than SOT, reaching means of 87.8% and 85.6% correspondingly, while SOT was on average close to the atmospheric equilibrium (98.9%). Although DEL did not show a significant relation between pH and salinity, clearly its more considerable range (21.3 psu) moved its prediction to lower pH values.

Given that the comparison (Fig 5.5) included ecosystems with very similar hydrologic characteristics, it is apparent that pH/O_2% dynamics respond to

local factors influencing aquatic metabolism. This highlights the importance of including a broad range of ecosystems in coastal monitoring to enlarge the understanding of the scales and magnitudes of fluctuations, as these are highly complex ecosystems and will differ among global regions.

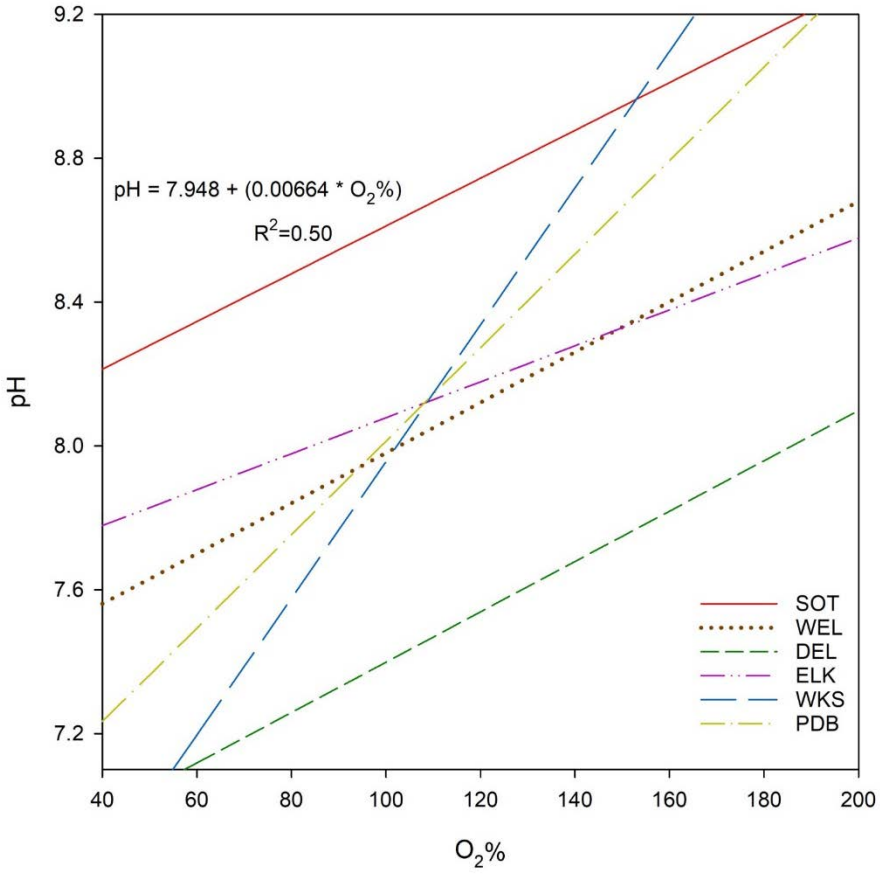

Fig. 5.5 Comparative analysis of the relationship between pH and oxygen saturation (O2%) in estuarine ecosystems. Southampton Water (SOT), Wells (WEL), Delaware (DEL), Elkhorn Slough (ELK), Weeks Bay (WKS) and Padilla Bay (PDB). Liner regression equations for the US National Estuarine Research Reserve System estuaries were taken from Baumann & Smith (2018).

5.3.4 Interannual and seasonal distribution of CO_2 air-sea fluxes

Coastal zones account for about 20% of total ocean FCO_2 (Ávila-López *et al*., 2017); nevertheless, a comprehensive description and analysis of the spatial and temporal variability of FCO_2 and its relation to environmental factors in estuaries is scarce (Raymond *et al*., 2000). When these summaries exist, they tend to poorly represent the wide variety of ecosystems due to the strong

spatial and temporal heterogeneity of coastal ecosystems (Ávila-López *et al*., 2017).

There is no general agreement on the role of estuaries on the exchange of CO_2 with the atmosphere (Borges & Frankignoulle, 2003). Several studies have indicated that estuaries are supersaturated with respect to CO_2 (heterotrophy) (Algesten *et al*., 2004; Ávila-López *et al*., 2017; Cai, 2011; Chen *et al*., 2013; Raymond *et al*., 2000; Yao *et al*., 2020), while some others have found a prevalence of undersaturated CO_2 conditions (autotrophy) (Crosswell *et al*., 2017; Guenther *et al*., 2017; Van Dam *et al*., 2018; Van Dam *et al*., 2019). The above statement exacerbates the importance in defining the trophic status of as many and diverse coastal ecosystems.

European estuaries have been reported to be CO_2 sources by Borges *et al*., (2006), and to have a significant impact on the regional CO_2 budget by contributing to an average of 50 mol C m^{-2} y^{-1}, equivalent to between 5–10% of the total anthropogenic CO_2 emissions from Western Europe, according to Cai (2011). Moreover, Borges (2005) calculated that the average FCO_2 from mid-latitude (30–60°) estuaries is 46 mol C m^{-2} y^{-1}, while Chen *et al*. (2013) specified a lower value for estuaries north of 50°N (36 mol C m^{-2} y^{-1}). Taking the global open estuarine water area of 1.05×10^{12} m^2, proposed by Cai (2011), and applying it to the results of this study (6.6 ± 10.4 mmol C m^{-2} d^{-1}), SOT presents an overall FCO_2 of 45.2 mol C m^{-2} y^{-1}, in agreement with the stated above estimate.

Furthermore, Borges & Frankignoulle (2003) found that the English Channel was a small net source of CO_2 (0.9 mmol C m^{-2} d^{-1}) and that the Eastern region was strongly influenced by freshwater inputs of organic matter influencing

respiration rates and probably accounting for higher levels of heterotrophy. In contrast, Kitidis *et al*. (2012) found that the L4 site in the Western English Channel, located ~12 km offshore of Plymouth, was a net sink for atmospheric CO_2 (-1.4 mmol C m^{-2} d^{-1}) over an annual cycle. In some way, this agrees with the widespread idea that estuarine mixing zones are considered as moderate CO_2 sources, whereas the adjacent ocean behaves as a CO_2 sink (Borges & Abril, 2011; Chen *et al*., 2013; Cotovicz *et al*., 2020; Frankignoulle *et al*., 1998).

In estuarine regions, a shift from an autotrophic to a heterotrophic state, mainly related to seasonal changes in water temperature and light availability, has been reported (Azevedo *et al*., 2006; Tang *et al*., 2015). In SOT, summer increased values of $\rho CO_{2\ sw}$ and FCO_2 were consistent with lower DIC, T_{Alk} and pH values. In contrast, lower $\rho CO_{2\ sw}$ and FCO_2 during winter corresponded to high DIC, Talk and pH. Ávila-López *et al*. (2017) reported shifts from net autotrophy in winter to net heterotrophy in summer in San Quintín Bay (Mexico), driven by upwelling events enhanced by warmer waters. SOT presented a similar change to autotrophy in winter of 2019, but in lesser magnitude, agreeing with the observation made by Kemp & Testa (2011) that the tropical ecosystems affected by upwelling season resemble many temperate estuaries and shallow coastal lagoons, where NCP peaks in spring influenced by annual light and temperature cycles. However, there is no evidence that SOT becomes significantly stratified given that there is no apparent CO_2 release from bottom waters right after the major productivity period and when temperatures start decreasing in autumn (e.g. Kitidis et al., 2012).

The analysis of seasonal variation in SOT (Table 5.2) found FCO_2 roughly follows the pattern of DIC, indicating that biology is an important factor in modulating CO_2 exchange with the atmosphere (e.g. Salisbury *et al*., 2009). The relationship between net heterotrophy from NCP and FCO_2 calculations was evident in seasonal CO_2 variation, especially in 2019, when maximum FCO_2 occurred in summer, corresponding to high temperatures, favouring elevated rates of respiration. Moreover, minimum FCO_2 values were observed in the winter when water temperatures are low and river discharge is high. Similar seasonal patterns in CO_2 were observed at the outer section of the York River estuary (USA) (Raymond *et al*., 2000) and in the Mission-Arkansas system (USA) (Yao *et al*., 2020). Lastly, a comparison with O2% showed that at higher $\rho CO_{2\ sw}$, oxygen saturation was often less than 100%, indicating the overall importance of respiration in the estuary. This same correlation was reported by Howland *et al*. (2000), for the Tweed estuary (UK), in their excess ρCO_2 model calculated from T_{Alk}, pH and temperature.

Although results from most studies agree that estuaries are sources of CO_2, it is clear that coastal ecosystems can also be considered net sinks, either seasonally or overall, since processes that modulate the carbonate chemistry system are driven by regionality, thermal effects and biological activities.

5.4 Conclusions

Results from the present work has shown that high-frequency carbonate system data in combination with meteorological and hydrological information, allows the description of short-term variability and long-term changes of CO_2 fluxes in the Southampton Water estuary.

Defining the trophic state of an ecosystem can potentially predict if it behaves as a sink or source of CO_2 to the atmosphere. In chapter 4, Southampton Water was classified as net heterotrophic, suggesting the estuary is generally supersaturated with CO_2 and agreeing with the independent CO_2 flux calculation of -6.6 ± 10.4 mmol C m^{-2} d^{-1}, based on discrete sampling of DIC and T_{Alk}, and the continuous monitoring of pH. FCO_2 estimations reinforced net community production calculations made in 2020 and, in autumn and parts of summer in 2019. Discrepancies between the estimations were attributed to possible seasonal stratification and wind speed affecting the calculation of O_2 fluxes and flushing times.

The frequency and magnitude of riverine inputs influenced the distribution of carbonate system parameters, presenting high partial pressure of CO_2 and therefore, increased degassing of CO_2 in summer when there was lower daily river discharge, and the highest DIC, T_{alk} and pH values corresponding to high riverine inflow during winter.

CO_2 fluxes were observed to follow the pattern of DIC, indicating that biology is an important controlling factor given the association with uptake and release of DIC to metabolic rates. Analysis of the fluctuation of the pH/oxygen saturation dynamics demonstrated that this relation can reflect the role of biological processes in the water column and that these respond to local factors. Although it is known that the rivers feeding into Southampton water are derived from chalk streams and have higher alkalinity values than the adjacent sea water, salinity was not a significant predictor of pH in the Southampton Water system.

Specific studies of the carbonate chemistry dynamics are needed for a global understanding of the estuarine carbon system. Results from the current research can be used as a baseline to assess future anthropogenic impacts and climate change alterations to the CO_2 flux between the aquatic system and the atmosphere in the Southampton Water estuary.

Chapter 6

Synthesis and conclusions

This chapter draws together the major findings of research presented in this thesis, and suggests the pending questions raised and future work where these findings might be applied.

6.1 Synthesis and conclusions

Coastal zones represent only 7% of the total ocean surface area (Kanuri *et al*., 2017) and within this region, estuaries can be highlighted due to their unique biogeochemical and complex ecological interactions (Lemley *et al*., 2020; Newton *et al*., 2014).

Phytoplankton communities are the basis of many marine ecosystems, estuaries not being the exception (e.g. Leterme *et al*., 2014). Therefore, the phytoplankton biomass distribution in an estuary can indicate the dynamics of the seasonal and annual variability of the ecosystem properties such as water quality and community metabolism (e.g. Cloern & Jassby, 2010).

Net community production, also known as net ecosystem metabolism (NCP) (e.g. Needoba *et al*., 2012), is a community-level process that integrates all processes affecting the balance between gross primary production (GPP) and ecosystem respiration (ER) (Duarte & Regaudie-De-Gioux, 2009; Garcia-Corral *et al*., 2021). If the NCP estimation is positive, the ecosystem is considered net autotrophic and exports or stores the excess organic carbon

and is a potential sink for atmospheric CO_2. Conversely, a net heterotrophic ecosystem is characterised by a negative NCP, requires stored or imported organic matter to maintain its metabolic state and acts as a net CO_2 source (Duarte & Agustí, 1998; Gazeau *et al*., 2005b; Nidzieko *et al*., 2014; Raymond *et al*., 2000).

Although estuaries account for about 20% of total ocean CO_2 flux, a comprehensive description and analysis of the spatial and temporal variability of factors influencing primary production, and therefore, CO_2 fluxes is scarce. Moreover, there is no general agreement on the 'trophic' state of estuaries (Borges & Frankignoulle, 2003). Although some studies have shown that estuaries are sources of CO_2 (heterotrophic) (Algesten et al., 2004; Ávila-López et al., 2017; Cai, 2011; C. T. A. Chen et al., 2013; Yao et al., 2020), it is clear that coastal ecosystems can also be considered net sinks (autotrophic) (Crosswell *et al*., 2017; Guenther *et al*., 2017; Van Dam *et al*., 2019), either seasonally or overall, since processes that modulate primary production are driven by regional factors, thermal effects and biological activities.

The overall aim of this study was to estimate interannual and seasonal changes in the primary production of two contrasting temperate estuaries, the Southampton Water estuary and Christchurch Harbour estuary, and identify the environmental factors influencing its variability by using continuous high-frequency environmental data. It was hypothesised that a net heterotrophic state will dominate in the two estuaries, implying a depletion of organic C and a net CO_2 release to the atmosphere, and that a shift to autotrophy will only be episodic and driven by phytoplankton blooms. This work was implemented through the three following objectives:

1. *To investigate temporal phytoplankton bloom dynamics and the environmental factors driving them in Southampton Water (2014 – 2020) and Christchurch Harbour (2014 – 2018).*

In chapter 3, an analysis of the correlation between phytoplankton blooms and environmental conditions using high-frequency water quality data collected in the Southampton Water (2014 – 2020) and Christchurch Harbour estuaries (2014 – 2018) is presented. The study of these extended time series allowed the identification of seasonal patterns, comparison among years and could open the possibility for predictions.

Phytoplankton distribution exhibited a seasonal variability in both estuaries, with the initiation of the spring bloom related to abrupt rises in the water column light availability and temperature. Temperatures above 11.8°C correlated with the appearance of blooms in Southampton Water, while rising water temperature overlapping with increased solar radiation seemed to initiate blooms in Christchurch Harbour.

Interannual variability in bloom magnitude was associated with sudden increases in water column irradiance synchronised with lower turbidity and wind speed periods. Christchurch Harbour displayed the typical dynamics observed in coastal temperate systems with mainly spring and autumn blooms, while Southampton Water presented a pattern with blooms in spring and summer.

In addition, an analysis of the neap-spring tidal cycle in the Southampton Water estuary identified that blooms typically developed during neap tides and dissipated during the following spring tide. The tidal cycle creates stronger

mixing conditions during spring tides leading to a turbidity increase and creating lower mixing, with possible stratification during neap tides enhancing phytoplankton biomass growth.

2. *To examine seasonal and interannual variation in productivity rates and the interactions between them and environmental variables in Southampton Water (2014 – 2020) and Christchurch Harbour (2014 – 2018).*

In chapter 4, the open water oxygen diel method was applied to the time series analysed in chapter 3 for Southampton Water and Christchurch Harbour, in order to estimate ecosystem respiration (ER), gross primary production (GPP), and net community production (NCP). To my knowledge, this is the first study to apply high-resolution oxygen diel data to calculate NCP and productivity rates in both of these estuaries.

The open water diel oxygen method appeared to provide reasonable estimates of ecosystem production and respiration rates in both estuaries. ER showed no clear dependence on water temperature, in agreement with the assumption that respiration rates are constant during day and night, however, an overestimation in the air-water transfer due to high winds was found.

Trends in the overall trophic state of the two estuaries were identified, with Southampton Water becoming more net heterotrophic over the 7-year time series (from -1.3 to -48.7 mmol O_2 m^{-2} d^{-1}), while Christchurch Harbour showed an increasing net autotrophic state (-11.7 to 19.8 mmol O_2 m^{-2} d^{-1}) in the 5 years studied.

In both estuaries, a pattern was observed where autotrophic conditions prevailed during summer and spring due to the dominant factors driving

metabolic rates being related to seasonal changes in light availability and temperature, with the addition of riverine inflow affecting Christchurch Harbour.

Threshold values for the Southampton estuary and Christchurch Harbour of temperature (10.5 & 10.3 °C), surface water irradiance (1520 & 1240 Wh m^{-2} d^{-1}) and mean water column irradiance (415 & 950 Wh m^{-2} d^{-1}) were related to the appearance of extreme autotrophic and heterotrophic conditions. Christchurch Harbour, being a shallower with a more turbid water column, is more affected by disturbances in the mean water column irradiance.

The relationship between ecosystem respiration and gross primary production allowed estimations of metabolic balance (GPP:ER). This showed that the primary production needed to drive Southampton Water towards net autotrophic metabolism is four orders of magnitude greater than that required for the shallower Christchurch Harbour. This approach also allowed classification of both estuaries between oligotrophic and mesotrophic states, with Southampton particularly leaning towards mesotrophic conditions.

A prevalence of ER>GPP at lower rates and a tendency for GPP>ER at higher metabolic rates was observed, implying that metabolic balance in these systems relies to some extent on allochthonous inputs of organic matter. Variance in Chl '*a*' concentration during phytoplankton blooms was explained by NCP rates in more than 75% for both estuaries.

3. *To explore the primary controls and temporal variability of carbonate system parameters in Southampton Water (2019 – 2020) and their influence on air-sea CO_2 fluxes.*

In chapter 5, an estimation of carbonate systems parameters (CO_2 flux, partial pressure of CO_2 [$\rho CO_{2\,sw}$], dissolved inorganic carbon [DIC], total alkalinity [T_{alk}] and pH) was carried out at hourly intervals for a position in the Southampton Water estuary in 2019 and 2020. The software CO_2^{calc}, as described in chapter 2, used inputs of discrete sample values of dissolved inorganic carbon and total alkalinity and the continuous monitoring of pH.

The estuary presented an annual average of 6.6 ± 10.4 mmol C m^{-2} d^{-1}, acting as a source of CO_2 to the atmosphere and agreeing with the overall net heterotrophic classification result from chapter 4. CO_2 flux estimations reinforced net community production calculations made in 2020 and, in autumn and parts of summer in 2019. Discrepancies among estimations were attributed to possible seasonal stratification, wind speed affecting the calculation of O_2 fluxes and estuarine flushing times.

Frequency and magnitude of riverine inputs influenced the distribution of carbonate system parameters, presenting high partial pressure of CO_2 and therefore, increased degassing of CO_2 in summer when there was lower daily river discharge, and the highest DIC, T_{alk} and pH values corresponding to high riverine inflow during winter.

An analysis of the fluctuation of the pH/oxygen saturation dynamics demonstrated that this relation can reflect the role of biological processes in the water column and that these respond to local factors. Although it is known that the rivers feeding into Southampton water are derived from chalk streams and have higher alkalinity values than the adjacent seawater, salinity was not a significant predictor of pH in the Southampton Water system.

The high-resolution simulation of the carbonate chemistry dynamics presented in this chapter is the first performed for the Southampton Water estuary and can be used as a baseline to assess future anthropogenic impacts and climate change alterations to the CO_2 flux between the aquatic system and the atmosphere in the ecosystem.

6.2 Recommendations

Open water diel oxygen method application

In this study, it was proven that the use of high frequency dissolved oxygen measurements using optodes for estimating metabolic rates in estuaries, through the open water diel oxygen method, is possible and reliable. However, before applying this method to any ecosystem, a review of the underlying assumptions and limitations needs to be done. For instance, in systems with persistent stratification, calculations of surface and bottom layers are necessary to estimate water column net community production more accurately, since the method assumes homogeneous plankton production/respiration rates throughout the water column depth. Another important consideration recognised in this thesis, is that wind mixing leading to O_2 air–sea exchange is an important component of the metabolic rate calculations, and it is especially important in shallow systems. It is recommended to use time-specific gas transfer velocity coefficients instead of using a constant, in order to minimised error propagation.

Coastal monitoring

Despite the ecological importance of estuaries, description and analysis of the variability in relation to environmental factors of these ecosystems is limited.

Furthermore, when these summaries exist, they tend to poorly represent the variety of systems from around the globe adequately enough to support a precise global synthesis, due to the strong spatial and temporal heterogeneity of coastal areas. It is suggested to increase studies using high-frequency, multi-parameter observations in estuarine systems, as long as they are accompanied by consistent quality control and sensor calibration. This will allow better understanding of local and regional primary production dynamics and develop adequate long-term monitoring strategies. It is also recommended to analysed, when possible, several different sites in each estuary to extend the spatial comprehension of freshwater and seawater mixing, and its implications for metabolic rates.

Climate change response

Studies have tended to focus on those estuaries that receive substantial anthropogenic alterations, providing much less attention to estuaries that receive little human impact. However, increasing atmospheric CO_2 conditions will impact globally and given the ecological and economic importance of shallow-water estuarine environments, further efforts to predict how these alterations could disturb production-respiration balances are essential to the effective management of these environments. Results from the current research can be used as a baseline to assess future anthropogenic impacts and climate change alterations to the aquatic trophic state in Southampton Water and Christchurch Harbour estuaries. Understanding the heterogeneity of coastal zones can provide a powerful tool to recognizing the symptoms of developing change.

6.3 Future work: advances in marine *in situ* sensors

Advances in phytoplankton community assessment

In the present study, phytoplankton diversity was not measured. However, it is known that by describing the phytoplankton community of a specific ecosystem, and its relationship with biotic and abiotic factors, interpretation of the ecosystem function and resilience can be improved (Campbell *et al*., 2022). Phytoplankton dynamics in marine ecosystems has been advanced, in the last decade, by using in situ molecular and imaging instrumentation (Spanbauer *et al*., 2020). These tools provide the opportunity of determining the impact of phytoplankton community structure on carbon export fluxes, coastal water quality and surveillance of blooms, including harmful algal blooms (HABs) (Baird *et al*., 2022). The vast majority of research effort in this area is concentrated on ecogenomic sensors: 'autonomous sensors, which apply molecular techniques on an *in situ* platform that allows for remote sample collection, processing, and molecular analyses' (Smith *et al*., 2022). Projects like TechOceanS (https://techoceans.eu/), are betting on developing ecogenomic samplers that autonomously perform in situ molecular analyses and provide real-time data with the idea of revolutionising ocean monitoring. The possibility of a low-cost, in situ and automated systems for biological sensing would enable covering a spatio-temporal resolution difficult to obtain by manual sampling since conditions in estuaries can vary considerably within days and even hours, as the present study corroborated

Biochemical sensor development

It is clear that long-term observations and measurements of the marine environment are needed to understand the variability caused by both anthropogenic and natural processes. With an increasing number of nutrients (e.g. NO_3, PO_4 and SiO_4), carbonate system parameters (pH, DIC, T_{alk} and *p*CO2) and other dissolved gases (e.g. O_2 and CH_4) to be monitored (Nightingale, Beaton, & Mowlem, 2015), a need has been identified to design and development multifunctional sensor systems capable of sharing data in real-time (Precheur & Delory, 2018). Data from these systems, deployed directly or on autonomous platforms, have changed our understanding of marine systems and processes (e.g. D'asaro & Mcneil, 2013). Sensors are clearly playing an major role in environmental monitoring and recent technological advances are certain to facilitate the application of new sensing devices (Pejcic *et al*., 2022). In order to miniaturised existing chemical analytical methods so they can be easily deploy on moorings and mobile platforms, the development of novel Lab-on-Chip microfluidic analysers has been gaining momentum in the last few years (e.g. Nightingale *et al*., 2019). Currently, this technology aims to reduce uncertainty in estimations of marine macronutrient data (Birchill *et al*., 2019) and, hopefully, one day it will lead to the integration of affordable and easily deployable carbonate system measurements and, even primary productivity rate sensors.

Appendix A

Nutrient data in Southampton Water estuary (2018 – 2020)

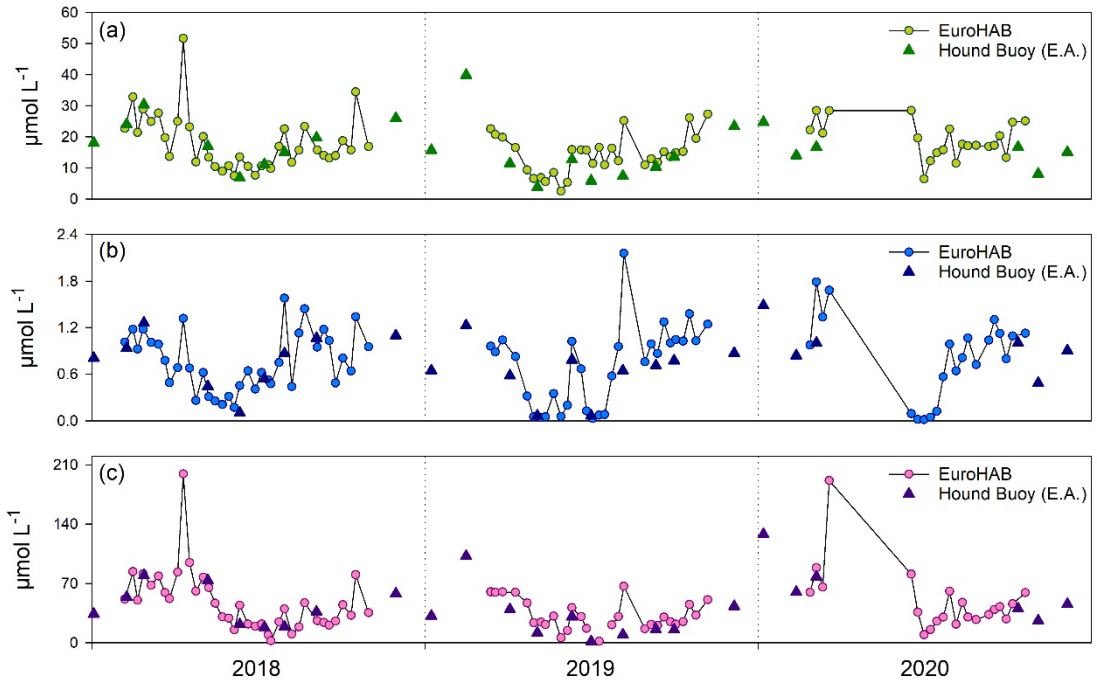

Fig. A1 Temporal variation of (a) SiO_2, (b) PO_4 and (c) NO_3 at the Environment Agency Hound Buoy sampling site and from discrete sampling part of the EuroHAB project at the Data Buoy system (Southampton Water estuary) from 2018 to 2020.

Appendix B

Salinity models for Southampton Water

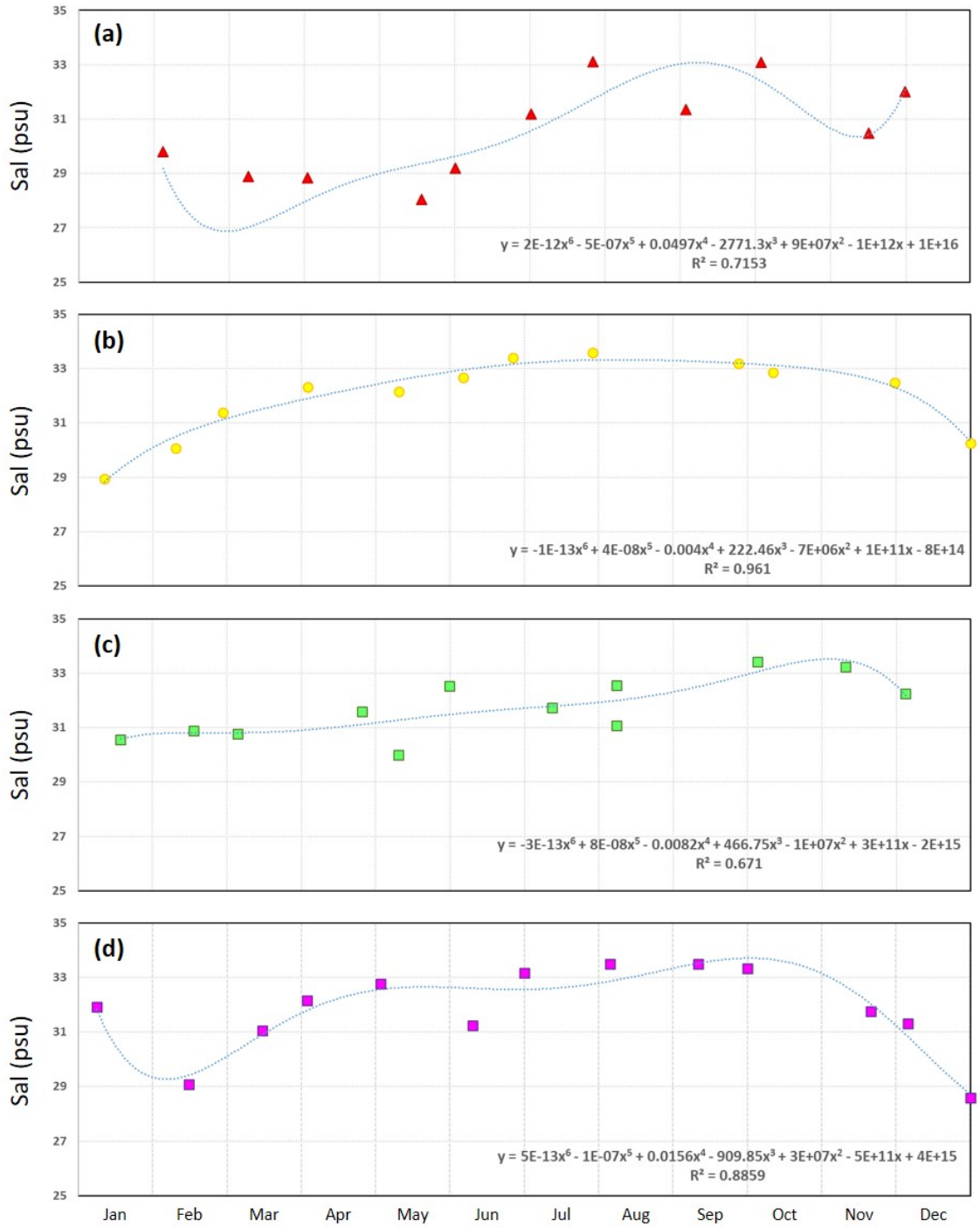

Fig. B1 Polynomial curve fitting for salinity data from Environment Agency sampling in (a) 2014, (b) 2015, (c) 2016 and (d) 2020.

Appendix C

Temporal variability of phytoplankton biomass and net community production in a macrotidal temperate estuary

At the time of submission of this thesis, data for the Southampton Water estuary in 2019, included in Chapter 4 and Chapter 5, have been submitted as:

Gomez-Castillo, A.P., Panton A. & Purdie, D. A. 2022. Temporal variability of phytoplankton biomass and net community production in a macrotidal temperate estuary. Submitted to *Estuarine, Coastal and Shelf Science*.

Temporal variability of phytoplankton biomass and net community production in a macrotidal temperate estuary

Estuarine, Coastal and Shelf Science

Africa P. Gomez-Castillo[1*], Anouska Panton[1], Duncan A. Purdie[1]

[1]School of Ocean and Earth Science, University of Southampton, National Oceanography Centre, European Way, Southampton SO14 3ZH, UK.

*Corresponding author: A.P.Gomez-Castillo@soton.ac.uk

Abstract

Coastal zones play a significant role in Earth's biogeochemical processes. Within these regions, estuaries are particularly important due to their complex ecological interactions and spatial and temporal variability. The aim of this study was to apply a year long high-frequency (15 minute) environmental data time series to identify both the timing and factors influencing phytoplankton blooms in the Southampton Water estuary. Dissolved oxygen measurements from an *in situ* deployed optode were applied to the open diel oxygen method to estimate daily integrated rates of gross primary production (GPP), ecosystem respiration (ER) and net community production (NCP). Additional water quality data including temperature, salinity, chlorophyll concentration and turbidity allowed the relationship between physical and biological processes occurring over different time scales to be investigated. The occurrence of major phytoplankton blooms during the spring-summer period were associated with critical values of estuarine water temperature and mean water column irradiance. In addition, neap tides were found to promote the initiation of phytoplankton blooms in late spring and summer months. Annual daily average NCP for the estuarine ecosystem presented an estimated net heterotrophic state (-0.8 mmol O_2 m^{-2} d^{-1}), although seasonal productivity events shifted this state for several days and sometimes weeks to net autotrophic conditions. The results of this study have demonstrated how high frequency *in situ* dissolved oxygen measurements from an optode can make a valuable contribution to understanding the key factors influencing bloom events in a temperate macrotidal estuary. This approach if applied more widely to other coastal sites could therefore contribute to consolidating global annual primary production budgets for coastal regions.

Keywords

Estuarine ecosystems

High-frequency data

Dissolved oxygen

Net community production

Phytoplankton blooms

1. Introduction

Coastal zones represent around 7% of the total ocean surface area (Kanuri *et al*., 2017), however, they are responsible for 14–33% of total oceanic production (Garcia-Corral *et al*., 2021). Within these regions, estuaries play a major role in hydrographic and biogeochemical processes of marine ecosystems (Mahoney & Bishop, 2017; Ruiz-Ruiz *et al*., 2017) due to the mixing of riverine freshwater with seawater carried in by the tides (Srichandan *et al*., 2015).

Given that phytoplankton communities form the base of most marine ecosystems (Leterme et al., 2014), the phytoplankton biomass distribution in an estuary can indicate the dynamics of the seasonal and annual variability of the system properties such as water quality and the aquatic trophic state (Cloern & Jassby, 2010; Haskell *et al*., 2019).

Several techniques are used to determine aquatic rates of net primary production, the most common being measurements of radioactive carbon 14 isotope ($^{14}CO_2$) incorporation by a natural community of microplankton incubated in bottles (Oczkowski *et al*., 2016). Alternatively, changes in dissolved oxygen (DO) can be measured in small volume glass bottle incubations in the dark and light to define rates of planktonic respiration and net production (Langdon & Garcia-Martin, 2021). The problems inherent in these short term, small volume incubation techniques however

63 are exacerbated in the highly dynamic heterogeneous coastal zone, where the seasonal
64 oxygen change shows marked variability (Queste *et al*., 2016). Interaction between
65 physical and biological processes within estuaries tends to vary over diurnal, semi-
66 diurnal and sometimes episodic timescales, making acquiring frequent data critical to
67 accurately assess ecosystem health for these periods (Bianchi, 2012; Nidzieko *et al*.,
68 2014).
69 An alternative, more integrative, method to estimate primary production relies on the
70 calculation of the in situ oxygen mass-balance from continuous measurements of DO,
71 the open diel oxygen water method, first proposed by Odum (1956) and later modified
72 to apply it to estuarine systems (Caffrey, 2003, 2004; Emerson *et al*., 2008). This
73 method quantifies the in situ diel oscillations in DO concentration to estimate daily
74 integrated gross primary production (GPP), ecosystem respiration (ER) and net
75 community production (NCP), also known as net ecosystem metabolism (Demars *et*
76 *al*., 2015).
77 NCP is a community-level process that integrates all processes affecting the balance
78 between GPP and ER (Duarte & Regaudie-De-Gioux, 2009; Garcia-Corral *et al*.,
79 2021). If the NCP estimation is positive, the ecosystem is considered net autotrophic
80 and exports or stores the excess organic carbon and is a potential sink for atmospheric
81 CO2. Conversely, a net heterotrophic ecosystem is characterised by a negative NCP
82 that requires stored or imported organic matter to maintain its metabolic state and acts
83 as a net CO2 source (Feng *et al*., 2012; Nidzieko *et al*., 2014).
84 The aim of this study was to estimate daily and seasonal changes in estuarine primary
85 production and identify the environmental factors influencing its variability by using
86 continuous high-frequency environmental data in the macrotidal Southampton Water
87 estuary, over a period of one year. To our knowledge, this is the first study to apply

high-resolution oxygen diel data to calculate productivity rates and relate them to phytoplankton blooms in a UK estuarine system. While our study is regional, the heterogeneity of coastal zones is of global concern and results from this study will allow a better understanding of local and regional primary production dynamics as well as provide a baseline to assess future anthropogenic impacts and climate change alterations to the aquatic trophic state of the Southampton Water estuary.

2. Materials and methods

2.1 Study sites

The Southampton Water estuary is part of the Solent estuarine system, considered the largest on the south coast of the UK (Fig. 1). It is an approximately linear body of water about 2 km wide and 10 km long with a central channel continuously dredged to a minimum depth of 12.2 m below the local Chart Datum. Three main rivers discharge into Southampton water: the River Test and Itchen towards the head of the estuary and the river Hamble, nearer to the mouth on the eastern side (Iriarte & Purdie, 2004).

The estuary is characterised by a semi-diurnal tidal regime where each tide consists of a double high water, ~2 h apart, followed by a short ebb-tide. The tidal range varies between 1.5 m on neaps and 5.0 m on springs (Crawford *et al.*, 1997). It is considered a partially mixed system, with minimal stratification occurring throughout the semi-diurnal tidal cycle with the highest vertical density gradient occurring at low water and well-mixed conditions at high water (Levasseur *et al.*, 2007).

2.2 Data Sources

Water quality data were collected using a YSI EXO2 sonde deployed since 2018 on a solar-powered Xylem Analytics UK EMM700 Data Buoy located at 50.871° N, -1.373° W, in the Southampton Water estuary (Fig. 1). The sonde was placed into an

open flow PVC tube fixed to the Data Buoy at a depth of 1.6m below the sea surface; the average water depth at the site was 10m. Parameters recorded by the sonde included dissolved oxygen (DO) concentration (mg L^{-1}) and oxygen saturation (%), temperature (°C), salinity, chlorophyll '*a*' (µg L^{-1}) and turbidity (FNU). The sonde is connected to a Storm data logger situated within the Data Buoy system that regularly uploads data, via a mobile phone connection, to a dedicated webpage within the Storm Central cloud data collection service (https://stormcentral.waterlog.com/). Data was recorded at high-frequency (every 15 minutes) from January 2019 to December 2019, but with hourly averages calculated for the purpose of this study. Two gaps in data collection occurred: the first between 13/02/2019 and 19/03/2019, caused by the sonde being recovered while the Data Buoy mooring chain was replaced and the sonde and PVC tube cleaned of biofouling and the second gap from 23/11/2019 to 04/12/2019 due to some problems backfilling data when the Storm Central server migrated from one IP address to another. All data was carefully inspected for unreliable values, and outliers plus negative or occasional inconsistent high magnitude values (typically caused by biofouling) were discarded manually.

The Data Buoy system was originally fitted with a met sensor, but this stopped recording on 12/09/18 due to damage from a boat collision. Hourly barometric pressure measurements during 2019 were taken from a Met Office met station mounted on the roof of the National Oceanography Centre (archived in the Met Office's MIDAS database). Additionally, the National Oceanography Centre meteorological database was used to obtained hourly wind speed and solar radiation values, measured at the same site (50.892° N, -1.394° W).

A set of water quality measurements from the Southampton Water estuary was acquired from the Environment Agency Water Quality Archive

(https://environment.data.gov.uk/water-quality/view/download/new). Data from the Hound navigation Buoy sampling site (50.861° N, -1.358° W) was selected to compare with the Xylem Analytics Data Buoy measurements due to its close proximity. Environment Agency data included monthly surface records of DO (mg L^{-1} and % sat.), temperature (°C), salinity (psu), chlorophyll '*a*' (µg L^{-1}), and turbidity (FNU).

The Associated British Ports (ABP) Marine Environmental Research provided minute-interval sea surface elevation data measured with a Tidalite tide gauge located at Dock Head, Eastern Docks Southampton (Fig. 1). Daily minimum and maximum values were extracted from the raw time series, and the difference plotted to indicate changes in the daily tidal range.

2.3 Field sampling

Discrete water samples were periodically collected using a Niskin bottle deployed at 2 m below the sea surface close to the Data Buoy from the RV *Callista*. Sets of three replicate glass bottles (~60ml) were filled from the Niskin to measure DO concentration on several dates during winter and spring 2019. The chemical determination of oxygen concentration was based on the method first proposed by Winkler (1888) and modified by Parsons *et al*. (1984). Winkler titrations were performed using a photometric end-point detector (Carrit & Carpenter, 1966).

Surface water samples for phytoplankton analysis were collected biweekly from the data buoy and 100 ml added to a darkened glass bottle and preserved in acidic Lugol's iodine to a final concentration of 1%. For analysis, 10 ml of preserved sample was settled in a glass sedimentation chamber for 24 h and cells then identified and counted using a Leica inverted light microscope (Utermöhl, 1958). Samples for later nutrient analysis were filtered through a 25 mm diameter GF/F filter using an inline syringe unit and then frozen in 50ml plastic bottles prior to analysis. Concentrations of nitrate

plus nitrite, phosphate and silicate were determined on a QuAAtro segmented flow nutrient analyser (SEAL Analytical, UK) as described by Panton et al. (2020).

2.4 Mean water column irradiance

Photosynthetic Active Radiation (PAR) within the water column varies according to changes in surface incident solar irradiance, turbidity, and depth (Cloern *et al*., 2014). Therefore, the mean water column irradiance (I_m) was calculated following Riley (1967) as:

$$I_m = I_0 \frac{(1-e^{-k_{PAR}h})}{k_{PAR}h} \quad (1)$$

where I_0 is the daily surface irradiance (W h m^{-2} d^{-1}), k_{PAR} is the diffuse attenuation coefficient (m^{-1}), and h is the mixed layer depth (10 m). The diffuse attenuation coefficient was estimated from the slope of a linear regression of turbidity against k_{PAR} data previously generated for the estuary by Iriarte & Purdie (2004), with k_{PAR} ranging between 0.2 and 2.0 m^{-1}.

2.5 Optode-based oxygen sensor validation

Semi-continuous oxygen measurements were determined from the EXO2 sonde deployed optode. While optodes have proven useful in describing biogeochemical processes (Bittig & Körtzinger, 2015), to ensure high quality dissolved oxygen data were being recorded, we compared the optode data to measurements made on discrete water samples (Haskell *et al*., 2019; Uchida *et al*., 2008). The following correction steps were therefore made prior to using the oxygen time-series data to calculate NCP rates: (i) Some missing salinity measurements from the time series were estimated since the optode DO sensor installed on the EXO2 sonde measures oxygen saturation and then salinity and temperature data are used to calculate DO concentration. During 2019, the salinity sensor on the sonde showed some periods of drifting, and a more reliable sensor was not replaced until November. Thus, Environment Agency

188 measured salinity data was compared against existing and reliable salinity data from
189 the EXO2 sonde, and an equation from that correlation was used to substitute missing
190 salinity data. (ii) Recalculating DO concentration values from polynomial temperature
191 and salinity dependant equations (Feistel, 2008). (iii) Lastly, discrete oxygen
192 measurements from Winkler titrations and Environment Agency collected
193 measurements were used to formulate a standard linear regression (see supplementary
194 material Fig. A.1) model to correct optode derived DO concentration values.

195 2.6 Open diel oxygen method

196 The open diel method (Needoba *et al*., 2012) was applied to calculate daily NCP by
197 calculating oxygen mass-balance in the surface mixed layer (see supplementary
198 material). An essential assumption of this model is that all measurements come from
199 a well-mixed water column; therefore, the water mass recorded presents the same
200 metabolic history (Caffrey *et al*., 2014).

201 The hourly biological oxygen production (BOP) calculation incorporated equations
202 used by Hull *et al*. (2016) and Murrell *et al.* (2018). In Eq. (2) C_0 is the oxygen
203 concentration at $t = 0$ and C_1 oxygen concentration at the time step (for the present
204 study, 1 hour), and it is analytically solved by using the air-sea diffusion flux
205 calculation F and a transfer velocity correction t, caused by wind-induced turbulence
206 in the mixed water column (h).

207 $$BOP = th\left(\frac{C_1 - C_0}{1 - e^{-rt}} + C_0\right) - Fh \quad (2)$$

208 The diffusive exchange of gases across the air– sea interface F (Eq. 3) was calculated
209 as a function of gas transfer velocity k_w (Eq. 4) and diffusion through bubbles B. P_{atm}
210 corresponds to an atmospheric pressure standard value of 101,325 Pa, P_{slp} is the
211 atmospheric air pressure at sea level, C^* is the calculated oxygen concentration in

equilibrium with the atmosphere as a function of temperature and salinity (Feistel, 2008) and C is the oxygen concentration in the surface mixed layer.

$$F = \frac{k_w}{h} C^* (1 + B) \frac{P_{slp}}{P_{atm}} + \frac{1}{h} \frac{\partial h}{\partial t} C \quad (3)$$

k_w (Eq. 4) is the parameterisation proposed by Wanninkhof (2014), as function of salinity and temperature through the relation between the Schmidt number Sch_{O_2} for oxygen and the normalised Schmidt number for CO_2 at 20°C and salinity of 35 (constant value of 660 in Eq. 4). U corresponds to wind speed measured at 10m above sea level but as stated above can be considered the same as at sea level at the position of the Data Buoy .

$$k_w = 0.251 U^2 \left(\frac{Sch_{O_2}}{660}\right)^{-0.5} \quad (4)$$

BOP data were averaged separately into "day" and "night" periods using light data from the MIDAS Met station. Respiration rates were assumed to be constant during a diel cycle; thus, respiration was extrapolated to 24 hours to obtain daily ecosystem respiration (ER). Finally, daily NCP (Eq. 5) was calculated as a function of the difference between daily gross primary production (GPP) and ER.

$$NCP = GPP - ER \quad (5)$$

2.7 Statistical analysis

None of the environmental data nor productivity rates were normally distributed, despite different transforms being applied. Consequently, the non-parametric Spearman's Rank-Order Correlation Coefficient (p<0.05) was used to evaluate the strength of associations among calculated productivity rates and measured environmental variables throughout the study period (Table 1). Data were divided into

separate groups (Table 2), and the Kruskal-Wallis One Way Analysis of Variance on Ranks (p<0.05) and the all pairwise Dunn's test (p<0.05) were used to evaluate whether environmental conditions and productivity rates changed between major bloom event periods and the remaining days over the 12-month period. In order to explain the sources of variability in bloom events, Principal Component Analysis was applied. This method allows reducing the dimensionality of large datasets without losing its variability by transforming original variables into a new and smaller set of uncorrelated variables (Jollife & Cadima, 2016). Statistical analysis was performed using the statistical package in SigmaPlot version 13.0.

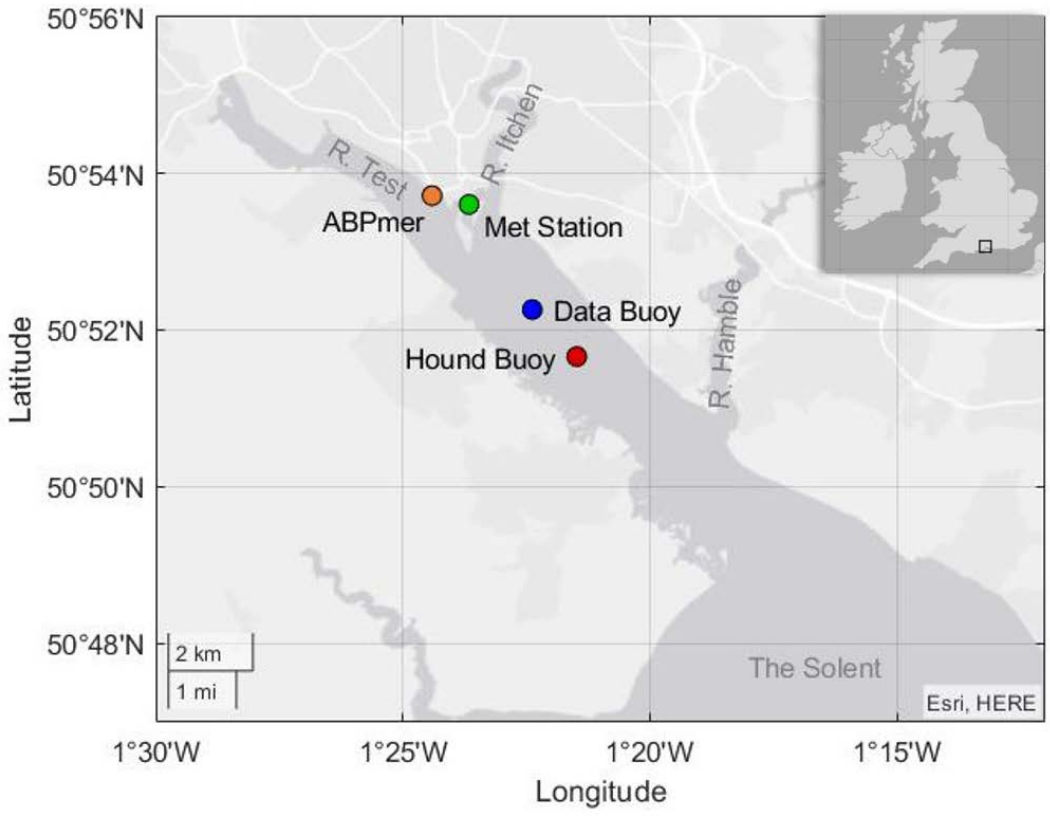

Fig. 1. Map of the Southampton Water estuary located on the south coast of The UK (inset). Data sets were collected from the Meteorological station at the National Oceanography Centre (green circle ●), tide gauge data from ABP Marine Environmental Research (orange circle ●), Xylem Analytics Data Buoy system (blue circle ●) and Environment Agency samples from Hound navigation buoy (red circle ●).

3 Results

3.1 Variation of environmental conditions

The estuarine water temperature reflected a seasonal warming, with monthly average values of ~7°C during January and February (Fig. 2a), then steadily increasing until reaching an average of 20.3°C for July and August and later decreasing to a value of 8.7°C in December 2019.

Salinity showed low variation across the whole year, with an average of 31.8 ± 1.2 (Fig. 2b). Some differences, although not significant, were found over 24 hr periods, but as seen in previous studies (Levasseur *et al*., 2007), salinity at this point of the estuary is mainly driven by the semi-diurnal tidal cycle and typically ranges between 28.0 and 32.9.

Oxygen concentration presented a year minimum of 165 µmol L^{-1} during July and a maximum of 450.4 µmol L^{-1} in June (Fig. 2c). Elevated daily concentrations were detected between April-July; however, periods before April and after July showed more constant values. The oxygen concentration during the first 3 months remained at ~300 µmol L^{-1}, while from August to December, a gradual monthly average increase occurred, with averages from 225.2 to 287.3 µmol L^{-1}. An average value of oxygen saturation over the whole year of 100.8% indicated an overall balance in the oxygen saturation (Fig. 2d). Oxygen percentage presented mainly oversaturated conditions between April and July and similar to oxygen concentration, consistently showed the greatest daily variations, with the lowest value in July (71.1%), while the highest in June (183.5%). During the rest of the year, oxygen conditions remained slightly undersaturated. Both oxygen parameters displayed peaks during the high productivity

period, comprising days of continuous values >115% saturation and >300 µmol L^{-1} concentration.

Chl '*a*' showed a clear period of increased concentration from late April to late August (Fig. 2e). Outside of this period, average Chl '*a*' concentration remained below 1.5 µg L^{-1}. Four phytoplankton bloom events of different duration and magnitude were observed (Table 1): (i) in late April, a peak dominated by the colonial phytoplankton *Phaeocystis* was observed for 14 days with an overall average of 4.2 µg L^{-1} and, (ii) at the end of May, a bloom comprising of the diatom *Guinardia delicatula* was sustained for 15 days with an average of 8.7 µg L^{-1} and reached a maximum hourly value of 27.1 µg L^{-1}. (iii) The most prolonged bloom was observed for about 48 days during June-July and was mainly attributed to the photosynthetic ciliate *Mesodinium rubrum,* presenting the hourly year maximum value of 28.3 µg L^{-1} and an event average of 7.5 µg L^{-1} and finally, (iv) a short bloom was observed at the end of August for 5 days with a mean concentration of 5 µg L^{-1}. The major bloom events in late April, early June and late August developed following a spring tide and peaked during the next neap tide (Fig. 2). The more prolonged bloom dominated by *Mesodinium rubrum* in July started on a neap tide in late June but was then sustained over two further spring/neap periods until late July.

Turbidity measurements ranged between 1.2 and 16.6 FTU, with a marked period from May to July of low turbidity when daily averages remained below 6 FTU (Fig. 2f). Increased daily variation in turbidity was observed from September to December, but this could have been caused by some biofouling of the turbidity sensor since Chl '*a*' for this period remained unaffected. Highest turbidity values corresponded to maximum tidal ranges during peak spring tides (Fig. 2f).

297 The first two weeks of March, showed high wind speeds in comparison to the rest of
298 the year, with sustained daily values above 6 m s^{-1} and gusts reaching up to 16.8 m s^{-1}.
299 Following this a period lasting until the end of July of lower wind speeds (>5 m s^{-1})
300 was identified (Fig. 2g).
301 For I_0, values ranged between 165.9 and 3313.6 W h m^{-2} d^{-1} in January and July,
302 respectively (Fig. 3a). A sudden increase in values was observed at the end of March,
303 reaching slightly above 2000 W h m^{-2} d^{-1} but then decreasing to ~1300 W h m^{-2} d^{-1} for
304 two weeks, before increasing again and remaining mainly above 2000 W h m^{-2} d^{-1} for
305 the period between April and August.
306 I_m showed a large variation throughout the year, with a monthly range from 55.9 W h
307 m^{-2} d^{-1} in November to 1004.6 W h m^{-2} d^{-1} in May (Fig. 3.b). Sustained values above
308 the annual average of 321.4 W h m^{-2} d^{-1} were observed from April to late September,
309 after which a drop in values remained for the rest of the year. An exceptionally high
310 I_m period occurred in late April and throughout the whole of May, with three different
311 events, lasting from 3 to 9 days, of sustained values above 1000 W h m^{-2} d^{-1}.
312 3.2 Fluctuation of productivity rates
313 Estimated daily values of ER are presented in Figure 4. Calculated values ranged from
314 0.1 (June) to 437.5 (August) mmol O_2 m^{-2} d^{-1} with a yearly average of 37.6 mmol O_2
315 m^{-2} d^{-1}. ER rates did not show a particularly well defined seasonality with occasional
316 periods of ~7 days of peaks in activity throughout the year, notably from May to
317 November. From August to October, monthly values were above 50.0 mmol O_2 m^{-2} d^{-1}.
318 Conversely, March presented a particularly low monthly value of 2.9 mmol O_2 m^{-2}
319 d^{-1} (although only 12 days of estimates were available).
320 GPP presented an annual daily average of 36.7 mmol O_2 m^{-2} d^{-1} and varied from 0.1
321 to 411.2 mmol O_2 m^{-2} d^{-1} with both values occurring in the second half of June, only

11 days apart, as seen in Figure 4. A period of increased productivity was noted from late April to mid-August, with the average productivity rate for this time being 58.6 mmol O_2 m^{-2} d^{-1}, compared to only 11.1 mmol O_2 m^{-2} d^{-1} for the rest of the year. In addition, daily values outside this period were below 100.0 mmol O_2 m^{-2} d^{-1}, while ~20% of daily observations from April to May were above this rate.

Positive daily values of NCP indicate net autotrophy within the water column while negative values suggest net heterotrophy. NCP showed a relatively balanced annual average of -0.8 mmol O_2 m^{-2} d^{-1}. Positive NCP estimations exhibited a seasonal pattern with a highly productive period from April to July (Fig. 4), reflecting net autotrophic conditions with an average of +34.8 mmol O_2 m^{-2} d^{-1} across the 4-month period. The highest positive NCP value of the year (+229.6 mmol O_2 m^{-2} d^{-1}) was observed at the end of a 57-day period of continuous autotrophic conditions, that averaged +44.1 mmol O_2 m^{-2} d^{-1}, and matched the peak in Chl '*a*' concentration at the end of May. This peak was followed closely by a second observed in late-June (+197.1 mmol O_2 m^{-2} d^{-1}), when an additional extended autotrophic period (29 days) averaged +72.2 mmol O_2 m^{-2} d^{-1}. Heterotrophic conditions were nearly absent from March to May, presenting less than ~15% of total observations in this period. However, in August (-366.8 mmol O_2 m^{-2} d^{-1}) and October (-309.8 mmol O_2 m^{-2} d^{-1}) some high negative daily rates of NCP were estimated. From August to November, a heterotrophic state averaging -30.0 mmol O_2 m^{-2} d^{-1} was calculated.

3.3 Relation between environmental conditions and bloom events

Spearman's rank coefficients analysis (Table 1, $p<0.05$) showed that NCP was strongly positively ($\rho>0.55$) correlated with I_m, DO in percentage and concentration of Chl '*a*' and negatively correlated ($\rho=0.43$) with turbidity. GPP showed a strong positive correlation ($\rho>0.55$) with Chl '*a*' concentration. Moderate positive correlations were

also found between GPP and I_m (ρ=0.40), average wind speed (ρ=0.47) and temperature (ρ=0.41). ER was found to strongly negatively correlate with average wind speed (ρ>0.55).

For this study, a major bloom was considered when 1-hour average values of Chl '*a*' concentration were sustained above 10 µg L^{-1} and when the biomass gain corresponded to NCP values >+20 mmol O_2 m^{-2} d^{-1}. In order to evaluate differences among parameters during bloom events and the rest of the days studied (identified as low productivity periods LPP), a Kruskal-Wallis analysis (p<0.05) was conducted, paired with Dunn's test (p<0.05) to identify specific groups (Table 2). Both Chl '*a*' and I_m showed a clear separation between bloom groups and LPP, presenting higher average values during bloom events, particularly during Bloom 2. On average, oversaturated oxygen values were observed during Bloom 1, 2 and 3, while during Bloom 4 and LPP water was slightly undersaturated. For NCP, Bloom 4 and LPP presented average values closer to production balance (=0), while Bloom 1, 2 and 3 showed mean values reflecting a more autotrophic state (>0). Bloom 4 was grouped with LPP for GPP data due to its lower mean value. For ER, Bloom 4 presented a tighter range and lower average than the other groups; hence was separated. Grouping blooms based on temperature placed those occurring during summer (Bloom 3 and 4) and those in winter-spring periods (LPP and Bloom 1) in different groups, with Bloom 2 (late spring) overlapping among the two groups (Table 2).

Further analysis of how individual environmental conditions contribute to each major bloom event is shown in the PCA (Fig. 5). The first two principal components accounted for ~58% of the total variance. PC1 explained 32.82% of the total variability in the dataset while PC2 described 25.54%. The main factors contributing to PC1 positive eigenvalues (R^2>0.80) were I_0, I_m, O_2% and Chl '*a*'. In comparison, river

flow and turbidity correlated with negative eigenvalues of PC1 (R^2>-0.41), and to a lesser extend (R^2>-0.20) tidal range, wind speed and ER. Trophic state was associated with PC1, with blooms being mainly associated to positive loadings, correlating to autotrophic conditions. Positive values of PC2 were mainly described (R^2>0.84) by temperature and salinity, followed by ER, turbidity, I_0 and wind speed (R^2>0.33). Conversely, river inflow and [O_2] were the main contributors (R^2<-0.81) to negative eigenvalues. PC2 described the influence of river input to the estuary, associating Bloom 1 and Bloom 2 (Fig. 5) with higher freshwater flow while Bloom 3 and Bloom 4 were distributed across daily rates during lower riverine inflow.

Table 1

Spearman's correlation coefficients relating environmental conditions and productivity rates

	I_m	Tidal Range	Wind Speed	Temp.	Sal.	O_2%	[O_2]	Chl '*a*'	Turb.
NCP	**0.61**	-0.10	**-0.15**	**0.24**	**-0.19**	**0.60**	**0.37**	**0.61**	**-0.43**
GPP	**0.40**	-0.10	**0.47**	**0.41**	0.10	**0.28**	**0.12**	**0.57**	**-0.15**
ER	**0.21**	-0.00	**-0.66**	**-0.12**	**-0.22**	**0.27**	**0.15**	0.04	**-0.24**

Values in bold $p < 0.05$. Values underlined represent absolute coefficient with strong correlation, ρ > 0.55.

Table 2

Average and range of daily measured environmental conditions and calculated productivity rates for different major bloom events (continuous chlorophyll' *a*' concentration values higher than 10 µg L^{-1}) and low productivity period LPP (studied days without blooms).

	I_m	Tidal range	Wind speed	Temp.	Sal.	O_2 %	[O_2]	Chl '*a*'	Turb.	NCP	GPP	ER
LPP	221.7[a]	3.3[a]	4.3	12.7[a]	31.7[a]	95.9[a]	274.8[a]	0.9[a]	5.4[a]	-21.2[a]	18.0[a]	-39.3[a]
(283)	(26.9 : 2001.9)	(1.6 : 4.8)	(1.1 : 13.1)	(5.7 : 22.0)	(28.8 : 33.6)	(81.5 : 116.9)	(205.8 : 361.4)	(0.1 : 3.3)	(1.8 : 10.9)	(-366.8 : 91.9)	(0.2 : 117.9)	(-437.5 : -0.2)
Bloom 1	625.1[b]	3.0[ab]	4.2	12.9[a]	31.3[a]	120.6[b]	330.7[b]	4.2[b]	3.8[a]	59.9[b]	110.2[b]	-50.3[a]
(111–124)	(188.3 : 1337.6)	(1.7 : 4.4)	(2.0 : 8.9)	(12.3 : 13.5)	(29.9 : 31.7)	(113.4 : 129.1)	(310.3 : 356.1)	(3.0 : 5.5)	(1.9 : 7.4)	(20.6 : 154.0)	(39.1 : 284.2)	(-212.6 : -4.9)
Bloom 2	1006.6[b]	2.9[ab]	4.0	15.9[ab]	31.8[a]	120.3[b]	312.3[b]	8.7[b]	2.3[b]	87.0[b]	123.1[b]	-36.1[a]
(142–156)	(650.3 : 1388.9)	(2.0 : 3.9)	(2.7 : 5.1)	(15.0 : 16.7)	(30.9 : 32.4)	(104.2 : 134.5)	(269.7 : 355.0)	(2.0 : 14.3)	(1.9 : 2.8)	(7.9 : 229.6)	(9.1 : 277.9)	(-80.0 : -1.3)
Bloom 3	426.4[b]	3.2[ab]	3.6	19.9[b]	32.3[ab]	113.5[b]	270.0[a]	7.5[b]	4.6[a]	44.3[b]	74.5[b]	-30.1[a]
(169–216)	(136.3 : 783.5)	(2.0 : 4.4)	(1.5 : 9.7)	(16.5 : 22.0)	(30.8 : 33.5)	(84.6 : 146.8)	(202.7 : 349.8)	(2.6 : 16.2)	(2.9 : 8.8)	(-172.1 : 197.1)	(0.1 : 411.2)	(-214.1 : -0.1)
Bloom 4	698.6[b]	2.3[b]	2.8	20.5[b]	33.6[b]	96.8[ab]	237.6[a]	5.0[b]	3.1[ab]	2.2[ab]	6.4[a]	-4.2[b]
(236–240)	(570.7 : 817.6)	(1.9 : 3.1)	(2.0 : 4.4)	(19.7 : 20.9)	(33.6 : 33.6)	(94.4 : 99.1)	(234.3 : 241.7)	(3.3 : 6.5)	(2.8 : 3.4)	(-1.2 : 6.2)	(1.6 : 12.0)	(-6.6 : -2.5)

Included mean water column irradiance I_m (W h m^{-2} d^{-1}), tidal range (m), wind speed (m s^{-1}), temperature (°C), salinity, dissolved oxygen (% and µmol L^{-1}), chlorophyll '*a*' (µg L^{-1}) and turbidity (FNU). Calculated productivity rates: NCP, GPP and ER in mmol O_2 m^{-2} d^{-1}.

Letters in superscript indicate a significant difference from one/all other groups (Dunn's test; $p<0.05$).

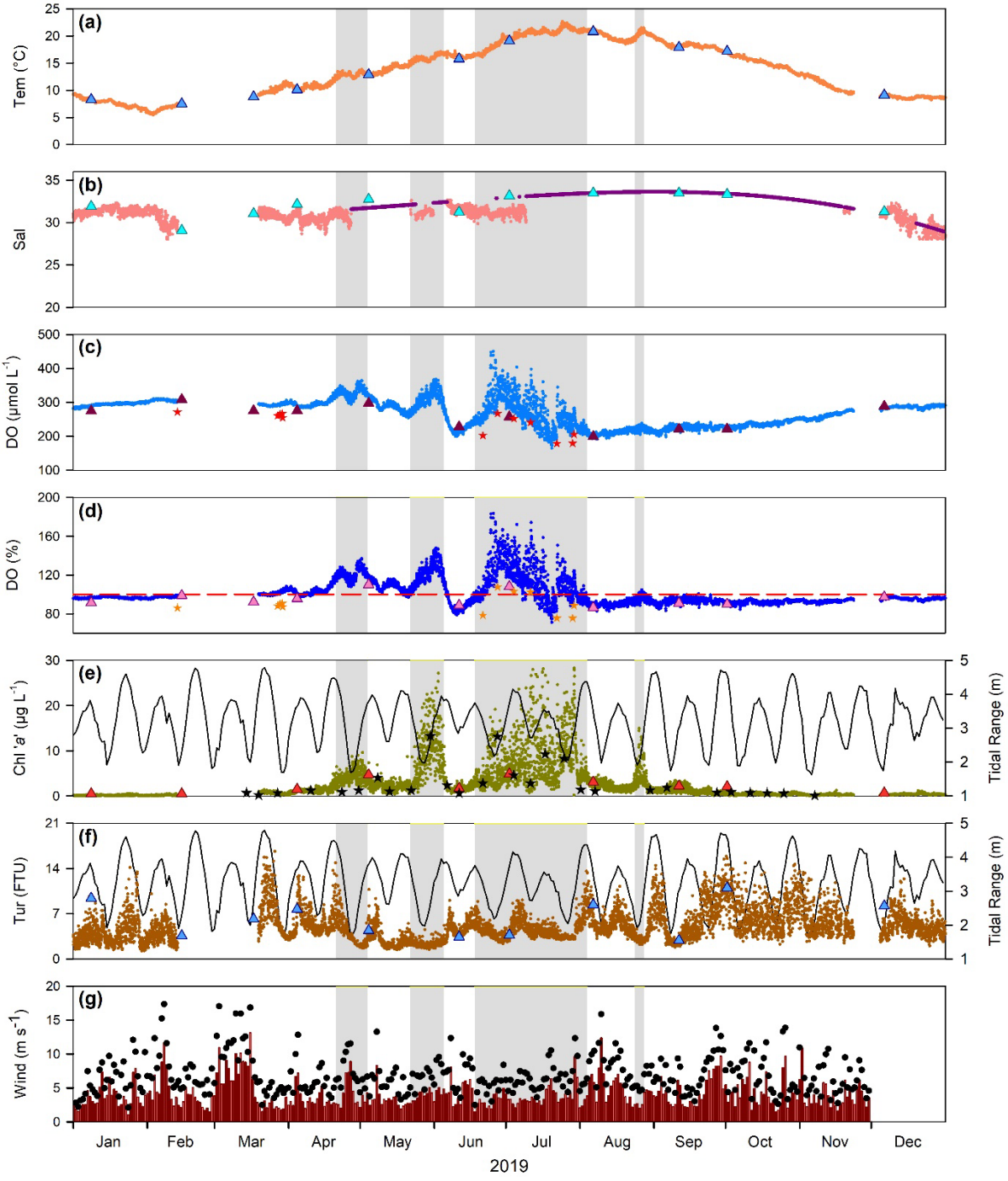

Fig. 2. Hourly time series of environmental conditions at the Xylem Data Buoy in Southampton Water in 2019: (a) temperature, (b) salinity, (c) DO in concentration and (d) DO in percentage saturation , (e) chlorophyll '*a*', (f) turbidity and (g) wind speed, represented as daily mean in vertical bars ▮ and maximum daily values in black circles ●. In a to g, the 4 major blooms identified are shown as a grey background ▮. In d, the red dashed line – – represents 100% of saturation. In c, d and f discrete samples are shown as ★ in different colours. In e and f, the daily tidal range is indicated with a black line. In a to f, Environmental agency sampling points are shown as triangles ▲ in different colours.

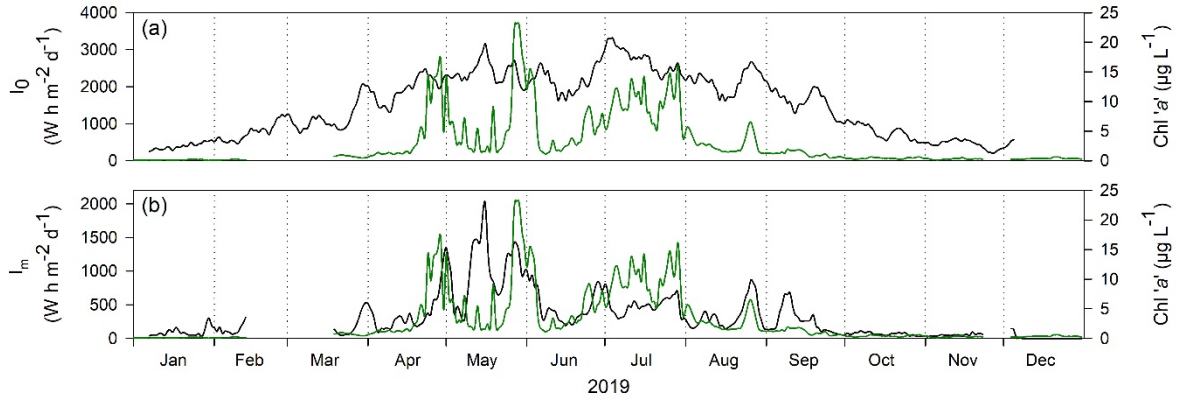

397

398 **Fig. 3.** Temporal variations (7-day running mean) in (a) surface irradiance I_0 and (b) mean water

399 column irradiance I_m with daily mean chlorophyll '*a*' concentration included in (a) and (b) as a green

400 line —.

401

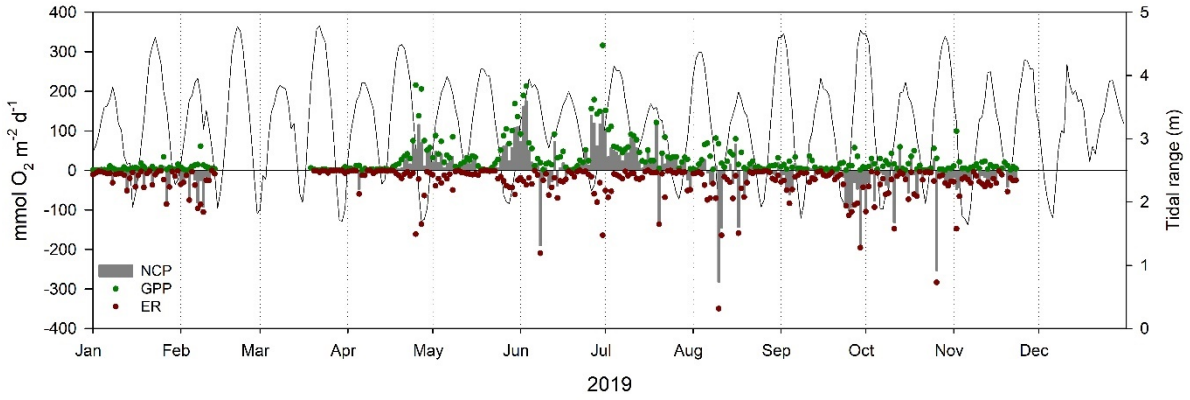

402

403 **Fig. 4.** Calculated daily net community production NCP (vertical bars ▮), ecosystem respiration ER

404 (red circles ●) and gross primary production GPP (green circles ●). Respiration data are displayed as

405 negative values. Change in the daily tidal range is indicated — as a black continuous line.

406

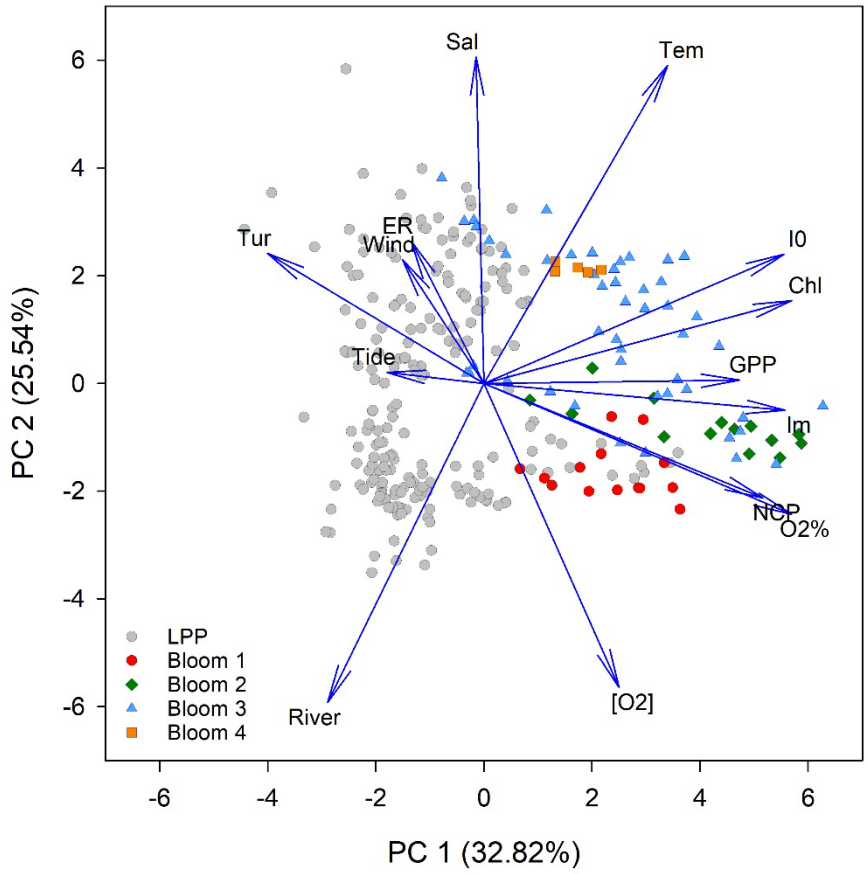

407

408 **Fig. 5.** Principal Component Analysis (PCA) of environmental conditions. The data clustering and the
409 primary (PC1: 32.82% of the variance) and secondary (PC2: 25.54% of the variance) axes represent
410 58.36% of the total variance. Bloom events have been used as factors to illustrate the clusters: Bloom 1
411 (red circles ●), Bloom 2 (green diamonds ♦), Bloom 3 (blue triangles ▲) and Bloom 4 (orange squares
412 ■). Tem=temperature, Sal=salinity, Chl=chlorophyll '*a*', I0=surface water irradiance, Im=mean water
413 column irradiance, O2%=DO in percentage saturation, [O2]=DO concentration, Wind=wind speed,
414 Tur=turbidity, Tide=tidal range, River=river inflow, GPP=gross primary production, ER=ecosystem
415 respiration and NCP=net community production.

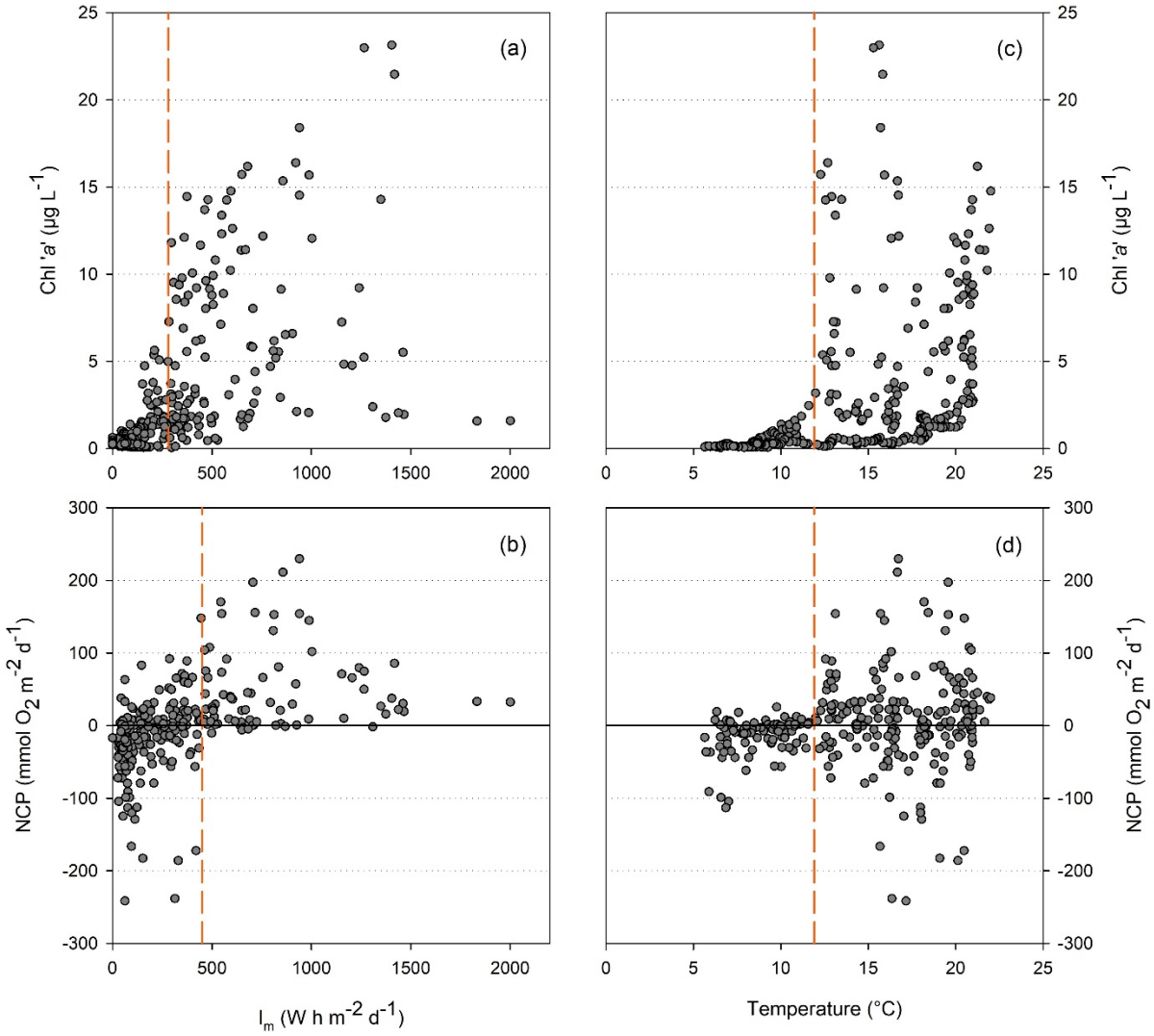

Fig. 6. Daily mean water column irradiance I_m compared with (a) daily chlorophyll '*a*' and (b) net community production NCP; and daily temperature averages compared with (c) daily chlorophyll '*a*' and (d) net community production NCP. References lines — for water column irradiance I_m of 280 (a) and 450 W h m^{-2} d^{-1} (b), and temperature of 11.91 °C (c and d) were added in.

4 Discussion

4.1 Drivers of phytoplankton bloom events

Blooms are a fundamental feature of phytoplankton dynamics, defined as events of fast growth and accumulation of biomass, occurring at different magnitudes and duration according to environmental conditions (Shi *et al.*, 2016). Three major phytoplankton bloom events were observed in the mid Southampton Water estuary

between late April and the beginning of August 2019, plus a fourth minor bloom detected at the end of August.

Daily peaks in Chl '*a*' recorded during bloom events in the present study compare well with previous observations in the estuary (Iriarte & Purdie, 2004; Torres-Valdés & Purdie, 2006), where values reached nearly 20 µg L^{-1} during spring blooms. The magnitude of coastal phytoplankton blooms is highly variable across the world; ranging from coastal ecosystems with typically low concentrations of Chl '*a*' such as the Thau Lagoon (France) presenting mean values between 2.8 and 3.6 µg L^{-1} during intense bloom events (Trombetta *et al*., 2019) to the Lagoon and Bay of Bizerte (Tunisia) described by Salhi *et al*. (2018) displaying more comparable maximum mean values during a summer bloom (15.8 and 8.5 µg L^{-1}). It is also possible to find highly eutrophicated systems like the Sundays Estuary in South Africa where exceptional maximum chlorophyll values during blooms above 100 µg L^{-1} have been reported (Lemley *et al*., 2018).

Nutrient input from runoff can supply ecosystems with nutrients, stimulating phytoplankton production and leading to the accumulation of biomass and bloom formation (Cloern & Jassby, 2010; Trombetta *et al*., 2019). However, in the present study nutrient measurements from surface water samples collected from near the data Buoy showed no clear relationship to appearance of blooms although nitrate, phosphate and silicate concentrations reached minimum levels in late May following the *Guinardia delicatula* bloom (see supplementary Figure A.2). Nutrient concentrations then increased during June with nitrate and phosphate concentrations declining to almost undetectable levels for the first 3 weeks of July during the *Mesodinium rubrum* bloom.

One of the main factors limiting water column primary production is light availability, in shallow and turbid coastal systems (Brito & Newton, 2013). A comparison between the temporal variation of average daily Chl '*a*' concentration and I_m (Fig. 6a), showed that Chl '*a*' values above 10 µg L^{-1} only occurred when I_m was greater than 280 W h m^{-2} d^{-1}. A similar comparison between NCP values and I_m (Fig. 6b) resulted in positive values, therefore production exceeding respiration, when I_m was above 450 W h m^{-2} d^{-1}. Riley (1967), proposed a theoretical I_m critical value for a sustained increase in phytoplankton biomass, in temperate coastal and estuarine waters, of 200 W h m^{-2} d^{-1}, a threshold value below that found in the present study. However, previous research in Southampton Water (Iriarte & Purdie, 2004) found that Chl '*a*' levels above 10 µg L^{-1} occurred, when I_m averaged for the previous 7 days exceeded 380 W h m^{-2} d^{-1}.

In temperate latitudes, water temperature is a critical parameter influencing phytoplankton bloom development (Lemley *et al*., 2018b; Trombetta *et al*., 2019). Furthermore, phytoplankton growth rates increase with temperature, almost doubling with each 10 °C rise (Rose & Caron, 2007). Given the range of temperature observed during 2019 in Southampton Water (5.7 – 22 °C), phytoplankton growth rates will have increased by more than double during the annual period studied. A comparison of temporal variation in water temperature against daily average Chl '*a*' concentration (Fig. 6c) and NCP (Fig. 6d) found that bloom conditions only occurred when temperature values were above 11.9 °C for both parameters. A similar result was reported by (Iriarte & Purdie, 2004) in their previous 5-year study where all major bloom events in Southampton Water occurred when water temperature was greater than 12 °C. An identical reference value of 12 °C was found by (Carstensen *et al*., 2015) for coastal sites in the Rhine-Meuse-Scheldt delta and the Wadden Sea, indicating phytoplankton communities of temperate coastal ecosystems, at comparable

latitudes, tend to bloom at around the similar threshold temperature. When compared against a coastal ecosystem at a lower latitude (southern France), the spring bloom generally occurred at a slightly increased temperature of 14 °C (Trombetta *et al*., 2019).

Water level data analysed showed a positive correlation (data not shown) between tidal range and turbidity, indicating that turbidity in the system generally increased during spring tides. Bucci *et al*. (2012) reported phytoplankton summer blooms in the São Vicente estuary (Brazil) usually occurred towards the end of neap tides, but no significant correlation with tidal cycles was found. This lack of correlation with tidal range, in addition to the strong correlations between phytoplankton peaks and I_m and temperature, indicate that blooms in the Southampton Water estuary are not only regulated by turbulent mixing due to tides but a combination of factors affecting the solar radiation attenuation throughout the water column (Cloern *et al*., 2014). In most shallow estuaries where the neap-spring cycle is present, fortnightly patterns of reduced mixing during neap tides can be observed (Carstensen *et al*., 2015), and it is during these periods that phytoplankton net biomass growth is enhanced. A similar pattern was reported by Cloern (1996) in his review of phytoplankton bloom dynamics in the San Francisco Bay, a system with a similar depth (~10m) to the Southampton Water estuary, but with a smaller tidal range (2m).

4.2 Net community production

High-frequency DO measurements represent a useful opportunity to link productivity rate dynamics and net community production response to short-period changes in environmental conditions, as well as episodic events, such as storms or increased river inputs (Staehr *et al*., 2012). The annual average rate of NCP for Southampton Water of -0.8 mmol O_2 m^{-2} d^{-1} showed an overall more or less balance between GPP and ER,

leaning slightly towards a heterotrophic state. A more heterotrophic annual average value of -5 mmol O_2 m^{-2} d^{-1} was reported for a shallow bank in the mouth of the Thames estuary, calculated using the open diel method (Hull *et al*., 2016). Reports of more highly heterotrophic ecosystems are widely described in the literature: such as the Ria Formosa Lagoon, South Portugal with DO dynamics used to calculate an annual value of -244 mmol O_2 m^{-2} d^{-1} (Cravo *et al*., 2020) and the use of the LOICZ biogeochemical model applied to four different coastal lagoons in the Gulf of California reported all of them to be heterotrophic for the time studied (Valenzuela-Siu *et al*., 2007). Caffrey *et al*. (2014) calculated the annual NCP, for three different estuaries in the Gulf of Mexico, and found all sites were net heterotrophic for most of the year with the greatest heterotrophy during the summer. On the other hand, an example of an ecosystem inclining to an autotrophic state is that reported by Haskell *et al*. (2019) in a productive coastal zone in southern California where NCP values of +0.16 and +0.18 mmol O_2 m^{-2} d^{-1} were calculated for 2013 and 2014, respectively through glider-measured oxygen concentrations.

Results from the current study showed a noticeable pattern of NCP behaving more similarly to GPP than to ER, and both showing a strong correlation to Chl '*a*' concentration (Table 1), suggesting productivity rates could be regulated by factors influencing autotrophic processes. The same tendency of GPP influencing NCP trends more strongly and correlations with Chl '*a*' were observed by Agusti *et al*. (2018) in their study of the productive Matilda Bay in Australia, where they found that over an annual period, ER rates were less variable than GPP rates. Lack of correlation between ER and Chl '*a*', while presenting a strong relation to GPP, was also observed by Murrell *et al*. (2018) in their study of a river-dominated estuary located in the Gulf of Mexico.

ER showed no clear seasonal pattern, while GPP produced maximum rates during the spring-summer period (Fig. 4). This was reflected in moderate correlations between GPP and temperature and I_m (Table 1), with higher values converging during summer. Since NCP closely reflected GPP trends, the highest positive NCP calculated value of 175 mmol O_2 m^{-2} d^{-1}, was observed in the middle of the spring-summer period. This maximum value is lower than others have reported during spring-summer NCP peaks in the Ria de Vigo, Spain (Alonso-Pérez *et al*., 2015) and in the mouth of the River Thames (Hull *et al*., 2016), of ~300 mmol O_2 m^{-2} d^{-1} and 485 mmol O_2 m^{-2} d^{-1}, respectively.

Photosynthetic rates generally present a close relation to light availability in the water column, although coastal ecosystem respiration is sometimes unaffected directly by light levels (Kemp & Testa, 2011). An analysis of NCP and light availability (Fig. 6b) showed that when I_m reached values of 450 W h m^{-2} d^{-1} and above, NCP was consistently positive, indicating at these levels of I_m, productivity was consistently exceeding respiration; hence, the system was net autotrophic.

As shown with Chl 'a' concentration peaks, NCP daily values during the high productivity period (April to August) were related to neap tides (Fig. 4). During this time, NCP showed a biweekly pattern peaking during the monthly low neap tide. This reveals the system was strongly autotrophic during these tides and moving to a less autotrophic state or, sometimes, even shifting to heterotrophic conditions with the onset of the spring tide. The closest comparison to these results was the two-month study done by Nidzieko *et al*. (2014) in a tidal creek/marsh area in the deeper main channel of Elkhorn Slough, California, where they found net heterotrophic conditions during spring tides and mostly in balance conditions during neap tides.

Although our results showed that the Southampton Water estuary presented an overall net heterotrophic annual state in 2019, where input of external organic matter is needed, and CO_2 is released to the atmosphere (Tang *et al*., 2015), seasonal productivity events shifted this state for a few days and sometimes weeks to autotrophic conditions, particularly during the highly productive period in spring-summer. This change meant that for brief periods, the ecosystem was a strong CO_2 sink and a source of organic matter and oxygen (Lee *et al*., 2017), consistent with the hypothesis that primary production during these brief episodes is a substantial component of annual primary production (Cloern *et al*., 2014).

4.3 Method implications

The open diel oxygen method coupled with high-frequency water quality monitoring is a powerful tool to help understand the influence of physical and biological processes on DO changes through time, particularly since the principal biological process influencing the ocean's declining DO concentration is phytoplankton respiration (Robinson, 2019). The increasing availability of improved and affordable instrumentation has made it possible to create high-frequency time-series from which more reliable estimations of net community production can be derived and evaluate different spatial and temporal variability within ecosystems (Aristegi *et al*., 2009; Staehr *et al*., 2012).

As with any method, assumptions must be made in order to apply the approach to different ecosystems and data availability. Since it frames the possibility of applying the open diel method to a particular ecosystem, one of the main assumptions is that the water column monitored must be reasonably homogenous and well mixed (Caffrey *et al*., 2014). Vertical profiles of temperature, salinity and DO% made previous to the 2019 data time series (see supplementary Figure A.3) presented temperature

differences between the surface and bottom waters that ranged from 0.1°C in late April to 2.0°C in July. DO saturation throughout the water column presented higher variability in August (9%) and did not correspond with the profile presenting the greater temperature variation or the highest temperature (July). Both DO saturation and temperature showed less variability through the water column than data in Murrell et al. (2018) study (26% and ~4°C). Among other complications previously encountered using this methodology is the necessity to separate air-sea O_2 exchange (Staehr *et al*., 2012). Direct measurements of air-water exchange can present great difficulty, and some past works have opted for assumed constant values for similar systems (Caffrey, 2004). Since air-water exchange varies due to surface turbulence, water viscosity and the solubility of O_2 (Holtgrieve *et al*., 2010); to minimize error propagation, in the present study it was calculated for every time-step (1 hour) as a function of diffusion through bubbles and gas transfer velocity, which in turn included the Schmidt number encapsulating influences of water temperature and salinity. However, a correlation between values of calculated ER and wind speed (Table 1) suggest highly negative NCP rates related to wind gusts above 9 m s^{-1} (data not shown) and, although it is known that in shallow ecosystems, wind stress can induce rates of sediment resuspension stimulating ER and reducing GPP (Kemp & Testa, 2011), this seems to be an overestimating heterotrophic condition from the bubble supersaturation term.

Contributions from partially dissolved bubbles and overestimation in the air-water transfer has been reported previously (Haskell *et al*., 2019; Hull *et al*., 2016; Liang *et al*., 2013). A final generalisation is that ER rates are assumed constant through the diel cycle since CO_2 fixation through chemoautotrophic processes is usually smaller than that fixed by photosynthesis. In most coastal ecosystems (Testa *et al*., 2012), processes

such as nitrification and photooxidation are assumed to be insignificant compared to estimates of 'night respiration' (Demars *et al*., 2015).

There are several methods available to estimate aquatic primary production, but few provide the opportunity to calculate directly continuous productivity rates for long periods at a low cost and fieldwork intensity, and at the same time, make available easy validation using independent estimations, like the open diel oxygen method (Briggs *et al*., 2018). Climate change and variability in environmental conditions will have an effect on both ER and GPP and, consequently, on NCP (Staehr *et al*., 2012), therefore, it is vital to increase understanding of how these factors influence productivity rates across a broader range of coastal regions, and at a scale that allows prevention and mitigation management in future years.

5 Conclusions

The collection of high-frequency estuarine water quality data allowed the correlation of abiotic environmental conditions with biological rate processes occurring over different time scales. Two independent variables were used to identify major phytoplankton bloom events in the Southampton Water estuary; Chl '*a*' concentration and calculated rates of NCP from high frequency dissolved oxygen concentrations. The initiation of major phytoplankton bloom events during the spring-summer period were correlated with critical values of temperature above 12 °C and mean water column irradiance I_m greater than 280 W h m^{-2} d^{-1}. Additionally, an analysis of the neap-spring tidal cycle identified that blooms typically developed during neap tides and dissipated during the following spring tide. The tidal cycle creates stronger mixing conditions during spring tides leading to increased turbidity compared with lower mixing, and possible stratification, during neap tides enhancing phytoplankton biomass growth. Annual daily average NCP for the estuary detailed a net heterotrophic

state (-0.8 mmol O_2 m^{-2} d^{-1},) but seasonal productive events, shifted this state for several days and sometimes weeks to net autotrophic conditions. The results of this study have demonstrated the opportunity of coupling high-frequency data on estuarine water quality and the use of the open oxygen diel method for a broader understanding of the bloom phenomenon in estuarine and coastal waters. Collectively, these studies can provide predictors of future phytoplankton bloom occurrence across a diversity of aquatic ecosystems.

Acknowledgements

This work was based on the support from CONACyT (the Mexican National Council for Science and Technology) through the grant 'CONACyT-Gobierno del Estado de Sinaloa' reference 472065 and GSNOCS (Graduate School of the National Oceanography Centre Southampton) that provided funding to the lead author, Africa P. Gomez-Castillo. The research was also supported by a European Regional Development Fund grant as part of the Interreg S-3 EuroHAB Project. Water quality data was downloaded from the Water Quality Data Archive via the Environment Agency Open WIMS collection. The authors thank the crew of the RV *Callista* for their skilled work in handling the Data Buoy deployments and supporting discrete sampling. We also thank the Associated British Ports (ABP) Marine Environmental Research for providing sea surface elevation data.

References

Agusti, S., Vigoya, L., & Duarte, C. M. (2018). Annual plankton community metabolism in estuarine and coastal waters in Perth (Western Australia). *PeerJ, 6*, e5081. https://doi.org/10.7717/peerj.5081

Alonso-Pérez, F., Zúñiga, D., Arbones, B., Figueiras, F. G., & Castro, C. G. (2015). Benthic fluxes, net ecosystem metabolism and seafood harvest: Completing the

organic carbon balance in the Ría de Vigo (NW Spain). *Estuarine, Coastal and Shelf Science*, *163*(PB), 54–63. https://doi.org/10.1016/j.ecss.2015.05.038

Aristegi, L., Izagirre, O., & Elosegi, A. (2009). Comparison of several methods to calculate reaeration in streams, and their effects on estimation of metabolism. *Hydrobiologia*, *635*(1), 113–124. https://doi.org/10.1007/s10750-009-9904-8

Bianchi, T. S. (2012). Estuarine Chemistry. In J. W. Day, B. C. Crump, W. M. Kemp, & A. Yáñez-Arancibia (Eds.), *Estuarine Ecology* (2nd ed., pp. 39–83). Wiley-Blackwell.

Bittig, H. C., & Körtzinger, A. (2015). Tackling oxygen optode drift: Near-surface and in-air oxygen optode measurements on a float provide an accurate in situ reference. *Journal of Atmospheric and Oceanic Technology*, *32*(8), 1536–1543. https://doi.org/10.1175/JTECH-D-14-00162.1

Briggs, N., Guemundsson, K., Cetinić, I., D'Asaro, E., Rehm, E., Lee, C., & Perry, M. J. (2018). A multi-method autonomous assessment of primary productivity and export efficiency in the springtime North Atlantic. *Biogeosciences*, *15*(14), 4515–4532. https://doi.org/10.5194/bg-15-4515-2018

Brito, A. C., & Newton, A. (2013). Measuring Light Attenuation in Shallow Coastal Systems. *Journal of Ecosystem & Ecography*, *03*(01). https://doi.org/10.4172/2157-7625.1000122

Bucci, A. F., Ciotti, Á. M., Gonçalves Pollery, R. C., de Carvalho, R., Cavalcanti De Albuquerque, H., Tomida, L., & Simões, S. (2012). Temporal variability of Chlorophyll-a in the Sao Vicente Estuary. *BRAZILIAN JOURNAL OF OCEANOGRAPHY*, *60*(4), 485–499.

674 Caffrey, J. M. (2003). Production, respiration and net ecosystem metabolism in U.S.
675 estuaries. *Environmental Monitoring and Assessment*, *81*(1–3), 207–219.
676 https://doi.org/10.1023/a:1021385226315
677 Caffrey, J. M. (2004). Factors Controlling Net Ecosystem Metabolism in U . S .
678 Estuaries. *Estuaries*, *27*(1), 90–101. https://doi.org/10.1007/BF02803563
679 Caffrey, J. M., Murrell, M. C., Amacker, K. S., Harper, J. W., Phipps, S., & Woodrey,
680 M. S. (2014). Seasonal and Inter-annual Patterns in Primary Production,
681 Respiration, and Net Ecosystem Metabolism in Three Estuaries in the Northeast
682 Gulf of Mexico. *Estuaries and Coasts*, *37*(S1), 222–241.
683 https://doi.org/10.1007/s12237-013-9701-5
684 Carrit, D. E., & Carpenter, J. H. (1966). Comparison and Evaluation of Currently
685 Employed Modifications of the Winkler Method for Determining Dissolved
686 Oxygen in Seawater; a NASCO Report. *Journal of Marine Research*, *24*, 286–
687 318.
688 Carstensen, J., Klais, R., & Cloern, J. E. (2015). Phytoplankton blooms in estuarine
689 and coastal waters: Seasonal patterns and key species. *Estuarine, Coastal and*
690 *Shelf Science*, *162*, 98–109. https://doi.org/10.1016/j.ecss.2015.05.005
691 Cloern, J. E. (1996). Phytoplankton bloom dynamics in coastal ecosystems: A review
692 with some general lessons from sustained investigation of San Francisco Bay,
693 California. In *Reviews of Geophysics* (Vol. 34, Issue 2, pp. 127–168). Blackwell
694 Publishing Ltd. https://doi.org/10.1029/96RG00986
695 Cloern, J. E., Foster, S. Q., & Kleckner, A. E. (2014). Phytoplankton primary
696 production in the world's estuarine-coastal ecosystems. *Biogeosciences*, *11*(9),
697 2477–2501. https://doi.org/10.5194/bg-11-2477-2014

Cloern, J. E., & Jassby, A. D. (2010). Patterns and scales of phytoplankton variability in estuarine-coastal ecosystems. *Estuaries and Coasts*, *33*(2), 230–241. https://doi.org/10.1007/s12237-009-9195-3

Cravo, A., Rosa, A., Jacob, J., & Correia, C. (2020). Dissolved oxygen dynamics in Ria Formosa Lagoon (South Portugal) - A real time monitoring station observatory. *Marine Chemistry*, *223*. https://doi.org/10.1016/j.marchem.2020.103806

Crawford, D. W., Purdie, D. A., Lockwood, A. P. M., & Weissman, P. (1997). Recurrent Red-tides in the Southampton Water Estuary Caused by the Phototrophic Ciliate Mesodinium rubrum. In *Estuarine, Coastal and Shelf Science* (Vol. 45).

Demars, B. O. L., Thompson, J., & Manson, J. R. (2015). Stream metabolism and the open diel oxygen method: Principles, practice, and perspectives. *Limnology and Oceanography: Methods*, *13*(7), 356–374. https://doi.org/10.1002/lom3.10030

Duarte, C. M., & Regaudie-De-Gioux, A. (2009). Thresholds of gross primary production for the metabolic balance of marine planktonic communities. *Limnology and Oceanography*, *54*(3), 1015–1022.

Emerson, S., Stump, C., & Nicholson, D. (2008). Net biological oxygen production in the ocean: Remote in situ measurements of O2 and N2 in surface waters. *Global Biogeochemical Cycles*, *22*(3), 1–13. https://doi.org/10.1029/2007GB003095

Feistel, R. (2008). A Gibbs function for seawater thermodynamics for -6 to 80 °C and salinity up to 120 g kg-1. *Deep-Sea Research Part I: Oceanographic Research Papers*, *55*(12), 1639–1671. https://doi.org/10.1016/j.dsr.2008.07.004

Feng, M. L., Sun, T., Zhang, L. X., & Shen, X. M. (2012). Net Ecosystem Metabolism Simulation by Dynamic Dissolved Oxygen Model in Yellow River Estuary,

China. *Procedia Environmental Sciences*, *13*(2011), 807–817. https://doi.org/10.1016/j.proenv.2012.01.074

Garcia-Corral, L. S., Duarte, C. M., & Agusti, S. (2021). Plankton Community Metabolism in Western Australia: Estuarine, Coastal and Oceanic Surface Waters. *Frontiers in Marine Science*, *7*. https://doi.org/10.3389/fmars.2020.582136

Haskell, W. Z., Hammond, D. E., Prokopenko, M. G., Teel, E. N., Seegers, B. N., Ragan, M. A., Rollins, N., & Jones, B. H. (2019). Net Community Production in a Productive Coastal Ocean From an Autonomous Buoyancy-Driven Glider. *Journal of Geophysical Research: Oceans*, *124*(6), 4188–4207. https://doi.org/10.1029/2019JC015048

Holtgrieve, G. W., Schindlern, D. E., Branch, T. A., & Teresa A'Mar, Z. (2010). Simultaneous quantification of aquatic ecosystem metabolism and reaeration using a Bayesian statistical model of oxygen dynamics. *Limnology and Oceanography*, *55*(3), 1047–1063. https://doi.org/10.4319/lo.2010.55.3.1047

Hull, T., Greenwood, N., Kaiser, J., & Johnson, M. (2016). Uncertainty and sensitivity in optode-based shelf-sea net community production estimates. *Biogeosciences*, *13*(4), 943–959. https://doi.org/10.5194/bg-13-943-2016

Iriarte, A., & Purdie, D. A. (2004). Factors controlling the timing of major spring bloom events in an UK south coast estuary. *Estuarine, Coastal and Shelf Science*, *61*(4), 679–690. https://doi.org/10.1016/j.ecss.2004.08.002

Jollife, I. T., & Cadima, J. (2016). Principal component analysis: A review and recent developments. In *Philosophical Transactions of the Royal Society A: Mathematical, Physical and Engineering Sciences* (Vol. 374, Issue 2065). Royal Society of London. https://doi.org/10.1098/rsta.2015.0202

748 Kanuri, V. V., Gijjapu, D. R., Munnooru, K., Sura, A., Patra, S., Vinjamuri, R. R., &
749 Karri, R. (2017). Scales and drivers of seasonal pCO2 dynamics and net
750 ecosystem exchange along the coastal waters of southeastern Arabian Sea.
751 *Marine Pollution Bulletin*, *121*(1–2), 372–380.
752 https://doi.org/10.1016/j.marpolbul.2017.06.016
753 Kemp, W. M., & Testa, J. M. (2011). Metabolic Balance between Ecosystem
754 Production and Consumption. In E. Wolansky & D. S. McLusky (Eds.), *Treatise*
755 *on Estuarine and Coastal Science* (Vol. 7, pp. 83–118). Waltham: Academic
756 Press.
757 Langdon, C., & Garcia-Martin, E. E. (2021). Light and dark dissolved oxygen rate
758 measurements using the Winkler method. In R. A. Vandermeulen & J. E. Chaves
759 (Eds.), *Aquatic Primary Productivity Field Protocols for Satellite Validation and*
760 *Model Synthesis* (Vol. 7, p. 195). NASA.
761 Lee, J., Kim, S., & An, S. (2017). Dynamics of the Physical and Biogeochemical
762 Processes during Hypoxia in Jinhae Bay, South Korea. *Journal of Coastal*
763 *Research*, *33*(4), 854–863. https://doi.org/10.2112/JCOASTRES-D-16-00122.1
764 Lemley, D. A., Adams, J. B., & Strydom, N. A. (2018). Triggers of phytoplankton
765 bloom dynamics in permanently eutrophic waters of a South African estuary.
766 *African Journal of Aquatic Science*, *43*(3), 229–240.
767 https://doi.org/10.2989/16085914.2018.1478794
768 Lemley, D. A., Adams, J. B., & Rishworth, G. M. (2018b). Unwinding a Tangled Web:
769 a Fine-Scale Approach towards Understanding the Drivers of Harmful Algal
770 Bloom Species in a Eutrophic South African Estuary. *Estuaries and Coasts*,
771 *41*(5), 1356–1369. https://doi.org/10.1007/s12237-018-0380-0

772 Leterme, S. C., Jendyk, J. G., Ellis, A. v., Brown, M. H., & Kildea, T. (2014). Annual
773 phytoplankton dynamics in the Gulf Saint Vincent, South Australia, in 2011.
774 *Oceanologia*, *56*(4), 757–778. https://doi.org/10.5697/oc.56-4.757
775 Levasseur, A., Shi, L., Wells, N. C., Purdie, D. A., & Kelly-Gerreyn, B. A. (2007). A
776 three-dimensional hydrodynamic model of estuarine circulation with an
777 application to Southampton Water, UK. *Estuarine, Coastal and Shelf Science*,
778 *73*(3–4), 753–767. https://doi.org/10.1016/j.ecss.2007.03.018
779 Liang, J. H., Deutsch, C., McWilliams, J. C., Baschek, B., Sullivan, P. P., & Chiba, D.
780 (2013). Parameterizing bubble-mediated air-sea gas exchange and its effect on
781 ocean ventilation. *Global Biogeochemical Cycles*, *27*(3), 894–905.
782 https://doi.org/10.1002/gbc.20080
783 Mahoney, P. C., & Bishop, M. J. (2017). Assessing risk of estuarine ecosystem
784 collapse. *Ocean and Coastal Management*, *140*, 46–58.
785 https://doi.org/10.1016/j.ocecoaman.2017.02.021
786 Murrell, M. C., Caffrey, J. M., Marcovich, D. T., Beck, M. W., Jarvis, B. M., & Hagy,
787 J. D. (2018). Seasonal Oxygen Dynamics in a Warm Temperate Estuary: Effects
788 of Hydrologic Variability on Measurements of Primary Production, Respiration,
789 and Net Metabolism. *Estuaries and Coasts*, *41*(3), 690–707.
790 https://doi.org/10.1007/s12237-017-0328-9
791 Needoba, J. A., Peterson, T. D., & Johnson, K. S. (2012). Method for the
792 Quantification of Aquatic Primary Production and Net Ecosystem Metabolism
793 Using In Situ Dissolved Oxygen Sensors. In S. M. Tiquia-Arashiro (Ed.),
794 *Molecular Biological Technologies for Ocean Sensing*. Springer Protocols
795 Handbooks. https://doi.org/10.1007/978-1-61779-915-0

796 Nidzieko, N. J., Needoba, J. A., Monismith, S. G., & Johnson, K. S. (2014). Fortnightly
797 Tidal Modulations Affect Net Community Production in a Mesotidal Estuary.
798 *Estuaries and Coasts*, *37*(S1), 91–110. https://doi.org/10.1007/s12237-013-9765-
799 2
800 Oczkowski, A., Hunt, C. W., Miller, K., Oviatt, C., Nixon, S., & Smith, L. (2016).
801 Comparing Measures of Estuarine Ecosystem Production in a Temperate New
802 England Estuary. *Estuaries and Coasts*, *39*(6), 1827–1844.
803 https://doi.org/10.1007/s12237-016-0113-1
804 Odum, H. T. (1956). Primary production in flowing waters. *Limnology and*
805 *Oceanography*, *1*, 102–117.
806 Panton, A., Couceiro, F., Fones, G. R., & Purdie, D. A. (2020). The impact of rainfall
807 events, catchment characteristics and estuarine processes on the export of
808 dissolved organic matter from two lowland rivers and their shared estuary.
809 *Science of the Total Environment*, *735*.
810 https://doi.org/10.1016/j.scitotenv.2020.139481
811 Parsons, T., Maita, Y., & Lalli, C. (1984). 4.3 - Fluorometric Determination of
812 Chlorophylls. In T. Parsons, Y. Maita, & C. Lalli (Eds.), *A Manual of Chemical*
813 *& Biological Methods for Seawater Analysis* (pp. 107–109). Pergamon.
814 https://doi.org/https://doi.org/10.1016/C2009-0-07774-5
815 Queste, B. Y., Fernand, L., Jickells, T. D., Heywood, K. J., & Hind, A. J. (2016).
816 Drivers of summer oxygen depletion in the central North Sea. *Biogeosciences*,
817 *13*(4), 1209–1222. https://doi.org/10.5194/bg-13-1209-2016
818 Riley, G. A. (1967). The plankton in estuaries. In G. H. Lauff (Ed.), *Estuaries* (pp.
819 316–326). American Association for the Advancement of Science Publication.

Robinson, C. (2019). Microbial Respiration, the Engine of Ocean Deoxygenation. *Frontiers in Marine Science*, *5*(January), 1–13. https://doi.org/10.3389/fmars.2018.00533

Rose, J. M., & Caron, D. A. (2007). Does low temperature constrain the growth rates of heterotrophic protists? Evidence and implications for algal blooms in cold waters. In *Limnol. Oceanogr* (Vol. 52, Issue 2). http://www.aslo.org/lo/toc/vol_52/

Ruiz-Ruiz, T. M., Arreola-Lizárraga, J. A., Morquecho, L., Mendez-Rodríguez, L. C., Martínez-López, A., & Mendoza-Salgado, R. A. (2017). Detecting Eutrophication Symptoms in a Subtropical Semi-Arid Coastal Lagoon by Means of Three Different Methods. *Wetlands*, 1–14. https://doi.org/10.1007/s13157-017-0944-y

Salhi, N., Zmerli Triki, H., Molinero, J. C., Laabir, M., Sehli, E., Bellaaj-Zouari, A., Daly Yahia, N., & Kefi-Daly Yahia, O. (2018). Seasonal variability of picophytoplankton under contrasting environments in northern Tunisian coasts, southwestern Mediterranean Sea. *Marine Pollution Bulletin*, *129*(2), 866–874. https://doi.org/10.1016/j.marpolbul.2017.10.029

Shi, J., Liu, Y., Mao, X., Guo, X., Wei, H., & Gao, H. (2016). Interannual variation of spring phytoplankton bloom and response to turbulent energy generated by atmospheric forcing in the central Southern Yellow Sea of China: Satellite observations and numerical model study. *Continental Shelf Research*, *143*(December 2015), 1–14. https://doi.org/10.1016/j.csr.2016.06.008

Srichandan, S., Kim, J. Y., Kumar, A., Mishra, D. R., Bhadury, P., Muduli, P. R., Pattnaik, A. K., & Rastogi, G. (2015). Interannual and cyclone-driven variability

in phytoplankton communities of a tropical coastal lagoon. *Marine Pollution Bulletin*, *101*(1), 39–52. https://doi.org/10.1016/j.marpolbul.2015.11.030

Staehr, P. A., Testa, J. M., Kemp, W. M., Cole, J. J., Sand-Jensen, K., & Smith, S. v. (2012). The metabolism of aquatic ecosystems: History, applications, and future challenges. In *Aquatic Sciences* (Vol. 74, Issue 1, pp. 15–29). https://doi.org/10.1007/s00027-011-0199-2

Tang, S., Sun, T., Shen, X. M., Qi, M., & Feng, M. L. (2015). Modeling net ecosystem metabolism influenced by artificial hydrological regulation: AN application to the Yellow River Estuary, China. *Ecological Engineering*, *76*, 84–94. https://doi.org/10.1016/j.ecoleng.2014.04.025

Testa, J. M., Kemp, W. M., Hopkinson, C. S., & Smith, S. v. (2012). Ecosystem Metabolism. In W. J. Day, B. C. Crump, W. M. Kemp, & A. Yáñez-Arancibia (Eds.), *Estuarine Ecology* (2nd ed., pp. 381–416). Wiley-Blackwell. https://doi.org/10.1002/9781118412787

Torres-Valdés, S., & Purdie, D. A. (2006). Nitrogen removal by phytoplankton uptake through a temperate non-turbid estuary. *Estuarine, Coastal and Shelf Science*, *70*(3), 473–486. https://doi.org/10.1016/j.ecss.2006.06.028

Trombetta, T., Vidussi, F., Mas, S., Parin, D., Simier, M., & Mostajir, B. (2019). Water temperature drives phytoplankton blooms in coastal waters. *PLoS ONE*, *14*(4). https://doi.org/10.1371/journal.pone.0214933

Uchida, H., Kawano, T., Kaneko, I., & Fukasawa, M. (2008). In situ calibration of optode-based oxygen sensors. *Journal of Atmospheric and Oceanic Technology*, *25*(12), 2271–2281. https://doi.org/10.1175/2008JTECHO549.1

867 Valenzuela-Siu, M., Arreola-Lizárraga, J. A., Sánchez-Carrillo, S., & Padilla-
868 Arredondo, G. (2007). Flujos de nutrientes y metabolismo neto de la laguna
869 costera Lobos, México. *Hidrobiologica*, *17*(3), 193–202.
870 Wanninkhof, R. (2014). Relationship between wind speed and gas exchange over the
871 ocean revisited. *Limnology and Oceanography: Methods*, *12*(JUN), 351–362.
872 https://doi.org/10.4319/lom.2014.12.351
873 Winkler, L. W. (1888). Die Bestimmung des im Wasser gelosten Sauerstoffes.
874 *Berichte Der Deutschen Chemischen Gesellschaft*, *21*(2), 2843–2854.
875 https://doi.org/https://doi.org/10.1002/cber.188802102122

References

Adams, J. B., Taljaard, S., van Niekerk, L., & Lemley, D. A. (2020). Nutrient enrichment as a threat to the ecological resilience and health of South African microtidal estuaries. *African Journal of Aquatic Science*, *45*(1–2), 23–40. https://doi.org/10.2989/16085914.2019.1677212

Agusti, S., Vigoya, L., & Duarte, C. M. (2018). Annual plankton community metabolism in estuarine and coastal waters in Perth (Western Australia). *PeerJ*, *6*, e5081. https://doi.org/10.7717/peerj.5081

Ahlgren, J., Grimvall, A., Omstedt, A., Rolff, C., & Wikner, J. (2017). Temperature, DOC level and basin interactions explain the declining oxygen concentrations in the Bothnian Sea. *Journal of Marine Systems*, *170*, 22–30. https://doi.org/10.1016/j.jmarsys.2016.12.010

Algesten, G., Wikner, J., Sobek, S., Tranvik, L. J., & Jansson, M. (2004). Seasonal variation of CO2 saturation in the Gulf of Bothnia: Indications of marine net heterotrophy. *Global Biogeochemical Cycles*, *18*(4), 1–7. https://doi.org/10.1029/2004GB002232

Alonso-Pérez, F., Zúñiga, D., Arbones, B., Figueiras, F. G., & Castro, C. G. (2015). Benthic fluxes, net ecosystem metabolism and seafood harvest: Completing the organic carbon balance in the Ría de Vigo (NW Spain). *Estuarine, Coastal and Shelf Science*, *163*(PB), 54–63. https://doi.org/10.1016/j.ecss.2015.05.038

Aranguren-Gassis, M., Serret, P., Fernández, E., Herrera, J. L., Domínguez, J. F., Pérez, V., & Escanez, J. (2011). Production and respiration control the marine microbial metabolic balance in the eastern north atlantic subtropical gyre. *Deep-Sea Research Part I: Oceanographic Research Papers*, *58*(7), 768–775. https://doi.org/10.1016/j.dsr.2011.05.003

Aristegi, L., Izagirre, O., & Elosegi, A. (2009). Comparison of several methods

to calculate reaeration in streams, and their effects on estimation of metabolism. *Hydrobiologia*, *635*(1), 113–124. https://doi.org/10.1007/s10750-009-9904-8

Ávila-López, M. C., Hernández-Ayón, J. M., Camacho-Ibar, V. F., Bermúdez, A. F., Mejía-Trejo, A., Pacheco-Ruiz, I., & Sandoval-Gil, J. M. (2017). Air–Water CO2 Fluxes and Net Ecosystem Production Changes in a Baja California Coastal Lagoon During the Anomalous North Pacific Warm Condition. *Estuaries and Coasts*, *40*(3), 792–806. https://doi.org/10.1007/s12237-016-0178-x

Azevedo, I. C., Duarte, P. M., & Bordalo, A. A. (2006). Pelagic metabolism of the Douro estuary (Portugal) - Factors controlling primary production. *Estuarine, Coastal and Shelf Science*, *69*(1–2), 133–146. https://doi.org/10.1016/j.ecss.2006.04.002

Baird, M., Dutkiewicz, S., Hickman, A., Mongin, M., Soja-Wozniak, M., Skerratt, J., & Wild-Allen, K. (2022). *Modeling phytoplankton processes in multiple functional types*. *Advances in Phytoplankton Ecology*. Elsevier Inc. https://doi.org/10.1016/b978-0-12-822861-6.00016-9

Barnes, M. K., Tilstone, G. H., Suggett, D. J., Widdicombe, C. E., Bruun, J., Martinez-Vicente, V., & Smyth, T. J. (2015). Temporal variability in total, micro- and nano-phytoplankton primary production at a coastal site in the Western English Channel. *Progress in Oceanography*, *137*, 470–483. https://doi.org/10.1016/j.pocean.2015.04.017

Barone, B., Nicholson, D., Ferrón, S., Firing, E., & Karl, D. (2019). The estimation of gross oxygen production and community respiration from autonomous time-series measurements in the oligotrophic ocean. *Limnology and Oceanography: Methods*, *17*(12), 650–664. https://doi.org/10.1002/lom3.10340

Baumann, H., & Smith, E. M. (2018). Quantifying Metabolically Driven pH and Oxygen Fluctuations in US Nearshore Habitats at Diel to Interannual Time Scales. *Estuaries and Coasts*, *41*(4), 1102–1117.

https://doi.org/10.1007/s12237-017-0321-3

Baumann, H., Wallace, R. B., Tagliaferri, T., & Gobler, C. J. (2015). Large Natural pH, CO2 and O2 Fluctuations in a Temperate Tidal Salt Marsh on Diel, Seasonal, and Interannual Time Scales. *Estuaries and Coasts*, *38*(1), 220–231. https://doi.org/10.1007/s12237-014-9800-y

Beck, M. W., Hagy, J. D., & Murrell, M. C. (2015). Improving estimates of ecosystem metabolism by reducing effects of tidal advection on dissolved oxygen time series. *Limnology and Oceanography: Methods*, *13*(12), 731–745. https://doi.org/10.1002/lom3.10062

Behrenfeld, M. J., O'Malley, R. T., Siegel, D. A., McClain, C. R., Sarmiento, J. L., Feldman, G. C., … Boss, E. S. (2006). Climate-driven trends in contemporary ocean productivity. *Nature*, *444*(7120), 752–755. https://doi.org/10.1038/nature05317

Bianchi, T. S. (2012). Estuarine Chemistry. In J. W. Day, B. C. Crump, W. M. Kemp, & A. Yáñez-Arancibia (Eds.), *Estuarine Ecology* (2nd ed., pp. 39–83). New Jersey: Wiley-Blackwell.

Bianchi, T. S., Allison, M. A., & Cai, W.-J. (2013). An introduction to the biogeochemistry of river-coastal systems. In T. S. Bianchi, M. A. Allison, & W.-J. Cai (Eds.), *Biogeochemical Dynamics at Major River-Coastal Interfaces Linkages with Global Change* (pp. 3–18). Ney York: Cambridge University Press.

Birchill, A. J., Clinton-Bailey, G., Hanz, R., Mawji, E., Cariou, T., White, C., … Mowlem, M. (2019). Realistic measurement uncertainties for marine macronutrient measurements conducted using gas segmented flow and Lab-on-Chip techniques. *Talanta*, *200*(March), 228–235. https://doi.org/10.1016/j.talanta.2019.03.032

Bittig, H. C., & Körtzinger, A. (2015). Tackling oxygen optode drift: Near-surface and in-air oxygen optode measurements on a float provide an accurate in situ reference. *Journal of Atmospheric and Oceanic Technology*, *32*(8), 1536–1543. https://doi.org/10.1175/JTECH-D-14-

00162.1

Bittig, H. C., Körtzinger, A., Neill, C., van Ooijen, E., Plant, J. N., Hahn, J., … Emerson, S. R. (2018). Oxygen Optode Sensors: Principle, Characterization, Calibration, and Application in the Ocean. *Frontiers in Marine Science*, *4*(January), 1–25. https://doi.org/10.3389/fmars.2017.00429

Borges, A. V. (2005). *Do We Have Enough Pieces of the Jigsaw to Integrate CO 2 Fluxes in the Coastal Ocean? Source: Estuaries* (Vol. 28). Retrieved from https://www.jstor.org/stable/3526933?seq=1&cid=pdf-reference#references_tab_contents

Borges, A. V., & Abril, G. (2011). Carbon Dioxide and Methane Dynamics in Estuaries. In *Treatise on Estuarine and Coastal Science* (pp. 119–161). Elsevier Inc. https://doi.org/https://doi.org/10.1016/B978-0-12-374711-2.00504-0

Borges, A. V., & Frankignoulle, M. (2003). Distribution of surface carbon dioxide and air-sea exchange in the English Channel and adjacent areas. *Journal of Geophysical Research*, *108*(C5), 1–12. https://doi.org/10.1029/2000jc000571

Borges, A. V., Delille, B., Schiettecatte, L.-S., Gazeau, F., Abril, G., & Frankignoulle, M. (2004). Gas transfer velocities of CO2 in three European estuaries (Randers Fjord, Scheldt, and Thames). *Limnology and Oceanography*, *49*(5), 1630–1641. https://doi.org/10.4319/lo.2004.49.5.1630

Borges, A. V., Ruddick, K., Schiettecatte, L. S., & Delille, B. (2008). Net ecosystem production and carbon dioxide fluxes in the Scheldt estuarine plume. *BMC Ecology*, *8*. https://doi.org/10.1186/1472-6785-8-15

Borges, A. V., Schiettecatte, L. S., Abril, G., Delille, B., & Gazeau, F. (2006). Carbon dioxide in European coastal waters. *Estuarine, Coastal and Shelf Science*, *70*(3), 375–387. https://doi.org/10.1016/j.ecss.2006.05.046

Bricker, S. B., Longstaff, B., Dennison, W., Jones, A., Boicourt, K., Wicks, C., & Woerner, J. (2008). Effects of nutrient enrichment in the nation's estuaries: A decade of change. *Harmful Algae*, *8*(1), 21–32. https://doi.org/10.1016/j.hal.2008.08.028

Briggs, N., Guemundsson, K., Cetinić, I., D'Asaro, E., Rehm, E., Lee, C., & Perry, M. J. (2018). A multi-method autonomous assessment of primary productivity and export efficiency in the springtime North Atlantic. *Biogeosciences*, *15*(14), 4515–4532. https://doi.org/10.5194/bg-15-4515-2018

Brito, A. C., & Newton, A. (2013). Measuring Light Attenuation in Shallow Coastal Systems. *Journal of Ecosystem & Ecography*, *03*(01). https://doi.org/10.4172/2157-7625.1000122

Bucci, A. F., Ciotti, Á. M., Gonçalves Pollery, R. C., De Carvalho, R., Cavalcanti De Albuquerque, H., Tomida, L., & Simões, S. (2012). Temporal variability of Chlorophyll-a in the Sao Vicente Estuary. *BRAZILIAN JOURNAL OF OCEANOGRAPHY*, *60*(4), 485–499.

Butron, A., Iriarte, A., & Madariaga, I. (2009). Size-fractionated phytoplankton biomass, primary production and respiration in the Nervion-Ibaizabal estuary: A comparison with other nearshore coastal and estuarine ecosystems from the Bay of Biscay. *Continental Shelf Research*, *29*, 1088–1102. https://doi.org/10.1016/j.csr.2008.11.013

Caffrey, J. M. (2003). Production, respiration and net ecosystem metabolism in U.S. estuaries. *Environmental Monitoring and Assessment*, *81*(1–3), 207–219. https://doi.org/10.1023/a:1021385226315

Caffrey, J. M. (2004). Factors Controlling Net Ecosystem Metabolism in U . S . Estuaries. *Estuaries*, *27*(1), 90–101. https://doi.org/10.1007/BF02803563

Caffrey, J. M., Murrell, M. C., Amacker, K. S., Harper, J. W., Phipps, S., & Woodrey, M. S. (2014). Seasonal and Inter-annual Patterns in Primary Production, Respiration, and Net Ecosystem Metabolism in Three

Estuaries in the Northeast Gulf of Mexico. *Estuaries and Coasts*, *37*(S1), 222–241. https://doi.org/10.1007/s12237-013-9701-5

Cai, W. J. (2011). Estuarine and coastal ocean carbon paradox: CO 2 sinks or sites of terrestrial carbon incineration? *Annual Review of Marine Science*, *3*, 123–145. https://doi.org/10.1146/annurev-marine-120709-142723

Cai, W. J., Guo, X., Chen, C. T. A., Dai, M., Zhang, L., Zhai, W., … Wang, Y. (2008). A comparative overview of weathering intensity and HCO3- flux in the world's major rivers with emphasis on the Changjiang, Huanghe, Zhujiang (Pearl) and Mississippi Rivers. *Continental Shelf Research*, *28*(12), 1538–1549. https://doi.org/10.1016/j.csr.2007.10.014

Cai, W. J., Huang, W. J., Luther, G. W., Pierrot, D., Li, M., Testa, J., … Michael Kemp, W. (2017). Redox reactions and weak buffering capacity lead to acidification in the Chesapeake Bay. *Nature Communications*, *8*(1), 1–12. https://doi.org/10.1038/s41467-017-00417-7

Campbell, L., Gaonkar, C. C., & Henrichs, D. W. (2022). *Integrating imaging and molecular approaches to assess phytoplankton diversity*. *Advances in Phytoplankton Ecology*. Elsevier Inc. https://doi.org/10.1016/b978-0-12-822861-6.00013-3

Carrit, D. E., & Carpenter, J. H. (1966). Comparison and Evaluation of Currently Employed Modifications of the Winkler Method for Determining Dissolved Oxygen in Seawater; a NASCO Report. *Journal of Marine Research*, *24*, 286–318.

Carstensen, J., Klais, R., & Cloern, J. E. (2015). Phytoplankton blooms in estuarine and coastal waters: Seasonal patterns and key species. *Estuarine, Coastal and Shelf Science*, *162*, 98–109. https://doi.org/10.1016/j.ecss.2015.05.005

Chavez, F. P., Messié, M., & Pennington, J. T. (2011). Marine primary production in relation to climate variability and change. *Annual Review of Marine Science*, *3*, 227–260. https://doi.org/10.1146/annurev.marine.010908.163917

Chen, C-T. A., & Borges, A. V. (2009). Reconciling opposing views on carbon cycling in the coastal ocean: Continental shelves as sinks and near-shore ecosystems as sources of atmospheric CO2. *Deep-Sea Research Part II*, *56*(8–10), 578–590. https://doi.org/10.1016/j.dsr2.2009.01.001

Chen, C-T. A., Huang, T. H., Chen, Y. C., Bai, Y., He, X., & Kang, Y. (2013). Air-sea exchanges of coin the world's coastal seas. *Biogeosciences*, *10*(10), 6509–6544. https://doi.org/10.5194/bg-10-6509-2013

Cloern, J. E. (1996). Phytoplankton bloom dynamics in coastal ecosystems: A review with some general lessons from sustained investigation of San Francisco Bay, California. *Reviews of Geophysics*. Blackwell Publishing Ltd. https://doi.org/10.1029/96RG00986

Cloern, J. E., & Jassby, A. D. (2008). Complex seasonal patterns of primary producers at the land-sea interface. *Ecology Letters*, *11*(12), 1294–1303. https://doi.org/10.1111/j.1461-0248.2008.01244.x

Cloern, J. E., & Jassby, A. D. (2010). Patterns and scales of phytoplankton variability in estuarine-coastal ecosystems. *Estuaries and Coasts*, *33*(2), 230–241. https://doi.org/10.1007/s12237-009-9195-3

Cloern, J. E., Foster, S. Q., & Kleckner, A. E. (2014). Phytoplankton primary production in the world's estuarine-coastal ecosystems. *Biogeosciences*, *11*(9), 2477–2501. https://doi.org/10.5194/bg-11-2477-2014

Cotovicz, L. C., Vidal, L. O., de Rezende, C. E., Marcelo C. Bernardes, M. C., Knoppers, B. A., Sobrinho, R. L., Muniz, M., dos Anjos, R. M., Biehler, A., & Abril, G. (2020). Carbon dioxide sources and sinks in the delta of the Paraíba do Sul River (Southeastern Brazil) modulated by carbonate thermodynamics, gas exchange and ecosystem metabolism during estuarine mixing. *Marine Chemistry*, *226*(August), 103869. https://doi.org/10.1016/j.marchem.2020.103869

Cravo, A., Rosa, A., Jacob, J., & Correia, C. (2020). Dissolved oxygen dynamics in Ria Formosa Lagoon (South Portugal) - A real time monitoring station observatory. *Marine Chemistry*, *223*.

https://doi.org/10.1016/j.marchem.2020.103806

Crawford, D. W., Purdie, D. A., Lockwood, A. P. M., & Weissman, P. (1997). *Recurrent Red-tides in the Southampton Water Estuary Caused by the Phototrophic Ciliate Mesodinium rubrum*. *Estuarine, Coastal and Shelf Science* (Vol. 45).

Crosswell, J. R., Anderson, I. C., Stanhope, J. W., Van Dam, B., Brush, M. J., Ensign, S., Piehler, M. F., McKee, B., Bost, M., & Paerl, H. W. (2017). Carbon budget of a shallow, lagoonal estuary: Transformations and source-sink dynamics along the river-estuary-ocean continuum. *Limnology and Oceanography*, *62*, S29–S45. https://doi.org/10.1002/lno.10631

D'asaro, E. A., & Mcneil, C. (2013). Calibration and stability of oxygen sensors on autonomous floats. *Journal of Atmospheric and Oceanic Technology*, *30*(8), 1896–1906. https://doi.org/10.1175/JTECH-D-12-00222.1

Davidson, K., Gowen, R. J., Harrison, P. J., Fleming, L. E., Hoagland, P., & Moschonas, G. (2015). Anthropogenic nutrients and harmful algae in coastal waters. *Acta Gastro-Enterologica Belgica*, *78*(3), 282–286. https://doi.org/10.1016/j.jenvman.2014.07.002

Davidson, K., Gowen, R. J., Tett, P., Bresnan, E., Harrison, P. J., McKinney, A., Milligan, S., Mills, D. K., Silke, J., & Crooks, A-M. (2012). Harmful algal blooms: How strong is the evidence that nutrient ratios and forms influence their occurrence? *Estuarine, Coastal and Shelf Science*, *115*, 399–413. https://doi.org/10.1016/j.ecss.2012.09.019

Demars, B. O. L., Thompson, J., & Manson, J. R. (2015). Stream metabolism and the open diel oxygen method: Principles, practice, and perspectives. *Limnology and Oceanography: Methods*, *13*(7), 356–374. https://doi.org/10.1002/lom3.10030

Dickson, A. G. (1990). Standard potential of the reaction: AgCl(s) + 1.21-12(g) = Ag(s) + HCl(aq.) and acidity constant of the ion HSO−4 in synthetic sea water from 273.15 to 318.15. *Journal of Chemical Thermodynamics*,

22(2), 113–127.

Dlugokencky, E. J., Mund, J. W., Crotwell, A. M., Crotwell, M. J., & Thoning, K. W. (2021). Atmospheric Carbon Dioxide Dry Air Mole Fractions. NOAA GML Carbon Cycle Cooperative Global Air Sampling Network, 1968-2020, Version: 2021-07-30. Retrieved August 9, 2021, from https://doi.org/10.15138/wkgj-f215

Duarte, C. M., & Agustí, S. (1998). The CO2 balance of unproductive aquatic ecosystems. *Science*, *281*(5374), 234–236. https://doi.org/10.1126/science.281.5374.234

Duarte, C. M., & Prairie, Y. T. (2005). Prevalence of heterotrophy and atmospheric CO2 emissions from aquatic ecosystems. *Ecosystems*, *8*(7), 862–870. https://doi.org/10.1007/s10021-005-0177-4

Duarte, C. M., & Regaudie-De-Gioux, A. (2009). Thresholds of gross primary production for the metabolic balance of marine planktonic communities. *Limnology and Oceanography*, *54*(3), 1015–1022.

Duarte, C. M., Hendriks, I. E., Moore, T. S., Olsen, Y. S., Steckbauer, A., Ramajo, L., Carstensen, J., Trotter, J. A., & McCulloch, M. (2013a). Is Ocean Acidification an Open-Ocean Syndrome? Understanding Anthropogenic Impacts on Seawater pH. *Estuaries and Coasts*, *36*(2), 221–236. https://doi.org/10.1007/s12237-013-9594-3

Duarte, C. M., Regaudie-de-Gioux, A., Arrieta, J. M., Delgado-Huertas, A., & Agustí, S. (2013b). The Oligotrophic Ocean Is Heterotrophic. *Annual Review of Marine Science*, *5*(1), 551–569. https://doi.org/10.1146/annurev-marine-121211-172337

Dumousseaud, C., Achterberg, E. P., Tyrrell, T., Charalampopoulou, A., Schuster, U., Hartman, M., & Hydes, D. J. (2010). Contrasting effects of temperature and winter mixing on the seasonal and inter-annual variability of the carbonate system in the Northeast Atlantic Ocean. *Biogeosciences*, *7*(5), 1481–1492. https://doi.org/10.5194/bg-7-1481-2010

Emerson, S., Stump, C., & Nicholson, D. (2008). Net biological oxygen production in the ocean: Remote in situ measurements of O2 and N2 in surface waters. *Global Biogeochemical Cycles*, *22*(3), 1–13. https://doi.org/10.1029/2007GB003095

Feng, M. L., Sun, T., Zhang, L. X., & Shen, X. M. (2012). Net Ecosystem Metabolism Simulation by Dynamic Dissolved Oxygen Model in Yellow River Estuary, China. *Procedia Environmental Sciences*, *13*(2011), 807–817. https://doi.org/10.1016/j.proenv.2012.01.074

Frankignoulle, M., Abril, G., Borges, A., Bourge, I., Canon, C., Delille, B., Libert, E., & Théate, J.-M. (1998). Carbon Dioxide Emission from European Estuaries. *Science*, *282*, 434–436. Retrieved from https://www.science.org

Frankignoulle, M., & Middelburg, J. J. (2002). Biogases in tidal European estuaries: the BIOGEST project. *Biogeochemestry*, *59*, 1–4.

Friedrich, J., Janssen, F., Aleynik, D., Bange, H. W., Boltacheva, N., Çagatay, M. N., Dale, A. W., Etiope, G., Erdem, Z., Geraga, M, Gilli, A., Gomoiu, M. T., Hall, P. O. J., Hansson, D., He, Y., Holtappels, M., Kirf, M. K., Kononets, M., Konovalov, S., Lichtschlag, A., Livingstone, D. M., Marinaro, G., Mazlumyan, S., Naeher, S., North, R. P., Papatheodorou, G., Pfannkuche, O., Prien, R., Rehder, G., Schubert, C. J., Soltwedel, T., Sommer, S., Stahl, H., Stanev, E. V., Teaca, A., Tengberg, A., Waldmann, C., Wehrli, B., & Wenzhöfer, F. (2014). Investigating hypoxia in aquatic environments: diverse approaches to addressing a complex phenomenon. *Biogeosciences*, *11*(4), 1215–1259. https://doi.org/10.5194/bg-11-1215-2014

Gammal, J., Norkko, J., Pilditch, C. A., & Norkko, A. (2017). Coastal Hypoxia and the Importance of Benthic Macrofauna Communities for Ecosystem Functioning. *Estuaries and Coasts*, *40*(2), 457–468. https://doi.org/10.1007/s12237-016-0152-7

Garcia-Corral, L. S., Duarte, C. M., & Agusti, S. (2021). Plankton Community

Metabolism in Western Australia: Estuarine, Coastal and Oceanic Surface Waters. *Frontiers in Marine Science*, *7*. https://doi.org/10.3389/fmars.2020.582136

Gazeau, F, Duarte, C. M., J.-P. Gattuso, C. Barrón, N. Navarro, S. Ruiz, … Borges, and A. V. (2005a). Whole-system metabolism and CO2 fluxes in a Mediterranean Bay dominated by seagrass beds (Palma Bay, NW Mediterranean). *Biogeosciences*, 43–60.

Gazeau, F., Borges, A. V., Barrón, C., Duarte, C. M., Iversen, N., Middelburg, J. J., … Gattuso, J. P. (2005b). Net ecosystem metabolism in a micro-tidal estuary (Randers Fjord, Denmark): Evaluation of methods. *Marine Ecology Progress Series*, *301*, 23–41. https://doi.org/10.3354/meps301023

Gazeau, F., Gattuso, J. P., Middelburg, J. J., Brion, N., Schiettecatte, L. S., Frankignoulle, M., & Borges, A. V. (2005c). Planktonic and whole system metabolism in a nutrient-rich estuary (the Scheldt estuary). *Estuaries*, *28*(6), 868–883. https://doi.org/10.1007/BF02696016

Gazeau, F., Smith, S. V., Gentili, B., Frankignoulle, M., & Gattuso, J. P. (2004). The European coastal zone: Characterization and first assessment of ecosystem metabolism. *Estuarine, Coastal and Shelf Science*, *60*(4), 673–694. https://doi.org/10.1016/j.ecss.2004.03.007

Godrijan, J., Marić, D., Tomažić, I., Precali, R., & Pfannkuchen, M. (2013). Seasonal phytoplankton dynamics in the coastal waters of the north-eastern Adriatic Sea. *Journal of Sea Research*, *77*, 32–44. https://doi.org/10.1016/j.seares.2012.09.009

Golubkov, S., Golubkov, M., Tiunov, A., & Nikulina, V. (2017). Long-term changes in primary production and mineralization of organic matter in the Neva Estuary (Baltic Sea). *Journal of Marine Systems*, *171*, 73–80. https://doi.org/10.1016/j.jmarsys.2016.12.009

Grundle, D. S., Timothy, D. A., & Varela, D. E. (2009). Variations of phytoplankton productivity and biomass over an annual cycle in Saanich

Inlet, a British Columbia fjord. *Continental Shelf Research*, *29*(19), 2257–2269. Retrieved from https://doi.org/10.1016/j.csr.2009.08.013

Guenther, M., Araújo, M., Flores-Montes, M., Gonzalez-Rodriguez, E., & Neumann-Leitão, S. (2015). Eutrophication effects on phytoplankton size-fractioned biomass and production at a tropical estuary. *Marine Pollution Bulletin*, *91*(2), 537–547. https://doi.org/10.1016/j.marpolbul.2014.09.048

Guenther, M., Araújo, M., Noriega, C., Flores-Montes, M., Gonzalez-Rodriguez, E., & Neumann-Leitão, S. (2017). Plankton carbon metabolism and air–water CO2 fluxes at a hypereutrophic tropical estuary. *Marine Ecology*, *38*(2), 1–12. https://doi.org/10.1111/maec.12423

Gupta, G. V. M., Sarma, V. V. S. S., Robin, R. S., Raman, A. V., Jai Kumar, M., Rakesh, M., & Subramanian, B. R. (2008). Influence of net ecosystem metabolism in transferring riverine organic carbon to atmospheric CO2in a tropical coastal lagoon (Chilka Lake, India). *Biogeochemistry*, *87*(3), 265–285. https://doi.org/10.1007/s10533-008-9183-x

Hall, R. O., Yackulic, C. B., Kennedy, T. A., Yard, M. D., Rosi-Marshall, E. J., Voichick, N., & Behn, K. E. (2015). Turbidity, light, temperature, and hydropeaking control primary productivity in the Colorado River, Grand Canyon. *Limnology and Oceanography*, *60*(2), 512–526. https://doi.org/10.1002/lno.10031

Hansen, H. P. (1999). Determination of oxygen. In K. Grasshoff, K. Kremling, & M. Ehrhardt (Eds.), *Methods of Seawater Analysis* (3rd ed., pp. 75–89). Wiley-VCH Verlag GmbH.

Haskell, W. Z., Hammond, D. E., Prokopenko, M. G., Teel, E. N., Seegers, B. N., Ragan, M. A., Rollins, N., & Jones, B. H. (2019). Net Community Production in a Productive Coastal Ocean From an Autonomous Buoyancy-Driven Glider. *Journal of Geophysical Research: Oceans*, *124*(6), 4188–4207. https://doi.org/10.1029/2019JC015048

Henderikx-Freitas, F., White, A. E., & Quay, P. D. (2020). Diel Measurements of Oxygen- and Carbon-Based Ocean Metabolism Across a Trophic

Gradient in the North Pacific. *Global Biogeochemical Cycles*, *34*(11). https://doi.org/10.1029/2019GB006518

Henson, S. A., Robinson, I., Allen, J. T., & Waniek, J. J. (2006). Effect of meteorological conditions on interannual variability in timing and magnitude of the spring bloom in the Irminger Basin, North Atlantic. *Deep-Sea Research Part I: Oceanographic Research Papers*, *53*(10), 1601–1615. https://doi.org/10.1016/j.dsr.2006.07.009

Herrmann, M., Najjar, R. G., Da, F., Friedman, J. R., Friedrichs, M. A. M., Goldberger, Menendez, A., Shadwick, E. H., Stets, E. G., & St-Laurent, P. (2020). Challenges in Quantifying Air-Water Carbon Dioxide Flux Using Estuarine Water Quality Data: Case Study for Chesapeake Bay. *Journal of Geophysical Research: Oceans*, *125*(7), 1–19. https://doi.org/10.1029/2019JC015610

Herrmann, M., Najjar, R. G., Michael, K. W., Alexander, R. B., Boyer, E. W., Cai, W-J., Griffith, P. C., Kroeger, K. D., McCallister, S. L., & Smith, R. A. (2014). Net ecosystem production and organic carbon balance of U.S. East Coast estuaries: A synthesis approach. *Global Biogeochemical Cycles*, *29*, 96–111. https://doi.org/10.1002/2013GB004736.Received

Holley, S. E., Purdie, D. A., Hydes, D. J., & Hartman, M. C. (2007). *5 years of plankton monitoring in Southampton Water and the Solent including FerryBox, Dock Monitor and discrete sample data*. Southampton, UK.

Holtgrieve, G. W., Schindlern, D. E., Branch, T. A., & Teresa A'Mar, Z. (2010). Simultaneous quantification of aquatic ecosystem metabolism and reaeration using a Bayesian statistical model of oxygen dynamics. *Limnology and Oceanography*, *55*(3), 1047–1063. https://doi.org/10.4319/lo.2010.55.3.1047

Hopkinson, C. S., & Smith, E. M. (2005). Estuarine respiration: an overview of benthic, pelagic, and whole system respiration. In Paul A. del Giorgio & P. J. L. B. Williams (Eds.), *Respiration in Aquatic Ecosystems* (pp. 1–328). Oxford University Press.

https://doi.org/10.1093/acprof:oso/9780198527084.001.0001

Howland, R. J. M., Tappin, A. D., Uncles, R. J., Plummer, D. H., & Bloomer, N. J. (2000). *Distributions and seasonal variability of pH and alkalinity in the Tweed Estuary, UK*. *The Science of the Total Environment* (Vol. 251).

Hu, X., Yao, H., Staryk, C. J., McCutcheon, M. R., Wetz, M. S., & Walker, L. (2020). Disparate Responses of Carbonate System in Two Adjacent Subtropical Estuaries to the Influence of Hurricane Harvey – A Case Study. *Frontiers in Marine Science*, *7*. https://doi.org/10.3389/fmars.2020.00026

Huggett, R. D., Haigh, I. D., & Purdie, D. A. (2021a). Modelling the impact of river flow, macronutrients and solar radiation on the eutrophication status of small shallow estuaries. *Journal of Marine Systems*, *222*. https://doi.org/10.1016/j.jmarsys.2021.103606

Huggett, R. D., Purdie, D. A., & Haigh, I. D. (2021b). Modelling the Influence of Riverine Inputs on the Circulation and Flushing Times of Small Shallow Estuaries. *Estuaries and Coasts*, *44*(1), 54–69. https://doi.org/10.1007/s12237-020-00776-3

Hull, T., Greenwood, N., Kaiser, J., & Johnson, M. (2016). Uncertainty and sensitivity in optode-based shelf-sea net community production estimates. *Biogeosciences*, *13*(4), 943–959. https://doi.org/10.5194/bg-13-943-2016

Iriarte, A., & Purdie, D. A. (1994). Size distribution of chlorophyll a biomass and primary production in a temperate estuary (Southampton Water): The contribution of photosynthetic picoplankton. *Marine Ecology Progress Series*, *115*(3), 283–298. https://doi.org/10.3354/meps115283

Iriarte, A., & Purdie, D. A. (2004). Factors controlling the timing of major spring bloom events in an UK south coast estuary. *Estuarine, Coastal and Shelf Science*, *61*(4), 679–690. https://doi.org/10.1016/j.ecss.2004.08.002

Jeffrey, L. C., Santos, I. R., Tait, D. R., Makings, U., & Maher, D. T. (2018). Seasonal Drivers of Carbon Dioxide Dynamics in a Hydrologically

Modified Subtropical Tidal River and Estuary (Caboolture River, Australia). *Journal of Geophysical Research: Biogeosciences*, *123*(6), 1827–1849. https://doi.org/10.1029/2017JG004023

Johnson, K. S., & Bif, M. B. (2021). Constraint on net primary productivity of the global ocean by Argo oxygen measurements. *Nature Geoscience*, *14*(10), 769–774. https://doi.org/10.1038/s41561-021-00807-z

Jollife, I. T., & Cadima, J. (2016). Principal component analysis: A review and recent developments. *Philosophical Transactions of the Royal Society*, *374*(2065). https://doi.org/10.1098/rsta.2015.0202

Kanuri, V. V., Gijjapu, D. R., Munnooru, K., Sura, A., Patra, S., Vinjamuri, R. R., & Karri, R. (2017). Scales and drivers of seasonal pCO2 dynamics and net ecosystem exchange along the coastal waters of southeastern Arabian Sea. *Marine Pollution Bulletin*, *121*(1–2), 372–380. https://doi.org/10.1016/j.marpolbul.2017.06.016

Keller, A. A., Taylor, C., Oviatt, C., Dorrington, T., Holcombe, G., & Reed, L. (2001). Phytoplankton production patterns in Massachusetts Bay and the absence of the 1998 winter–spring bloom. *Marine Biology Research*, *138*, 1051–1062. Retrieved from https://doi.org/10.1007/s002270000525

Kemp, W. M., & Testa, J. M. (2011). Metabolic Balance between Ecosystem Production and Consumption. In E. Wolansky & D. S. McLusky (Eds.), *Treatise on Estuarine and Coastal Science* (Vol. 7, pp. 83–118). Waltham: Academic Press.

Kifle, D., & Purdie, D. A. (1993). *The seasonal abundance of the phototrophic ciliate Mesodinium rubrum in Southampton Water, England*. *Journal of Plankton Research* (Vol. 15). Retrieved from https://academic.oup.com/plankt/article/15/7/823/1472966

Kitidis, V., Hardman-Mountford, N. J., Litt, E., Brown, I., Cummings, D., Hartman, Hydes, D., Fishwick, J. R., Harris, C., Martinez-Vicente, V., Woodward, E. M. S., & Smyth, T. J. (2012). Seasonal dynamics of the carbonate system in the Western English Channel. *Continental Shelf*

Research, *42*, 30–40. https://doi.org/10.1016/j.csr.2012.04.012

Kitsiou, D., & Karydis, M. (2011). Coastal marine eutrophication assessment: A review on data analysis. *Environment International*, *37*(4), 778–801. https://doi.org/10.1016/j.envint.2011.02.004

Laane, R. W. P. M., & Middelburg, J. J. (2011). Biogeochemestry, An Introduction. In Eric Wolanski & D. McLusky (Eds.), *Treatise on Estuarine and Coastal Science* (Vol. 5, pp. 1–5). Academic Press.

Langdon, C., & Garcia-Martin, E. E. (2021). Light and dark dissolved oxygen rate measurements using the Winkler method. In R. A. Vandermeulen & J. E. Chaves (Eds.), *Aquatic Primary Productivity Field Protocols for Satellite Validation and Model Synthesis* (Vol. 7, p. 195). NASA.

Laurent, A., Fennel, K., Cai, W-J., Huang, W-J., Barbero, L., & Wanninkhof, R. (2012). Eutrophication induced CO2-acidification of subsurface coastal waters: Interactive effects of temperature, salinity, and atmospheric P CO2. *Environmental Science and Technology*, *46*(2), 10651–10659. https://doi.org/10.1021/es300626f

Lauria, M. Lou, Purdie, D. A., & Sharples, J. (1999). *Contrasting phytoplankton distributions controlled by tidal turbulence in an estuary*. *Journal of Marine Systems* (Vol. 21).

Lee, J. S., Kim, S-H., Min, W-G., Choi, D. M., Lee, E. K., Kim, K-T., An, S-U., Baek, J-W., Lee, W-C., & Park, C. H. (2022). In-Situ Estimates of Net Ecosystem Metabolisms in the Rocky Habitats of Dokdo Islets in the East Sea of Korea, *10*(7), 887. https://doi.org/https://doi.org/10.3390/jmse10070887

Lee, K., Kim, T. W., Byrne, R. H., Millero, F. J., Feely, R. A., & Liu, Y. M. (2010). The universal ratio of boron to chlorinity for the North Pacific and North Atlantic oceans. *Geochimica et Cosmochimica Acta*, *74*(6), 1801–1811. https://doi.org/10.1016/j.gca.2009.12.027

Lee, K., Tong, L. T., Millero, F. J., Sabine, C. L., Dickson, A. G., Goyet, C.,

Park, G-H., Wanninkhof, R., Feely, R. A., & Key, R. M. (2006). Global relationships of total alkalinity with salinity and temperature in surface waters of the world's oceans. *Geophysical Research Letters*, *33*(19), 1–5. https://doi.org/10.1029/2006GL027207

Lemley, D. A., Adams, J. B., & Strydom, N. A. (2018). Triggers of phytoplankton bloom dynamics in permanently eutrophic waters of a South African estuary. *African Journal of Aquatic Science*, *43*(3), 229–240. https://doi.org/10.2989/16085914.2018.1478794

Lemley, D. A., Adams, J. B., Rishworth, G. M., & Purdie, D. A. (2020). Harmful algal blooms of Heterosigma akashiwo and environmental features regulate Mesodinium cf. rubrum abundance in eutrophic conditions. *Harmful Algae*, *100*. https://doi.org/10.1016/j.hal.2020.101943

Leterme, S. C., Jendyk, J. G., Ellis, A. V., Brown, M. H., & Kildea, T. (2014). Annual phytoplankton dynamics in the Gulf Saint Vincent, South Australia, in 2011. *Oceanologia*, *56*(4), 757–778. https://doi.org/10.5697/oc.56-4.757

Levasseur, A., Shi, L., Wells, N. C., Purdie, D. A., & Kelly-Gerreyn, B. A. (2007). A three-dimensional hydrodynamic model of estuarine circulation with an application to Southampton Water, UK. *Estuarine, Coastal and Shelf Science*, *73*(3–4), 753–767. https://doi.org/10.1016/j.ecss.2007.03.018

Levasseur, M., Therriault, J.-C., & Legendre, L. (1984). *Hierarchical control of phytoplankton succession by physical factors*. *Source: Marine Ecology Progress Series* (Vol. 19). Retrieved from https://www.jstor.org/stable/24816037

Lewis, E., & Wallace, D. (1998). Program developed for CO2 system calculations. *Ornl/Cdiac-105*. Retrieved from http://cdiac.esd.ornl.gov/oceans/co2rprtnbk.html

Liang, J. H., Deutsch, C., McWilliams, J. C., Baschek, B., Sullivan, P. P., & Chiba, D. (2013). Parameterizing bubble-mediated air-sea gas exchange

and its effect on ocean ventilation. *Global Biogeochemical Cycles*, *27*(3), 894–905. https://doi.org/10.1002/gbc.20080

Liu, T-K., Chen, P., & Chen, H-Y. (2015). Comprehensive assessment of coastal eutrophication in Taiwan and its implications for management strategy. *Marine Pollution Bulletin*, *97*(1–2), 440–450. https://doi.org/10.1016/j.marpolbul.2015.05.055

Loken, L. C., Van Nieuwenhuyse, E. E., Dahlgren, R. A., Lenoch, L. E. K., Stumpner, P. R., Burau, J. R., & Sadro, S. (2021). Assessment of multiple ecosystem metabolism methods in an estuary. *Limnology and Oceanography: Methods*, *19*(11), 741–757. https://doi.org/10.1002/lom3.10458

López-Abbate, M. C., Molinero, J. C., Guinder, V. A., Perillo, G. M. E., Freije, R. H., Sommer, U., Spetter, C. V., & Marcovecchio, J. E. (2017). Time-varying environmental control of phytoplankton in a changing estuarine system. *Science of the Total Environment*, *609*, 1390–1400. https://doi.org/10.1016/j.scitotenv.2017.08.002

López-Urrutia, A., San Martin, E., Harris, R. P., & Irigoien, X. (2011). Scaling the metabolic balance of the oceans. *Proceedings of the National Academy of Sciences of the United States of America*, *103*(23), 8739–8744. Retrieved from www.pnas.orgcgidoi10.1073pnas.0601137103

Mahoney, P. C., & Bishop, M. J. (2017). Assessing risk of estuarine ecosystem collapse. *Ocean and Coastal Management*, *140*, 46–58. https://doi.org/10.1016/j.ocecoaman.2017.02.021

Martellucci, R., Salon, S., Cossarini, G., Piermattei, V., & Marcelli, M. (2021). Coastal phytoplankton bloom dynamics in the Tyrrhenian Sea: Advantage of integrating in situ observations, large-scale analysis and forecast systems. *Journal of Marine Systems*, *218*. https://doi.org/10.1016/j.jmarsys.2021.103528

May, C. L., Koseff, J. R., Lucas, L. V., Cloern, J. E., & Schoellhamer, D. H. (2003). Effects of spatial and temporal variability of turbidity on

phytoplankton blooms. *Marine Ecology Progress Series*, *254*, 111–128.

McAndrew, P. M., Björkman, K. M., Church, M. J., Morris, P. J., Jachowski, N., Williams, P. J. L. B., & Karl, D. M. (2007). Metabolic response of oligotrophic plankton communities to deep water nutrient enrichment. *Marine Ecology Progress Series*, *332*(C), 63–75. https://doi.org/10.3354/meps332063

McKinnon, A. D., Duggan, S., Logan, M., & Lonborg, C. (2017). Plankton respiration, production, and trophic state in tropical coastal and shelf waters adjacent to Northern Australia. *Frontiers in Marine Science*, *4*(OCT). https://doi.org/10.3389/fmars.2017.00346

Met Office. (2020). MIDAS Open: UK hourly weather observation data, v202007. Centre for Environmental Data Analysis. Retrieved August 24, 2020, from http://dx.doi.org/10.5285/8d85f664fc614ba0a28af3a2d7ef4533

Millero, F. J. (2010). Carbonate constants estuarine waters. *Marine and Freshwater Research*, *61*, 139–142.

Mortazavi, B., Riggs, A. A., Caffrey, J. M., Genet, H., & Phipps, S. W. (2012). The Contribution of Benthic Nutrient Regeneration to Primary Production in a Shallow Eutrophic Estuary, Weeks Bay, Alabama. *Estuaries and Coasts*, *35*(3), 862–877. https://doi.org/10.1007/s12237-012-9478-y

Murrell, M. C., Caffrey, J. M., Marcovich, D. T., Beck, M. W., Jarvis, B. M., & Hagy, J. D. (2018). Seasonal Oxygen Dynamics in a Warm Temperate Estuary: Effects of Hydrologic Variability on Measurements of Primary Production, Respiration, and Net Metabolism. *Estuaries and Coasts*, *41*(3), 690–707. https://doi.org/10.1007/s12237-017-0328-9

Narasimha, M. K., Sarma, N. S., Pandi, S. R., Chiranjeevulu, G., Kiran, R., & Muralikrishna, R. (2017). Hydrodynamic control of microphytoplankton bloom in a coastal sea. *Journal of Earth System Science*, *126*(6). https://doi.org/10.1007/s12040-017-0867-2

Nedwell, D. B., Dong, L. F., Sage, A., & Underwood, G. J. C. (2002). Variations of the nutrients loads to the mainland U.K. estuaries: Correlation with catchment areas, urbanization and coastal eutrophication. *Estuarine, Coastal and Shelf Science*, *54*(6), 951–970. https://doi.org/10.1006/ecss.2001.0867

Needoba, J. A., Peterson, T. D., & Johnson, K. S. (2012). Method for the Quantification of Aquatic Primary Production and Net Ecosystem Metabolism Using In Situ Dissolved Oxygen Sensors. In S. M. Tiquia-Arashiro (Ed.), *Molecular Biological Technologies for Ocean Sensing*. New York: Springer Protocols Handbooks. https://doi.org/10.1007/978-1-61779-915-0

Newton, A., Icely, J., Cristina, S., Brito, A., Cardoso, A. C., Colijn, F., Riva, S. D., Gertz, F., Hansen, J. W., Holmer, M., Ivanova, K., Leppäkoski, E., Canu, D. M., Mocenni, C., Mudge, S., Murray, N., Pejrup, M., Razinkovas, A., Reizopoulou, S., Pérez-Ruzafa, A., Schernewski, G., Schubert, H., Carr, L., Solidoro, C., Viaroli, P., & Zaldívar, J-M. (2014). An overview of ecological status, vulnerability and future perspectives of European large shallow, semi-enclosed coastal systems, lagoons and transitional waters. *Estuarine, Coastal and Shelf Science*, *140*, 95–122. https://doi.org/10.1016/j.ecss.2013.05.023

Nezlin, N. P., Kamer, K., Hyde, J., & Stein, E. D. (2009). Dissolved oxygen dynamics in a eutrophic estuary, Upper Newport Bay, California. *Estuarine, Coastal and Shelf Science*, *82*(1), 139–151. https://doi.org/10.1016/j.ecss.2009.01.004

Nicholson, D. P., Wilson, S. T., Doney, S. C., & Karl, D. M. (2015). Quantifying subtropical North Pacific gyre mixed layer primary productivity from Seaglider observations of diel oxygen cycles. *Geophysical Research Letters*, *42*(10), 4032–4039. https://doi.org/10.1002/2015GL063065

Nidzieko, N. J., Needoba, J. A., Monismith, S. G., & Johnson, K. S. (2014). Fortnightly Tidal Modulations Affect Net Community Production in a Mesotidal Estuary. *Estuaries and Coasts*, *37*(S1), 91–110.

https://doi.org/10.1007/s12237-013-9765-2

Nightingale, A. M., Beaton, A. D., & Mowlem, M. C. (2015). Trends in microfluidic systems for in situ chemical analysis of natural waters. *Sensors and Actuators, B: Chemical*, *221*, 1398–1405. https://doi.org/10.1016/j.snb.2015.07.091

Nightingale, A. M., Hassan, S-U., Warren, B. M., Makris, K., Evans, G. W. H., Papadopoulou, E., Coleman, S., & Niu, X. (2019). A Droplet Microfluidic-Based Sensor for Simultaneous in Situ Monitoring of Nitrate and Nitrite in Natural Waters. *Environmental Science and Technology*, *53*(16), 9677–9685. https://doi.org/10.1021/acs.est.9b01032

Niu, L., van Gelder, P. H. A. J. M., Zhang, C., Guan, Y., & Vrijling, J. K. (2016). Physical control of phytoplankton bloom development in the coastal waters of Jiangsu (China). *Ecological Modelling*, *321*, 75–83. https://doi.org/10.1016/j.ecolmodel.2015.10.008

Nixon, S. W. (1995). Coastal marine eutrophication: A definition, social causes, and future concerns. *Ophelia*. https://doi.org/10.1080/00785236.1995.10422044

Nixon, S. W., Oczkowski, A. J., Pilson, M. E. Q., Fields, L., Oviatt, C. A., & Hunt, C. W. (2015). On the Response of pH to Inorganic Nutrient Enrichment in Well-Mixed Coastal Marine Waters. *Estuaries and Coasts*, *38*(1), 232–241. https://doi.org/10.1007/s12237-014-9805-6

O'Boyle, S., McDermott, G., Noklegaard, T., & Wilkes, R. (2013). A Simple Index of Trophic Status in Estuaries and Coastal Bays Based on Measurements of pH and Dissolved Oxygen. *Estuaries and Coasts*, *36*(1), 158–173. https://doi.org/10.1007/s12237-012-9553-4

O'Boyle, S., McDermott, G., & Wilkes, R. (2009). Dissolved oxygen levels in estuarine and coastal waters around Ireland. *Marine Pollution Bulletin*, *58*(11), 1657–1663. https://doi.org/10.1016/j.marpolbul.2009.07.002

Oczkowski, A., Hunt, C. W., Miller, K., Oviatt, C., Nixon, S., & Smith, L. (2016).

Comparing Measures of Estuarine Ecosystem Production in a Temperate New England Estuary. *Estuaries and Coasts*, *39*(6), 1827–1844. https://doi.org/10.1007/s12237-016-0113-1

Odum, H. T. (1956). Primary production in flowing waters. *Limnology and Oceanography*, *1*, 102–117.

Paerl, H. W., & Justic, D. (2013). Estuarine phytoplankton. In John W. Day, B. C. Crump, W. M. Kemp, & A. Yañez-Arancibia (Eds.), *Estuarine ecology* (2nd ed.). Wiley-Blackwell.

Panton, A., Couceiro, F., Fones, G. R., & Purdie, D. A. (2020). The impact of rainfall events, catchment characteristics and estuarine processes on the export of dissolved organic matter from two lowland rivers and their shared estuary. *Science of the Total Environment*, *735*. https://doi.org/10.1016/j.scitotenv.2020.139481

Parsons, T., Maita, Y., & Lalli, C. (1984). Fluorometric Determination of Chlorophylls. In T. Parsons, Y. Maita, & C. Lalli (Eds.), *A Manual of Chemical & Biological Methods for Seawater Analysis* (pp. 107–109). Pergamon. https://doi.org/https://doi.org/10.1016/C2009-0-07774-5

Peierls, B. L., Hall, N. S., & Paerl, H. W. (2012). Non-monotonic responses of phytoplankton biomass accumulation to hydrologic variability: A comparison of two coastal plain north carolina estuaries. *Estuaries and Coasts*, *35*(6), 1376–1392. https://doi.org/10.1007/s12237-012-9547-2

Pejcic, B., Myers, M., Crooke, E., & Cooper, J. S. (2022). *Chem/Bio Sensors for Marine Applications*. *Reference Module in Biomedical Sciences*. Elsevier Inc. https://doi.org/10.1016/b978-0-12-822548-6.00108-4

Peperzak, L. (1993). *Daily irradiance governs growth rate and colony formation of Phaeocystis (Prymnesiophyceae)*. *Journal of Planktoa Research* (Vol. 15). Retrieved from https://academic.oup.com/plankt/article/15/7/809/1472944

Pierrot, D., Lewis, E., & Wallace, D. W. R. (2006). MS Excel program

developed for CO2 system calculations: ORNL/CDIAC-105a. Oak Ridge,Tennesse: Oak Ridge National Laboratory.

Pohlmann, J. T., & Leitner, D. W. (2003). *A Comparison of Ordinary Least Squares and Logistic Regression 1*. *OHIO J SCI* (Vol. 103).

Precheur, H., & Delory, E. (2018). Ocean in situ sensors: New developments in biogeochemistry sensors. In *Challenges and Innovations in Ocean In Situ Sensors: Measuring Inner Ocean Processes and Health in the Digital Age* (pp. 27–80). https://doi.org/10.1016/B978-0-12-809886-8.00002-8

Queste, B. Y., Fernand, L., Jickells, T. D., Heywood, K. J., & Hind, A. J. (2016). Drivers of summer oxygen depletion in the central North Sea. *Biogeosciences*, *13*(4), 1209–1222. https://doi.org/10.5194/bg-13-1209-2016

Raven, J. A., Gobler, C. J., & Hansen, P. J. (2020). Dynamic CO2 and pH levels in coastal, estuarine, and inland waters: Theoretical and observed effects on harmful algal blooms. *Harmful Algae*, *91*. https://doi.org/10.1016/j.hal.2019.03.012

Raymond, P. A., Bauer, J. E., & Cole, J. J. (2000). *Atmospheric CO 2 evasion, dissolved inorganic carbon production, and net heterotrophy in the York River estuary*. *Limnol. Oceanogr* (Vol. 45). Retrieved from http://www.

Riley, G. A. (1967). The plankton in estuaries. In G. H. Lauff (Ed.), *Estuaries* (pp. 316–326). American Association for the Advancement of Science Publication.

Robbins, L. L., Hansen, M. E., Kleypas, J. A., & Meylan, S. C. (2010). *CO2calc: A user-friendly carbon calculator for Windows , Mac OS X , and iOS (iPhone)*. *U.S. Geological Survey* (Vol. Open-File). Retrieved from https://pubs.usgs.gov/of/2010/1280/pdf/ofr_2010-1280.pdf%0Ahttps://pubs.er.usgs.gov/publication/ofr20101280

Robinson, C. (2019). Microbial Respiration, the Engine of Ocean Deoxygenation. *Frontiers in Marine Science*, *5*(January), 1–13.

https://doi.org/10.3389/fmars.2018.00533

Robinson, C., & Williams, P. J. le B. (2005). Respiration and its measurement in surface marine waters. In P. A. del Giorgio & P. J. L. B. Williams (Eds.), *Respiration in Aquatic Ecosystems* (pp. 147–180). Oxford: Oxford University Press.

Rodríguez-Gallego, L., Achkar, M., Defeo, O., Vidal, L., Meerhoff, E., & Conde, D. (2017). Effects of land use changes on eutrophication indicators in five coastal lagoons of the Southwestern Atlantic Ocean. *Estuarine, Coastal and Shelf Science*, *188*, 116–126. https://doi.org/10.1016/j.ecss.2017.02.010

Rose, J. M., & Caron, D. A. (2007). *Does low temperature constrain the growth rates of heterotrophic protists? Evidence and implications for algal blooms in cold waters*. *Limnol. Oceanogr* (Vol. 52). Retrieved from http://www.aslo.org/lo/toc/vol_52/

Ruiz-Ruiz, T. M., Arreola-Lizárraga, J. A., Morquecho, L., Mendez-Rodríguez, L. C., Martínez-López, A., & Mendoza-Salgado, R. A. (2017). Detecting Eutrophication Symptoms in a Subtropical Semi-Arid Coastal Lagoon by Means of Three Different Methods. *Wetlands*, 1–14. https://doi.org/10.1007/s13157-017-0944-y

Ruiz, J., Macías, D., Losada, M. A., Díez-Minguito, M., & Prieto, L. (2013). A simple biogeochemical model for estuaries with high sediment loads: Application to the Guadalquivir River (SW Iberia). *Ecological Modelling*, *265*, 194–206. https://doi.org/10.1016/j.ecolmodel.2013.06.012

Rumyantseva, A., Henson, S., Martin, A., Thompson, A. F., Damerell, G. M., Kaiser, J., & Heywood, K. J. (2019). Phytoplankton spring bloom initiation: The impact of atmospheric forcing and light in the temperate North Atlantic Ocean. *Progress in Oceanography*, *178*. https://doi.org/10.1016/j.pocean.2019.102202

Salhi, N., Zmerli Triki, H., Molinero, J. C., Laabir, M., Sehli, E., Bellaaj-Zouari, A., Daly Yahia, N., & Kefi-Daly Yahia, O. (2018). Seasonal variability of

picophytoplankton under contrasting environments in northern Tunisian coasts, southwestern Mediterranean Sea. *Marine Pollution Bulletin*, *129*(2), 866–874. https://doi.org/10.1016/j.marpolbul.2017.10.029

Salisbury, J. E., Vandemark, D., Hunt, C. W., Campbell, J. W., McGillis, W. R., & McDowell, W. H. (2008a). Seasonal observations of surface waters in two Gulf of Maine estuary-plume systems: Relationships between watershed attributes, optical measurements and surface pCO2. *Estuarine, Coastal and Shelf Science*, *77*(2), 245–252. https://doi.org/10.1016/j.ecss.2007.09.033

Salisbury, J. E., Green, M., Hunt, C., & Campbell, J. (2008b). Coastal Acidification by Rivers: A Threat to Shellfish? *EOS, Transactions, American Geophysical Union*, *89*(50), 513–528.

Salisbury, J. E., Vandemark, D., Hunt, C., Campbell, J., Jonsson, B., Mahadevan, A., McGillis, W., & Xue, H. (2009). Episodic riverine influence on surface DIC in the coastal Gulf of Maine. *Estuarine, Coastal and Shelf Science*, *82*(1), 108–118. https://doi.org/10.1016/j.ecss.2008.12.021

Serret, P., Fernandez, E., & Robinson, C. (2002). Biogeographic differences in the net ecosystem metabolism of the open ocean. *Ecology*, *83*(11), 3225–3234.

Shen, C., Testa, J. M., Li, M., Cai, W-J., Waldbusser, G. G., Ni, W., Kemp, W. M., Cornwell, J., Chen, B., Brodeur, J., & Su, J. (2019a). Controls on Carbonate System Dynamics in a Coastal Plain Estuary: A Modeling Study. *Journal of Geophysical Research: Biogeosciences*, *124*(1), 61–78. https://doi.org/10.1029/2018JG004802

Shen, X., Sun, T., Liu, F., Xu, J., & Pang, A. (2015). Aquatic metabolism response to the hydrologic alteration in the Yellow River estuary, China. *Journal of Hydrology*, *525*, 42–54. https://doi.org/10.1016/j.jhydrol.2015.03.013

Shen, X., Sun, T., Su, M., Dang, Z., & Yang, Z. (2019b). Short-term response of aquatic ecosystem metabolism to turbidity disturbance in experimental

estuarine wetlands. *Ecological Engineering*, *136*, 55–61. https://doi.org/10.1016/j.ecoleng.2019.06.005

Shen, X., Su, M., Sun, T., Lv, S., Dang, Z., & Yang, Z. (2020). Net heterotrophy and low carbon dioxide emissions from biological processes in the Yellow River Estuary, China. *Water Research*, *171*. https://doi.org/10.1016/j.watres.2019.115457

Shi, J., Liu, Y., Mao, X., Guo, X., Wei, H., & Gao, H. (2016). Interannual variation of spring phytoplankton bloom and response to turbulent energy generated by atmospheric forcing in the central Southern Yellow Sea of China: Satellite observations and numerical model study. *Continental Shelf Research*, *143*(December 2015), 1–14. https://doi.org/10.1016/j.csr.2016.06.008

Shi, L. (2000). *Development and application of a three-dimensional water quality model in a partially-mixed estuary, Southampton Water, UK*. University of Southampton.

Silkin, V. A., Pautova, L. A., Giordano, M., Chasovnikov, V. K., Vostokov, S. V., Podymov, O. I., Pakhomova, S. V., & Moskalenko, L. V. (2019). Drivers of phytoplankton blooms in the northeastern Black Sea. In *Marine Pollution Bulletin* (Vol. 138, pp. 274–284). Elsevier Ltd. https://doi.org/10.1016/j.marpolbul.2018.11.042

Smith, M. C., Bodrossy, L., & Craw, P. (2022). *Advances in in situ molecular systems for phytoplankton research and monitoring*. *Advances in Phytoplankton Ecology*. Elsevier Inc. https://doi.org/10.1016/b978-0-12-822861-6.00014-5

Smyth, T. J., Fishwick, J. R., Al-Moosawi, L., Cummings, D. G., Harris, C., Kitidis, V., Rees, A., Martinez-Vicente, V., & Woodward, E. M. S. (2010). A broad spatio-temporal view of the Western English Channel observatory. *Journal of Plankton Research*, *32*(5), 585–601. https://doi.org/10.1093/plankt/fbp128

Spanbauer, T. L., Briseño-Avena, C., Pitz, K. J., & Suter, E. (2020). Salty

sensors, fresh ideas: The use of molecular and imaging sensors in understanding plankton dynamics across marine and freshwater ecosystems. *Limnology And Oceanography Letters*, *5*(2), 169–184. https://doi.org/10.1002/lol2.10128

Staehr, P. A., Testa, J., & Carstensen, J. (2017). Decadal Changes in Water Quality and Net Productivity of a Shallow Danish Estuary Following Significant Nutrient Reductions. *Estuaries and Coasts*, *40*(1), 63–79. https://doi.org/10.1007/s12237-016-0117-x

Staehr, P. A., Testa, J. M., Kemp, W. M., Cole, J. J., Sand-Jensen, K., & Smith, S. V. (2012). The metabolism of aquatic ecosystems: History, applications, and future challenges. *Aquatic Sciences*, *74*(1), 15–29. https://doi.org/10.1007/s00027-011-0199-2

Steckbauer, A., Duarte, C. M., Carstensen, J., Vaquer-Sunyer, R., & Conley, D. J. (2011). Ecosystem impacts of hypoxia: Thresholds of hypoxia and pathways to recovery. *Environmental Research Letters*, *6*(2). https://doi.org/10.1088/1748-9326/6/2/025003

Steemann-Nielsen, E. (1952). The Use of Radio-active Carbon (C14) for Measuring Organic Production in the Sea. *Journal Du Conseil .Conseil Permanent International Pour l'Exploration de La Mer: Copenhagen.*, *18*, 117–140. Retrieved from https://academic.oup.com/icesjms/article/18/2/117/887431

Strickland, J. D. H., & Parsons, T. R. (1972). Pigment anlysis. In J. C. Stevenson, J. Watson, J. M. Reinhart, D. G. Cook, J. Camp, & M. I. Smith (Eds.), *A practical handbook of seawater analysis* (2nd ed., pp. 185–193). Ottawa: Alger Press Ltd.

Taddei, D., Cuet, P., Frouin, P., Esbelin, C., & Clavier, J. (2008). Low community photosynthetic quotient in coral reef sediments. *Comptes Rendus - Biologies*, *331*(9), 668–677. https://doi.org/10.1016/j.crvi.2008.06.006

Tang, S., Sun, T., Shen, X. M., Qi, M., & Feng, M. L. (2015). Modeling net

ecosystem metabolism influenced by artificial hydrological regulation: AN application to the Yellow River Estuary, China. *Ecological Engineering*, *76*, 84–94. https://doi.org/10.1016/j.ecoleng.2014.04.025

Testa, J M, & Kemp, W. M. (2011). Oxygen-Dynamics and Biogeochemical Consequences. In E. Wolanski & D. S. McLusky (Eds.), *Treatise on Estuarine and Coastal Science* (pp. 163–199). Academic Press.

Testa, Jeremy M., Kemp, W. M., Hopkinson, C. S., & Smith, S. V. (2012). Ecosystem Metabolism. In W. J. Day, B. C. Crump, W. M. Kemp, & A. Yáñez-Arancibia (Eds.), *Estuarine Ecology* (2nd ed., pp. 381–416). New Jersey: Wiley-Blackwell. https://doi.org/10.1002/9781118412787

Tilstone, G., Smyth, T., Poulton, A., & Hutson, R. (2009). Measured and remotely sensed estimates of primary production in the Atlantic Ocean from 1998 to 2005. *Deep-Sea Research Part II: Topical Studies in Oceanography*, *56*(15), 918–930. https://doi.org/10.1016/j.dsr2.2008.10.034

Trombetta, T., Vidussi, F., Mas, S., Parin, D., Simier, M., & Mostajir, B. (2019). Water temperature drives phytoplankton blooms in coastal waters. *PLoS ONE*, *14*(4). https://doi.org/10.1371/journal.pone.0214933

Turner, E. L., Paudel, B., & Montagna, P. A. (2015). Baseline nutrient dynamics in shallow well mixed coastal lagoon with seasonal harmful algal blooms and hypoxia formation. *Marine Pollution Bulletin*, *96*(1–2), 456–462. https://doi.org/10.1016/j.marpolbul.2015.05.005

Uchida, H., Kawano, T., Kaneko, I., & Fukasawa, M. (2008). In situ calibration of optode-based oxygen sensors. *Journal of Atmospheric and Oceanic Technology*, *25*(12), 2271–2281. https://doi.org/10.1175/2008JTECHO549.1

Uthicke, S., Furnas, M., & Lønborg, C. (2014). Coral reefs on the edge? Carbon chemistry on inshore reefs of the great barrier reef. *PLoS ONE*, *9*(10). https://doi.org/10.1371/journal.pone.0109092

Valenzuela-Siu, M., Arreola-Lizárraga, J. A., Sánchez-Carrillo, S., & Padilla-Arredondo, G. (2007). Flujos de nutrientes y metabolismo neto de la laguna costera Lobos, México. *Hidrobiologica*, *17*(3), 193–202.

Van Dam, B. R., Crosswell, J. R., Anderson, I. C., & Paerl, H. W. (2018). Watershed-Scale Drivers of Air-Water CO2Exchanges in Two Lagoonal North Carolina (USA) Estuaries. *Journal of Geophysical Research: Biogeosciences*, *123*(1), 271–287. https://doi.org/10.1002/2017JG004243

Van Dam, B. R., Edson, J. B., & Tobias, C. (2019). Parameterizing Air-Water Gas Exchange in the Shallow, Microtidal New River Estuary. *Journal of Geophysical Research: Biogeosciences*, *124*(7), 2351–2363. https://doi.org/10.1029/2018JG004908

Van Der Struijk, L. F., & Kroeze, C. (2010). Future trends in nutrient export to the coastal waters of South America: Implications for occurrence of eutrophication. *Global Biogeochemical Cycles*, *24*(2), 1–14. https://doi.org/10.1029/2009GB003572

Wallace, R. B., Baumann, H., Grear, J. S., Aller, R. C., & Gobler, C. J. (2014). Coastal ocean acidification: The other eutrophication problem. *Estuarine, Coastal and Shelf Science*, *148*, 1–13. https://doi.org/10.1016/j.ecss.2014.05.027

Wanninkhof, R. (2014). Relationship between wind speed and gas exchange over the ocean revisited. *Limnology and Oceanography: Methods*, *12*(JUN), 351–362. https://doi.org/10.4319/lom.2014.12.351

Weiss, R. F. (1974). The impact of sedimentary alkalinity release on the water column CO2 system in the North Sea. *Biogeosciences*, *2*, 203–2015. https://doi.org/10.5194/bg-13-841-2016

Williams, P. J. le B., Quay, P. D., Westberry, T. K., & Behrenfeld, M. J. (2012). The Oligotrophic Ocean Is Autotrophic. *Annual Review of Marine Science*, *5*(1), 535–549. https://doi.org/10.1146/annurev-marine-121211-172335

Winder, M., & Cloern, J. E. (2010). The annual cycles of phytoplankton biomass. *Philosophical Transactions of the Royal Society B: Biological Sciences*, *365*(1555), 3215–3226. https://doi.org/10.1098/rstb.2010.0125

Winkler, L. W. (1888). Die Bestimmung des im Wasser gelosten Sauerstoffes. *Berichte Der Deutschen Chemischen Gesellschaft*, *21*(2), 2843–2854. https://doi.org/https://doi.org/10.1002/cber.188802102122

Wright, P. N., Hydes, D. J., Lauria, M. Lou, Sharples, J., & Purdie, D. A. (1997). Data Buoy Measurements of Phytoplankton Dynamics in Southampton Water, UK, a Temperate Latitude Estuary with High Nutrient Inputs. *Deutsche Hydrographische Zeitschrift German Journal of Hydrography*, *49*(3).

Xia, M., & Jiang, L. (2015). Influence of wind and river discharge on the hypoxia in a shallow bay. *Ocean Dynamics*, *65*(5), 665–678. https://doi.org/10.1007/s10236-015-0826-x

Yao, H., McCutcheon, M. R., Staryk, C. J., & Hu, X. (2020). Hydrologic controls on CO2 chemistry and flux in subtropical lagoonal estuaries of the northwestern Gulf of Mexico. *Limnology and Oceanography*, *65*(6), 1380–1398. https://doi.org/10.1002/lno.11394

Yuan, X., Huang, H., Zhou, W., Yuan, T., Li, X., Gao, Y., & Liu, S. (2016). Long-term variations in oxygen in sub-tropical coastal waters: Influence of sewage effluent. *Aquatic Ecosystem Health and Management*, *19*(4), 336–344. https://doi.org/10.1080/14634988.2016.1240554

Zehrer, R. F., Burns, C. W., & Flöder, S. (2015). Sediment resuspension, salinity and temperature affect the plankton community of a shallow coastal lake. *Marine and Freshwater Research*, *66*(4), 317–328. https://doi.org/10.1071/MF13221

Zhu, Y., McCowan, A., & Cook, P. L. M. (2017). Effects of changes in nutrient loading and composition on hypoxia dynamics and internal nutrient cycling of a stratified coastal lagoon. *Biogeosciences*, *14*(19), 4423–4433. https://doi.org/10.5194/bg-14-4423-2017

Zingone, A., Phlips, E. J., & Harrison, P. J. (2010). Multiscale variability of twenty-two coastal phytoplankton time series: A global scale comparison. *Estuaries and Coasts*, *33*(2), 224–229. https://doi.org/10.1007/s12237-009-9261-x